DISSECTING THE GENETIC INTERACTION OF BRCA1 AND ATM IN HOMOLOGY-DIRECTED DNA REPAIR

A Dissertation

Presented to the Faculty of the Weill Cornell Graduate School

of Medical Sciences

in Partial Fulfillment of the Requirements for the Degree of

Doctor of Philosophy

by

Chun-Chin Chen

May 2018

DISSECTING THE GENETIC INTERACTION OF BRCA1 AND ATM IN HOMOLOGY-DIRECTED DNA REPAIR

Chun-Chin Chen, Ph.D.

Cornell University 2018

Homology-directed repair (HDR) plays a crucial role in the repair of DNA double-strand breaks. Defects in genes involved in HDR compromise genome integrity and predispose cells to tumorigenesis. The breast tumor suppressor BRCA1 is essential for HDR in part through antagonizing the nonhomologous end joining factor 53BP1. The ATM kinase is involved in various aspects of DNA damage signaling. Both BRCA1 and ATM have functions in the early steps of HDR, however their epistatic relationship is largely unclear. In this study we address how mutations in BRCA1 affect its genetic interaction with ATM and 53BP1 in HDR. In a *Brca1*^{S1598F} mouse model carrying a mutation in the phosphoprotein-binding BRCT domain at the C terminus, ATM becomes critical to support HDR and this regulation is independent of the BRCA1-53BP1 antagonism. Deficiency of ATM leads to synthetic lethality in the *Brca1*^{S1598F} mutant mice associated with severely compromised HDR. On the other hand, in a *Brca1*^{ex11} mutant expressing the BRCA1 Δ11 splicing isoform lacking the central region, whether ATM supports HDR is modulated by the status of 53BP1: Only in the absence of 53BP1 does ATM promote HDR. These results suggest that mutations in the BRCT domain and the exon 11-encoding region of BRCA1 differentially affect how ATM kinase participates in HDR. Importantly, while normally not essential, ATM could be critical for HDR proficiency in certain contexts of BRCA1 deficiency, providing a new perspective for targeting *BRCA1* mutant tumors.

BIOGRAPHICAL SKETCH

Chun-Chin Chen graduated from National Sun Yat-Sen University in Taiwan in 2007 majoring in biology. He subsequently obtained his master's degree in 2009 for work performed in Fung-Fang Wang's laboratory at National Yang-Ming University, where he studied p53-mediated regulation on cell migration. He came to Weill Cornell Graduate School of Medical Sciences to pursue his Ph.D. in 2011. He worked on his dissertation research from 2012 to 2018 in Maria Jasin's laboratory at Memorial Sloan Kettering Cancer Center, in which he studied the mechanisms of DNA double-strand break repair.

This dissertation is dedicated to my parents who have fully supported my endeavors.

謹以此論文感謝父母對我的教養與支持

ACKNOWLEDGEMENTS

I want to express sincere gratitude to my Ph.D. mentor, Maria Jasin, whose passion for knowledge and reason exemplifies the quality of a true scientist. I also want to thank my thesis committee members Jayanta Chaudhuri and Xiaolan Zhao for their critical input and career advice during these years. I am grateful to my former mentors in Taiwan: Fung-Fang Wang, who laid a solid foundation for my training during my master's program and inspired me to study abroad and see a different world, as well as Pei-Jung Lu, who sparked my interest in biomedical science during my undergraduate research. Finally, I want to thank all the present and former members of the Jasin lab - in particular, Elizabeth Kass, who provided tremendous assistance to my project from the beginning, my friends on different continents, and most importantly my family.

TABLE OF CONTENTS

LIST OF FIGURES

Chapter 1

Chapter 2

Chapter 3

CHAPTER ONE

INTRODUCTION - THE ROLES OF BRCA1 AND ATM IN HOMOLOGY-DIRECTED REPAIR*

DNA molecules in cells are constantly undergoing damage from both endogenous and exogenous sources that generate a variety of DNA lesions (1, 2). Among them, a double-strand break (DSB) is one of the most cytotoxic types of DNA damage that poses a significant threat to genome integrity. DSBs are repaired by two major pathways in mammalian cells: homology-directed repair (HDR), also known as homologous recombination, and nonhomologous end joining (NHEJ) (3). HDR is considered a relatively error-free repair mechanism, and defects in HDR subject the cells to the utilization of more error-prone repair such as NHEJ that predispose cells to genome instability and tumorigenesis.

A critical step initiating HDR is the resection of DNA ends to generate 3' single-stranded DNA (ssDNA) for recombination (4). Evidence suggests that this process occurs through a two-step mechanism (5, 6). The initial stage of limited resection is mediated by the MRE11 endonuclease activity of the MRE11-RAD50-NBS1 (MRN) complex stimulated by the co-factor CtIP. This is followed by an extensive, bi-directional resection involving the 3'-5' exonuclease activity of MRE11 together with the 5'-3' exonuclease activity of EXO1 and DNA2. The ssDNA overhang is then bound by the recombination protein RAD51, which displaces RPA and promotes strand exchange with a homologous template, typically the sister chromatids during S/G2 phases of the cell cycle, thus allowing for the faithful restoration of wild-type sequence (Figure 1.1). In canonical NHEJ (C-NHEJ), DNA

* Chen CC, Feng W, et al. (2018) Homology-Directed Repair and the Role of BRCA1, BRCA2, and Related Proteins in Genome Integrity and Cancer. Annu. Rev. Cancer Biol. 2:313–336. (Co-first authors)

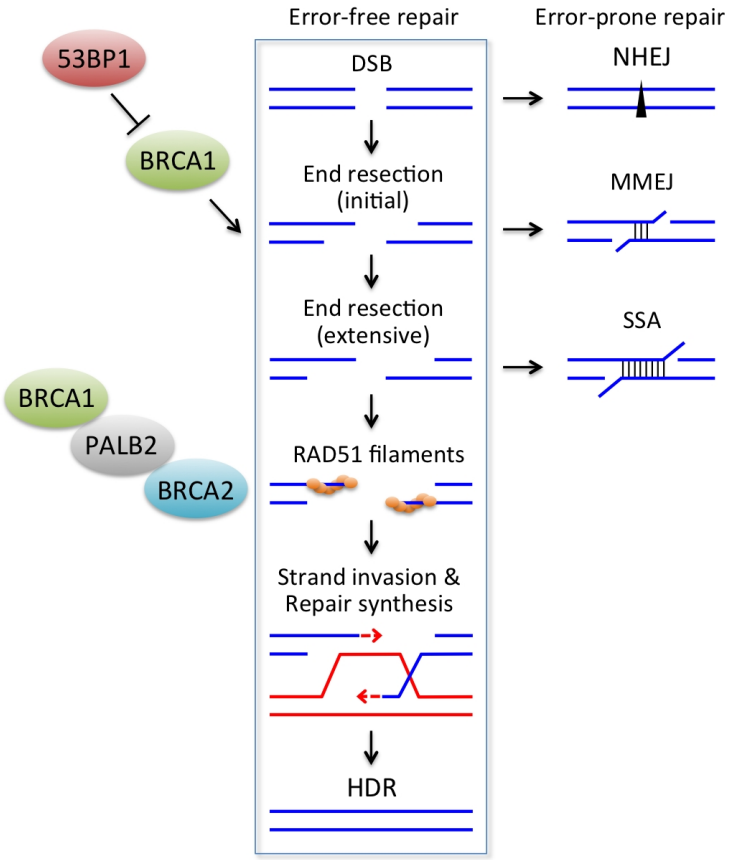

Figure 1.1 Homology-directed repair (HDR) and other pathways for the repair of double-strand breaks (DSBs).
HDR is a major pathway for the error-free repair of DSBs in S/G2 phases. An early determinant of repair pathway choice is end resection that generates 3' single strands. This is regulated by BRCA1 in competition with 53BP1 and can occur through an initial phase to produce short 3' overhangs (<100 base pairs) and a more extensive phase to produce longer 3' overhangs (hundreds of base pairs), as shown in yeast. BRCA1 also promotes the later steps of HDR via interaction with PALB2, which in turn recruits BRCA2. The defining step of HDR is controlled by BRCA2 that promotes the formation of RAD51 filaments on the 3' single strands, followed by strand invasion into a homologous DNA, typically the sister chromatid, priming repair DNA synthesis. DSBs can also be repaired by error-prone repair pathways. Canonical nonhomologous end joining (NHEJ) can occur during any cell cycle phase and is considered the other major DSB repair pathway. In NHEJ, DNA ends are protected from end resection, but often undergo some processing before joining that results in small insertions/deletions. Initial and extensive end resection also provides intermediates for two other DSB repair pathways, alternative NHEJ involving microhomology, also termed microhomology-mediated end joining (MMEJ), and single-strand annealing (SSA) involving longer stretches of homology. Consistent with their involvement in different steps of HDR, BRCA1 promotes HDR and SSA, whereas BRCA2 promotes HDR and suppresses SSA.

ends are bound by the Ku70/80 heterodimer, which then recruits the DNA-PK catalytic subunit (DNA-PKcs) forming the DNA-PK holoenzyme, and joined directly by the XRCC4-DNA Ligase IV complex (7). This process is considered to be active throughout the cell cycle and is frequently accompanied by mutagenic insertions or deletions at the junctions due to the activity of polymerases or nucleases. DSBs can also be repaired by other minor pathways including alternative end joining (alt-EJ) and single-strand annealing (SSA), both are considered error-prone mechanisms (8, 9) (Figure 1.1). Alt-EJ can occur in the absence of C-NHEJ machinery and involves noncanonical factors such as DNA Ligase III for the joining activity. Some end joining events could also rely on a few base pairs of microhomologous sequence exposed on short stretches of ssDNA following limited resection, hence termed microhomology-mediated end joining (MMEJ). More extensive resection could reveal longer stretches of homology on both ends of broken DNA that promote the annealing of each other via SSA. This process is facilitated by RAD52 and the protruding 3' flaps are then removed, leading to the deletion of sequence within the two homologies.

The roles of breast tumor suppressor BRCA1 in HDR

The BRCA1 protein is a key player in HDR and an important suppressor of tumors, in particular hereditary breast and ovarian cancers. Complete loss of BRCA1 leads to early embryonic lethality in mouse models due to the requirement of HDR proficiency for embryo development, whereas hypomorphic mutations of BRCA1 in mice can be viable but confer genome instability and tumor predisposition (10). Human carriers heterozygous for *BRCA1* mutations show a significant increase in cancer risks, in particular those of the breast (~30-fold higher risk at ages 30-39 then decreasing with age) and ovarian cancers (11, 12). Loss of heterozygosity on the wild-type allele is frequently observed in breast tumors from carries with deleterious *BRCA1* mutations

(13). The recent discovery of a patient with biallelic *BRCA1* mutations has led to the classification of *BRCA1* as a Fanconi anemia susceptibility gene (*FANCS*) *(14)*.

BRCA1 participates in both early and later steps of HDR: Following DSB formation, BRCA1 is involved in counteracting the NHEJ factor 53BP1 to facilitate DNA end resection (see below), an early step in HDR. BRCA1 also interacts with the PALB2 protein (15, 16), which in turn recruits BRCA2 to facilitate RAD51 filament formation, a later step in HDR. Patient-derived mutations of *BRCA1* that impair HDR typically also reduce SSA, another DSB repair pathway that requires end resection (17, 18). The exceptions are missense mutations in the coiled-coil domain that specifically disrupt BRCA1 interaction with PALB2 (Figure 1.2), which show reduced HDR but increased SSA, similar to BRCA2 deficiency (17, 18).

Mutations of *BRCA1* in familial breast cancers are frequently located at the evolutionally conserved N-terminal RING and C-terminal BRCT domains, such as the founder mutations 185delAG and 5382insC, respectively (19, 20) (Figure 1.2). The interaction of the RING domain with the BARD1 protein is important for tumor suppression and HDR activity (21, 22), whereas the E3 ubiquitin ligase activity of BRCA1 itself is dispensable for these processes but has a role in other functions such as spermatogenesis (23). The BRCT domain is also critical for tumor suppression and other repair functions of BRCA1, particularly in the regulation of chromatin localization and HDR (23, 24). The BRCT domain interacts with a number of phosphoproteins containing a pSer-X-X-Phe motif, namely Abraxas, BRIP1 (also called BACH1), and CtIP, leading to the mutually exclusive formation of the BRCA1-A, -B, and -C complexes, respectively (25). The components of the BRCA1-A complex, namely Abraxas and RAP80, help localize BRCA1 to the ubiquitylated chromatin modified by RNF8 E3 ubiquitin ligase (26-29). Loss of Abraxas or RAP80 increases genome instability and tumor incidence in mice (30, 31), but how HDR is

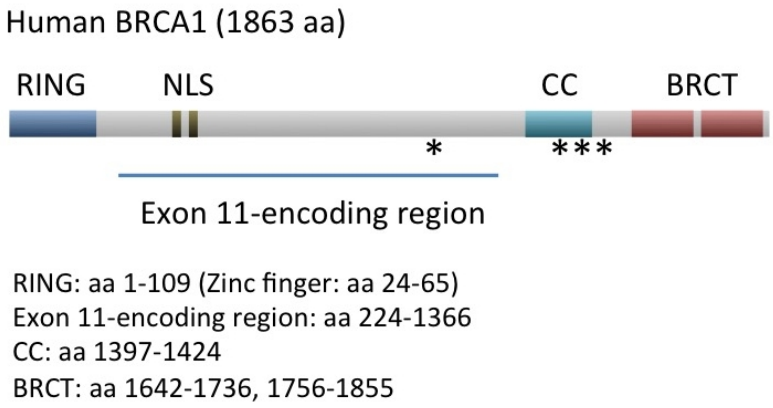

Figure 1.2 Domain structure of the BRCA1 protein.
BRCA1 is composed of an N-terminal RING E3 ubiquitin ligase domain that interacts with the RING domain of its binding partner BARD1; an exon 11-encoding central region containing nuclear localization signals (NLSs) and other activities (e.g., interaction with DNA and RAD51 protein); a coiled-coil (CC) domain for PALB2 binding, with an overlapping SQ cluster targeted by the ATM kinase; and tandem BRCT repeats at the C terminus for interaction with phosphoproteins. The approximate locations of mapped ATM phosphorylation sites are marked by asterisks: A few of them are located in the exon 11-encoding region whereas the rest are located at or adjacent to the CC domain (Cortez et al., 1999; Matsuoka et al., 2007). At least 4 ATM target sites are conserved in mice that are equivalent to human S1189 (in exon 11) and S1387/S1466/S1524 (around CC); note that S1189 is a SP motif which is different from the canonical ATM target site. Domain positions are based on annotations in the UniProtKB database (http://www.uniprot.org/). aa: amino acids.

affected by the loss of the BRCA1-A complex is controversial and several studies show that end resection is actually increased leading to excessive end processing (28, 32, 33). The significance of the BRCA1-C complex in HDR is also elusive, but some evidence suggests that the interaction of CtIP with BRCA1 can facilitate CtIP-mediated resection and the loss of it confers a moderate sensitivity to topoisomerase inhibitors in cells (34-38). These studies point out a possible role of BRCA1 in fine-tuning the extent of end resection through the formation of distinct complexes via its BRCT domain.

Antagonism of BRCA1 and 53BP1 in DSB repair pathway choice

The repair pathway choice of HDR versus NHEJ is regulated in a cell cycle-dependent manner through a mutual antagonism between BRCA1 and 53BP1 (39, 40). The 53BP1 protein is recruited to DSB sites through association with histone markers such as the dimethylated histone H4K20 and ubiquitylated H2AK15 (41-43) (Figure 1.3). 53BP1 is not a core component of the end-joining complex but contributes to NHEJ in certain contexts. For example, 53BP1 has important roles in lymphocyte development by promoting the class switching recombination (CSR) of immunoglobulin heavy chains and the synapsis of long-range V(D)J recombination for T cell receptors (44-46). 53BP1 also regulates chromatin mobility that contributes to the end-to-end fusion of uncapped telomeres (47). In G1 phase, 53BP1 suppresses end resection in an ATM-dependent manner, thus allowing for efficient NHEJ. Deficiency of 53BP1 abrogates the protection of DNA ends and predisposes mice to lymphoma particularly in the p53-deficient condition due to the increased levels of end processing and oncogenic translocations (46, 48-50). On the other hand, in S/G2 phases, BRCA1 is required to counteract 53BP1 in order to promote end resection. This ensures that HDR occurs when sister chromatids are available to template HDR. Importantly, loss of 53BP1

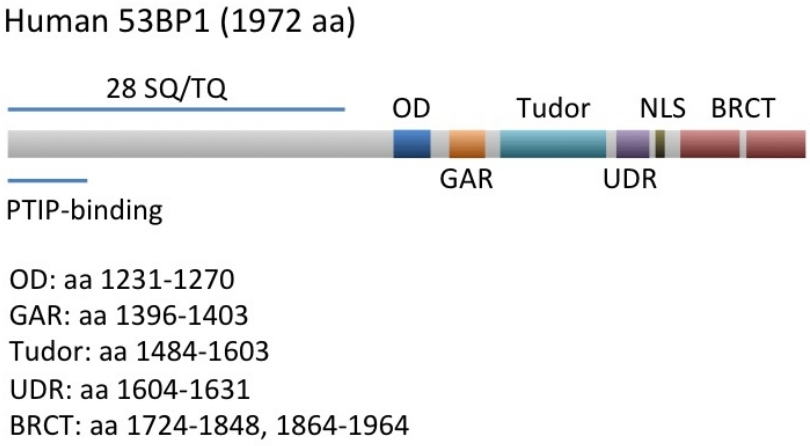

Figure 1.3 Domain structure of the 53BP1 protein.
53BP1 is composed of an N-terminal 28 SQ/TQ cluster that interacts with RIF1 and PTIP (via the 8 sites at the very N terminus) in an ATM-dependent manner; an oligomerization domain (OD) involved in damage foci formation; a glycine arginine rich (GAR) motif; a Tudor domain that binds to dimethylated H4K20 and is important for 53BP1's functions in resection inhibition and class switching; a ubiquitination-dependent recruitment (UDR) motif that binds to ubiquitylated H2AK15; a nuclear localization signal (NLS); and C-terminal tandem BRCT repeats for interaction with proteins such as p53. Domain positions are based on annotations in the UniProtKB database (http://www.uniprot.org/). aa: amino acids.

rescues the HDR defects and lethality of BRCA1- but not BRCA2-deficient cells (51-53). Thus, the role of BRCA1 in antagonizing 53BP1 is likely more pivotal than a direct role for BRCA1 in end resection per se. Besides the BRCA1-53BP1 antagonism, other mechanisms also contribute to the cell cycle-dependent regulation of HDR. For example, phosphorylation of CtIP by CDK in S/G2 phases is crucial for its resection function in cooperation with the MRE11 (54-56). The ubiquitination of PALB2 by the E3 ubiquitin ligase CRL3-KEAP1 in G1 phase suppresses the BRCA1-PALB2 interaction and recombination (57). Notably, depletion of 53BP1 and KEAP1 together with the expression of the $CtIP^{T847E}$ phosphomimetic mutant allow HDR to occur in G1 cells (57), highlighting how multiple factors coordinate to restrict the untimely activation of HDR outside S/G2 phases.

Given the additional, later role for BRCA1 in HDR, it seems surprising that 53BP1 loss can fully restore HDR in BRCA1-deficient settings. Possibly, 53BP1 loss creates more resected ssDNA that mitigates the requirement for BRCA1 in mediating PALB2 and BRCA2 recruitment for RAD51 filament formation (58, 59). Alternatively, additional factors such as ATM/ATR-mediated phosphorylation may contribute to the regulation of PALB2 in this context (60). Importantly, some aspects of BRCA1 function cannot be rescued by 53BP1 loss, such as interstrand crosslink repair and replication fork protection (61-63), suggesting a distinct role of BRCA1 in repairing stalled fork lesions.

ATM-mediated phosphorylation of 53BP1 is required for the interaction of several 53BP1-binding proteins, namely RIF1 and PTIP, to suppress end resection in G1 phase (34, 64-69). The interaction with PTIP depends on the phosphorylation of the 8 most N-terminal SQ/TQ sites on 53BP1, whereas RIF1 binding is partially dependent on the 7 SQ/TQ sites immediately downstream of the 8 PTIP-recognizing residues and is abrogated when all 28 SQ/TQ sites at the N terminus of 53BP1 are

mutated (Figure 1.3). Loss of RIF1 in mice leads to CSR defects and hyper-resection at DSBs at the immunoglobulin heavy chain genes and at uncapped telomeres, similar to the phenotypes of 53BP1-deficient mice. However, RIF1 loss does not rescue the HDR defect of BRCA1-deficient cells to the same extent as 53BP1 loss. By contrast, PTIP appears to a more prominent role than RIF1 in counteracting BRCA1. PTIP deficiency attenuates the fusion of uncapped telomeres but does not affect the NHEJ aspect of CSR. Notably, loss of PTIP in BRCA1-deficient cells almost completely rescues HDR and suppresses chromosome aberrations following treatment with poly(ADP-ribose) polymerase (PARP) inhibitors (see below). These observations illustrate how 53BP1 regulates repair pathway choice through distinct interacting proteins in different contexts.

The mechanism by which BRCA1 counteracts 53BP1 to allow for end resection is not well understood and is likely to be complex. CtIP, which interacts with BRCA1, is a critical resection factor (70), such that 53BP1 loss fails to rescue the lethality of CtIP-deficient mice (71). It is possible that BRCA1 stimulates the end resection machinery, including CtIP, to have limited generation of ssDNA that in turn displaces NHEJ components. For example, activities of the resection factors MRE11 and CtIP can limit the accumulation of Ku at DSB ends (72, 73). However, depletion of Ku cannot rescue cellular lethality associated with BRCA1 deficiency in mice, despite a reduction in chromosome aberrations (62). Given that Ku binds only to DNA ends whereas 53BP1 binds modified histones surrounding the DSB site, the presence of ssDNA alone may not be sufficient to abolish 53BP1 action. Consistent with the notion, the transition from a 53BP1 block of resection to BRCA1-mediated HDR can be facilitated by several chromatin modifying proteins (e.g., histone acetyltransferases TIP60/KAT5 and MOF/KAT8) or chromatin remodelers (e.g., SMARCAD1 and CSB) (74-77). BRCA1 may also actively disrupt the function of the 53BP1 complex to

abrogate the blockade of HDR. For example, BRCA1 disrupts the interaction of 53BP1 and RIF1 in S/G2 phases through promoting the dephosphorylation of 53BP1 by the PP4C phosphatase and targeting RIF1 by an E3 ubiquitin ligase UHRF1 (78, 79). BRCA1 also induces an active repositioning of 53BP1 as observed in the exclusion of 53BP1 signal from the core of DNA damage foci in S/G2 phases (80, 81).

Loss of end resection suppressors confers resistance to PARP inhibitor

Studies have demonstrated that HDR-deficient cells are extremely sensitive to the inhibition of PARP (82, 83). The activity of PARP is involved in the efficient repair of single-strand breaks, and PARP inhibition (PARPi) results in the accumulation of DSBs converted from single-strand breaks during replication and the trapping of the inactive PARP1/2 enzymes on DNA that require HDR machinery to resolve (84-86). Chromosome aberrations arising from toxic NHEJ events also contribute to the sensitivity to PARPi in HDR-deficient human cells (87). These studies have led to the concept of synthetic lethality that targets tumors defective in BRCA1/2 or other HDR factors with PARPi (88).

Despite the effective response to PARPi in HDR-deficient tumors, the development of resistance has been a crucial problem in the clinic (88). Elevated expression of membrane transporters can promote drug efflux. Reduced levels of PARP1/2 enzyme expression or activity can attenuate the pharmacological actions of PARPi. The most common mechanism of acquired resistance is through reversions in the *BRCA1/2* genes that recover wild-type sequence or new frame-restoring isoforms regaining some levels of HDR proficiency. Recent studies demonstrate that BRCA1 mutant mouse and human cells can bypass nonsense mutations within the N-terminal RING domain by expressing a RING-less truncated protein that is not proficient in tumor suppression but is partially competent in HDR, leading to poor therapeutic

responses (89, 90). Another resistance mechanism related to BRCA1 deficiency is the restoration of HDR through the loss of resection suppressors such as 53BP1. Constitutional loss of 53BP1 reduces the spontaneous mammary tumorigenesis in BRCA1-deficient mice (52, 53), consistent with the notion that HDR proficiency suppresses tumors. However, BRCA1-deficient mammary tumors arising in 53BP1 wild-type mice can acquire PARPi resistance through somatic loss of 53BP1 (91). Furthermore, selection of PARPi-resistant BRCA1-mutated tumor cells is also associated with reduced 53BP1 expression (91, 92). Notably, however, because BRCA1 has distinct roles in interstrand crosslink repair (63), 53BP1 loss does not lead to cross-resistance to platinum drugs (62).

Loss of other proteins that affect the levels of end-resected DNA, such as REV7 and HELB, are similarly found to confer PARPi resistance (87, 93-96). These proteins could operate in the same pathway as 53BP1 or in independent steps, such as in the extensive end resection. Notably, given that ATM contributes to HDR in the BRCA1-53BP1 double mutant cells (52), evidence suggests that the HDR-restored BRCA1-deficient tumor cells can be re-sensitized to PARPi by treatments with ATM kinase inhibitors (93, 94). ATR kinase also has a role in bypassing the requirement for BRCA1 for HDR in PARPi-resistant cells by promoting RAD51 recruitment to damage sites (97). Given the use of bioavailable inhibitors of ATM or ATR in combination with genotoxic therapies in mouse tumor models (98-100), the combined treatments with PARPi and ATM/ATR inhibitors have the potential for treating BRCA1-deficient tumors.

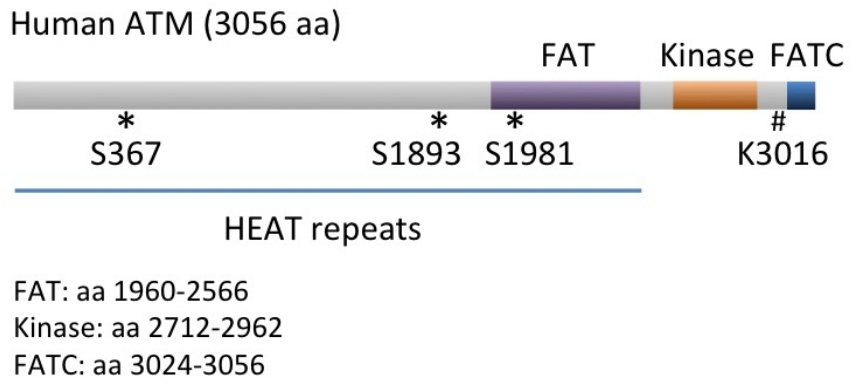

Figure 1.4 Domain structure of the ATM kinase.
ATM kinase is comprised an N-terminal helical solenoid region formed by consecutive HEAT repeats; a FAT domain involved in the trans-inhibition of ATM kinase activity in the dimerized form; a PI3K-related Ser/Thr kinase domain that preferentially recognizes SQ or TQ motif on substrates; and a C-terminal FAT (FATC) domain that interacts with Tip60 histone acetyltransferase contributing to ATM activation. The activity of ATM is regulated by three major autophosphorylation sites S367/S1893/S1981 as well as a Tip60-mediated acetylation site on K3016. Domain positions are based on annotations in the UniProtKB database (http://www.uniprot.org/). aa: amino acids.

The roles of ATM kinase in HDR

The ATM kinase has critical roles in the DNA damage response and checkpoint regulation following DSBs (101). ATM is a Ser/Thr kinase belonging to the PI3K-related kinase family (Figure 1.4), whose members also include ATR and DNA-PKcs which are also important for the DNA damage response. Biallelic *ATM* mutations result in the neurodegenerative syndrome ataxia-telangiectasia (A-T), which is highly associated with tumor predisposition, primarily lymphoid tumors during childhood whose incidence correlates with the absence of any residual ATM kinase activity (102-104). A-T patients who survive to adulthood are also prone to solid tumors, in particular those of the breast (~30-fold increased risk) (102). Monoallelic *ATM* mutations in carriers also lead to a moderate but significant increase in breast cancer risk (~2-fold), making *ATM* a putative breast cancer susceptibility gene (105-107). Evidence also suggests mice heterozygous for an *Atm* nullizygous allele could promote mammary tumorigenesis under certain backgrounds (108-110). The majority of *ATM* mutations associated with A-T are truncations, however, studies suggest that those associated with cancers tend to be missense mutations, frequently in the kinase domain of ATM (103, 111, 112). Inhibition of ATM kinase activity is shown to promote the transformation of normal human mammary epithelial cells (113), in agreement with its association with breast cancer suppression.

ATM kinase is activated in response to multiple conditions including DSBs, chromatin perturbation, and oxidative stress (114). ATM is normally maintained as catalytic inactive dimers in cells and is activated through a monomerization process following DSBs (115, 116). Studies *in vitro* suggest that the monomerization of ATM is facilitated by the MRN complex in the presence of DNA ends that result in the phosphorylation of ATM substrates (117, 118). Activation of ATM upon oxidative stress involves crosslinked dimers formed via oxidized disulfide bonds and is

independent of the MRN-mediated monomerization (119). In human cells undergoing DNA damage, autophosphorylation of ATM on S1981 is shown to unmask the trans-inhibition of its kinase domain in the dimer, which is critical for the monomerization and activation of ATM (115, 120). However, other reports suggest that autophosphorylation is mainly responsible for the retention of active ATM at the breaks but not the initial recruitment (121), and *in vitro* studies using human ATM also suggest that autophosphorylation is not required for the activation process or substrate phosphorylation (117). In mice, mutation on the residue equivalent to human S1981 alone or together with mutations on two additional autophosphorylation sites does not affect the functions of ATM in the DNA damage response (122, 123), raising the possibility of species difference in the regulatory mechanisms of ATM.

In addition to its roles in checkpoint signaling, ATM activity is also implicated in DSB repair mechanisms. ATM functions in NHEJ in part through maintaining the fidelity of the joining process particularly during distant joining, which is important for the V(D)J recombination and CSR in B and T lymphocytes (124-127). Deficiency of ATM leads to aberrant repair of RAG-induced DSBs and chromosomal translocations that, together with the lack of an ATM-mediated G1/S checkpoint, promote the development of lymphoid tumors both in A-T patients and mouse models (128-132). On the other hand, the association of ATM deficiency with breast cancer risk and the sensitivity of ATM-deficient cells to PARPi (87, 133-135) raise the question of a potential role for ATM in HDR. Loss of ATM has been shown to impact HDR in some contexts but not in others depending on the cell types, nature of DNA breaks, or the HDR assays examined (133, 136-141). This may be in part due to the redundancy of substrate phosphorylation by related kinases including ATR and DNA-PKcs (142) or simply a context-dependent requirement for ATM. However, a number of ATM targets have been clearly implicated in the HDR machinery. For example,

phosphorylation of CtIP by CDK and ATM on a number of residues is critical for end resection and HDR (56, 143-145). ATM has also been shown to phosphorylate MRE11 and EXO1 to modulate the extent of end resection for optimal recombination activity (146, 147). Loss of ATM or inhibition of its activity reduces the levels of ssDNA generated from resection as measured by nuclear RPA foci or PCR-based resection assays (140, 148-151). ATM has also been shown to function in later steps of HDR (60, 152). Another aspect of ATM function is to promote heterochromatin relaxation by phosphorylating and inactivating KAP1 to allow for the access of the repair machinery (153).

Recent studies in mice have shown that expression of a kinase-dead ATM protein leads to embryonic lethality in mice and a more severe HDR defect than loss of the ATM protein itself (112, 154, 155). In particular, kinase-dead *Atm* mutant mouse cells are more sensitive to a topoisomerase I inhibitor than *Atm*-null cells in part due to the inability to remove the DNA adducts, providing implications for targeting cancers carrying kinase-inactivating mutations of *ATM* (112). The kinase-dead ATM protein can still localize to the sites of DNA damage, however, cells heterozygous for the kinase-dead *Atm* allele do not have observable repair defects (154, 155). It is possible that the kinase-dead ATM protein is deficient in certain self-regulatory mechanisms, e.g., dissociation from breaks, thus leading to more prominent interference with DSB repair in the absence of wild-type ATM.

Summary

The epistatic relationships between ATM, BRCA1, and 53BP1 in the early steps of DSB repair are not fully understood. Although the interaction of 53BP1 with RIF1 or PTIP in G1 phase depends on ATM, inhibition of ATM activity in 53BP1-deficient lymphocytes reduces the hyper-resection of RAG-induced DSBs and also

partially rescues CSR defects (48, 156-158), suggesting ATM-mediated end resection can occur in G1 phase following 53BP1 loss. On the other hand, ATM also phosphorylates BRCA1 following DNA damage at multiple sites that promote the functions of BRCA1 in checkpoint regulation (159-162). Although the significance of these phosphorylations on BRCA1-mediated HDR is not clear, combined mutations of three phosphorylation sites (human residues S1423/S1387/S1524) abrogate the ability of BRCA1 to support cellular viability (163). Given that ATM is a master regulator at DSB sites, it would be important to determine if ATM has active roles in regulating the choice of DSB repair pathways and how this could affect the therapeutic responses or resistance mechanisms in HDR-deficient tumors.

REFERENCES

1. De Bont R & van Larebeke N (2004) Endogenous DNA damage in humans: a review of quantitative data. *Mutagenesis* 19(3):169-185.
2. Lomax ME, Folkes LK, & O'Neill P (2013) Biological consequences of radiation-induced DNA damage: relevance to radiotherapy. *Clin Oncol (R Coll Radiol)* 25(10):578-585.
3. Moynahan ME & Jasin M (2010) Mitotic homologous recombination maintains genomic stability and suppresses tumorigenesis. *Nat. Rev. Mol. Cell Biol.* 11(3):196-207.
4. Daley JM, Niu H, Miller AS, & Sung P (2015) Biochemical mechanism of DSB end resection and its regulation. *DNA repair* 32:66-74.
5. Garcia V, Phelps SE, Gray S, & Neale MJ (2011) Bidirectional resection of DNA double-strand breaks by Mre11 and Exo1. *Nature* 479(7372):241-244.
6. Mimitou EP & Symington LS (2008) Sae2, Exo1 and Sgs1 collaborate in DNA double-strand break processing. *Nature* 455(7214):770-774.
7. Chang HHY, Pannunzio NR, Adachi N, & Lieber MR (2017) Non-homologous DNA end joining and alternative pathways to double-strand break repair. *Nat. Rev. Mol. Cell Biol.* 18(8):495-506.
8. Verma P & Greenberg RA (2016) Noncanonical views of homology-directed DNA repair. *Genes Dev.* 30(10):1138-1154.
9. Sfeir A & Symington LS (2015) Microhomology-Mediated End Joining: A Back-up Survival Mechanism or Dedicated Pathway? *Trends Biochem. Sci.* 40(11):701-714.
10. Evers B & Jonkers J (2006) Mouse models of BRCA1 and BRCA2 deficiency: past lessons, current understanding and future prospects. *Oncogene* 25(43):5885-5897.
11. Antoniou A*, et al.* (2003) Average risks of breast and ovarian cancer associated with BRCA1 or BRCA2 mutations detected in case Series unselected for family history: a combined analysis of 22 studies. *Am. J. Hum. Genet.* 72(5):1117-1130.
12. Brose MS*, et al.* (2002) Cancer risk estimates for BRCA1 mutation carriers identified in a risk evaluation program. *J. Natl. Cancer Inst.* 94(18):1365-1372.
13. Osorio A*, et al.* (2002) Loss of heterozygosity analysis at the BRCA loci in tumor samples from patients with familial breast cancer. *Int. J. Cancer* 99(2):305-309.
14. Sawyer SL*, et al.* (2015) Biallelic mutations in BRCA1 cause a new Fanconi anemia subtype. *Cancer Discov* 5(2):135-142.
15. Zhang F*, et al.* (2009) PALB2 links BRCA1 and BRCA2 in the DNA-damage response. *Curr. Biol.* 19(6):524-529.
16. Sy SM, Huen MS, & Chen J (2009) PALB2 is an integral component of the BRCA complex required for homologous recombination repair. *Proc. Natl. Acad. Sci. U. S. A.* 106(17):7155-7160.

17. Anantha RW, *et al.* (2017) Functional and mutational landscapes of BRCA1 for homology-directed repair and therapy resistance. *Elife* 6.
18. Stark JM, Pierce AJ, Oh J, Pastink A, & Jasin M (2004) Genetic steps of mammalian homologous repair with distinct mutagenic consequences. *Mol. Cell. Biol.* 24(21):9305-9316.
19. Couch FJ & Weber BL (1996) Mutations and polymorphisms in the familial early-onset breast cancer (BRCA1) gene. Breast Cancer Information Core. *Hum. Mutat.* 8(1):8-18.
20. Clark SL, Rodriguez AM, Snyder RR, Hankins GD, & Boehning D (2012) Structure-Function Of The Tumor Suppressor BRCA1. *Computational and structural biotechnology journal* 1(1).
21. Westermark UK, *et al.* (2003) BARD1 participates with BRCA1 in homology-directed repair of chromosome breaks. *Mol. Cell. Biol.* 23(21):7926-7936.
22. Drost R, *et al.* (2011) BRCA1 RING function is essential for tumor suppression but dispensable for therapy resistance. *Cancer Cell* 20(6):797-809.
23. Shakya R, *et al.* (2011) BRCA1 tumor suppression depends on BRCT phosphoprotein binding, but not its E3 ligase activity. *Science* 334(6055):525-528.
24. Li M & Yu X (2013) Function of BRCA1 in the DNA damage response is mediated by ADP-ribosylation. *Cancer Cell* 23(5):693-704.
25. Wu Q, Jubb H, & Blundell TL (2015) Phosphopeptide interactions with BRCA1 BRCT domains: More than just a motif. *Prog. Biophys. Mol. Biol.* 117(2-3):143-148.
26. Kim H, Chen J, & Yu X (2007) Ubiquitin-binding protein RAP80 mediates BRCA1-dependent DNA damage response. *Science* 316(5828):1202-1205.
27. Sobhian B, *et al.* (2007) RAP80 targets BRCA1 to specific ubiquitin structures at DNA damage sites. *Science* 316(5828):1198-1202.
28. Wang B, *et al.* (2007) Abraxas and RAP80 form a BRCA1 protein complex required for the DNA damage response. *Science* 316(5828):1194-1198.
29. Wang B & Elledge SJ (2007) Ubc13/Rnf8 ubiquitin ligases control foci formation of the Rap80/Abraxas/Brca1/Brcc36 complex in response to DNA damage. *Proc Natl Acad Sci U S A* 104(52):20759-20763.
30. Yin Z, *et al.* (2012) RAP80 is critical in maintaining genomic stability and suppressing tumor development. *Cancer Res.* 72(19):5080-5090.
31. Castillo A, *et al.* (2014) The BRCA1-interacting protein Abraxas is required for genomic stability and tumor suppression. *Cell Rep* 8(3):807-817.
32. Coleman KA & Greenberg RA (2011) The BRCA1-RAP80 complex regulates DNA repair mechanism utilization by restricting end resection. *J. Biol. Chem.* 286(15):13669-13680.
33. Hu Y, *et al.* (2011) RAP80-directed tuning of BRCA1 homologous recombination function at ionizing radiation-induced nuclear foci. *Genes Dev.* 25(7):685-700.
34. Escribano-Diaz C, *et al.* (2013) A cell cycle-dependent regulatory circuit composed of 53BP1-RIF1 and BRCA1-CtIP controls DNA repair pathway choice. *Mol. Cell* 49(5):872-883.

35. Yun MH & Hiom K (2009) CtIP-BRCA1 modulates the choice of DNA double-strand-break repair pathway throughout the cell cycle. *Nature* 459(7245):460-463.
36. Nakamura K, *et al.* (2010) Collaborative action of Brca1 and CtIP in elimination of covalent modifications from double-strand breaks to facilitate subsequent break repair. *PLoS Genet.* 6(1):e1000828.
37. Reczek CR, Szabolcs M, Stark JM, Ludwig T, & Baer R (2013) The interaction between CtIP and BRCA1 is not essential for resection-mediated DNA repair or tumor suppression. *J. Cell Biol.* 201(5):693-707.
38. Cruz-Garcia A, Lopez-Saavedra A, & Huertas P (2014) BRCA1 Accelerates CtIP-Mediated DNA-End Resection. *Cell Rep.* 9(2):451-459.
39. Panier S & Boulton SJ (2014) Double-strand break repair: 53BP1 comes into focus. *Nat. Rev. Mol. Cell Biol.* 15(1):7-18.
40. Zimmermann M & de Lange T (2014) 53BP1: pro choice in DNA repair. *Trends Cell Biol.* 24(2):108-117.
41. Botuyan MV, *et al.* (2006) Structural basis for the methylation state-specific recognition of histone H4-K20 by 53BP1 and Crb2 in DNA repair. *Cell* 127(7):1361-1373.
42. Fradet-Turcotte A, *et al.* (2013) 53BP1 is a reader of the DNA-damage-induced H2A Lys 15 ubiquitin mark. *Nature* 499(7456):50-54.
43. Huyen Y, *et al.* (2004) Methylated lysine 79 of histone H3 targets 53BP1 to DNA double-strand breaks. *Nature* 432(7015):406-411.
44. Ward IM, *et al.* (2004) 53BP1 is required for class switch recombination. *J. Cell Biol.* 165(4):459-464.
45. Manis JP, *et al.* (2004) 53BP1 links DNA damage-response pathways to immunoglobulin heavy chain class-switch recombination. *Nat. Immunol.* 5(5):481-487.
46. Difilippantonio S, *et al.* (2008) 53BP1 facilitates long-range DNA end-joining during V(D)J recombination. *Nature* 456(7221):529-533.
47. Dimitrova N, Chen YC, Spector DL, & de Lange T (2008) 53BP1 promotes non-homologous end joining of telomeres by increasing chromatin mobility. *Nature* 456(7221):524-528.
48. Bothmer A, *et al.* (2010) 53BP1 regulates DNA resection and the choice between classical and alternative end joining during class switch recombination. *J. Exp. Med.* 207(4):855-865.
49. Jankovic M, *et al.* (2013) 53BP1 alters the landscape of DNA rearrangements and suppresses AID-induced B cell lymphoma. *Mol. Cell* 49(4):623-631.
50. Morales JC, *et al.* (2006) 53BP1 and p53 synergize to suppress genomic instability and lymphomagenesis. *Proc. Natl. Acad. Sci. U. S. A.* 103(9):3310-3315.
51. Bouwman P, *et al.* (2010) 53BP1 loss rescues BRCA1 deficiency and is associated with triple-negative and BRCA-mutated breast cancers. *Nat. Struct. Mol. Biol.* 17(6):688-695.
52. Bunting SF, *et al.* (2010) 53BP1 inhibits homologous recombination in Brca1-deficient cells by blocking resection of DNA breaks. *Cell* 141(2):243-254.

53. Cao L*, et al.* (2009) A selective requirement for 53BP1 in the biological response to genomic instability induced by Brca1 deficiency. *Mol. Cell* 35(4):534-541.
54. Huertas P & Jackson SP (2009) Human CtIP mediates cell cycle control of DNA end resection and double strand break repair. *J. Biol. Chem.* 284(14):9558-9565.
55. Anand R, Ranjha L, Cannavo E, & Cejka P (2016) Phosphorylated CtIP Functions as a Co-factor of the MRE11-RAD50-NBS1 Endonuclease in DNA End Resection. *Mol. Cell* 64(5):940-950.
56. Wang H*, et al.* (2013) The interaction of CtIP and Nbs1 connects CDK and ATM to regulate HR-mediated double-strand break repair. *PLoS Genet.* 9(2):e1003277.
57. Orthwein A*, et al.* (2015) A mechanism for the suppression of homologous recombination in G1 cells. *Nature* 528(7582):422-426.
58. Buisson R*, et al.* (2010) Cooperation of breast cancer proteins PALB2 and piccolo BRCA2 in stimulating homologous recombination. *Nat. Struct. Mol. Biol.* 17(10):1247-1254.
59. Dray E*, et al.* (2010) Enhancement of RAD51 recombinase activity by the tumor suppressor PALB2. *Nat. Struct. Mol. Biol.* 17(10):1255-1259.
60. Ahlskog JK, Larsen BD, Achanta K, & Sorensen CS (2016) ATM/ATR-mediated phosphorylation of PALB2 promotes RAD51 function. *EMBO reports* 17(5):671-681.
61. Ray Chaudhuri A*, et al.* (2016) Replication fork stability confers chemoresistance in BRCA-deficient cells. *Nature* 535(7612):382-387.
62. Bunting SF*, et al.* (2012) BRCA1 functions independently of homologous recombination in DNA interstrand crosslink repair. *Mol. Cell* 46(2):125-135.
63. Long DT, Joukov V, Budzowska M, & Walter JC (2014) BRCA1 promotes unloading of the CMG helicase from a stalled DNA replication fork. *Mol. Cell* 56(1):174-185.
64. Feng L, Fong KW, Wang J, Wang W, & Chen J (2013) RIF1 counteracts BRCA1-mediated end resection during DNA repair. *J. Biol. Chem.* 288(16):11135-11143.
65. Zimmermann M, Lottersberger F, Buonomo SB, Sfeir A, & de Lange T (2013) 53BP1 regulates DSB repair using Rif1 to control 5' end resection. *Science* 339(6120):700-704.
66. Di Virgilio M*, et al.* (2013) Rif1 prevents resection of DNA breaks and promotes immunoglobulin class switching. *Science* 339(6120):711-715.
67. Chapman JR*, et al.* (2013) RIF1 is essential for 53BP1-dependent nonhomologous end joining and suppression of DNA double-strand break resection. *Mol. Cell* 49(5):858-871.
68. Callen E*, et al.* (2013) 53BP1 mediates productive and mutagenic DNA repair through distinct phosphoprotein interactions. *Cell* 153(6):1266-1280.
69. Bothmer A*, et al.* (2011) Regulation of DNA end joining, resection, and immunoglobulin class switch recombination by 53BP1. *Mol Cell* 42(3):319-329.

70. Sartori AA, *et al.* (2007) Human CtIP promotes DNA end resection. *Nature* 450(7169):509-514.
71. Polato F, *et al.* (2014) CtIP-mediated resection is essential for viability and can operate independently of BRCA1. *J. Exp. Med.* 211(6):1027-1036.
72. Chanut P, Britton S, Coates J, Jackson SP, & Calsou P (2016) Coordinated nuclease activities counteract Ku at single-ended DNA double-strand breaks. *Nat Commun* 7:12889.
73. Mimitou EP & Symington LS (2010) Ku prevents Exo1 and Sgs1-dependent resection of DNA ends in the absence of a functional MRX complex or Sae2. *EMBO J.* 29(19):3358-3369.
74. Gupta A, *et al.* (2014) MOF phosphorylation by ATM regulates 53BP1-mediated double-strand break repair pathway choice. *Cell Rep* 8(1):177-189.
75. Densham RM, *et al.* (2016) Human BRCA1-BARD1 ubiquitin ligase activity counteracts chromatin barriers to DNA resection. *Nat. Struct. Mol. Biol.* 23(7):647-655.
76. Tang J, *et al.* (2013) Acetylation limits 53BP1 association with damaged chromatin to promote homologous recombination. *Nat. Struct. Mol. Biol.* 20(3):317-325.
77. Batenburg NL, *et al.* (2017) ATM and CDK2 control chromatin remodeler CSB to inhibit RIF1 in DSB repair pathway choice. *Nat Commun* 8(1):1921.
78. Isono M, *et al.* (2017) BRCA1 Directs the Repair Pathway to Homologous Recombination by Promoting 53BP1 Dephosphorylation. *Cell Rep* 18(2):520-532.
79. Zhang H, *et al.* (2016) A cell cycle-dependent BRCA1-UHRF1 cascade regulates DNA double-strand break repair pathway choice. *Nat Commun* 7:10201.
80. Chapman JR, Sossick AJ, Boulton SJ, & Jackson SP (2012) BRCA1-associated exclusion of 53BP1 from DNA damage sites underlies temporal control of DNA repair. *J. Cell Sci.* 125(Pt 15):3529-3534.
81. Kakarougkas A, *et al.* (2013) Co-operation of BRCA1 and POH1 relieves the barriers posed by 53BP1 and RAP80 to resection. *Nucleic Acids Res.* 41(22):10298-10311.
82. Farmer H, *et al.* (2005) Targeting the DNA repair defect in BRCA mutant cells as a therapeutic strategy. *Nature* 434(7035):917-921.
83. Bryant HE, *et al.* (2005) Specific killing of BRCA2-deficient tumours with inhibitors of poly(ADP-ribose) polymerase. *Nature* 434(7035):913-917.
84. Helleday T (2011) The underlying mechanism for the PARP and BRCA synthetic lethality: clearing up the misunderstandings. *Mol. Oncol.* 5(4):387-393.
85. Murai J, *et al.* (2012) Trapping of PARP1 and PARP2 by Clinical PARP Inhibitors. *Cancer Res.* 72(21):5588-5599.
86. Strom CE, *et al.* (2011) Poly (ADP-ribose) polymerase (PARP) is not involved in base excision repair but PARP inhibition traps a single-strand intermediate. *Nucleic Acids Res.* 39(8):3166-3175.

87. Patel AG, Sarkaria JN, & Kaufmann SH (2011) Nonhomologous end joining drives poly(ADP-ribose) polymerase (PARP) inhibitor lethality in homologous recombination-deficient cells. *Proc. Natl. Acad. Sci. U. S. A.* 108(8):3406-3411.
88. Lord CJ & Ashworth A (2013) Mechanisms of resistance to therapies targeting BRCA-mutant cancers. *Nat. Med.* 19(11):1381-1388.
89. Drost R*, et al.* (2016) BRCA1185delAG tumors may acquire therapy resistance through expression of RING-less BRCA1. *J. Clin. Invest.* 126(8):2903-2918.
90. Li M*, et al.* (2016) 53BP1 ablation rescues genomic instability in mice expressing 'RING-less' BRCA1. *EMBO reports* 17(11):1532-1541.
91. Jaspers JE*, et al.* (2013) Loss of 53BP1 causes PARP inhibitor resistance in Brca1-mutated mouse mammary tumors. *Cancer Discov.* 3(1):68-81.
92. Johnson N*, et al.* (2013) Stabilization of mutant BRCA1 protein confers PARP inhibitor and platinum resistance. *Proc. Natl. Acad. Sci. U. S. A.* 110(42):17041-17046.
93. Tkac J*, et al.* (2016) HELB Is a Feedback Inhibitor of DNA End Resection. *Mol. Cell* 61(3):405-418.
94. Xu G*, et al.* (2015) REV7 counteracts DNA double-strand break resection and affects PARP inhibition. *Nature* 521(7553):541-544.
95. Wang J*, et al.* (2014) PTIP associates with Artemis to dictate DNA repair pathway choice. *Genes Dev.* 28(24):2693-2698.
96. Boersma V*, et al.* (2015) MAD2L2 controls DNA repair at telomeres and DNA breaks by inhibiting 5' end resection. *Nature* 521(7553):537-540.
97. Yazinski SA*, et al.* (2017) ATR inhibition disrupts rewired homologous recombination and fork protection pathways in PARP inhibitor-resistant BRCA-deficient cancer cells. *Genes Dev.* 31(3):318-332.
98. Degorce SL*, et al.* (2016) Discovery of Novel 3-Quinoline Carboxamides as Potent, Selective, and Orally Bioavailable Inhibitors of Ataxia Telangiectasia Mutated (ATM) Kinase. *J. Med. Chem.* 59(13):6281-6292.
99. Fokas E*, et al.* (2012) Targeting ATR in vivo using the novel inhibitor VE-822 results in selective sensitization of pancreatic tumors to radiation. *Cell Death Dis.* 3:e441.
100. Vendetti FP*, et al.* (2015) The orally active and bioavailable ATR kinase inhibitor AZD6738 potentiates the anti-tumor effects of cisplatin to resolve ATM-deficient non-small cell lung cancer in vivo. *Oncotarget* 6(42):44289-44305.
101. Shiloh Y & Ziv Y (2013) The ATM protein kinase: regulating the cellular response to genotoxic stress, and more. *Nat. Rev. Mol. Cell Biol.* 14(4):197-210.
102. Reiman A*, et al.* (2011) Lymphoid tumours and breast cancer in ataxia telangiectasia; substantial protective effect of residual ATM kinase activity against childhood tumours. *Br. J. Cancer* 105(4):586-591.
103. Stankovic T*, et al.* (1998) ATM mutations and phenotypes in ataxia-telangiectasia families in the British Isles: expression of mutant ATM and the

risk of leukemia, lymphoma, and breast cancer. *Am. J. Hum. Genet.* 62(2):334-345.
104. Verhagen MM*, et al.* (2012) Presence of ATM protein and residual kinase activity correlates with the phenotype in ataxia-telangiectasia: a genotype-phenotype study. *Hum. Mutat.* 33(3):561-571.
105. Renwick A*, et al.* (2006) ATM mutations that cause ataxia-telangiectasia are breast cancer susceptibility alleles. *Nat. Genet.* 38(8):873-875.
106. Thompson D*, et al.* (2005) Cancer risks and mortality in heterozygous ATM mutation carriers. *J. Natl. Cancer Inst.* 97(11):813-822.
107. Walsh T & King MC (2007) Ten genes for inherited breast cancer. *Cancer Cell* 11(2):103-105.
108. Umesako S*, et al.* (2005) Atm heterozygous deficiency enhances development of mammary carcinomas in p53 heterozygous knockout mice. *Breast Cancer Res.* 7(1):R164-170.
109. Bowen TJ*, et al.* (2005) Atm heterozygosity cooperates with loss of Brca1 to increase the severity of mammary gland cancer and reduce ductal branching. *Cancer Res.* 65(19):8736-8746.
110. Mao JH*, et al.* (2008) Atm heterozygosity does not increase tumor susceptibility to ionizing radiation alone or in a p53 heterozygous background. *Oncogene* 27(51):6596-6600.
111. Scott SP*, et al.* (2002) Missense mutations but not allelic variants alter the function of ATM by dominant interference in patients with breast cancer. *Proc. Natl. Acad. Sci. U. S. A.* 99(2):925-930.
112. Yamamoto K*, et al.* (2016) Kinase-dead ATM protein is highly oncogenic and can be preferentially targeted by Topo-isomerase I inhibitors. *Elife* 5.
113. Mandriota SJ*, et al.* (2010) Ataxia telangiectasia mutated (ATM) inhibition transforms human mammary gland epithelial cells. *J. Biol. Chem.* 285(17):13092-13106.
114. Paull TT (2015) Mechanisms of ATM Activation. *Annu Rev Biochem* 84:711-738.
115. Bakkenist CJ & Kastan MB (2003) DNA damage activates ATM through intermolecular autophosphorylation and dimer dissociation. *Nature* 421(6922):499-506.
116. Wang X*, et al.* (2016) Structure of the intact ATM/Tel1 kinase. *Nat Commun* 7:11655.
117. Lee JH & Paull TT (2005) ATM activation by DNA double-strand breaks through the Mre11-Rad50-Nbs1 complex. *Science* 308(5721):551-554.
118. Lee JH & Paull TT (2004) Direct activation of the ATM protein kinase by the Mre11/Rad50/Nbs1 complex. *Science* 304(5667):93-96.
119. Guo Z, Kozlov S, Lavin MF, Person MD, & Paull TT (2010) ATM activation by oxidative stress. *Science* 330(6003):517-521.
120. Berkovich E, Monnat RJ, & Kastan MB (2007) Roles of ATM and NBS1 in chromatin structure modulation and DNA double-strand break repair. *Nat Cell Biol* 9(6):683-690.

121. So S, Davis AJ, & Chen DJ (2009) Autophosphorylation at serine 1981 stabilizes ATM at DNA damage sites. *J Cell Biol* 187(7):977-990.
122. Daniel JA*, et al.* (2008) Multiple autophosphorylation sites are dispensable for murine ATM activation in vivo. *J Cell Biol* 183(5):777-783.
123. Pellegrini M*, et al.* (2006) Autophosphorylation at serine 1987 is dispensable for murine Atm activation in vivo. *Nature* 443(7108):222-225.
124. Bennardo N & Stark JM (2010) ATM limits incorrect end utilization during non-homologous end joining of multiple chromosome breaks. *PLoS Genet.* 6(11):e1001194.
125. Bhargava R, Carson CR, Lee G, & Stark JM (2017) Contribution of canonical nonhomologous end joining to chromosomal rearrangements is enhanced by ATM kinase deficiency. *Proc Natl Acad Sci U S A* 114(4):728-733.
126. Bredemeyer AL*, et al.* (2006) ATM stabilizes DNA double-strand-break complexes during V(D)J recombination. *Nature* 442(7101):466-470.
127. Reina-San-Martin B, Chen HT, Nussenzweig A, & Nussenzweig MC (2004) ATM is required for efficient recombination between immunoglobulin switch regions. *J Exp Med* 200(9):1103-1110.
128. Liao MJ & Van Dyke T (1999) Critical role for Atm in suppressing V(D)J recombination-driven thymic lymphoma. *Genes Dev* 13(10):1246-1250.
129. Callen E*, et al.* (2007) ATM prevents the persistence and propagation of chromosome breaks in lymphocytes. *Cell* 130(1):63-75.
130. Zha S*, et al.* (2010) ATM-deficient thymic lymphoma is associated with aberrant tcrd rearrangement and gene amplification. *J Exp Med* 207(7):1369-1380.
131. Huang CY*, et al.* (2007) Defects in coding joint formation in vivo in developing ATM-deficient B and T lymphocytes. *J Exp Med* 204(6):1371-1381.
132. Hathcock KS*, et al.* (2015) ATM deficiency promotes development of murine B-cell lymphomas that resemble diffuse large B-cell lymphoma in humans. *Blood* 126(20):2291-2301.
133. Rass E, Chandramouly G, Zha S, Alt FW, & Xie A (2013) Ataxia telangiectasia mutated (ATM) is dispensable for endonuclease I-SceI-induced homologous recombination in mouse embryonic stem cells. *J. Biol. Chem.* 288(10):7086-7095.
134. Weston VJ*, et al.* (2010) The PARP inhibitor olaparib induces significant killing of ATM-deficient lymphoid tumor cells in vitro and in vivo. *Blood* 116(22):4578-4587.
135. Williamson CT*, et al.* (2010) ATM deficiency sensitizes mantle cell lymphoma cells to poly(ADP-ribose) polymerase-1 inhibitors. *Mol. Cancer Ther.* 9(2):347-357.
136. Alvarez-Quilon A*, et al.* (2014) ATM specifically mediates repair of double-strand breaks with blocked DNA ends. *Nat. Commun.* 5:3347.
137. Kass EM*, et al.* (2013) Double-strand break repair by homologous recombination in primary mouse somatic cells requires BRCA1 but not the ATM kinase. *Proc. Natl. Acad. Sci. U. S. A.* 110(14):5564-5569.

138. White JS, Choi S, & Bakkenist CJ (2010) Transient ATM kinase inhibition disrupts DNA damage-induced sister chromatid exchange. *Sci. Signal.* 3(124):ra44.
139. Morrison C*, et al.* (2000) The controlling role of ATM in homologous recombinational repair of DNA damage. *EMBO J.* 19(3):463-471.
140. Beucher A*, et al.* (2009) ATM and Artemis promote homologous recombination of radiation-induced DNA double-strand breaks in G2. *EMBO J.* 28(21):3413-3427.
141. Chen CC*, et al.* (2017) ATM loss leads to synthetic lethality in BRCA1 BRCT mutant mice associated with exacerbated defects in homology-directed repair. *Proc. Natl. Acad. Sci. U. S. A.* 114(29):7665-7670.
142. Tomimatsu N, Mukherjee B, & Burma S (2009) Distinct roles of ATR and DNA-PKcs in triggering DNA damage responses in ATM-deficient cells. *EMBO reports* 10(6):629-635.
143. You Z*, et al.* (2009) CtIP links DNA double-strand break sensing to resection. *Mol. Cell* 36(6):954-969.
144. Shibata A*, et al.* (2011) Factors determining DNA double-strand break repair pathway choice in G2 phase. *EMBO J.* 30(6):1079-1092.
145. Makharashvili N*, et al.* (2014) Catalytic and noncatalytic roles of the CtIP endonuclease in double-strand break end resection. *Mol. Cell* 54(6):1022-1033.
146. Kijas AW*, et al.* (2015) ATM-dependent phosphorylation of MRE11 controls extent of resection during homology directed repair by signalling through Exonuclease 1. *Nucleic Acids Res.* 43(17):8352-8367.
147. Bolderson E*, et al.* (2010) Phosphorylation of Exo1 modulates homologous recombination repair of DNA double-strand breaks. *Nucleic Acids Res.* 38(6):1821-1831.
148. Zhou Y & Paull TT (2013) DNA-dependent protein kinase regulates DNA end resection in concert with Mre11-Rad50-Nbs1 (MRN) and ataxia telangiectasia-mutated (ATM). *J. Biol. Chem.* 288(52):37112-37125.
149. Jazayeri A*, et al.* (2006) ATM- and cell cycle-dependent regulation of ATR in response to DNA double-strand breaks. *Nat. Cell Biol.* 8(1):37-45.
150. Cuadrado M*, et al.* (2006) ATM regulates ATR chromatin loading in response to DNA double-strand breaks. *J. Exp. Med.* 203(2):297-303.
151. Myers JS & Cortez D (2006) Rapid activation of ATR by ionizing radiation requires ATM and Mre11. *J. Biol. Chem.* 281(14):9346-9350.
152. Bakr A*, et al.* (2015) Involvement of ATM in homologous recombination after end resection and RAD51 nucleofilament formation. *Nucleic Acids Res.* 43(6):3154-3166.
153. Goodarzi AA & Jeggo PA (2012) The heterochromatic barrier to DNA double strand break repair: how to get the entry visa. *International journal of molecular sciences* 13(9):11844-11860.
154. Daniel JA*, et al.* (2012) Loss of ATM kinase activity leads to embryonic lethality in mice. *J. Cell Biol.* 198(3):295-304.
155. Yamamoto K*, et al.* (2012) Kinase-dead ATM protein causes genomic instability and early embryonic lethality in mice. *J. Cell Biol.* 198(3):305-313.

156. Yamane A*, et al.* (2013) RPA accumulation during class switch recombination represents 5'-3' DNA-end resection during the S-G2/M phase of the cell cycle. *Cell Rep.* 3(1):138-147.
157. Tubbs AT*, et al.* (2014) KAP-1 promotes resection of broken DNA ends not protected by gamma-H2AX and 53BP1 in G(1)-phase lymphocytes. *Mol. Cell. Biol.* 34(15):2811-2821.
158. Liu X*, et al.* (2012) Overlapping functions between XLF repair protein and 53BP1 DNA damage response factor in end joining and lymphocyte development. *Proc Natl Acad Sci U S A* 109(10):3903-3908.
159. Gatei M*, et al.* (2000) Role for ATM in DNA damage-induced phosphorylation of BRCA1. *Cancer Res.* 60(12):3299-3304.
160. Cortez D, Wang Y, Qin J, & Elledge SJ (1999) Requirement of ATM-dependent phosphorylation of brca1 in the DNA damage response to double-strand breaks. *Science* 286(5442):1162-1166.
161. Xu B, O'Donnell AH, Kim ST, & Kastan MB (2002) Phosphorylation of serine 1387 in Brca1 is specifically required for the Atm-mediated S-phase checkpoint after ionizing irradiation. *Cancer Res.* 62(16):4588-4591.
162. Xu B, Kim S, & Kastan MB (2001) Involvement of Brca1 in S-phase and G(2)-phase checkpoints after ionizing irradiation. *Mol. Cell. Biol.* 21(10):3445-3450.
163. Chang S, Biswas K, Martin BK, Stauffer S, & Sharan SK (2009) Expression of human BRCA1 variants in mouse ES cells allows functional analysis of BRCA1 mutations. *J. Clin. Invest.* 119(10):3160-3171.

CHAPTER TWO

ATM LOSS LEADS TO SYNTHETIC LETHALITY IN BRCA1 BRCT MUTANT MICE ASSOCIATED WITH EXACERBATED DEFECTS IN HOMOLOGY-DIRECTED REPAIR[*]

Abstract

BRCA1 is essential for homology-directed repair (HDR) of DNA double-strand breaks in part through antagonism of the nonhomologous end-joining factor 53BP1. The ATM kinase is involved in various aspects of DNA damage signaling and repair, but how ATM participates in HDR and genetically interacts with BRCA1 in this process is unclear. To investigate this question, we used the *Brca1*^{S1598F} mouse model carrying a mutation in the BRCT domain of BRCA1. Whereas ATM loss leads to a mild HDR defect in adult somatic cells, we find that ATM inhibition leads to severely reduced HDR in *Brca1*^{S1598F} cells. Consistent with a critical role for ATM in HDR in this background, loss of ATM leads to synthetic lethality of *Brca1*^{S1598F} mice. While both ATM and BRCA1 promote end resection, which can be regulated by 53BP1, *53bp1* deletion does not rescue the HDR defects of *Atm* mutant cells, in contrast to *Brca1* mutant cells. These results demonstrate that ATM has a role in HDR independent of the BRCA1-53BP1 antagonism and that its HDR function can become critical in certain contexts.

Introduction

A DNA double-strand break (DSB) is one of the most cytotoxic types of DNA damage and poses a significant threat to genome integrity. Two major DSB repair pathways

[*] Chen CC, et al. (2013) ATM loss leads to synthetic lethality in BRCA1 BRCT mutant mice associated with exacerbated defects in homology-directed repair Proc. Natl. Acad. Sci. U. S. A. 114(29):7665-7670.

exist in mammalian cells: homology-directed repair (HDR) and non-homologous end joining (NHEJ) (1, 2). In NHEJ, DNA ends are minimally processed before rejoining. By contrast, HDR initiates with resection of DNA ends to generate single-stranded DNA for RAD51-mediated strand invasion of a homologous template. HDR is considered a relatively error-free repair pathway, such that defects in HDR result in the use of more error-prone repair mechanisms that predispose cells to genome instability and tumorigenesis or cell death.

An essential HDR factor is the breast tumor suppressor BRCA1, which promotes the initial end resection step of HDR, as well as later steps of recombination (1, 3). HDR defects in BRCA1-deficient cells can be suppressed by loss of 53BP1, an NHEJ protein that impedes end resection (4-6). BRCA1 and 53BP1 operate antagonistically at different cell cycle phases: 53BP1 and its interacting proteins counteract BRCA1 in G1 phase to limit end resection; by contrast, BRCA1 suppresses 53BP1 function in S/G2 phases to promote HDR (3, 7). In addition to antagonizing 53BP1, BRCA1 binds to the resection factor CtIP and facilitates its activity, although the mechanisms merit further investigation (8-11)

ATM kinase is the master regulator of the DNA damage signaling and repair machinery in response to DSBs, and a suppressor of lymphoid and mammary tumors (12, 13). In repair, ATM is implicated in various aspects of NHEJ, e.g., in maintaining the fidelity of the joining process (14, 15). ATM-mediated phosphorylation is required for the proper functions of 53BP1 in NHEJ (3, 7) and for the destabilization of BRCA1-PALB2 complex to prevent HDR in G1 phase (16). Conversely, ATM is also proposed to participate in HDR (17, 18), e.g., by phosphorylating CtIP in cooperation with cyclin-dependent kinase (CDK) to stimulate end resection in S/G2 phases (19-23). However, several studies have shown that ATM is not essential for HDR in some contexts, e.g., mouse embryonic stem (ES) cells (24-27). Further, unlike the severe

phenotypes of mice deficient in core HDR factors such as BRCA1 (28), *Atm* nullizygous mice are viable (29, 30). Therefore, it remains an open question whether ATM plays a significant role in HDR.

In this study, we examine the genetic interactions between ATM, BRCA1, and 53BP1 in mice using a hypomorphic mutant, $Brca1^{S1598F}$ ($Brca1^{SF}$), carrying a breast cancer-derived mutation in the BRCT domain that disrupts the hydrogen bond interaction with the phosphate group of incoming phosphoproteins (31). We present evidence that ATM is critical for the residual HDR in $Brca1^{SF}$ cells, and that loss of ATM in $Brca1^{SF}$ mice leads to synthetic lethality, consistent with the embryonic lethality of mouse mutants with severe HDR defects. Interestingly, unlike in the $Brca1^{SF}$ mutant, the resection and HDR defects in the *Atm* mutant cannot be rescued by *53bp1* deletion. These genetic analyses indicate that ATM has a role in HDR independent of the BRCA1-53BP1 antagonism and, while normally not essential for HDR, this role becomes critical when certain functions of BRCA1 are compromised.

Results

ATM inhibition reduces HDR in $Brca1^{SF}$ embryonic stem cells.

Since BRCA1 and ATM have both been implicated in DNA end resection, the first step of HDR, we investigated the genetic interaction of the two proteins. While complete loss of BRCA1 leads to cell lethality, mice carrying the $Brca1^{S1598F}$ hypomorphic allele are viable (31) (Figure 2.1A). HDR was substantially reduced in the mouse $Brca1^{SF/SF}$ ES cells, as demonstrated using the direct repeat (DR)-GFP reporter assay (>5-fold) (31) (Figure 2.1B). By contrast, HDR levels were not significantly reduced in the $Atm^{-/-}$ cells (Figure 2.1B), as previously reported (25-27), indicating that ATM is not required for HDR in these cells. However, we observed that HDR was reduced at an earlier time point (24 versus 48 hours after transfection),

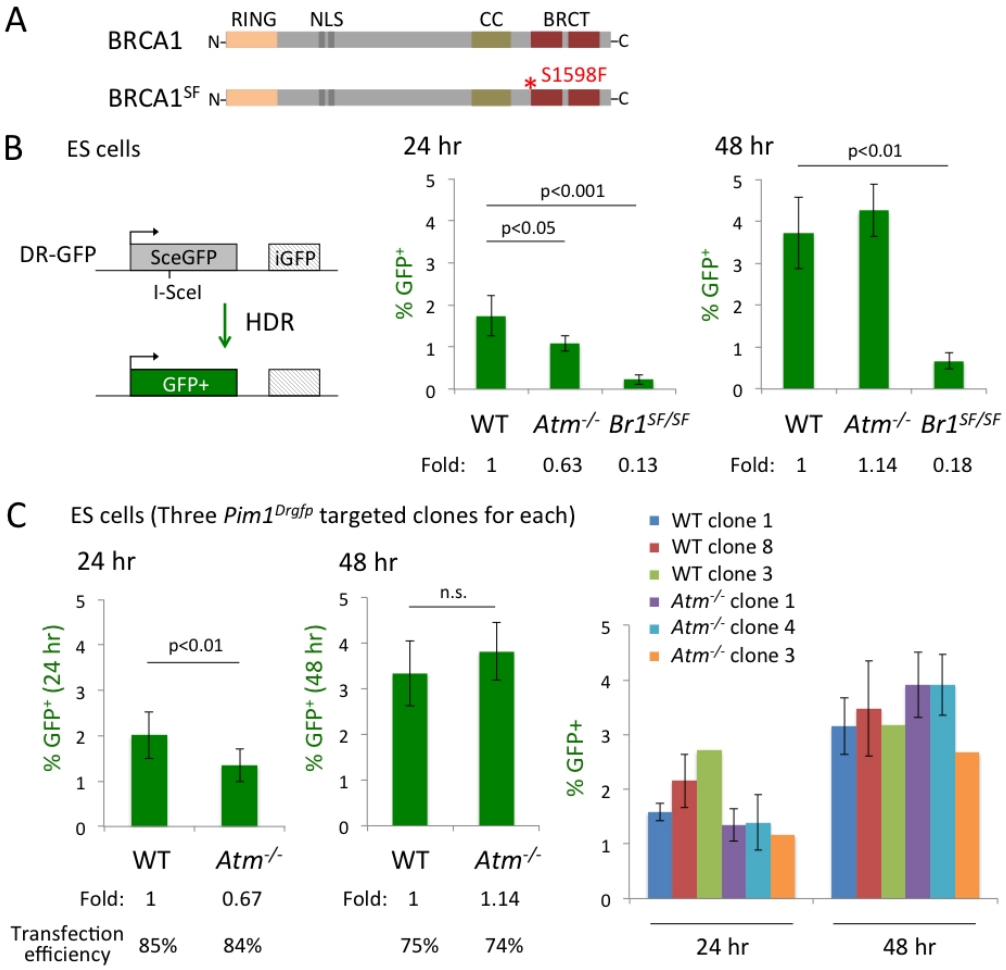

Figure 2.1 HDR is defective in *Brca1*$^{SF/SF}$ whereas only delayed in *Atm*$^{-/-}$ ES cells.
A. Mouse BRCA1 S1598F (SF) protein carries a breast cancer-derived point mutation in the BRCT domain that interrupts the interaction with phosphoproteins.
B. The DR-GFP reporter consists of two copies of mutant *GFP* genes. A DSB introduced by I-SceI endonuclease in *SceGFP* can be repaired by HDR using *iGFP* as a template and restore a functional *GFP*$^{+}$ gene. HDR is substantially reduced in *Brca1*$^{SF/SF}$ ES cells. HDR in *Atm*$^{-/-}$ ES cells has no significant difference from WT cells, however a ~1.6-fold reduction is seen at earlier time point (24 hr post transfection of an I-SceI expression vector). All error bars in the figures of this chapter represent one standard deviation from the mean. (n≥3)
C. To clarify the impact of ATM loss on HDR, three independent *Pim1*^{Drgfp} targeted clones of WT and *Atm*$^{-/-}$ ES cells, respectively, are examined. The average HDR of the three clones is reduced by ~1.5-fold in *Atm*$^{-/-}$ ES cells at 24 hr (left) but not 48 hr (middle) after transfection of an I-SceI expression vector, confirming a delay in HDR (WT n=12; *Atm*$^{-/-}$ n=13 transfections combined). The levels of HDR in individual clones are summarized (right) and are consistent with the notion above. J1 clone 8 and *Atm*$^{-/-}$ clone 1 are used for the rest of ES cell experiments in Chapter 2 and 3.

such that *Atm*$^{-/-}$ ES cells showed a delay in HDR, but eventually reached wild-type levels. We further analyzed the average levels of HDR of three independent clones integrated with the DR-GFP reporter for WT J1 and *Atm*$^{-/-}$ ES cells, respectively, and the comparison between them supported the notion of delayed HDR response in *Atm*$^{-/-}$ ES cells (Figure 2.1C).

To examine the interaction between ATM and the BRCA1 mutant, ES cells were treated with an ATM inhibitor (ATMi, KU-55933). ATMi treatment reduced HDR in both WT and *Brca1*$^{SF/SF}$ cells; the reduction was greater in *Brca1*$^{SF/SF}$ cells, leading to an overall 19-fold reduction in HDR compared to DMSO-treated WT cells (Figure 2.2A). These differences were not related to changes in cell cycle distribution (Figure 2.2B). Thus, ATM kinase activity supports HDR in *Brca1*$^{SF/SF}$ cells.

We also examined the response of these ES cell lines to olaparib, a poly(ADP-ribose) polymerase inhibitor (PARPi), treatment of which is synthetically lethal with HDR deficiency (32). Transient olaparib exposure had little effect on WT ES cells at the doses tested, but decreased colony formation of both mutants (Figure 2.2 C and D). Interestingly, *Atm*$^{-/-}$ ES cells (IC_{50}: 13.8 nM) showed a similar sensitivity as *Brca1*$^{SF/SF}$ cells (IC_{50}: 14.5 nM), despite only a kinetic delay in HDR in the DR-GFP assay, suggesting additional repair deficiencies such as processing of DNA ends at trapped PARP complexes (33). Notably, ATM inhibition in *Brca1*$^{SF/SF}$ cells further increased the sensitivity of these cells to olaparib in colony formation assays (Figure 2.2 C and D; IC_{50} with ATMi: 3.9 nM), consistent with the exacerbated HDR defect (Figure 2.2A).

The mouse *Brca1*^{SF} mutation encodes a protein that corresponds to the familial breast cancer mutation S1655F which disrupts the interaction of the BRCT domain with a number of phosphoproteins, including the resection factor CtIP (34). Previous studies have shown that phosphorylation of human CtIP at residue S327 (S326 in

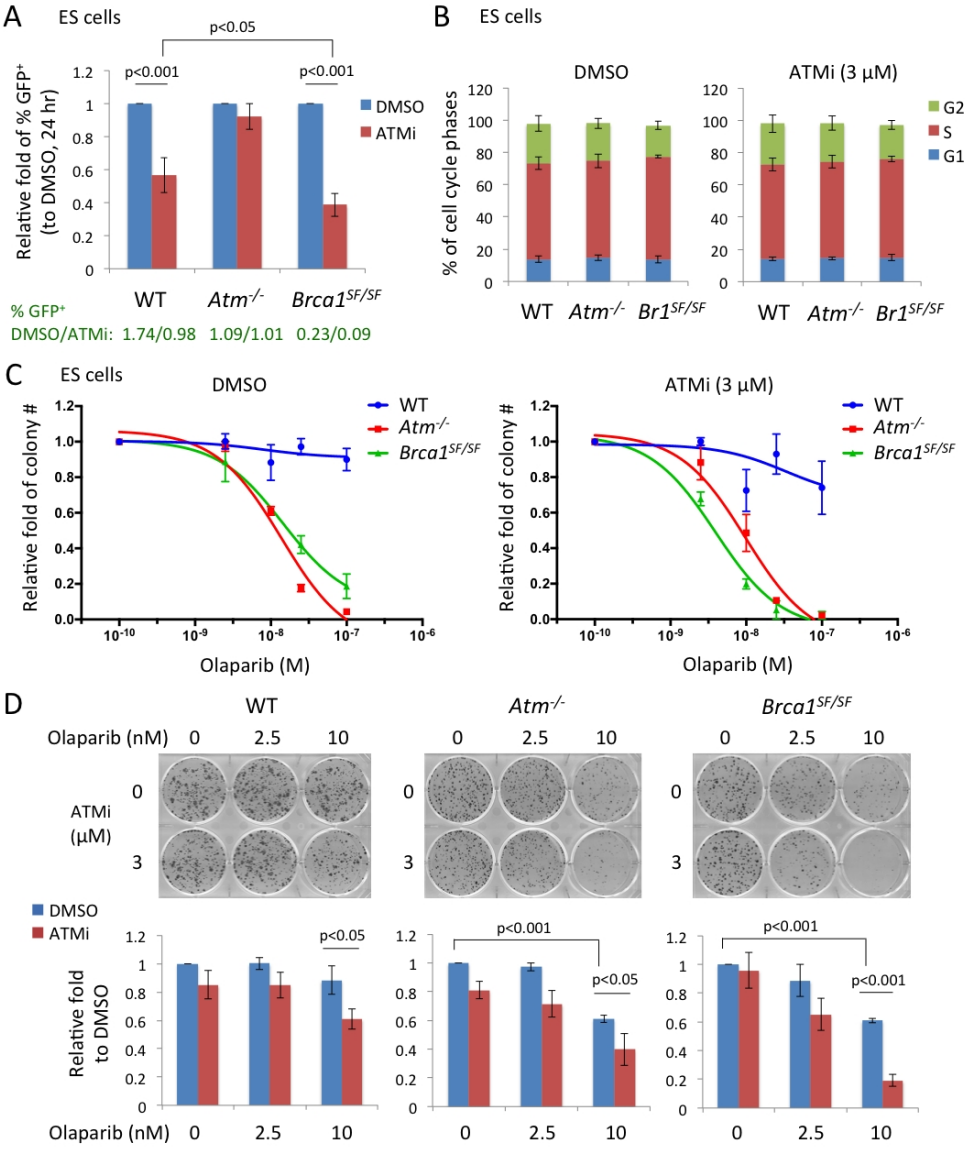

Figure 2.2 ATM inhibition further reduces HDR in *Brca1*$^{SF/SF}$ ES cells.
A. Treatment with ATMi (3 μM, 24 hr) suppresses HDR to a greater extent in *Brca1*$^{SF/SF}$ than in WT ES cells. (n=5)
B. Treatment with ATMi (3 μM, 24 hr) does not significantly affect cell cycle distribution of ES cells. (n=3)
C. ES cells are transiently treated with different doses of olaparib for 2 days with or without continuous ATMi treatment (3 μM). IC_{50} of olaparib treatment (2-day pulse) with/without ATMi: *Atm*$^{-/-}$, 13.8/9.8 nM; *Brca1*$^{SF/SF}$, 14.5/3.9 nM.
D. *Brca1*$^{SF/SF}$ ES cells show a further reduction in colony number upon the combined treatment with olaparib (2-day) and ATMi (continuous). The fold is relative to the colony number of DMSO treatment for each genotype. The colony reduction in ATMi-treated *Atm*$^{-/-}$ cells is likely due to off-target effects of the ATMi. (n=3)

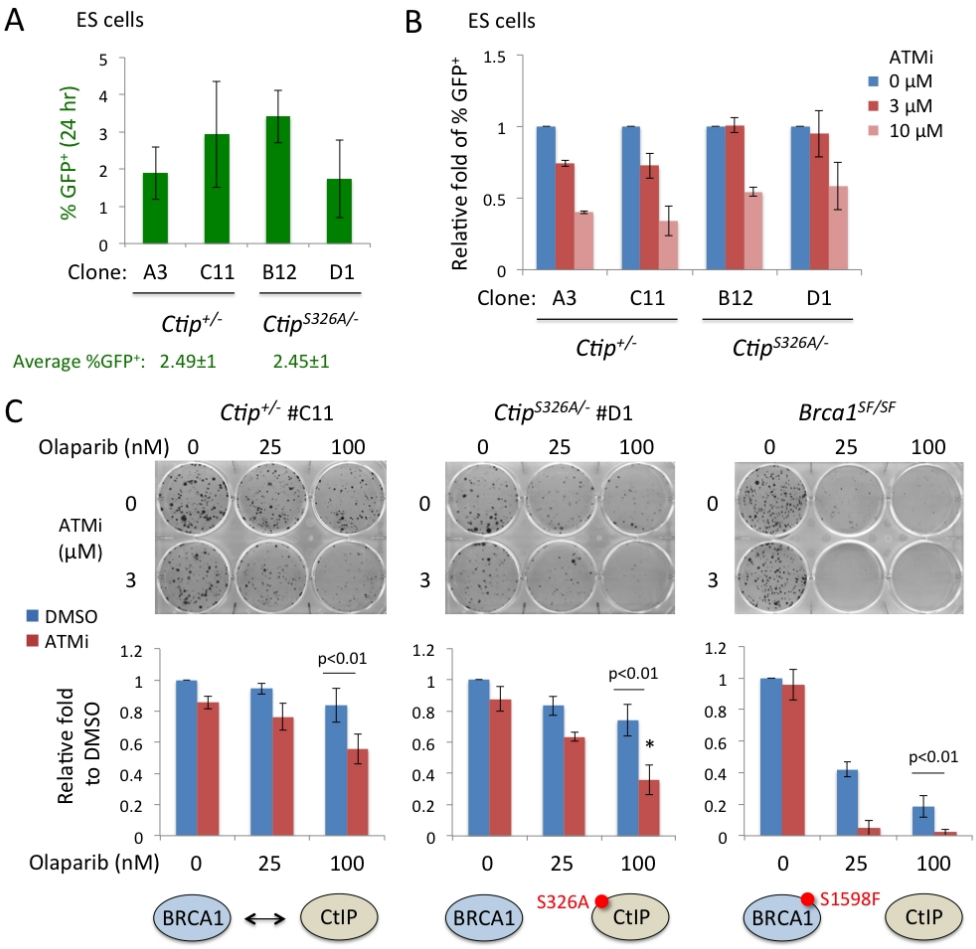

Figure 2.3 HDR in *Ctip*^{S326A} mutant does not recapitulate *Brca1*^{SF} in the response to ATMi.

A. HDR in *Ctip*$^{S326A/-}$ ES cells, which express a mutant CtIP deficient in binding BRCA1, is not significantly different from *Ctip*$^{+/-}$ control cells. Two independent clones are examined for each genotype. (n≥3 for each clone)

B. ATMi treatment in *Ctip*$^{S326A/-}$ ES cells does not reduce HDR to a greater extent than in the *Ctip*$^{+/-}$ cells. (n≥3)

C. ATMi-treated *Ctip*$^{S326A/-}$ ES cells are slightly more sensitive to olaparib compared to *Ctip*$^{+/-}$ cells in colony assay, however the level is not comparable to the hypersensitivity in *Brca1*$^{SF/SF}$ cells. * p<0.05 vs. *Ctip*$^{+/-}$ (n=4)

mouse) mediates its interaction with BRCA1 (35). CtIP phosphorylation at this residue is not essential for end resection but can stimulate the process (9).

We asked whether mouse cells expressing CtIP S326A, which is deficient in binding BRCA1 (8), recapitulate *Brca1*^{SF} mutant phenotypes and have a similar dependence on ATM for HDR. Unlike *Brca1*$^{SF/SF}$ ES cells, *Ctip*$^{S326A/-}$ ES cells showed no significant reduction in HDR, as reported previously (8) (Figure 2.3A), and ATMi treatment reduced HDR in *Ctip*$^{S326A/-}$ cells no more than that in *Ctip*$^{+/-}$ cells (Figure 2.3B). Further, *Ctip*$^{S326A/-}$ cells showed only a mild sensitivity to olaparib compared to *Brca1*$^{SF/SF}$ cells and, while inhibition of ATM in the olaparib-treated *Ctip*$^{S326A/-}$ cells reduced survival more than that in *Ctip*$^{+/-}$ cells, it was not equivalent to the extreme hypersensitivity of the similarly treated *Brca1*$^{SF/SF}$ cells (Figure 2.3C). Thus, disruption of the interaction of CtIP with BRCA1 does not recapitulate the phenotype of *Brca1*$^{SF/SF}$ cells, including the degree of dependence on ATM for HDR. Accordingly, the *Ctip*^{S326A} mutant mice also lack the tumor-prone phenotype observed in the *Brca1*^{SF} mutant mice (8, 31). This suggests that loss of interaction of the BRCT domain with other or additional factors may be responsible for the phenotype of *Brca1*^{SF} mutant.

***Brca1*^{SF} mutation is synthetically lethal with *Atm* nullizygosity.**

Brca1$^{\Delta 11/\Delta 11}$ mice that express the exon 10-12 spliced product of BRCA1 with an intact BRCT domain die during embryogenesis (36), but loss of ATM or CHK2 rescues the embryonic lethality (37). Presumably, unrepaired DNA damage triggers a DNA damage response through ATM-CHK2 that confers a survival disadvantage to *Brca1*$^{\Delta 11/\Delta 11}$ embryos. *Brca1*$^{SF/SF}$ mice show a less penetrant phenotype than *Brca1*$^{\Delta 11/\Delta 11}$ mice: *Brca1*$^{SF/SF}$ mice can be recovered, but they were observed at about half the expected Mendelian frequency at weaning (Figure 2.4A). To determine if the reduced survival of *Brca1*$^{SF/SF}$ mice could be rescued by dampening the DNA damage

A Viable Pups (Total: 463) $Atm^{+/-}Br1^{SF/+}$ x $Atm^{+/-}Br1^{SF/+}$ * 2 dead pups found at birth

Atm	+/+			+/-			-/-		
$Brca1^{SF}$	+/+	SF/+	SF/SF	+/+	SF/+	SF/SF	+/+	SF/+	SF/SF
Observed	33	72	16	63	157	44	31	47	*0
Expected	28.9	57.9	28.9	57.9	115.8	57.9	28.9	57.9	28.9

B Viable Pups (Total: 183) $Chk2^{+/-}Br1^{SF/+}$ x $Chk2^{+/-}Br1^{SF/+}$

Chk2	+/+			+/-			-/-		
$Brca1^{SF}$	+/+	SF/+	SF/SF	+/+	SF/+	SF/SF	+/+	SF/+	SF/SF
Observed	15	28	1	31	51	18	11	22	6
Expected	11.4	22.9	11.4	22.9	45.8	22.9	11.4	22.9	11.4

C E9.5-10.5 (Total: 37) $Atm^{+/-}Br1^{SF/+}$ x $Atm^{+/-}Br1^{SF/+}$

Atm	+/+			+/-			-/-		
$Brca1^{SF}$	+/+	SF/+	SF/SF	+/+	SF/+	SF/SF	+/+	SF/+	SF/SF
Observed	4	3	3	4	10	5	2	5	1
Expected	2.3125	4.625	2.3125	4.625	9.25	4.625	2.3125	4.625	2.3125

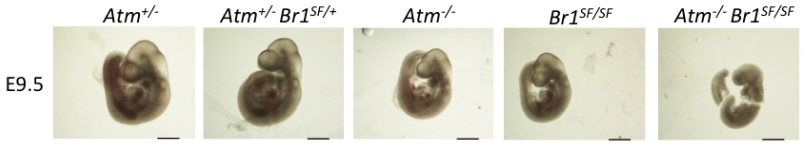

D E12.5-14.5 (Total: 56) $Atm^{+/-}Br1^{SF/+}$ x $Atm^{+/-}Br1^{SF/+}$

Atm	+/+			+/-			-/-		
$Brca1^{SF}$	+/+	SF/+	SF/SF	+/+	SF/+	SF/SF	+/+	SF/+	SF/SF
Observed	3	7	3	9	15	8	2	8	1
Expected	3.5	7	3.5	7	14	7	3.5	7	3.5

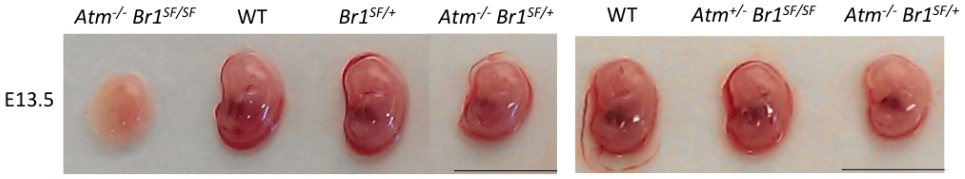

Figure 2.4 *Brca1*^{SF} hypomorphic allele shows synthetic lethality with *Atm* nullizygosity.

A. *Atm* heterozygosity rescues the sub-Mendelian ratio of $Brca1^{SF/SF}$ mice. However, no live $Atm^{-/-}Brca1^{SF/SF}$ double mutant mice are recovered at weaning.

B. Heterozygous and homozygous deletion of *Chk2* partially rescue the sub-Mendelian ratio of $Brca1^{SF/SF}$ mice. This cohort is the F2 generation of intercross with *Chk2* mice that are originally on B6 background, which likely causes the more unfavorable ratio of $Brca1^{SF/SF}$ mutant compared to the cross with *Atm* mice (mixed background).

C. One $Atm^{-/-}Brca1^{SF/SF}$ embryo is found at E9.5. The embryo appears slightly smaller than either $Atm^{-/-}$ or $Brca1^{SF/SF}$ single mutant. Scale bar: 1 mm.

D. One $Atm^{-/-}Brca1^{SF/SF}$ embryo is found at E13.5 that is much smaller than other siblings. The MEFs from this embryo fail to plate in culture while MEFs from all other embryos survive. Scale bar: 1 cm.

response or whether the role for ATM in HDR becomes important in this context, mating was performed to generate *Atm*$^{-/-}$*Brca1*$^{SF/SF}$ and *Chk2*$^{-/-}$*Brca1*$^{SF/SF}$ mice. Heterozygous *Atm* deletion, as well as heterozygous and homozygous deletion of *Chk2,* partially rescued the *Brca1*$^{SF/SF}$ mice (Figure 2.4 A and B), indicating that a DNA damage response reduces the survival of *Brca1*$^{SF/SF}$ mice. However, we did not recover viable *Atm*$^{-/-}$*Brca1*$^{SF/SF}$ double mutants, indicating that ATM is required for the survival of *Brca1*$^{SF/SF}$ mice (Figure 2.4A; see Appendix Figure A.1A for the photograph). These results suggest that the lethality associated with complete loss of ATM is due to another function of ATM such as in DNA repair, specifically HDR.

To approximate at what stage *Atm*$^{-/-}$*Brca1*$^{SF/SF}$ mice die, timed mating was set up to harvest embryos. *Atm*$^{-/-}$*Brca1*$^{SF/SF}$ embryos were underrepresented at mid-embryogenesis, although at both embryonic day E9.5 (Figure 2.4C) and E13.5 (Figure 2.4D) one double mutant was recovered; both embryos appeared smaller than their single mutant littermates. Mouse embryonic fibroblasts (MEFs) derived from the E13.5 embryo failed to proliferate in culture. Overall, our results indicate that *Atm* nullizygous mutation leads to a synthetic, embryonic lethality in the context of the *Brca1*^{SF} missense mutation, in contrast to the rescue of viability observed with the *Brca1*$^{\Delta 11}$ allele. The difference between the two *Brca1* alleles may relate to the BRCT domain, which is intact in the protein expressed from the *Brca1*$^{\Delta 11}$ allele (38).

HDR in *Brca1*^{SF} primary mouse fibroblasts is further reduced by ATM inhibition.

To investigate the mechanism of synthetic lethality, we examined HDR in primary cells derived from mice carrying an integrated DR-GFP reporter, a *CMV-rtTA* transactivator, and a doxycycline (Dox)-inducible transgene of I-SceI endonuclease (*TRE-I-SceI*) that allow for highly efficient DSB formation (27, 39). Primary ear fibroblasts from the *Brca1*$^{SF/SF}$ and *Atm*$^{-/-}$ mice showed 3- and 2-fold reductions in

HDR, respectively (Figure 2.5 A and B, left panels). To take into account animal variation in I-SceI expression, the percent GFP^+ cells was normalized to total DSB repair events using a site-loss assay (Figure 2.5C), which provided an estimate on the fraction of HDR among total repair events, i.e., % HDR (in graphs showing DR-GFP assays in Chapter 2 and 3, green and gray bars represent % GFP^+ and % HDR, respectively). The site-loss assay helped confirm the fold of reduction in HDR in these mutants (Figure 2.5 A and B, right panels). The HDR defect observed in *Atm* mutant fibroblasts was interesting, given that the influence of ATM loss on HDR varies between reports. The percentage of site loss for WT and $Atm^{-/-}$ ear fibroblasts was similar (44% for each), indicating that total repair efficiency was similar for both genotypes (Figure 2.5B, right panel). Thus, the fraction of HDR among total repair events was 25% for WT and 12% for $Atm^{-/-}$ ear fibroblasts, confirming that loss of ATM reduces HDR by 2-fold in this assay, whereas the rest of the repair events in $Atm^{-/-}$ cells were likely compensated by NHEJ. Unlike the delay of HDR seen in $Atm^{-/-}$ ES cells, a similar reduction in HDR in $Atm^{-/-}$ compared with control ear fibroblasts was observed at all time points following DSB induction (from 24 to 96 hr; other primary cell experiments were typically analyzed at 48 hr), suggesting persistent HDR defect (Figure 2.5D). Other somatic cell types from $Atm^{-/-}$ mice, e.g., splenic B cells (Figure 2.5E) and mammary epithelial cells (Figure 2.5F), showed similarly impaired HDR, as did a distinct *Atm* mutant (30) (Figure 2.5G; ear fibroblasts and mammary cells in upper and lower panels, respectively). Thus, loss of ATM causes a defect in HDR in mouse primary adult somatic cells, as measured by the DR-GFP reporter assay, although not to the same extent as with the hypomorphic $Brca1^{SF}$ allele (Figure 2.5 A and H). Although heterozygous mutations of *BRCA1* or *ATM* are associated to breast cancer risks in carries, heterozygosity of $Brca1^{SF}$ or *Atm* in mice did not

Figure 2.5 Primary somatic cells from *Brca1*^{SF} and *Atm* mutant mice show defects in HDR.

A. Examining HDR in primary cells using the inducible I-SceI/DR-GFP system. Primary ear fibroblasts from *Brca1*$^{SF/SF}$ mice have a ~3-fold reduction in HDR compared to WT cells either by analyzing % GFP$^+$ alone or by normalizing % GFP$^+$ to % I-SceI site loss (i.e., % HDR, the fraction of HDR in overall repair; see Figure 2.5C below). *I-SceI*$^{S/S}$: these mice are homozygous for the *TRE-I-SceI* allele when indicated. (n≥9)

B. Primary ear fibroblasts from *Atm*$^{-/-}$ mice have a 2-fold reduction in HDR. (n≥10)

C. To determine DSB efficiency in the DR-GFP reporter, the sequence flanking the DSB site in the *SceGFP* is amplified by primers, followed by *in vitro* digestion with I-SceI endonuclease. Repair by either HDR or imprecise NHEJ results in loss of the I-SceI site, which leaves an intact 0.9-kb product (right gel) in comparison to the digested 0.7- and 0.2-kb bands. This primer set does not amplify SSA or unrepaired events. The % site loss is calculated by dividing the intensity of 0.9-kb band with the sum of 0.9-kb plus 0.7-kb (* accounted for size difference) band. The % HDR, which normalizes % GFP$^+$ with % site loss, represents the ratio of HDR among total repair events. Dox: doxycycline.

D. Time course of Dox treatment shows that *Atm*$^{-/-}$ fibroblasts consistently have lower HDR than control cells (*Atm*$^{+/-}$ or WT). Cells are exposed to Dox continuously for 24, 48, or 72 hours or for a 48-hour pulse followed by 48-hour recovery to allow time for repair. (n≥3 for all time points except n=1 for 72h)

E. Primary splenic B cells from *Atm*$^{-/-}$ mice have a 2-fold reduction in HDR compared to WT cells (left). The % GFP$^+$ is measured from the purified B220$^+$ B cells stimulated with LPS and IL4 together with Dox for 5 days. The low dose of Dox (0.25 μg/ml) used here does not affect class switching per se, which is 3-fold lower in *Atm*$^{-/-}$ than WT B cells (right). (n=3)

F. Primary mammary epithelial cells harvested from *Atm*$^{-/-}$ mice have a ~2-fold reduction in HDR. Mammary gland from a 12-week-old *Atm*$^{-/-}$ mouse shows relatively normal elongation of ductal trees that fill the fat pad, albeit with less secondary branching compared to the littermate control (right panel). (n≥4)

G. All the *Atm* experiments in the paper are performed with the *Atm*^{b} mutant allele with the exons encoding the kinase domain deleted (29). For comparison, another strain of *Atm* mutant mice (*Atm*^{w} allele) is examined, which contains an exon deletion upstream of the kinase domain (30). Both *Atm* mutant alleles do not produce detectable ATM protein in fibroblasts (27). Primary ear fibroblasts and mammary cells harvested from the *Atm*^{w} mutant mice show a similar 2-fold reduction in HDR as the *Atm*^{b} allele. (n≥3)

H. Primary mammary epithelial cells from *Brca1*$^{SF/SF}$ mutant mice have a ~3-fold reduction in % HDR. (n≥3)

Figure 2.5

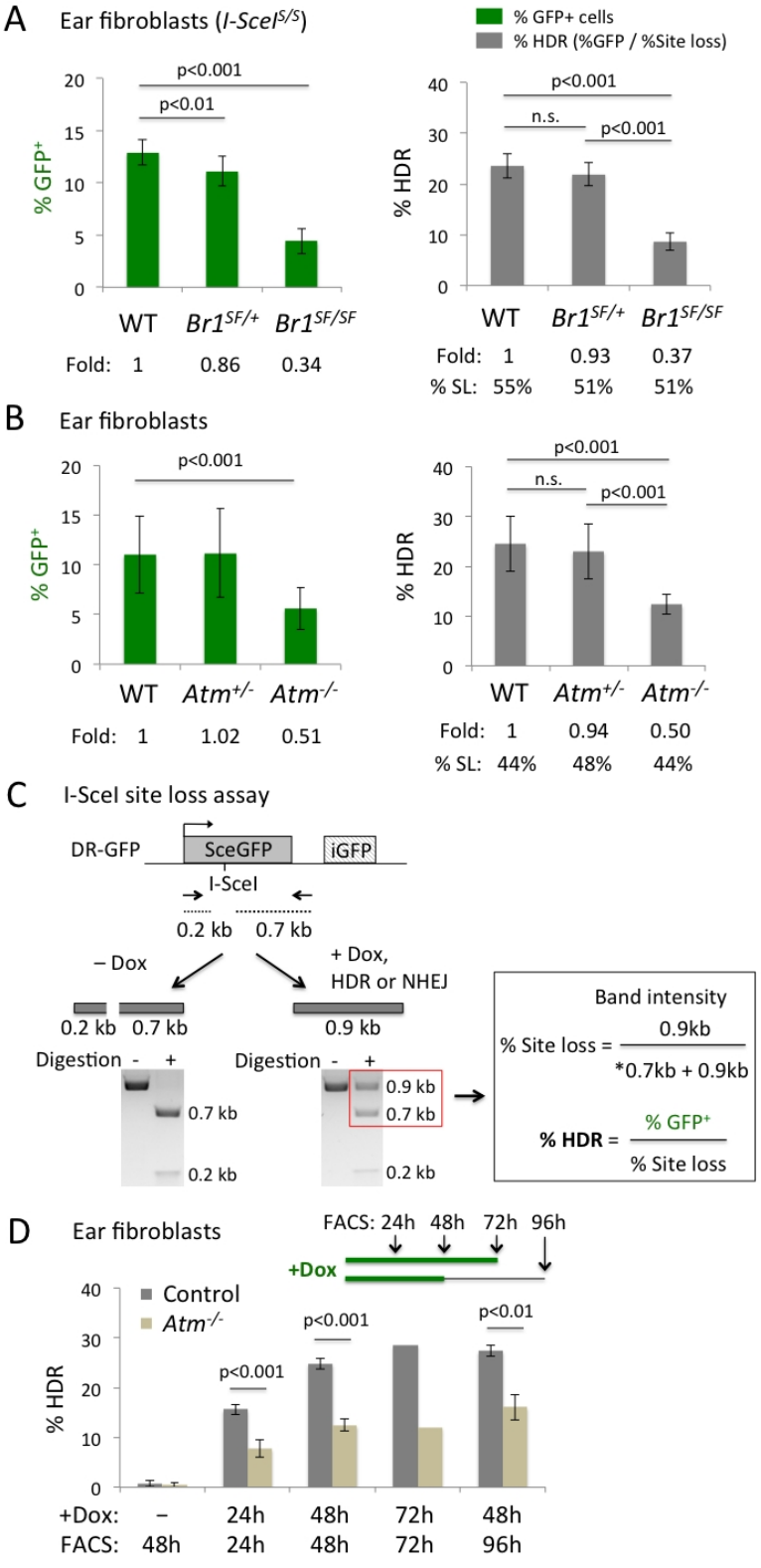
A
Ear fibroblasts (I-SceI^S/S)
% GFP+ cells
% HDR (%GFP / %Site loss)
% GFP+
% HDR
p<0.001
p<0.01
n.s.
WT
Br1^SF/+
Br1^SF/SF
Fold: 1 0.86 0.34
Fold: 1 0.93 0.37
% SL: 55% 51% 51%
B
Ear fibroblasts
Atm+/-
Atm-/-
Fold: 1 1.02 0.51
Fold: 1 0.94 0.50
% SL: 44% 48% 44%
C
I-SceI site loss assay
DR-GFP
SceGFP
iGFP
I-SceI
0.2 kb
0.7 kb
– Dox
+ Dox,
HDR or NHEJ
0.9 kb
Digestion - +
Band intensity
% Site loss = 0.9kb / *0.7kb + 0.9kb
% HDR = % GFP+ / % Site loss
D
Ear fibroblasts
FACS: 24h 48h 72h 96h
+Dox
Control
Atm-/-
+Dox: – 24h 48h 72h 48h
FACS: 48h 24h 48h 72h 96h

Figure 2.5 (Continued)

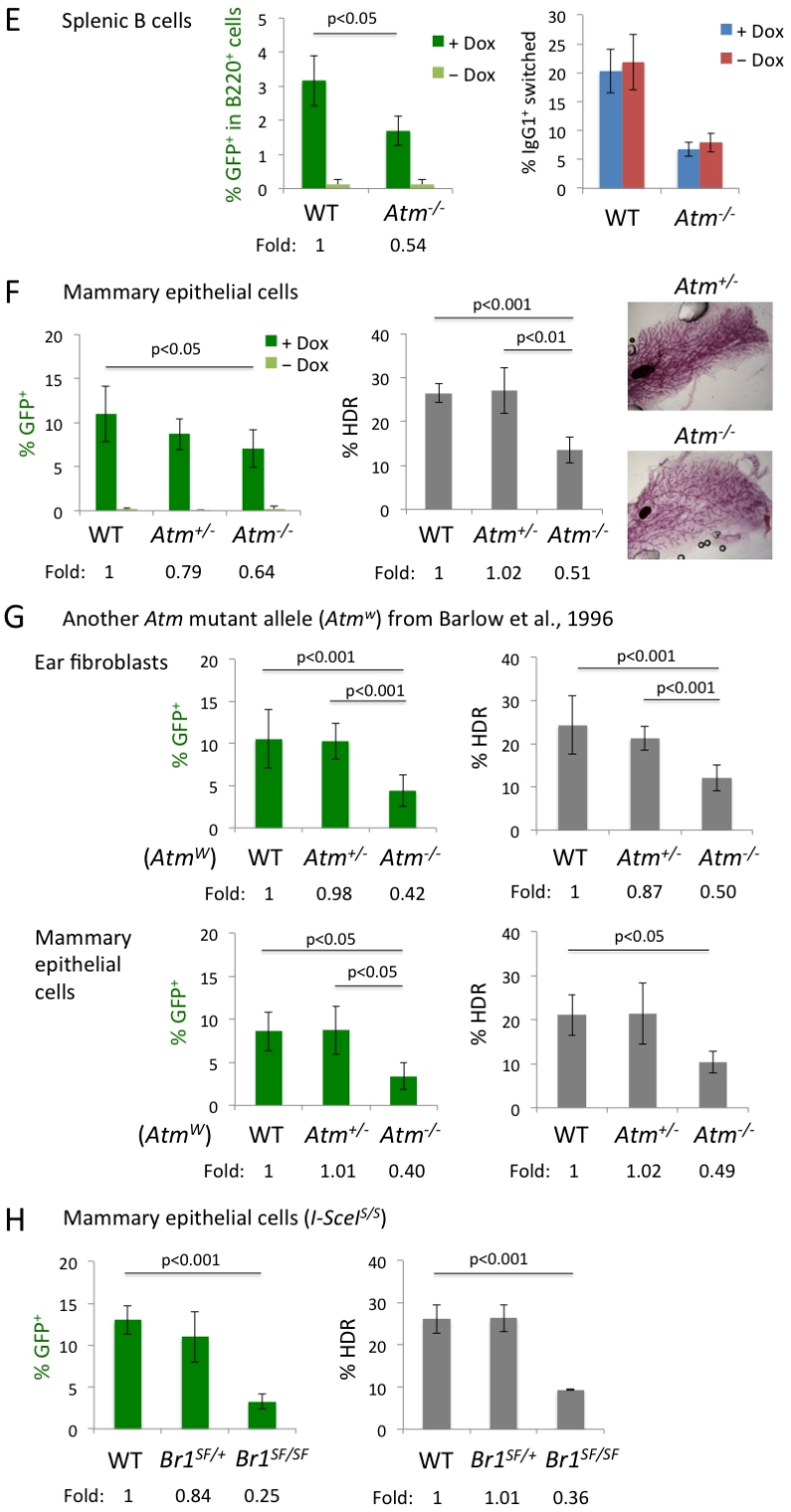

significantly affect HDR in either fibroblasts or mammary cells (Figure 2.5 A and B, see % HDR for normalized results).

Although ATM deficiency by itself caused only a 2-fold HDR defect (Figure 2.5B) and ATMi-treated WT cells showed a mild 1.6-fold HDR reduction (Figure 2.6A), ATM inhibition in *Brca1*$^{SF/SF}$ ear fibroblasts greatly exacerbated their HDR defect, such that the overall reduction of HDR relative to DMSO-treated WT cells was 14-fold (Figure 2.6A, % GFP^{+} 0.8 vs. 11.2). The large HDR reduction in ATMi-treated *Brca1*$^{SF/SF}$ cells was not related to changes in cell cycle distribution (Figure 2.6B). At the dose of 3 μM used, ATMi generally caused a 1.2-fold reduction in HDR in *Atm*$^{-/-}$ primary fibroblasts but this was still significantly less than the 1.6-fold reduction in WT cells (Figure 2.6A), which could be attributed to the off-target effects of the ATMi. Treatment with a CHK2 inhibitor slightly reduced HDR in the *Brca1*$^{SF/SF}$ ear fibroblasts, but the extent was not significantly different from that in WT or *Atm*$^{-/-}$ cells (Figure 2.6C), consistent with the notion that the reliance on ATM in the *Brca1*^{SF} mutant is related to its role in DNA repair.

We performed a similar analysis in MEFs. In untreated *Brca1*$^{SF/SF}$ MEFs, the reduction in HDR was larger than in ear fibroblasts, but was similar to ES cells (~8-fold; Figure 2.6D), suggesting that BRCA1 has a more pronounced role in HDR in embryonic cells than adult cells. Conversely, HDR was reduced to a somewhat lesser extent in *Atm*$^{-/-}$ MEFs (Figure 2.6D) and ATMi-treated WT MEFs (Figure 2.6E), indicating a less critical role for ATM in embryonic cells (see Appendix Figure A.1B for olaparib sensitivity in MEFs). This differential dependence of BRCA1 and ATM in adult cells versus embryonic cells is also confirmed by normalizing HDR with the site-loss assay. However, as with the ear fibroblasts, the HDR defect in *Brca1*$^{SF/SF}$ MEFs was further exacerbated by ATMi treatment, such that the overall reduction in

Figure 2.6 ATM inhibition exacerbates HDR defect in *Brca1*$^{SF/SF}$ primary cells.
A. ATMi treatment (3 μM) reduces HDR in *Brca1*$^{SF/SF}$ ear fibroblasts to a greater extent than in WT cells. (n≥3)
B. Cell cycle profiles show no significant difference between WT and *Brca1*$^{SF/SF}$ primary ear fibroblasts following ATMi treatment. Note that these cells are from +Dox 48 hr treatment and thus have higher G1 ratio than the profiles in Figure 2.10C. (n=2)
C. Inhibition of CHK2 slightly reduces HDR in *Brca1*$^{SF/SF}$ ear fibroblasts, but the extent is not significantly different from that of WT or *Atm*$^{-/-}$ cells. * *Brca1*$^{SF/SF}$: *Atm*$^{+/+}$ or *Atm*$^{+/-}$ (n=3 for WT and *Brca1*$^{SF/SF}$, n=2 for *Atm*$^{-/-}$)
D. *Brca1*$^{SF/SF}$ primary MEFs show a substantial reduction in HDR (~8-fold for % GFP^{+}; 6-fold for % HDR) compared to WT MEFs, whereas the reduction in *Atm*$^{-/-}$ MEFs is less profound (~1.5-fold). (n≥3 except n=2 for *Brca1*$^{SF/SF}$)
E. ATMi treatment (3 μM) reduces HDR in *Brca1*$^{SF/SF}$ MEFs to a greater extent than in WT MEFs. Similar to ATM loss, ATMi also shows less effect in suppressing HDR in WT MEFs compared to WT ear fibroblasts. (n≥3 except n=2 for *Atm*$^{-/-}$)

Figure 2.6

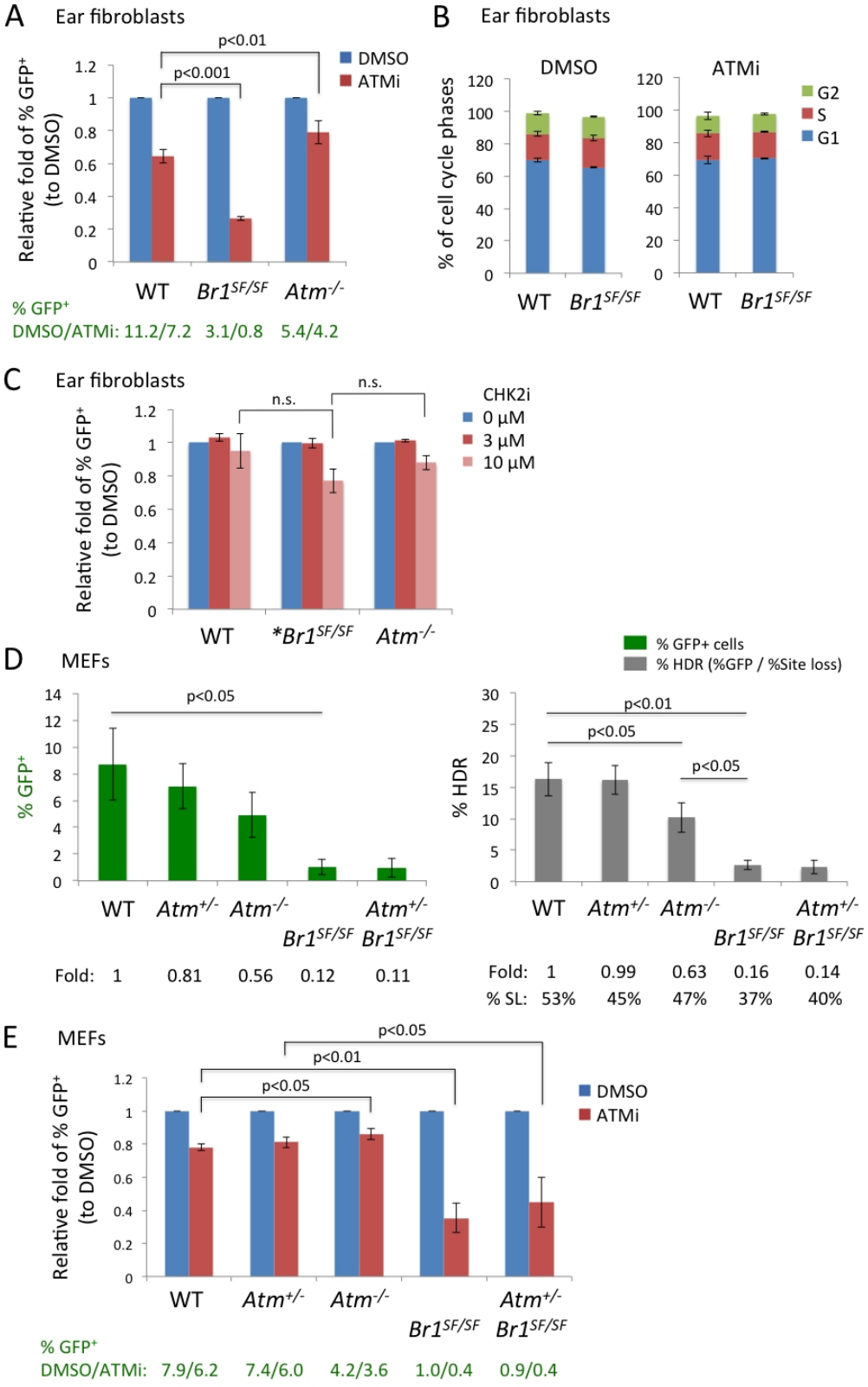
A
Ear fibroblasts
p<0.01
p<0.001
DMSO
ATMi
Relative fold of % GFP+ (to DMSO)
WT
Br1SF/SF
Atm-/-
% GFP+
DMSO/ATMi: 11.2/7.2 3.1/0.8 5.4/4.2
B
Ear fibroblasts
DMSO
ATMi
% of cell cycle phases
G2
S
G1
C
Ear fibroblasts
n.s.
n.s.
CHK2i
0 µM
3 µM
10 µM
Relative fold of % GFP+ (to DMSO)
WT
*Br1SF/SF
Atm-/-
D
MEFs
% GFP+ cells
% HDR (%GFP / %Site loss)
p<0.05
% GFP+
p<0.01
p<0.05
p<0.05
% HDR
WT
Atm+/-
Atm-/-
Br1SF/SF
Atm+/- Br1SF/SF
Fold: 1 0.81 0.56 0.12 0.11
Fold: 1 0.99 0.63 0.16 0.14
% SL: 53% 45% 47% 37% 40%
E
MEFs
p<0.05
p<0.01
p<0.05
DMSO
ATMi
Relative fold of % GFP+ (to DMSO)
WT
Atm+/-
Atm-/-
Br1SF/SF
Atm+/- Br1SF/SF
% GFP+
DMSO/ATMi: 7.9/6.2 7.4/6.0 4.2/3.6 1.0/0.4 0.9/0.4

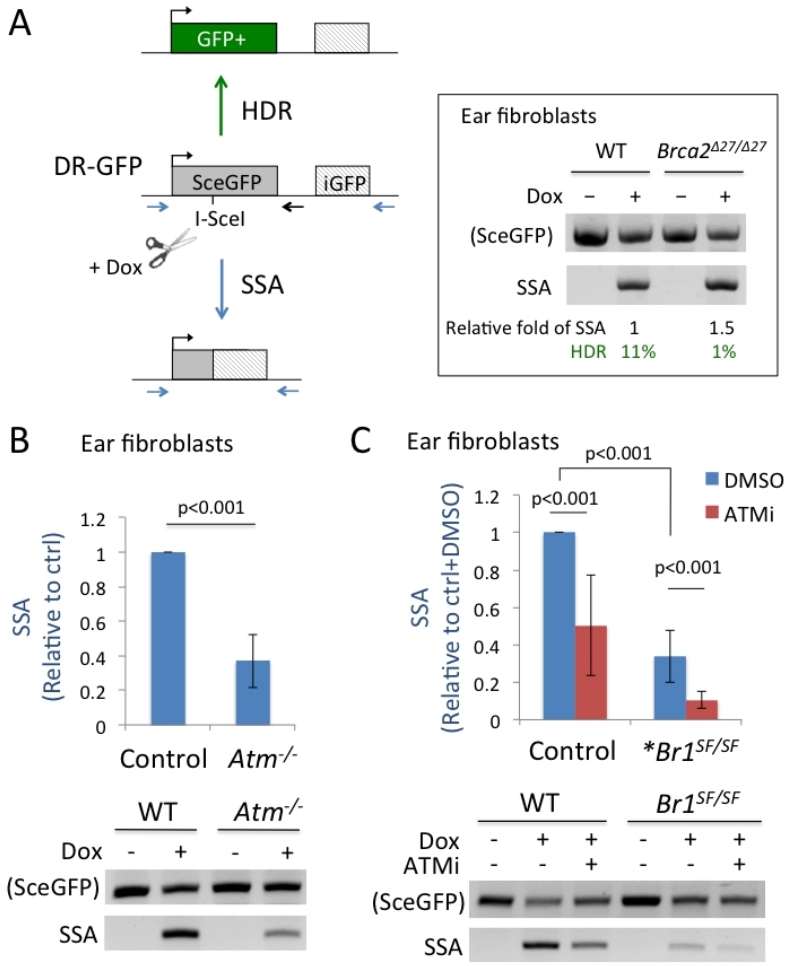

Figure 2.7 ATM inhibition exacerbates SSA defect in *Brca1*$^{SF/SF}$ primary cells.
A. Treatment with Dox induces I-SceI endonuclease, which introduces a DSB in the DR-GFP reporter that if repaired by HDR restores GFP expression. The DSB can also be repaired via SSA if resection exposes complementary strands in both *SceGFP* and *iGFP* which then anneal to give rise to a shortened reporter product. SSA events are detected using a specific primer set (blue forward/reverse) and the intensity is normalized to the structurally intact reporter using primers flanking *SceGFP* (blue forward, black reverse), followed by comparison between control and mutants. A positive control of this assay is depicted in the box showing that *Brca2*$^{\Delta 27/\Delta 27}$ primary fibroblasts have severely reduced HDR but increased SSA (40).
B. The relative levels of SSA are reduced by ~2.5 fold in *Atm*$^{-/-}$ ear fibroblasts compared to control cells (WT or *Atm*$^{+/-}$). The SSA product is observed only when I-SceI is induced by Dox. Relative fold is calculated between control and mutant cells on the same gel. (n=7)
C. The relative levels of SSA in *Brca1*$^{SF/SF}$ ear fibroblasts are ~3-fold lower than in control cells, and ATMi treatment further reduces SSA in *Brca1*$^{SF/SF}$ cells.
**Brca1*$^{SF/SF}$: *Atm*$^{+/+}$ or *Atm*$^{+/-}$ (n=8)

HDR was 20-fold compared to WT cells (Figure 2.6E, % GFP^+ 0.4 vs. 7.9). Overall, these results demonstrate that ATM is critical for much of the residual HDR in the *Brca1*$^{SF/SF}$ cells, potentially accounting for the synthetic lethality observed in double mutant mice.

ATM kinase inhibition further reduces SSA in *Brca1*^{SF} mutant cells.

Evidence suggests that both BRCA1 and ATM promote DNA end resection (6, 20, 40). End resection is a common step for HDR and another homology-based DSB repair pathway, single-strand annealing (SSA), in which complementary single strands generated by resection at sequence repeats anneal, resulting in a deletion of the sequence between the repeats; thus, a defect in end resection compromises both pathways (40). By contrast, defects in downstream steps of HDR such as RAD51 filament formation increase SSA. Using a PCR-based assay with the DR-GFP reporter to quantify SSA (41) (Figure 2.7A), we found that loss or inhibition of ATM reduced SSA by 2 to 2.5 fold in ear fibroblasts (Figure 2.7 B and C), as reported previously for mouse ES cells (42). The decreased levels of SSA are comparable to our HDR results and are consistent with a role for ATM in the end resection step of DSB repair.

As with HDR, *Brca1*$^{SF/SF}$ cells showed a 3-fold reduction in SSA (Figure 2.7C), similar to cells carrying the cognate human BRCA1 mutation (43). Notably, ATM inhibition further decreased SSA in *Brca1*$^{SF/SF}$ cells for an overall 10-fold reduction compared to DMSO-treated control cells, indicating that both end resection-dependent DSB repair pathways, HDR and SSA, rely heavily on ATM in *Brca1*^{SF} mutant cells.

***53bp1* deletion does not restore HDR in ATM-deficient cells.**

The NHEJ protein 53BP1 suppresses DNA end resection, such that loss of 53BP1 significantly restores HDR in BRCA1-deficient cells (5, 6). Thus, we hypothesized that loss of 53BP1 would rescue the survival of *Atm-Brca1*^{SF} double mutant animals.

As predicted, viable *Atm*$^{-/-}$*Brca1*$^{SF/SF}$*53bp1*$^{-/-}$ mice were recovered (Figure 2.8A; see Appendix Figure A.1C for survival analysis of the *Atm-Brca1*^{SF}*-53bp1* mutant mice). Interestingly, *53bp1* heterozygosity also led to a rescue of *Atm*$^{-/-}$*Brca1*$^{SF/SF}$ animals, although partial. In *Brca1*$^{SF/SF}$ ear fibroblasts (Figure 2.8B) and mammary epithelial cells (Figure 2.8C), homozygous deletion of *53bp1* fully rescued the HDR defect (Figure 2.8 B and C), indicating that the functions of BRCT domain are involved in counteracting 53BP1 (44-46). Interestingly, in both cell types, heterozygosity for the *53bp1* mutation also led to a moderate increase in HDR (~50%) (Figure 2.8 B and D). This may be in part related to the reduced levels of 53BP1 protein in the *53bp1* heterozygous cells (Figure 2.8E). Thus, even partial loss of 53BP1 protein increases HDR in the *Brca1*^{SF} mutant setting.

We investigated whether *53bp1* mutation would also rescue HDR defects in *Atm* mutant cells as it does in *Brca1* mutant cells. Importantly, *Atm*$^{-/-}$*53bp1*$^{-/-}$ ear fibroblasts showed the same ~2-fold decrease in HDR as *Atm*$^{-/-}$ cells (Figure 2.9A). The lack of rescue of the HDR defect in *Atm* mutant cells by *53bp1* loss indicates that ATM operates separately from the BRCA1-53BP1 antagonism in HDR. Consistent with this interpretation, HDR was ~2-fold lower in *Atm*$^{-/-}$*Brca1*$^{SF/SF}$*53bp1*$^{-/-}$ ear fibroblasts compared with *Brca1*$^{SF/SF}$*53bp1*$^{-/-}$ cells (Figure 2.9B), which is analogous to the HDR response following ATM loss in WT cells (Figure 2.9A). This indicates that *53bp1* loss specifically rescues the HDR defect caused by the *Brca1*^{SF} mutation but not that of the *Atm* mutation.

We also analyzed HDR in *Brca1*$^{SF/SF}$*53bp1*$^{-/-}$ ear fibroblasts treated with the ATMi. HDR was significantly restored in *Brca1*$^{SF/SF}$*53bp1*$^{-/-}$ cells compared to *Brca1*$^{SF/SF}$ cells, but treatment with ATMi still reduced it by ~30%, similar to the fold reduction in WT cells (Figure 2.9C). HDR in *53bp1*$^{-/-}$ cells was also reduced by ATMi

A Viable pups (Total: 512) $Atm^{+/-}Br1^{SF/+}53bp1^{+/-}$ x $Atm^{+/-}Br1^{SF/+}53bp1^{+/-}$

$Brca1^{SF}$	SF/SF									Others
53bp1	+/+			+/-			-/-			
Atm	+/+	+/-	-/-	+/+	+/-	-/-	+/+	+/-	-/-	
Observed	6	9	0	12	36	3	7	18	5	416
Expected	8	16	8	16	32	16	8	16	8	384

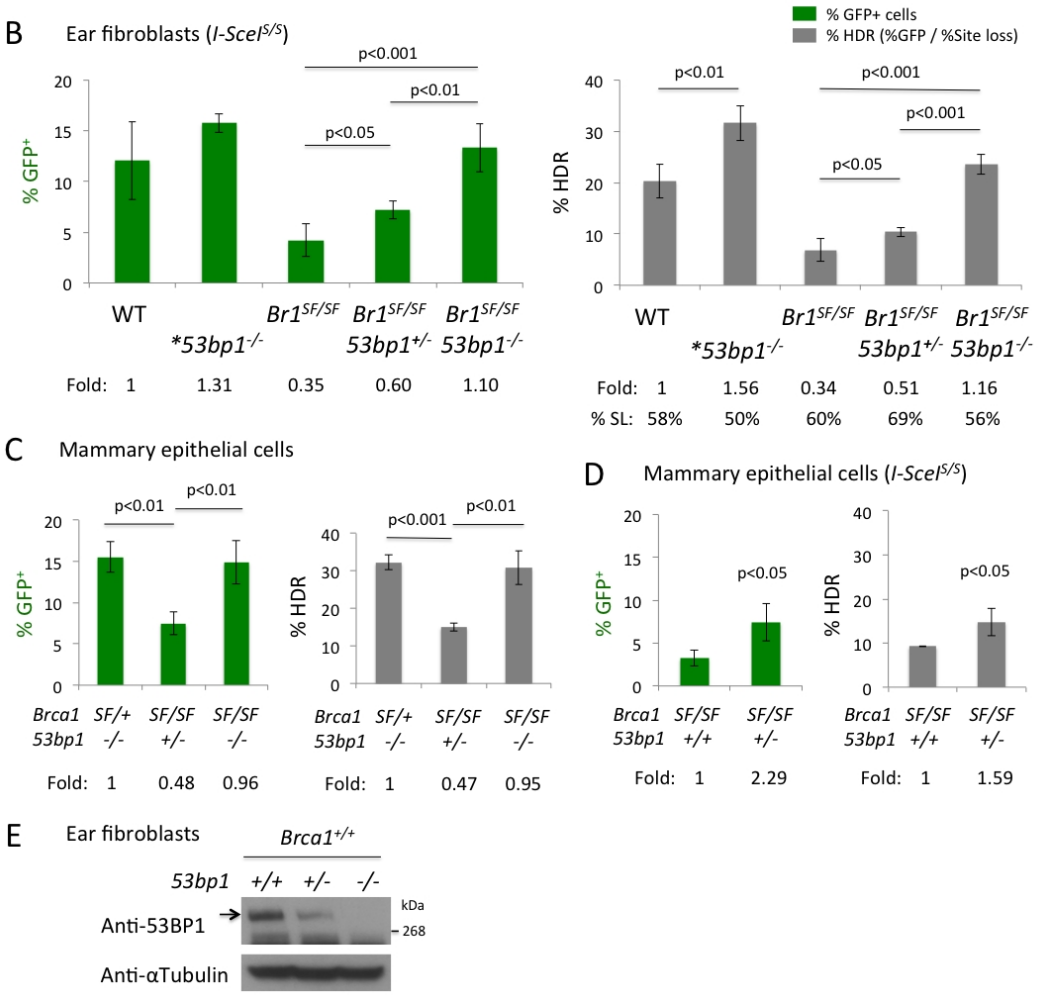

Figure 2.8 HDR defect in $Brca1^{SF/SF}$ primary cells is rescued by loss of 53BP1.
A. Heterozygous and homozygous deletion of *53bp1* rescue the viability of $Atm^{-/-}$ $Brca1^{SF/SF}$ double mutant mice.
B. Homozygous deletion of *53bp1* fully restores the levels of HDR in $Brca1^{SF/SF}$ ear fibroblasts. Heterozygous deletion of *53bp1* in $Brca1^{SF/SF}$ fibroblasts also increases HDR by ~1.5-fold. $*53bp1^{-/-}$: $Brca1^{+/+}$ or $Brca1^{SF/+}$ (n≥3 except n=2 for $53bp1^{-/-}$)
C. Homozygous deletion of *53bp1* restores HDR in $Brca1^{SF/SF}$ mammary cells. (n≥3)
D. Heterozygous deletion of *53bp1* significantly increases HDR in $Brca1^{SF/SF}$ mammary epithelial cells by ~1.6-fold. (n≥3)
E. The level of 53BP1 protein is partially reduced in $53bp1^{+/-}$ compared to $53bp1^{+/+}$ primary ear fibroblasts.

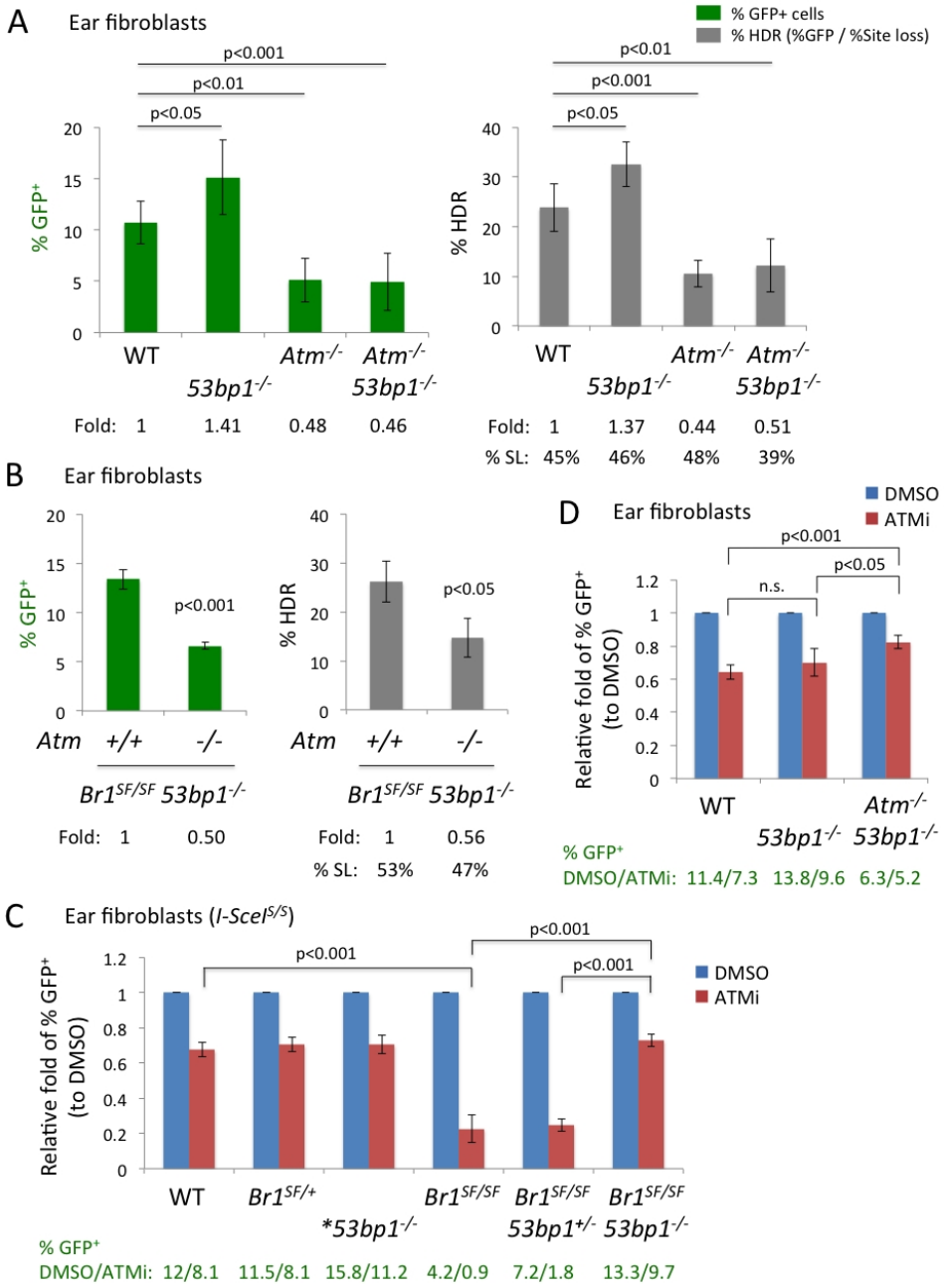

Figure 2.9 ATM promotes HDR independently of the BRCA1-53BP1 antagonism.
A. 53BP1 loss does not restore the 2-fold HDR defect in *Atm*$^{-/-}$ ear fibroblasts. (n≥4)
B. Loss of *Atm* in *Brca1*$^{SF/SF}$*53bp1*$^{-/-}$ ear fibroblasts still reduces HDR by ~2-fold. (n=5 for double mutant, n=2 for triple mutant)
C. Unlike in *Brca1*$^{SF/SF}$ ear fibroblasts, ATMi treatment (3 μM) reduces HDR in *Brca1*$^{SF/SF}$*53bp1*$^{-/-}$ cells to a similar extent as in WT or *53bp1*$^{-/-}$ cells. (n≥3 except n=2 for *53bp1*$^{-/-}$)
D. ATMi treatment reduces HDR in *53bp1*$^{-/-}$ ear fibroblasts to a similar extent as in WT cells. (n≥5)

to a similar extent as in WT cells (Figure 2.9D). Thus, 53BP1 loss does not rescue the HDR defect caused by either ATM loss or inhibition.

Although sensitive to ATM inhibition, the level of HDR in the *Brca1*$^{SF/SF}$*53bp1*$^{+/-}$ cells was still higher than in the *Brca1*$^{SF/SF}$ cells upon ATMi treatment (Figure 2.9C, with ATMi, % GFP^{+} 1.8 vs. 0.9), indicating that *53bp1* heterozygosity is effective in partially restoring HDR in the presence of ATMi. Thus, it seems plausible that HDR in *Atm*$^{-/-}$*Brca1*$^{SF/SF}$*53bp1*$^{+/-}$ mice may be restored above a threshold level that permits their survival (Figure 2.8A).

ATM supports HDR and SSA independently of the BRCA1-53BP1 antagonism. To further examine the interaction of the *Atm*, *Brca1*^{SF}, and *53bp1* mutations in HDR, we examined DNA damage-induced RAD51 and RPA foci in primary ear fibroblasts (Figure 2.10 A and B). As seen previously in other cell types, both *Atm*$^{-/-}$ and *Brca1*$^{SF/SF}$ fibroblasts showed a significant decrease compared to WT in the percentage of cells positive for RAD51 and RPA foci following ionizing radiation (IR) (~25% and ~40% reduction, respectively) (17, 18, 20, 31), whereas *53bp1*$^{-/-}$ cells showed a small increase (~10%). In *Brca1*$^{SF/SF}$*53bp1*$^{-/-}$ cells, RAD51 and RPA focus formation was significantly rescued compared to *Brca1*$^{SF/SF}$ cells, approaching that of WT cells (Figure 2.10 A and B; compare column a, c, and f). No significant changes in cell cycle distribution were observed in any of the genotypes at the time point of immunofluorescence staining (2 hours after IR; Figure 2.10C).

Consistent with the lack of rescue of HDR by 53BP1 loss (Figure 2.9A), the number of RAD51 and RPA foci-positive *Atm*$^{-/-}$*53bp1*$^{-/-}$ cells remained lower than WT cells (Figure 2.10 A and B; column a and e). Interestingly, however, a small increase was noted for the *Atm*$^{-/-}$*53bp1*$^{-/-}$ compared to *Atm*$^{-/-}$ cells, although this did not reach statistical significance (Figure 2.10 A and B; column b and e). It is possible that more recombination complexes are able to form with loss of 53BP1 that are not proficient at

Figure 2.10 Nuclear foci analysis confirms the epistasis of *Atm-Brca1^{SF}-53bp1* in resection and HDR.
A & B. Loss of *Atm* in *Brca1$^{SF/SF}$53bp1$^{-/-}$* primary ear fibroblasts still reduces % RAD51^{+} (A) and % RPA^{+} (B) cells following IR (column f versus h), supporting an independent role of ATM in resection and HDR. Although *53bp1$^{+/-}$* rescues the *Atm$^{-/-}$ Brca1$^{SF/SF}$* animal viability, fibroblasts derived from the animal have the lowest levels of RAD51 and RPA foci formation among all the mutants (column g, note the limited difference between IR+ and IR−), suggesting a severe repair defect in the *Atm-Brca1^{SF}* double mutant. Primary ear fibroblasts are plated overnight, treated with or without 10 Gy IR, and allowed for recovery for 2 hr before immunostaining. The analysis is performed with at least three animals for IR+ samples, each with ~200 total cells counted. For IR− samples, at least two animals are analyzed, except just one for RPA foci in triple mutant.
C. Cell cycle profiles show no apparent difference between WT and mutant fibroblasts 2 hr after 10 Gy IR (i.e., the same condition for staining of DNA damage foci).

Figure 2.10

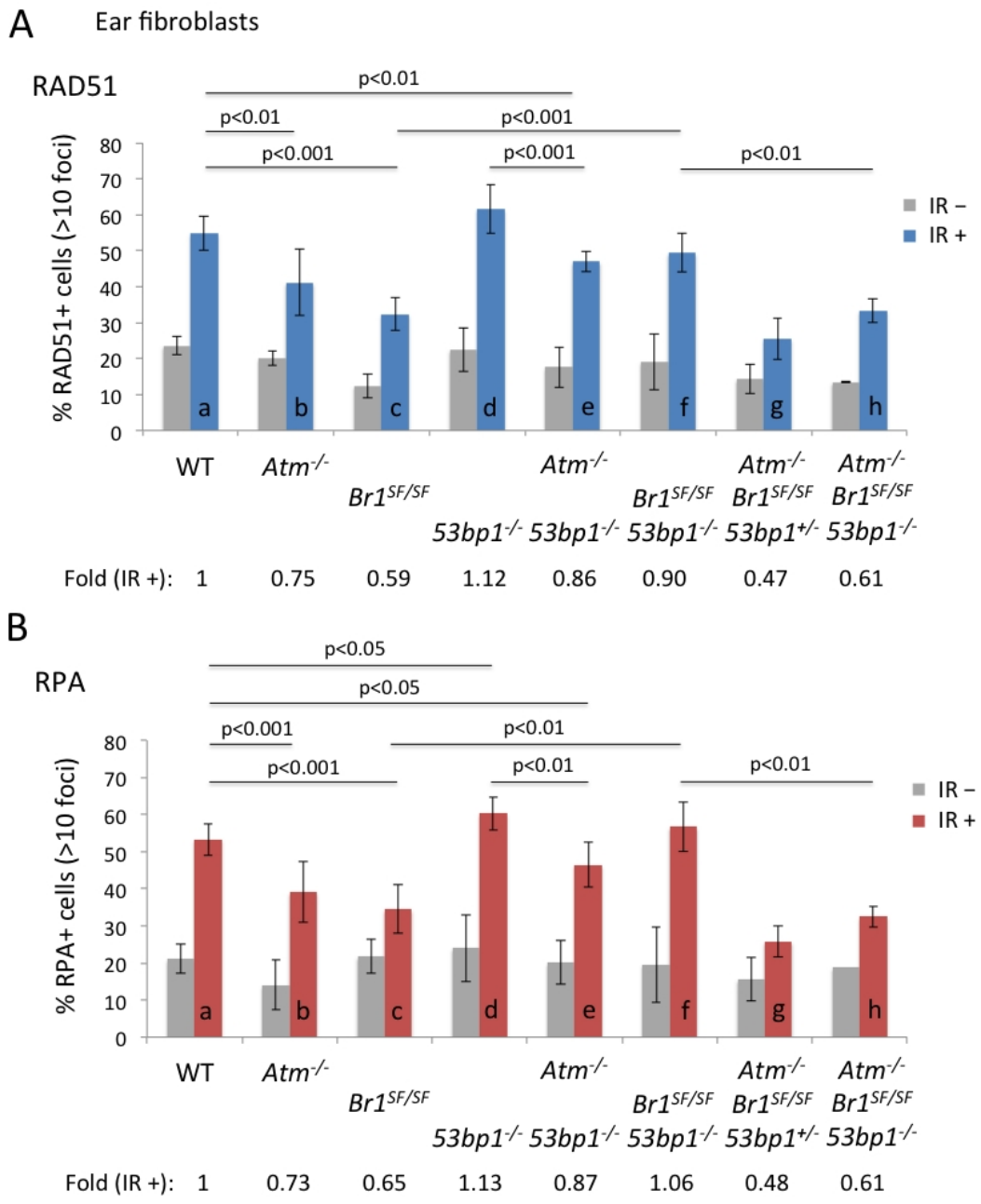
A
Ear fibroblasts
RAD51
p<0.01
p<0.01
p<0.001
p<0.001
p<0.001
p<0.01
% RAD51+ cells (>10 foci)
IR –
IR +
a
b
c
d
e
f
g
h
WT
Atm-/-
Br1SF/SF
Atm-/-
53bp1-/-
Br1SF/SF
53bp1-/-
Atm-/-
Br1SF/SF
53bp1+/-
Atm-/-
Br1SF/SF
53bp1-/-
Fold (IR +): 1 0.75 0.59 1.12 0.86 0.90 0.47 0.61
B
RPA
p<0.05
p<0.05
p<0.001
p<0.01
p<0.001
p<0.01
p<0.01
% RPA+ cells (>10 foci)
IR –
IR +
WT
Atm-/-
Br1SF/SF
Atm-/-
53bp1-/-
Br1SF/SF
53bp1-/-
Atm-/-
Br1SF/SF
53bp1+/-
Atm-/-
Br1SF/SF
53bp1-/-
Fold (IR +): 1 0.73 0.65 1.13 0.87 1.06 0.48 0.61

Figure 2.10 (Continued)

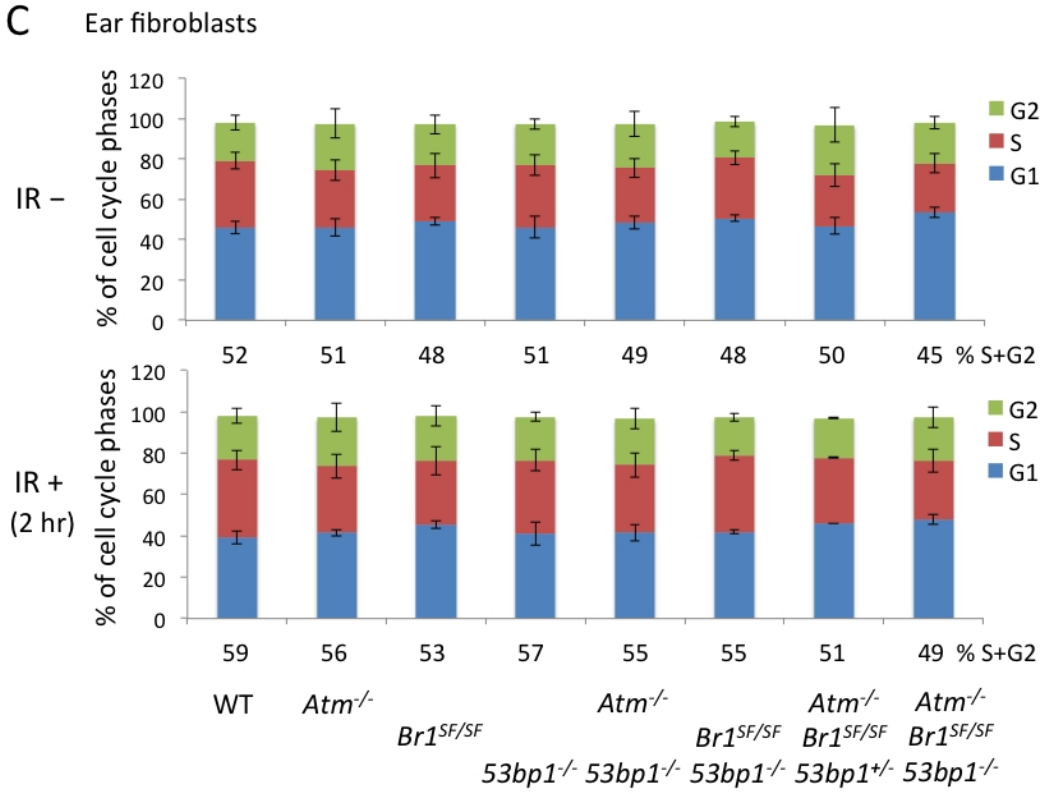

late-stage HDR (47); alternatively, more foci may become visible due to increased resection lengths (see Appendix Figure A.1E for quantification of the RPA foci number). The *Atm*$^{-/-}$*Brca1*$^{SF/SF}$*53bp1*$^{-/-}$ triple mutant also demonstrated reduced RAD51 and RPA foci-positive cells compared to *Brca1*$^{SF/SF}$*53bp1*$^{-/-}$ (Figure 2.10 A and B; column f and h), further supporting a role for ATM in generating end-resected intermediates for RAD51 filament formation in cells with compromised BRCA1 and 53BP1 functions.

These results suggest that ATM functions in HDR independently of 53BP1 and BRCA1 and that SSA in ATM-deficient cells would also not be fully restored by 53BP1 loss. While *53bp1*$^{-/-}$ cells had an ~1.5-fold increase in SSA, *Atm*$^{-/-}$*53bp1*$^{-/-}$ cells showed the same ~2-fold reduction as *Atm*$^{-/-}$ cells (Figure 2.11A). Similarly, while SSA was restored in *Brca1*$^{SF/SF}$*53bp1*$^{-/-}$ cells, it was reduced by ~2-fold in triple mutant *Atm*$^{-/-}$*Brca1*$^{SF/SF}$*53bp1*$^{-/-}$ cells (Figure 2.11A) and in ATMi-treated double mutant cells (Figure 2.11B). These results are consistent with a role for ATM in promoting resection-dependent repair independently of the BRCA1-53BP1 antagonism.

Discussion

The epistatic relationship of BRCA1 and ATM in HDR is not well understood in mice, in part because *Brca1* nullizygosity leads to early embryonic lethality (28). However, the viability of the hypomorphic *Brca1*^{SF} allele with a missense mutation in the BRCT domain (31) has allowed us to uncover synthetic lethality upon *Atm* loss. The findings support a critical role for ATM in maintaining a threshold level of HDR necessary for viability in the context of a breast cancer-associated *Brca1* mutation. Inhibition of ATM activity in *Brca1*$^{SF/SF}$ cells reduces HDR by up to 20-fold relative to WT cells. As HDR proficiency is essential for proliferation during mouse

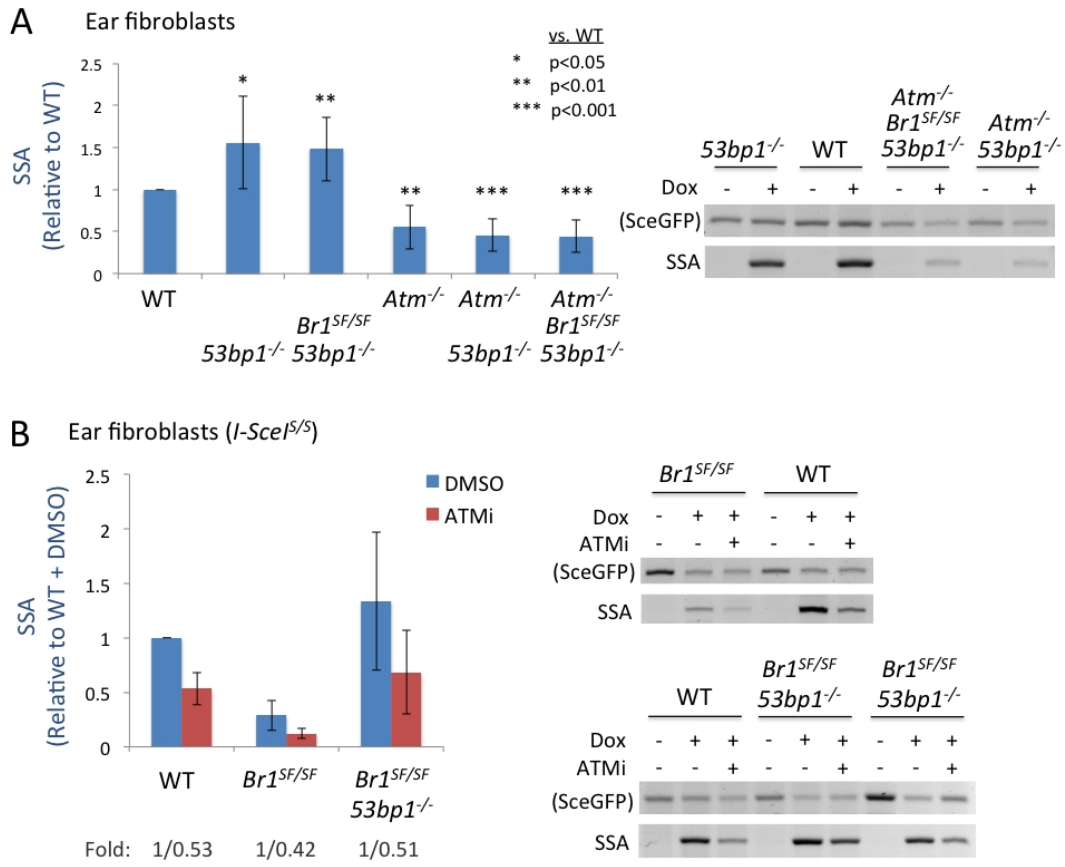

Figure 2.11 ATM promotes SSA independently of the BRCA1-53BP1 antagonism.

A. The levels of SSA in both *Atm*$^{-/-}$*53bp1*$^{-/-}$ and *Atm*$^{-/-}$*Brca1*$^{SF/SF}$*53bp1*$^{-/-}$ ear fibroblasts show the similar 2-fold reductions as in *Atm*$^{-/-}$ cells. (n=4 for *Atm*$^{-/-}$*53bp1*$^{-/-}$, n=2 for triple mutant).

B. While loss of *53bp1* rescues the SSA defect in *Brca1*$^{SF/SF}$ ear fibroblasts, treatment with ATMi still reduces SSA in the *Brca1*$^{SF/SF}$*53bp1*$^{-/-}$ cells by ~2-fold as in WT cells. (n≥3)

development (1), the contribution of ATM to HDR in *Brca1*$^{SF/SF}$ mice provides a mechanism for the compromised viability of *Atm-Brca1*^{SF} double mutant mice.

Previous studies have also demonstrated synthetic lethality of *Atm* mutant mice with deficiency of other DNA damage response factors such as *H2ax* and *Parp1* (48, 49). However, the mechanisms of synthetic lethality appear to differ from what we report here. In particular, *Atm-H2ax* double mutant cells do not show significant exacerbation in HDR defects compared to single mutant cells (26). Further, synthetic lethality of the *Atm-Parp1* mouse is likely due to deficiency in distinct pathways, given that PARP1 loss impairs single-strand break repair. The defect in HDR we report for *Atm* mutant mouse cells, however, makes it reasonable to consider that *Atm-Parp1* mice are unviable due to a role for ATM in repair of lesions generated by PARP1 loss (50).

Different BRCA1 mutations affect the genetic interaction with ATM

In addition to the *Brca1*^{SF} BRCT mutation, we have also examined the genetic interaction of ATM with another *Brca1* allele, *Brca1*^{tr} truncational mutation (51), which mimics a breast cancer founder mutation *2800delAA (52)*. The *Brca1*^{tr} allele is predicted to express a BRCA1 protein truncated in the exon 11-encoding region, leading to deletion of the C terminus including the BRCT domain (Appendix Figure A.2A). The *Brca1*$^{tr/tr}$ mice were born at sub-Mendelian ratio (observed 3, expected 11; Appendix Figure A.2B). Whereas the sub-viability of *Brca1*$^{tr/tr}$ mice was rescued by *Atm* heterozygosity (observed 18, expected 22), it was further reduced by nullizygosity of *Atm* (observed 1, expected 11). These results share similarity with the synthetic lethality of the *Atm-Brca1*^{SF} mutant mice (Figure 2.4A). HDR in *Brca1*$^{tr/tr}$ fibroblasts was suppressed by ATM deficiency to a greater extent than in WT cells, although not as much as that in *Brca1*$^{SF/SF}$ cells (Appendix Figure A.2 D and E), suggesting a moderate dependence on ATM for HDR in the *Brca1*^{tr} mutant. By contrast, in a

different *Brca1* hypomorphic mutant, BRCA1 exon 11-skipping isoform that lacks the central region but retains the BRCT domain (53), ATM deficiency leads to distinct HDR response that we will describe in Chapter 3. These observations raise the possibility that ATM has special roles in promoting HDR in the context of different BRCA1 mutations. Further work is needed to elucidate the mechanisms as well as the significance in the human context.

Context-dependent roles of ATM in HDR

While some studies have observed a role for ATM in HDR (17, 18), other studies have not (24-27). We previously did not detect a significant defect in HDR in $Atm^{-/-}$ primary mouse fibroblasts using an electroporation method with an I-SceI expression vector (27), which in primary cells is variable and relatively inefficient (~20%), such that the fraction of DSB repair events involving HDR could not be determined (see Appendix Figure A.3 for I-SceI transfection experiments in primary cells). The Dox-inducible I-SceI system utilized in this study, by contrast, results in DSB formation in a substantially higher percentage of cells (~50%) (39). This allows us to normalize HDR levels to total repair events to determine the percentage of cells that had repaired the DSB by either HDR or imprecise NHEJ. We present evidence here that primary somatic cells of multiple tissue types from *Atm* mutant mice consistently have a ~2-fold reduction in HDR following an I-SceI-induced DSB. In contrast to somatic cells, our results show that ATM loss in ES cells causes only a transient delay in HDR. The lack of a defect at later time points in ES cells in DR-GFP experiments is consistent with findings from other groups (25, 26).

Several possibilities may account for the different HDR response in $Atm^{-/-}$ ES cells. First, embryonic cells likely have a greater reliance on BRCA1 than ATM for HDR compared to somatic cells. We observed that $Brca1^{SF}$ mutation causes a greater HDR defect in MEFs than adult ear fibroblasts, whereas *Atm* mutation shows the

opposite trend (Figures 2.5 and 2.6). Consistent with this notion, *Brca1*-null mice are lethal (54), unlike the viability of *Atm*-null mice at birth (29, 30). Second, mouse ES cells have unique properties in DNA repair and cell cycle profiles compared to more differentiated cell types (55, 56). Studies suggest that mouse ES cells preferably use HDR over NHEJ for DSB repair (57). The high enrichment in S/G2 phases in these cells may facilitate phosphorylation of BRCA1 for its functions or provide high CDK activity for resection regulation (58-60), thus attenuating the requirement for ATM. The short G1 phase and lack of the G1/S checkpoint may also render mouse ES cells more dependent on replication-coupled repair and thus more reliance on the ATR kinase (55). Interestingly, studies in *Xenopus* extracts show that ATR can be activated directly by the MRN complex and can also facilitate CtIP-mediated resection of clean DSBs independently of ATM in the presence of the EXO1 exonuclease (61, 62). It is possible that ATR and/or EXO1 can serve as alternative pathways for resection in $Atm^{-/-}$ ES cells in the context of I-SceI-induced DSBs (see Appendix Figures A.4-6 for additional analysis of ES cells). Third, $Atm^{-/-}$ ES cells may still have defects in repairing high levels of DSBs or specific breaks located in heterochromatic regions compared to a single break at the DR-GFP reporter at *Pim1* locus. Despite the lack of significant defect in DR-GFP experiments, $Atm^{-/-}$ mouse ES cells are clearly very sensitive to olaparib (26, 63), similar to the phenotypes in *Atm* mutant human cells (64, 65). This suggests that loss of ATM protein indeed causes certain HDR deficiency that renders the cells unable to cope with global DSB accumulation following PARP inhibition. This may be due to the excessive DSB formation that highly activates the ATM pathway or the structural lesions generated by trapping of PARP1/2 proteins that involve ATM activity in the repair of blocked ends (33, 50, 66). Furthermore, PARPi-induced DSBs could be located in heterochromatins throughout the genome that depend on ATM for efficient repair (67).

ATM operates in HDR independently of the BRCA1-53BP1 antagonism

Although the reduced HDR in *Atm*$^{-/-}$ cells could be associated with a role for ATM in later steps of recombination (47, 68), the shared defects in both HDR and SSA together with the reduced RPA focus formation we and others observe (19, 20) argue that ATM loss impacts early steps of recombination, such as modulating the extent of end resection (21-23, 69-71) or the removal of Ku from DNA ends (72). HDR defects in *Atm* mutant cells have also been related to indirect aspects of ATM activity in chromatin relaxation (22, 73). A role for ATM in promoting end resection in HDR during S/G2 may seem contradictory, considering that ATM also functions in NHEJ: In G1 cells, ATM inhibits end resection by promoting 53BP1 functions (3, 7) and the γH2AX/MDC1 assembly (74). However, removing either 53BP1 or H2AX allows ATM-dependent resection to be observed (74-77), though G1 phase resection is not expected to be productive for HDR due to other restrictive mechanisms (16). Importantly, although not usually essential in wild-type cells, our results indicate that ATM becomes crucial for supporting the residual end resection and HDR in *Brca1*^{SF} hypomorphic cells, which is likely critical for the survival of *Brca1*^{SF} mice.

Our genetic epistasis indicates that the HDR and SSA defects in *Atm*$^{-/-}$ primary cells cannot be rescued by *53bp1* deletion, distinguishing the function of ATM from the 53BP1-mediated suppression of BRCA1 and HDR. Further, while *53bp1* loss can restore HDR and SSA in *Brca1*$^{SF/SF}$ cells, as with other *Brca1* mutant alleles, ATM deficiency in *Brca1*$^{SF/SF}$*53bp1*$^{-/-}$ cells reduces both types of DSB repair to a similar extent as in WT or *53bp1*$^{-/-}$ cells. Therefore, these observations suggest that ATM has a direct function in promoting end resection independently of the BRCA1-53BP1 mutual antagonism (Figure 2.12). We do not rule out the possibility that the BRCA1^{SF} protein, which maintains ATM-phosphorylation sites (78), requires ATM

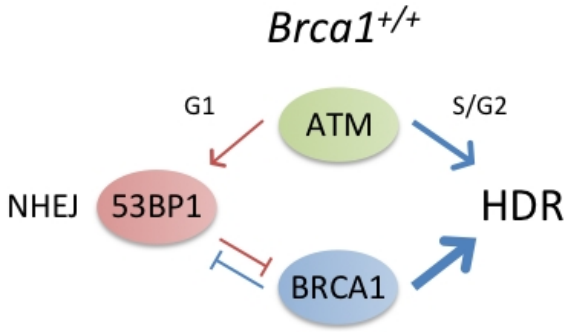

Figure 2.12 Model: The interplay of ATM and BRCA1 in HDR.
In *Brca1*$^{+/+}$ cells, ATM has a minor role in HDR that operates independently of the BRCA1-53BP1 antagonism. Loss of ATM in this setting only reduces HDR to a moderate degree (2-fold in mouse somatic cells) and does not compromise overall viability, e.g., in mouse development. However, in the context of a breast cancer-derived S1598F mutation on mouse BRCA1 that disrupts its BRCT domain functions, ATM becomes essential for supporting the residual end resection and HDR in *Brca1*$^{SF/SF}$ cells as well as the viability of *Brca1*$^{SF/SF}$ mice.

phosphorylation to sustain its hypomorphic function in HDR, in which case ATM may not be an entirely independent player but have crosstalk with BRCA1.

A number of mutations in the BRCT domain of BRCA1 have been associated with breast cancer (https://research.nhgri.nih.gov/projects/bic/), including S1655F equivalent to the mouse S1598F mutation. It remains to be seen how tumors carrying these mutations respond to DNA damaging agents upon ATM loss-of-function. The downregulation of resection suppressors such as 53BP1 has been identified as a mechanism for the acquired resistance to PARP inhibition in BRCA1-deficient mammary tumors (79-82). Given that ATM still plays a role in HDR in these resistant cells, we envision that inhibition of ATM kinase activity may have therapeutic potential for certain types of BRCA1-deficient cancers with acquired resistance to PARP inhibitor therapy.

Contribution

Elizabeth Kass (Maria Jasin lab) performed the *Brca1*^{SF} and *Brca1*^{SF}*-53bp1* mammary experiments and provided materials for the *I-SceI*$^{S/S}$ experiments. Wei-Feng Yen (Jayanta Chaudhuri lab) performed the *Atm* B cell experiments. Chun-Chin Chen performed all the rest of the experiments.

Materials and Methods

Mouse care and genotyping. The care and use of mice were performed with the approval of the Memorial Sloan Kettering Cancer Center (MSKCC) Institutional Animal Care and Use Committee in accordance with institutional guidelines. Genomic DNA was extracted from tail tips using Gentra Puregene Mouse Tail Kit (Qiagen). PCR reactions were performed with PuReTaq PCRbeads (GE Healthcare) with ~100 ng purified genomic DNA.

Pim1^{Drgfp} mice (27) were genotyped using primers Pim1Ex1F 5'-AAG ATC AAC TCC CTG GCC CAC CTG CG-3'; Pim1Ex4R 5'-TGT TCT CGT CCT TGA TGT CG-3'; Hyg3A 5'-CCG CTC GTC TGG CTA AGA T-3' under the following conditions: 94°C/3 min; 35 cycles of 94°C/30 sec, 62.9°C/45 sec and 72°C/1 min; and a final extension of 72°C/5 min. PCR products (WT: 786 bp; Targeted: 958 bp) were separated on a 1% agarose gel.

TRE-I-SceI mice (39) (founder line #10) were genotyped using primers F10.For.Chr6 5′-CTA CAT GTG GCA ACT GGC TCA ATC A-3′; F10.Rev.350 5′-CTG AGC CAT CTC TCT AGC CCA-3′ and SCE.Rev 5′-CTG CTT ATA TAG GCC TCC CAC CGT ACA-3′ under the following conditions: 95 °C/3 min; 32 cycles of 95 °C/30 sec, 58.5 °C/30 sec, and 72 °C/1 min; and a final extension of 72 °C/5 min. PCR products (WT: 350 bp; *I-SceI* allele: 550 bp) were separated on a 1.5% agarose gel. The *CMV-rtTA* transgene was genotyped using rtTA-specific forward primer 5′-GCT TGG TGT AGA GCA GCC TAC AC-3′ and reverse primer 5′-CAG CGC TGA GTG CAT ATA ACG CG-3′ under the following conditions: 94 °C/4 min; 35 cycles of 94 °C/30 sec, 55 °C/30 sec, and 72 °C, 30 sec, and a final extension of 72 °C/5 min. For *CMV-rtTA* PCR, the reaction contains 150-200 ng of genomic DNA and 2% DMSO. An ~310 bp product indicates presence of the transgene.

Atm^{b} mice (29) were genotyped using primers AtmWTFwd 5'-TGT AAT GTG CCT TAA AGA ACC TGG-3'; AtmNullFwd 5'-GGA AAA GCG CCT CCC CTA CCC-3'; AtmRev 5'-CCT CCT CAT ATT TGT AAC ACG CTG-3' under the following conditions: 94°C/2 min; 35 cycles of 94°C/30 sec, 62°C/45 sec, and 72°C/45 sec; and a final extension of 72°C/5 min. PCR products (WT: 362 bp; Mutant: ~500 bp) were resolved on a 1.5% agarose gel; note that a faint band may appear between the two PCR products.

Atm^{w} mice (30) were genotyped using primers AtmF 5'-GAC TTC TGT CAG ATG TTG CTG CC-3'; AtmB 5'-CGA ATT TGC AGG AGT TGC TGA G-3'; AtmN 5'-GGG TGG GAT TAG ATA AAT GCC TG-3' under the following conditions: 94°/2 min; 35 cycles of 94°C/20 sec, 58°C/30 sec, and 72°C/30 sec; and a final extension of 72°C/5 min. WT (162 bp) and mutant (440 bp) PCR products were separated on a 1.5% agarose gel.

Brca1^{S1598F} mice (31) were genotyped using primers S1598F.for 5'-CCC TTG TGC ACC TCC AGA GA-3'; S1598F.rev 5'-GCC ACG CCT ATG AAG GCT CT-3' and LNL3xpA 5'-GAC CTG CAG CCC AAG CTA GC-3' under the following conditions: 94°C/3 min; 35 cycles of 94°C/30 sec, 58°C/30 sec and 72°C/30 sec; and a final extension of 72°C/5 min. PCR products (WT: 259 bp; Mutant: 117 bp) were separated on a 1.5% agarose gel.

53bp1 mice (83) were genotyped using primers exon4 sense 5'-GAT TTT GCC TTA CCC AGT TCC CGA-3'; neo sense 5'-CTA CCC GGT AGA ATT GAC CTG CA-3' and intron antisense 5'-CCT TCT ATT CTA CTT CAG GCT CTG G-3' following the same condition as the *Brca1*^{S1598F} mice genotyping PCR. PCR products (WT: ~300 bp; Mutant: ~200 bp) were separated on a 1.5% agarose gel.

Chk2 mice (84) were genotyped using primers WT#1F 5'-GTG TGC GCC ACC ACT ATC CTG-3'; WT#2R 5'-CCC TTG GCC ATG TTT CAT CTG-3' and Neop53 5'-TCC TCG TGC TTT ACG GTA TC-3' following the same condition as the *Brca1*^{S1598F} mice genotyping PCR (WT: 439 bp; Mutant: ~600 bp).

Primary cell cultures and HDR assays. The tetracycline-inducible I-SceI transgenic system was established by Elizabeth Kass in the Jasin lab (39). All experimental mice were hemizygous for the *Pim1*^{drgfp} and *CMV-rtTA* alleles. The *TRE-I-SceI* allele was also hemizygous, except when labeled as *I-SceI*$^{S/S}$ to indicate homozygous alleles (all *I-SceI*$^{S/S}$ mice are directly provided by Elizabeth Kass). No significant difference in %

GFP^+ and % site-loss between hemizygous and homozygous *TRE-I-SceI* alleles was observed in the *ex vivo* HDR assays in the cohort.

Primary ear fibroblasts and MEFs were cultured in DMEM-HG medium supplemented with 10% tetracycline-free FBS (Clontech), 1X Pen-Strep, and 1X MEM/NEAA. Primary mammary epithelial cells were cultured in DMEM-HG:F12 medium with 10% tetracycline-free FBS, 1X Pen-Strep, 10 μg/ml insulin and 5 ng/ml EGF.

For ear fibroblast isolation, ear tips are cut from 6- to 8-week-old mice, minced with a razor blade, and dissociated in 5 ml serum-free DMEM medium containing 2 mg/ml collagenase A (Roche) and 1X Pen-Strep on a 37°C shaker for 3 hr. The dissociated tissues were passed through a 70-μm strainer, pelleted by centrifugation at 400 g for 8 min, and plated to 6-well plate for 1-2 days before experiments.

For MEF isolation, E12.5-E14.5 mouse embryos were separated from the placenta and embryonic sac, then minced following the removal of head and liver, and then dissociated in 0.05% trypsin at 37°C for 45 min in a 6-cm dish. The dissociated cells were resuspended by pipetting, pelleted at 400 g for 10 min, and plated to a 6-cm dish coated with 0.1% gelatin for 1-2 days.

For mammary epithelial cell isolation, the 4^{th} inguinal mammary glands from 8- to 10-week-old virgin female mice were minced and dissociated in 5 ml serum-free DMEM-HG:F12 containing 2 mg/ml collagenase A, 5 μg/ml insulin, and 1X Pen-Strep on a 37°C shaker for 2 hr. The dissociated cells were pelleted at 400 g for 10 min, resuspended in 6 ml serum-free DMEM-HG:F12 containing 10 μg/ml DNase I (Stem Cell Technologies) and inverted for 2 min, and then pelleted again by centrifugation. Red blood cells were lysed with ammonium chloride solution (Stem Cell Technologies), and the epithelial organoids were separated from other cell types

using two sequential short spins (10 and 5 sec) at 400 g, and then plated to 6-well plate coated with collagen I for 1 day.

For HDR assays, primary fibroblasts and mammary epithelial cells at passage one were plated at a density of 10^5 cells per single well of 6-well plate the night before, then treated with 1 μg/ml Dox (Clontech) to induce I-SceI expression. The percentage of GFP^+ cells was analyzed after 48 hr by flow cytometry. For inhibition of ATM, 3 μM KU-55933 (Calbiochem #118502, 10 mM solution) or equal volume of DMSO were added together with Dox and replenished at 24 hr. For CHK2 inhibition (EMD Millipore #220486), the same procedure is followed.

Primary B cells were purified from mouse spleens by CD43 negative selection (Miltenyi Biotec 130-049-801) as described (85). The B cells were cultured at a density of 10^6 cells/ml, stimulated with cytokines (10 μg/ml LPS, 2 μg/ml anti-CD40, and 25 μg/ml mouse IL4) in combination with 0.25 μg/ml Dox (can even go down to 0.1 μg/ml). The $B220^+GFP^+$ cells were analyzed by flow cytometry at 96 hr.

Mouse ES cell culture and transfection. The *Brca1*$^{SF/SF}$ mouse ES cell line carrying a *Pim1*^{Neo}-targeted DR-GFP allele (clone A8) (31) as well as the *Ctip*$^{+/-}$ and *Ctip*$^{S326A/-}$ DR-GFP clones (8) were provided by Thomas Ludwig at Ohio State University and subsequently weaned from MEF feeder layers after receiving. *Atm*$^{-/-}$ (29) and WT J1 (obtained from mouse targeting facility at MSKCC) ES cell lines were targeted with a linearized *Pim1*$^{Hyg/Puro}$ DR-GFP plasmid using a previously described method (86) to one allele of the *Pim1* locus on chromosome 17 and confirmed by Southern blotting (Appendix Figure A.7). Among the several heterozygous-targeted clones characterized for HDR assay (Figure 2.1C), J1 clone 8 and *Atm*$^{-/-}$ clone 1 showed more consistent HDR results and transfection efficiency and thus were used for most experiments. All mouse ES cell lines were cultured in DMEM-HG medium supplemented with 12.5% stem cell grade FBS (Gemini), 1X Pen-Strep, 1X MEM/NEAA, 1X L-Gln, 833 U/ml

LIF (Gemini), and 0.1 mM β-mercaptoethanol. Culture dishes were pre-coated with 0.1% gelatin. For electroporation, 3-4 × 10^6 ES cells per 10-cm dish were plated the night before. Typically a total of 3 × 10^6 cells and 30 μg plasmid DNA were used for each electroporation. The trypsinized cells were resuspended in 600 μl warm Opti-MEM, mixed with I-SceI-expressing pCBASce plasmid, and pulsed with a Gene Pulser Xcell (Bio-Rad) in a 0.4 cm cuvette at 250 V/950 μF. After pulsing, the cells were mixed with growth medium and plated to a 6-cm dish; for ATM inhibition, the transfection mixture was split to two wells of a 6-well plate containing ATMi KU-55933 or equal volume of DMSO, replenished at 24 hr. As a control for transfection efficiency, equal amount of pNZ-EGFP plasmid and pCAGGS empty vector were electroporated in independent reactions, respectively. Analysis of GFP^+ cells by flow cytometry was typically performed at the 24-hr time point for mouse ES cells, given that the transfection efficiency of pNZ-EGFP plasmid started to drop after 24 hr and the levels of % GFP^+ HDR usually reached plateau at 48 hr. The average transfection efficiency at 24 hr was around 80-90% and the background % GFP^+ without I-SceI transfection was less than 0.01% for these ES cell clones. Plasmids were prepared using PureLink Maxiprep kit (Invitrogen).

Site-loss PCR assays. Genomic DNA was extracted from primary cells following I-SceI induction using Gentra Puregene Mouse Tail Kit (Qiagen). The sequence spanning the I-SceI cleavage site in the *SceGFP* gene was amplified from 100 ng of genomic DNA using Advantage 2 Polymerase (Clontech) with forward primer dr.for 5'-CCC GCC ACC TGC CCC ATC TGC TA-3' and reverse primer dr.rev 5' -CCT CTA CAA ATG TGG TAT GGC TGA TTA TG-3'; this primer set does not amplify SSA products. The PCR condition is as follows: 95°C/1 min; 33 cycles of 95°C/15 sec and 70°C/2 min; and a final extension of 70°C/5 min. The reaction contains 2% DMSO. The PCR products were aliquoted in half and digested with 8 U I-SceI

endonuclease (Thermo Fisher Scientific) or buffer-only control *in vitro* at 37°C overnight and separated on a 1% agarose gel. Band intensities were quantified using ImageJ. The intensity of the uncut band (0.9 kb) was divided by the sum of the uncut (0.9 kb) plus the large cut band (0.7 kb; accounted for the size difference with a correction factor 1.3) to calculate % I-SceI site loss. Animals with % site loss smaller than 20%, which generally also show lower % GFP^+ signal and low I-SceI protein in western blot, were considered having inefficient DNA cutting due to low I-SceI induction and were usually excluded from the cohort analysis.

Site-loss PCR could also be performed with the same dr.for forward primer with another reverse primer dr.rev3 (5'-GGA CAA ACC ACA ACT AGA ATG CAG TG-3') that gave cleaner background for pCBASce plasmid-transfected samples; the amplified product for this primer set was 1.1 kb and the digested products were 0.9 and 0.2 kb.

Single-strand annealing PCR. SSA analysis was performed as described (41). Briefly, the products of SSA were amplified from 200 ng genomic DNA extracted from primary cells following I-SceI induction using PuReTaq PCR beads (GE Healthcare) with forward primer SA.F 5'-TTT GGC AAA GAA TTC AGA TCC-3' and reverse primer SA.R2 5'-ATG ACC ATG ATT ACG CCA AG-3'. For comparison, the structurally intact *SceGFP* gene (or one that had undergone HDR or NHEJ) was amplified using the same forward primer and a different reverse primer SA.R1 5'-CAA ATG TGG TAT GGC TGA TTA TG-3' from 100 ng genomic DNA. The band intensity of SSA product (0.9 kb) was normalized to that of SceGFP (1.1 kb) for each sample as an internal control, and the derived ratio of mutants was relative to that of control samples on the same gel. This SSA analysis only used control/mutant pairs that have similar % I-SceI site loss, i.e., similar DSB efficiency, for relative comparison.

Cell cycle analysis. Trypsinized cells were resuspended in 300 µl ice-cold PBS, and 700 µl of ice-cold 100% ethanol was added drop-wise to the cells while vortexing at low speed to a final concentration of 70% ethanol. The samples were fixed at -20°C at least overnight, then pelleted at 2000 g for 5 min, washed with PBS once, and incubated in 200 µl staining solution (25 µg/ml propidium iodide, 0.1 mg/ml RNase A, 0.05% Triton X-100 in PBS) at 37°C for 30 min followed by flow cytometry. The cell cycle distribution was analyzed using FlowJo cell cycle analysis tool.

Colony formation assay. Mouse ES cells were plated at a density of 1000-1200 cells per well in 6-well plates overnight. Cells were pre-treated with 3 µM ATMi KU-55933 or DMSO for 2 hr, and then treated with PARPi olaparib (synthesized in the MSKCC Organic chemistry core facility) in combination with ATMi or DMSO for 48 hr. All media were added along the wall to avoid disrupting colonies. After removing the olaparib-containing medium, the cells were gently washed with PBS once and then incubated with medium containing only ATMi or DMSO for another 3-4 days until colonies become visible. The colonies were fixed in 100% methanol for 20 min, stained in 3% Giemsa for 3-4 hr, and then washed in distilled water. Colony pictures were scanned and each experimental set was counted around the same time manually using ImageJ. IC_{50} is plotted by nonlinear regression using Prism 6 software.

Mammary gland whole mount staining. The 4^{th} inguinal mammary glands from >8-week-old virgin female mice were harvested and gently spread on microscope slides with a sheet of parafilm. The slides were fixed in Carnoy's fixative (60% ethanol, 30% chloroform, and 10% glacial acetic acid) overnight, defatted in acetone for 30 min, sequentially washed in 70%/50%/30% ethanol for 15 min each and in distilled water for 5 min. The rehydrated slides were incubated in carmine alum solution (2% carmine, 5% aluminum potassium sulfate in water) at room temperature (RT) overnight. After staining, the slides were dehydrated with sequential washes in

70%/95%/100% ethanol for 15 min each, incubated in fresh 100% ethanol for 15 min, cleared in CitriSolv (Fisher Scientific) overnight until the fat pads become transparent, and sealed in Permount mounting medium (Fisher Scientific) for photography.

Western blotting. Proliferating cells were scraped from dishes on ice and lysed for 30 min on ice in TEGN buffer (10 mM Tris, pH 8, 1 mM EDTA, 10% glycerol, 0.5% NP-40, and 400 mM NaCl) with freshly added 1 mM DTT and 1X protease/phosphatase inhibitor EDTA-free cocktails (Pierce #88669). Lysates were centrifuged at 13000 g for 20 min and the supernatant was collected. Protein concentration was quantified using Bradford protein assay (Bio-Rad). Typically an amount of 30 μg protein was diluted in 1X Blue SDS Loading Buffer (New England BioLabs) with 42 mM DTT and boiled at 95°C for 7 min before loading. 53BP1 was separated on 3-8% Tris-Acetate gels (Invitrogen) and transferred to a PVDF membrane in Tris-Glycine buffer containing 0.01% SDS and 10% methanol at 22V, 4°C overnight. Blocking was performed in 5% milk diluted in PBST (1X PBS/0.1% Tween-20) at RT for 1 hr. Primary antibodies were diluted in 2.5% milk and incubated at 4°C overnight on a rotator. HRP-conjugated secondary antibodies (GE Healthcare) were diluted 1:10000 in 2.5% milk and incubated at RT for 1 hr on a shaker. Each incubation was followed by three 10 min-washes in PBST. The membranes were developed using Enhanced ECL reagents (PerkinElmer). Primary antibodies used: Anti-53BP1, 1:4000 (Novus NB100-304); Anti-Clathrin heavy chain, 1:10000 (BD Biosciences 610500).

Immunofluorescence staining. Primary ear fibroblasts were plated in 8-well chamber slides (BD Falcon; pre-coated with poly-L-lysine) at a density of 2×10^4 cells per well overnight, followed by 10 Gy IR and 2 hr recovery in incubator. Cells were fixed in fresh 3% paraformaldehyde/2% sucrose/PBS at RT for 10 min. For RPA foci staining, cells were pre-extracted with cold 0.5% Triton X-100/PBS on ice for 5 min and

washed once with PBS before fixing; for RAD51 foci staining, cells were washed once with PBS and fixed directly without pre-extraction. After fixing, the slides are washed with PBS twice, permeabilized in 0.5% Triton X-100/PBS at RT for 10 min, and blocked in 1% IgG-free BSA (Jackson ImmunoResearch)/0.1% Triton X-100/PBS on a shaker at RT for 30 min. The slides were incubated with primary and secondary antibodies diluted in blocking buffer (70 µl/well) at RT on a shaker for 2 and 1 hr, respectively. Following each staining step the slides were washed with PBS three times, 10 min for each on a shaker. Finally, the slides were fixed in ProLong Gold Antifade Mountant with DAPI (Molecular Probes) and analyzed by microscopy. Antibodies used: Anti-RAD51, 1:400 (Calbiochem PC130). Anti-RPA2, 1:400 (Cell Signaling 2208). Alexa Fluor 488/594-conjugated secondary antibodies, 1:400 (Molecular Probes).

Statistical analysis. Statistical comparisons were calculated using two-tailed Student's t-test. All error bars in the figures represent one standard deviation from the mean.

REFERENCES

1. Moynahan ME & Jasin M (2010) Mitotic homologous recombination maintains genomic stability and suppresses tumorigenesis. *Nat. Rev. Mol. Cell Biol.* 11(3):196-207.
2. Chapman JR, Taylor MR, & Boulton SJ (2012) Playing the end game: DNA double-strand break repair pathway choice. *Mol. Cell* 47(4):497-510.
3. Panier S & Boulton SJ (2014) Double-strand break repair: 53BP1 comes into focus. *Nat. Rev. Mol. Cell Biol.* 15(1):7-18.
4. Cao L*, et al.* (2009) A selective requirement for 53BP1 in the biological response to genomic instability induced by Brca1 deficiency. *Mol. Cell* 35(4):534-541.
5. Bouwman P*, et al.* (2010) 53BP1 loss rescues BRCA1 deficiency and is associated with triple-negative and BRCA-mutated breast cancers. *Nat. Struct. Mol. Biol.* 17(6):688-695.
6. Bunting SF*, et al.* (2010) 53BP1 inhibits homologous recombination in Brca1-deficient cells by blocking resection of DNA breaks. *Cell* 141(2):243-254.
7. Zimmermann M & de Lange T (2014) 53BP1: pro choice in DNA repair. *Trends Cell Biol.* 24(2):108-117.
8. Reczek CR, Szabolcs M, Stark JM, Ludwig T, & Baer R (2013) The interaction between CtIP and BRCA1 is not essential for resection-mediated DNA repair or tumor suppression. *J. Cell Biol.* 201(5):693-707.
9. Cruz-Garcia A, Lopez-Saavedra A, & Huertas P (2014) BRCA1 Accelerates CtIP-Mediated DNA-End Resection. *Cell Rep.* 9(2):451-459.
10. Yun MH & Hiom K (2009) CtIP-BRCA1 modulates the choice of DNA double-strand-break repair pathway throughout the cell cycle. *Nature* 459(7245):460-463.
11. Polato F*, et al.* (2014) CtIP-mediated resection is essential for viability and can operate independently of BRCA1. *J. Exp. Med.* 211(6):1027-1036.
12. Shiloh Y & Ziv Y (2013) The ATM protein kinase: regulating the cellular response to genotoxic stress, and more. *Nat. Rev. Mol. Cell Biol.* 14(4):197-210.
13. Reiman A*, et al.* (2011) Lymphoid tumours and breast cancer in ataxia telangiectasia; substantial protective effect of residual ATM kinase activity against childhood tumours. *Br. J. Cancer* 105(4):586-591.
14. Bennardo N & Stark JM (2010) ATM limits incorrect end utilization during non-homologous end joining of multiple chromosome breaks. *PLoS Genet.* 6(11):e1001194.
15. Bredemeyer AL*, et al.* (2006) ATM stabilizes DNA double-strand-break complexes during V(D)J recombination. *Nature* 442(7101):466-470.
16. Orthwein A*, et al.* (2015) A mechanism for the suppression of homologous recombination in G1 cells. *Nature* 528(7582):422-426.
17. Morrison C*, et al.* (2000) The controlling role of ATM in homologous recombinational repair of DNA damage. *EMBO J.* 19(3):463-471.

18. Beucher A, *et al.* (2009) ATM and Artemis promote homologous recombination of radiation-induced DNA double-strand breaks in G2. *EMBO J.* 28(21):3413-3427.
19. Myers JS & Cortez D (2006) Rapid activation of ATR by ionizing radiation requires ATM and Mre11. *J. Biol. Chem.* 281(14):9346-9350.
20. Jazayeri A, *et al.* (2006) ATM- and cell cycle-dependent regulation of ATR in response to DNA double-strand breaks. *Nat. Cell Biol.* 8(1):37-45.
21. You Z, *et al.* (2009) CtIP links DNA double-strand break sensing to resection. *Mol. Cell* 36(6):954-969.
22. Shibata A, *et al.* (2011) Factors determining DNA double-strand break repair pathway choice in G2 phase. *EMBO J.* 30(6):1079-1092.
23. Wang H, *et al.* (2013) The interaction of CtIP and Nbs1 connects CDK and ATM to regulate HR-mediated double-strand break repair. *PLoS Genet.* 9(2):e1003277.
24. White JS, Choi S, & Bakkenist CJ (2010) Transient ATM kinase inhibition disrupts DNA damage-induced sister chromatid exchange. *Sci. Signal.* 3(124):ra44.
25. Yamamoto K, *et al.* (2016) Kinase-dead ATM protein is highly oncogenic and can be preferentially targeted by Topo-isomerase I inhibitors. *Elife* 5.
26. Rass E, Chandramouly G, Zha S, Alt FW, & Xie A (2013) Ataxia telangiectasia mutated (ATM) is dispensable for endonuclease I-SceI-induced homologous recombination in mouse embryonic stem cells. *J. Biol. Chem.* 288(10):7086-7095.
27. Kass EM, *et al.* (2013) Double-strand break repair by homologous recombination in primary mouse somatic cells requires BRCA1 but not the ATM kinase. *Proc. Natl. Acad. Sci. U. S. A.* 110(14):5564-5569.
28. Evers B & Jonkers J (2006) Mouse models of BRCA1 and BRCA2 deficiency: past lessons, current understanding and future prospects. *Oncogene* 25(43):5885-5897.
29. Xu Y & Baltimore D (1996) Dual roles of ATM in the cellular response to radiation and in cell growth control. *Genes Dev.* 10(19):2401-2410.
30. Barlow C, *et al.* (1996) Atm-deficient mice: a paradigm of ataxia telangiectasia. *Cell* 86(1):159-171.
31. Shakya R, *et al.* (2011) BRCA1 tumor suppression depends on BRCT phosphoprotein binding, but not its E3 ligase activity. *Science* 334(6055):525-528.
32. Helleday T (2011) The underlying mechanism for the PARP and BRCA synthetic lethality: clearing up the misunderstandings. *Mol. Oncol.* 5(4):387-393.
33. Murai J, *et al.* (2012) Trapping of PARP1 and PARP2 by Clinical PARP Inhibitors. *Cancer Res.* 72(21):5588-5599.
34. Wu Q, Jubb H, & Blundell TL (2015) Phosphopeptide interactions with BRCA1 BRCT domains: More than just a motif. *Prog. Biophys. Mol. Biol.* 117(2-3):143-148.

35. Yu X & Chen J (2004) DNA damage-induced cell cycle checkpoint control requires CtIP, a phosphorylation-dependent binding partner of BRCA1 C-terminal domains. *Mol. Cell. Biol.* 24(21):9478-9486.
36. Xu X*, et al.* (2001) Genetic interactions between tumor suppressors Brca1 and p53 in apoptosis, cell cycle and tumorigenesis. *Nat. Genet.* 28(3):266-271.
37. Cao L*, et al.* (2006) ATM-Chk2-p53 activation prevents tumorigenesis at an expense of organ homeostasis upon Brca1 deficiency. *EMBO J.* 25(10):2167-2177.
38. Huber LJ*, et al.* (2001) Impaired DNA damage response in cells expressing an exon 11-deleted murine Brca1 variant that localizes to nuclear foci. *Mol. Cell. Biol.* 21(12):4005-4015.
39. Kass EM, Lim PX, Helgadottir HR, Moynahan ME, & Jasin M (2016) Robust homology-directed repair within mouse mammary tissue is not specifically affected by Brca2 mutation. *Nat Commun* 7:13241.
40. Stark JM, Pierce AJ, Oh J, Pastink A, & Jasin M (2004) Genetic steps of mammalian homologous repair with distinct mutagenic consequences. *Mol. Cell. Biol.* 24(21):9305-9316.
41. Nakanishi K*, et al.* (2005) Human Fanconi anemia monoubiquitination pathway promotes homologous DNA repair. *Proc. Natl. Acad. Sci. U. S. A.* 102(4):1110-1115.
42. Gunn A, Bennardo N, Cheng A, & Stark JM (2011) Correct end use during end joining of multiple chromosomal double strand breaks is influenced by repair protein RAD50, DNA-dependent protein kinase DNA-PKcs, and transcription context. *J. Biol. Chem.* 286(49):42470-42482.
43. Anantha RW*, et al.* (2017) Functional and mutational landscapes of BRCA1 for homology-directed repair and therapy resistance. *Elife* 6.
44. Feng L*, et al.* (2015) Cell cycle-dependent inhibition of 53BP1 signaling by BRCA1. *Cell Discov* 1:15019.
45. Escribano-Diaz C*, et al.* (2013) A cell cycle-dependent regulatory circuit composed of 53BP1-RIF1 and BRCA1-CtIP controls DNA repair pathway choice. *Mol. Cell* 49(5):872-883.
46. Kakarougkas A*, et al.* (2013) Co-operation of BRCA1 and POH1 relieves the barriers posed by 53BP1 and RAP80 to resection. *Nucleic Acids Res.* 41(22):10298-10311.
47. Bakr A*, et al.* (2015) Involvement of ATM in homologous recombination after end resection and RAD51 nucleofilament formation. *Nucleic Acids Res.* 43(6):3154-3166.
48. Menisser-de Murcia J, Mark M, Wendling O, Wynshaw-Boris A, & de Murcia G (2001) Early embryonic lethality in PARP-1 Atm double-mutant mice suggests a functional synergy in cell proliferation during development. *Mol. Cell. Biol.* 21(5):1828-1832.
49. Zha S, Sekiguchi J, Brush JW, Bassing CH, & Alt FW (2008) Complementary functions of ATM and H2AX in development and suppression of genomic instability. *Proc. Natl. Acad. Sci. U. S. A.* 105(27):9302-9306.

50. Bryant HE & Helleday T (2006) Inhibition of poly (ADP-ribose) polymerase activates ATM which is required for subsequent homologous recombination repair. *Nucleic Acids Res.* 34(6):1685-1691.
51. Ludwig T, Fisher P, Ganesan S, & Efstratiadis A (2001) Tumorigenesis in mice carrying a truncating Brca1 mutation. *Genes Dev.* 15(10):1188-1193.
52. Liede A*, et al.* (2000) Evidence of a founder BRCA1 mutation in Scotland. *Br J Cancer* 82(3):705-711.
53. Gowen LC, Johnson BL, Latour AM, Sulik KK, & Koller BH (1996) Brca1 deficiency results in early embryonic lethality characterized by neuroepithelial abnormalities. *Nat. Genet.* 12(2):191-194.
54. Ludwig T, Chapman DL, Papaioannou VE, & Efstratiadis A (1997) Targeted mutations of breast cancer susceptibility gene homologs in mice: lethal phenotypes of Brca1, Brca2, Brca1/Brca2, Brca1/p53, and Brca2/p53 nullizygous embryos. *Genes Dev.* 11(10):1226-1241.
55. Ahuja AK*, et al.* (2016) A short G1 phase imposes constitutive replication stress and fork remodelling in mouse embryonic stem cells. *Nat. Commun.* 7:10660.
56. Stambrook PJ & Tichy ED (2010) Preservation of genomic integrity in mouse embryonic stem cells. *Adv. Exp. Med. Biol.* 695:59-75.
57. Tichy ED*, et al.* (2010) Mouse embryonic stem cells, but not somatic cells, predominantly use homologous recombination to repair double-strand DNA breaks. *Stem Cells Dev* 19(11):1699-1711.
58. Huertas P & Jackson SP (2009) Human CtIP mediates cell cycle control of DNA end resection and double strand break repair. *J. Biol. Chem.* 284(14):9558-9565.
59. Scully R*, et al.* (1997) Dynamic changes of BRCA1 subnuclear location and phosphorylation state are initiated by DNA damage. *Cell* 90(3):425-435.
60. Peterson SE*, et al.* (2011) Cdk1 uncouples CtIP-dependent resection and Rad51 filament formation during M-phase double-strand break repair. *J. Cell Biol.* 194(5):705-720.
61. Peterson SE*, et al.* (2013) Activation of DSB processing requires phosphorylation of CtIP by ATR. *Mol. Cell* 49(4):657-667.
62. Duursma AM, Driscoll R, Elias JE, & Cimprich KA (2013) A role for the MRN complex in ATR activation via TOPBP1 recruitment. *Mol. Cell* 50(1):116-122.
63. Chen CC*, et al.* (2017) ATM loss leads to synthetic lethality in BRCA1 BRCT mutant mice associated with exacerbated defects in homology-directed repair. *Proc. Natl. Acad. Sci. U. S. A.* 114(29):7665-7670.
64. Williamson CT*, et al.* (2010) ATM deficiency sensitizes mantle cell lymphoma cells to poly(ADP-ribose) polymerase-1 inhibitors. *Mol. Cancer Ther.* 9(2):347-357.
65. Weston VJ*, et al.* (2010) The PARP inhibitor olaparib induces significant killing of ATM-deficient lymphoid tumor cells in vitro and in vivo. *Blood* 116(22):4578-4587.

66. Alvarez-Quilon A, *et al.* (2014) ATM specifically mediates repair of double-strand breaks with blocked DNA ends. *Nat. Commun.* 5:3347.
67. Goodarzi AA, *et al.* (2008) ATM signaling facilitates repair of DNA double-strand breaks associated with heterochromatin. *Mol. Cell* 31(2):167-177.
68. Ahlskog JK, Larsen BD, Achanta K, & Sorensen CS (2016) ATM/ATR-mediated phosphorylation of PALB2 promotes RAD51 function. *EMBO reports* 17(5):671-681.
69. Kijas AW, *et al.* (2015) ATM-dependent phosphorylation of MRE11 controls extent of resection during homology directed repair by signalling through Exonuclease 1. *Nucleic Acids Res.* 43(17):8352-8367.
70. Bolderson E, *et al.* (2010) Phosphorylation of Exo1 modulates homologous recombination repair of DNA double-strand breaks. *Nucleic Acids Res.* 38(6):1821-1831.
71. Makharashvili N, *et al.* (2014) Catalytic and noncatalytic roles of the CtIP endonuclease in double-strand break end resection. *Mol. Cell* 54(6):1022-1033.
72. Chanut P, Britton S, Coates J, Jackson SP, & Calsou P (2016) Coordinated nuclease activities counteract Ku at single-ended DNA double-strand breaks. *Nat Commun* 7:12889.
73. Ziv Y, *et al.* (2006) Chromatin relaxation in response to DNA double-strand breaks is modulated by a novel ATM- and KAP-1 dependent pathway. *Nat. Cell Biol.* 8(8):870-876.
74. Helmink BA, *et al.* (2011) H2AX prevents CtIP-mediated DNA end resection and aberrant repair in G1-phase lymphocytes. *Nature* 469(7329):245-249.
75. Tubbs AT, *et al.* (2014) KAP-1 promotes resection of broken DNA ends not protected by gamma-H2AX and 53BP1 in G(1)-phase lymphocytes. *Mol. Cell. Biol.* 34(15):2811-2821.
76. Bothmer A, *et al.* (2010) 53BP1 regulates DNA resection and the choice between classical and alternative end joining during class switch recombination. *J. Exp. Med.* 207(4):855-865.
77. Yamane A, *et al.* (2013) RPA accumulation during class switch recombination represents 5'-3' DNA-end resection during the S-G2/M phase of the cell cycle. *Cell Rep.* 3(1):138-147.
78. Cortez D, Wang Y, Qin J, & Elledge SJ (1999) Requirement of ATM-dependent phosphorylation of brca1 in the DNA damage response to double-strand breaks. *Science* 286(5442):1162-1166.
79. Jaspers JE, *et al.* (2013) Loss of 53BP1 causes PARP inhibitor resistance in Brca1-mutated mouse mammary tumors. *Cancer Discov.* 3(1):68-81.
80. Johnson N, *et al.* (2013) Stabilization of mutant BRCA1 protein confers PARP inhibitor and platinum resistance. *Proc. Natl. Acad. Sci. U. S. A.* 110(42):17041-17046.
81. Xu G, *et al.* (2015) REV7 counteracts DNA double-strand break resection and affects PARP inhibition. *Nature* 521(7553):541-544.
82. Tkac J, *et al.* (2016) HELB Is a Feedback Inhibitor of DNA End Resection. *Mol. Cell* 61(3):405-418.

83. Ward IM, Minn K, van Deursen J, & Chen J (2003) p53 Binding protein 53BP1 is required for DNA damage responses and tumor suppression in mice. *Mol. Cell. Biol.* 23(7):2556-2563.
84. Hirao A*, et al.* (2002) Chk2 is a tumor suppressor that regulates apoptosis in both an ataxia telangiectasia mutated (ATM)-dependent and an ATM-independent manner. *Mol. Cell. Biol.* 22(18):6521-6532.
85. Zheng S*, et al.* (2015) Non-coding RNA Generated following Lariat Debranching Mediates Targeting of AID to DNA. *Cell* 161(4):762-773.
86. Moynahan ME, Pierce AJ, & Jasin M (2001) BRCA2 is required for homology-directed repair of chromosomal breaks. *Mol. Cell* 7(2):263-272.

CHAPTER THREE

ATM HAS DISTINCT EFFECTS ON HDR MODULATED BY 53BP1 IN MOUSE BRCA1 EXON 11-SKIPPING MUTANT CELLS

Abstract

Mutations across the major domains of BRCA1 are associated with various levels of HDR deficiency. Here we genetically dissect how two hypomorphic mutations of BRCA1 affect the interplay with ATM and 53BP1 in HDR in mouse ES cells. In a *Brca1*^{S1598F} mutant that disrupts the phosphoprotein-binding BRCT domain at the C terminus, ATM activity promotes HDR regardless of 53BP1 status. However, in a *Brca1*^{ex11} alternative splicing mutant that skips the central region of BRCA1 but retains the BRCT domain, whether ATM supports HDR is determined by the status of 53BP1: Only in the absence of 53BP1 does ATM promote HDR. The *Brca1*^{ex11} mutant also shows more augmented DNA damage and NHEJ-mediated suppression of HDR that correspond to its more severe repair defects. These results demonstrate that structural mutations of BRCA1 could differentially affect how ATM participates in HDR through a context-dependent regulation by 53BP1.

Introduction

Many cancer-associated *BRCA1* mutations result in frameshift and truncation of the protein, although missense mutations also occur throughout different domains of BRCA1 protein that could impact its DSB repair and tumor suppression functions (1, 2). Alternatively spliced transcripts of *BRCA1* have also been identified in various contexts, including proliferative and tumorigenic tissues as well as normal counterparts (3, 4). These alternative splicing events frequently occur around exon 11, the largest exon of BRCA1, resulting in various isoforms that lack part of the central

region of the BRCA1 protein (3, 5). The significance of the exon 11-encoding region is less defined compared to the N and C terminus of BRCA1. This region contains two nuclear localization signals, though these are not essential for BRCA1 nuclear import (6, 7), and other elements such as interaction sites for DNA and RAD51 as well as phosphorylation sites that together contribute to the functions of BRCA1 in DNA damage checkpoints and HDR (8-11). *BRCA1*-mutant breast tumors maintaining an isoform that skips most of the exon 11 (Δ11q) show partial resistance to PARPi compared to tumors with complete loss of BRCA1 expression (12). This residual function of Δ11q is in part dependent on the remaining interaction of the peptide with PALB2. Thus, these splicing isoforms of *BRCA1* could have a role in therapeutic resistance by preserving some levels of DSB repair activity.

A number of *Brca1* exon 11-skipping mouse alleles have been developed either by deleting the entire exon 11 via *Cre-loxP* recombination (referred to below as $Brca1^{\Delta 11}$) (13) or disrupting the splicing acceptor of exon 11 with a targeting cassette (referred to below as $Brca1^{ex11}$) (14, 15), both producing the exon 11-skipping peptide (Δ11) consisting of the N-terminal RING domain fused with the C-terminal coiled-coil and BRCT domains. In the presence of full-length BRCA1, this isoform appears to be dispensable for mouse development (16). However, mice exclusively expressing the $BRCA1^{\Delta 11}$ protein show embryonic lethality ranging from mid E9.5-10.5 (14, 15) to late E12.5-18 (17) stages depending on the structure of mutant allele, whereas mice carrying *Brca1* alleles that are considered nullizygous die at an earlier stage between E5.5-9.5 (18, 19), suggesting a hypomorphic phenotype for the exon 11-skipping mutants. Conditional deletion of *Brca1* exon 11 has also been studied, in particular in the mouse mammary gland where tumorigenesis has been observed (after one year (13)).

Studies have shown that HDR is reduced in both *Brca1*^{ex11} and *Brca1*^{S1598F} (SF) mutant ES cells (20-23). Our recent work demonstrates that ATM supports much of the residual levels of HDR in *Brca1*^{SF} BRCT mutant cells, and that loss of ATM further compromises the viability of *Brca1*$^{SF/SF}$ mice (Chapter 2, (24)). Intriguingly, this phenotype is distinct from that previously reported with *Brca1*$^{\Delta 11}$ mutant mice where *Atm* deletion restores viability of the animals (25). These two BRCA1 mutant proteins have very different structures, in that the BRCA1^{SF} protein is full length (although deficient in binding phosphoproteins via the BRCT domain) while the BRCA1$^{\Delta 11}$ peptide maintains an intact BRCT domain (Figure 3.1A). Although both *Brca1* mutants have compromised HDR that can be rescued by loss of the resection suppressor 53BP1 (24, 26), some aspects of the DNA damage response are different. For example, formation of DNA damage-induced BRCA1 foci is impaired upon mutation of the mouse S1598 or its human equivalent S1655 (20, 27) but is intact for the BRCA1$^{\Delta 11}$ isoform (28), likely related to the collaboration of RING and BRCT domain functions in BRCA1 chromatin association (29, 30). Particularly striking is the contrasting phenotypes in animal viability in the absence of ATM, raising the question whether these two BRCA1 hypomorphic mutants differentially affect the interplay with other regulators of DSB repair following ATM loss. Here, we show that in mouse cells expressing the BRCA1$^{\Delta 11}$ splicing isoform, loss of ATM activity has differential effects on HDR depending on the status of the NHEJ factor 53BP1: ATM suppresses HDR in these cells in the presence of 53BP1 but supports HDR in the absence of 53BP1. This is distinct from the *Brca1*^{SF} mutant and WT cells where ATM promotes HDR independently of 53BP1.

Results

Derivation of *Brca1*$^{ex11/ex11}$ DR-GFP mouse ES cells

We utilized a mouse *Brca1*$^{ex11/ex11}$ ES cell line from Beverly Koller's lab (UNC) carrying a *Brca1* allele that has half of exon 11 (encoding amino acid 223-763), including the splice acceptor, replaced by a *Neo*^{R} cassette (15, 23). This integration leads to alternative splicing from exons 9 to 12 and the expression of the BRCA1$^{\Delta 11}$ isoform (7). This cell line was previously modified by integrating the DR-GFP reporter at the *Pim1* locus and shown to be HDR defective (21). A derivative clone (#3) of this *Brca1*$^{ex11/ex11}$ DR-GFP ES cell line was used for *53bp1* targeting experiments (see below), which has the *Hyg*^{R} marker gene at the *Pim1*^{Drgfp} locus disrupted by CRISPR/Cas9-mediated mutagenesis to allow for the use of hygromycin-selection method during gene targeting; the expression of BRCA1$^{\Delta 11}$ isoform was confirmed by western blotting in this clone #3 before starting the targeting experiment (see below, Figure 3.7B). The *Brca1*$^{SF/SF}$ ES cell line carrying a *Pim1*-targeted DR-GFP reporter (clone A8), provided by Thomas Ludwig (OSUCCC), has been described in Chapter 2 (20).

Differential effects of ATM inhibition on HDR in *Brca1*^{S1598F} and *Brca1*^{ex11} cells.

Because ATM deficiency exacerbates the HDR defects in *Brca1*^{SF} mutant cells (24), we investigated whether ATM inhibition also affects HDR in cells expressing the BRCA1$^{\Delta 11}$ spliced isoform. Both *Brca1*$^{SF/SF}$ and *Brca1*$^{ex11/ex11}$ ES cells showed an ~8-fold reduction in HDR 24 hr after transfection of an I-SceI expression plasmid compared to a WT J1 ES cell line (Figure 3.1B, left panel). However, unlike *Brca1*$^{SF/SF}$ ES cells, in which treatment with an ATM kinase inhibitor (KU-55933) reduced the residual HDR by ~2.6-fold, we found that ATM inhibition actually increased HDR by ~1.7-fold in *Brca1*$^{ex11/ex11}$ cells (Figure 3.1B, right panel). The

Figure 3.1 ATM inhibition suppresses HDR in *Brca1*^{SF} but increases HDR in *Brca1*^{ex11} ES cells.

A. The mouse BRCA1 S1598F protein has a point mutation in the BRCT domain that disrupts the interaction with phosphoproteins. The BRCA1 Δ11 spliced isoform skips the exon 11-encoding central region but retains the downstream coiled-coil (CC) and BRCT domains. Both mutant proteins contain the RING domain at the N terminus. NLS: nuclear localization signal.

B. Both *Brca1*$^{SF/SF}$ and *Brca1*$^{ex11/ex11}$ mouse ES cell lines have severely reduced HDR (left). Treatment of an ATMi (3 μM, 24 hr) in *Brca1*$^{SF/SF}$ cells reduces HDR to a greater extent than in WT cells; by contrast, ATMi treatment increases HDR in *Brca1*$^{ex11/ex11}$ cells (right). All error bars in the figures of this chapter represent one standard deviation from the mean. (n=5)

C. Cell cycle profiles of the *Brca1* mutant ES cell lines are not significantly affected by ATM inhibition (3 μM, 24 hr) at the time point of HDR analysis. (n≥3)

D. Unlike in *Brca1*$^{SF/SF}$ ES cells, continuous treatment with ATMi (3 μM) does not further sensitize *Brca1*$^{ex11/ex11}$ ES cells to a 48-hr pulsed treatment with olaparib. IC_{50} of olaparib with/without ATMi: *Brca1*$^{SF/SF}$, 14.5/3.9 nM; *Brca1*$^{ex11/ex11}$, 8.9/9.3 nM. The fold is relative to the colony number of DMSO-only treatment. (n≥3)

Figure 3.1

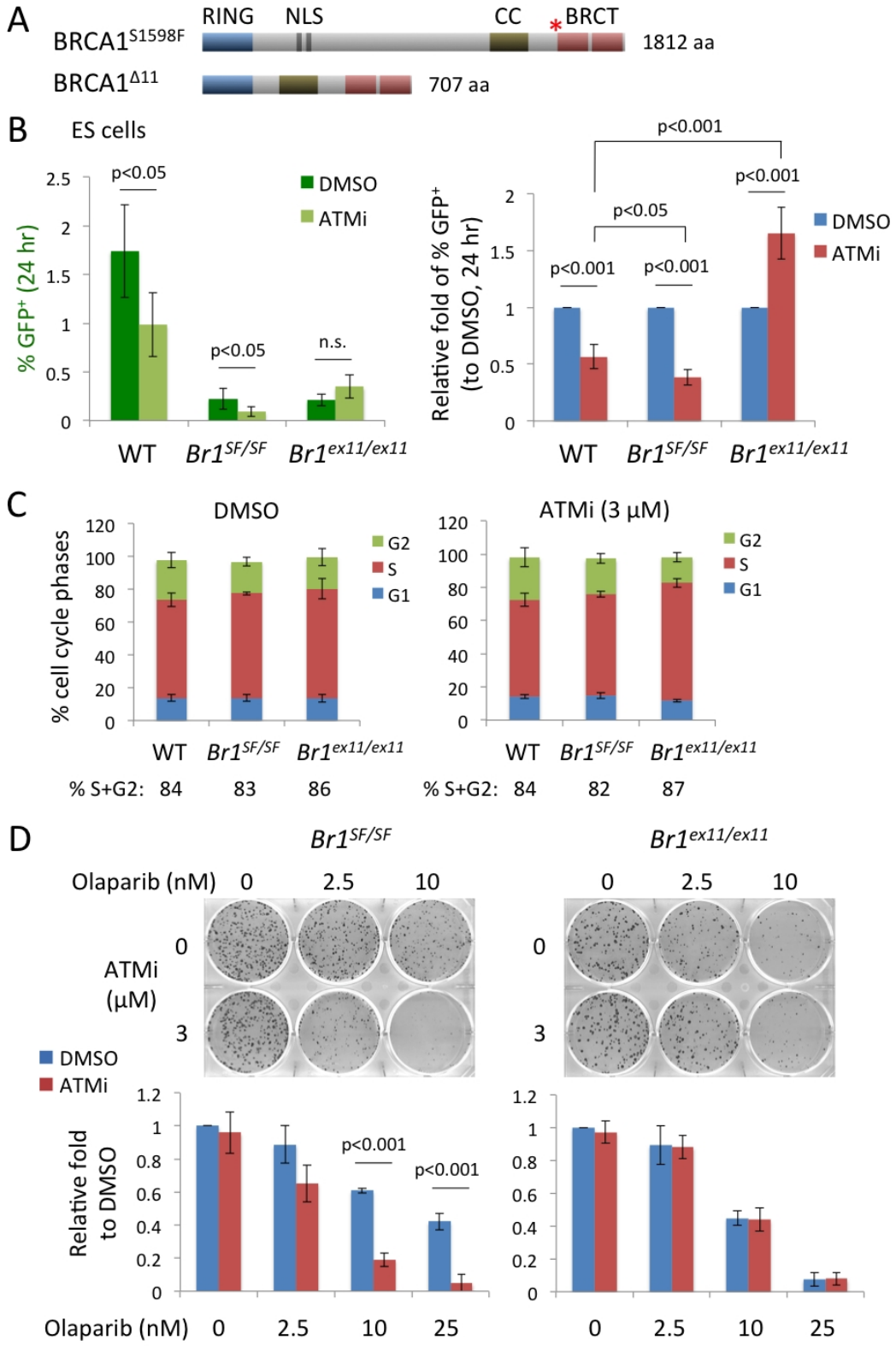
A
BRCA1S1598F
RING
NLS
CC
BRCT
1812 aa
BRCA1Δ11
707 aa
B
ES cells
% GFP+ (24 hr)
p<0.05
DMSO
ATMi
p<0.05
n.s.
WT
Br1SF/SF
Br1ex11/ex11
Relative fold of % GFP+ (to DMSO, 24 hr)
p<0.001
p<0.05
p<0.001
p<0.001
C
DMSO
ATMi (3 μM)
% cell cycle phases
G2
S
G1
% S+G2: 84 83 86
% S+G2: 84 82 87
D
Br1SF/SF
Br1ex11/ex11
Olaparib (nM) 0 2.5 10
ATMi (μM)
DMSO
ATMi
Relative fold to DMSO
p<0.001
p<0.001
Olaparib (nM) 0 2.5 10 25

difference was not related to any significant changes in cell cycle profiles (Figure 3.1C).

We also examined the colony formation capability of these *Brca1* mutant ES cell lines following a 48 hr pulse of different doses of olaparib. *Brca1*$^{ex11/ex11}$ ES cells showed more sensitivity to olaparib (IC_{50} 8.9 nM) than *Brca1*$^{SF/SF}$ cells (IC_{50} 14.5 nM) (Figure 3.1D). This differential sensitivity to this DNA damaging agent may be related to the more severe developmental defects of mice expressing the Δ11 isoform than the *Brca1*^{SF} mutant mice (17, 20). When we combined increasing doses of olaparib with a defined dose of the ATMi, colony formation of *Brca1*$^{SF/SF}$ cells was further suppressed compared to olaparib treatment alone (~5-fold reduction at 10 nM olaparib+ATMi versus ~1.7-fold reduction at 10 nM olaparib; Figure 3.1D, left panel), whereas the olaparib-treated *Brca1*$^{ex11/ex11}$ cells did not show any further colony reduction upon ATM inhibition (~2-fold reduction at 10 nM olaparib with or without ATMi; Figure 3.1D, right panel). The IC_{50} of olaparib in the combination with ATMi for *Brca1*$^{SF/SF}$ cells was thus decreased to 3.9 nM, whereas the IC_{50} for *Brca1*$^{ex11/ex11}$ cells remained similar at 9.3 nM. Together, these results suggest that ATM kinase activity supports HDR in *Brca1*^{SF} cells but conversely inhibits HDR in *Brca1*^{ex11} cells.

Mutation of *53bp1* in WT ES cells only moderately increases HDR

Given the roles of the NHEJ protein 53BP1 in suppressing end resection in different contexts, we also examined how loss of 53BP1 impacts HDR in ES cells. To mutate the *53bp1* gene, we followed a previously described CRISPR/Cas9 method in the lab (31) (see Appendix A.8 for *53bp1* targeting scheme and clonal analysis). Loss of 53BP1 protein following mutagenesis was confirmed by western blotting (Figure 3.2A). HDR in the *53bp1*$^{-/-}$ clone #26 was increased by ~1.4-fold at 24 hr compared to WT ES cells, but the difference was not significant, likely due to the variation of transfection efficiency (Figure 3.2A). We also examined HDR at a later time point

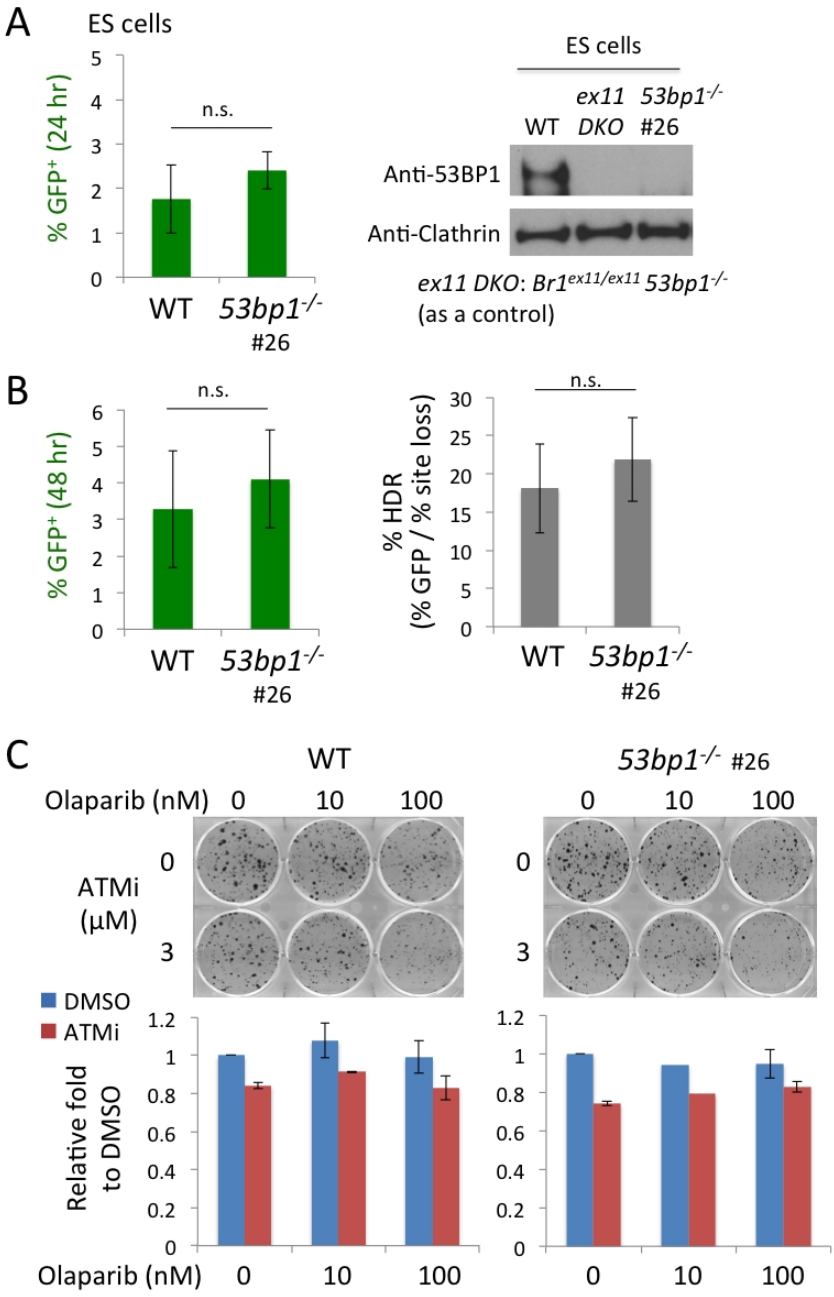

Figure 3.2 Loss of 53BP1 in the presence of BRCA1 only slightly increases HDR.
A. Mutation of *53bp1* in WT ES cells slightly increases HDR at 24 hr but this does not reach statistical significance. Loss of 53BP1 is confirmed by western blot using a *Brca1*$^{ex11/ex11}$*53bp1*$^{-/-}$ clone #60 as a negative control (see below). (n=4)
B. At 48 hr HDR is slightly higher in *53bp1*$^{-/-}$ cells but is not significantly different from WT (left). There is also no significant difference when normalizing % GFP^{+} to % I-SceI site-loss despite a ~1.2-fold increase in *53bp1*$^{-/-}$ cells (right). (n=4)
C. *53bp1*$^{-/-}$ ES cells respond to treatments with olaparib and/or ATMi similarly to WT cells. (n=2 for 100 nM dose)

(48 hr) which showed a ~1.3-fold increase in % GFP^+ in *53bp1*$^{-/-}$ cells, but this again did not reach significant difference (Figure 3.2B, left panel). To have a better measurement on the fraction of HDR over total repair events, we normalized % GFP^+ with overall repair efficiency using an I-SceI site loss assay (i.e., % HDR; see Chapter 2), which confirmed that HDR in *53bp1*$^{-/-}$ ES cells had a ~1.2-fold increase compared to WT cells (Figure 3.2B, right panel). The small elevation in HDR in *53bp1* mutant ES cells is similar to the observation in primary fibroblasts derived from *53bp1*$^{-/-}$ mice (Chapter 2, (24)), suggesting that loss of 53BP1 in the presence of wild-type BRCA1 promotes only a moderate increase in HDR. The *53bp1*$^{-/-}$ #26 cells also did not show any observable reduction in colony numbers upon treatment with olaparib alone, as expected, and had only a ~1.2-fold reduction upon the combined treatment with olaparib and ATMi, similar to the response in WT ES cells (Figure 3.2C).

53BP1 modulates the response of *Brca1*^{ex11} mutant cells to ATM inhibition.

53BP1 plays a major role in counteracting BRCA1 and is also regulated by ATM. Given the complex interplay of these three proteins in DSB repair, we performed mutagenesis of *53bp1* in the two *Brca1* mutant ES cell lines to address whether 53BP1 deficiency affects the distinct HDR responses following ATM inhibition. The *Brca1*$^{ex11/ex11}$ #3 derivative clone used for *53bp1* mutagenesis showed slightly lower baseline HDR (0.13% at 24 hr) than the parental *Brca1*$^{ex11/ex11}$ cells (0.21% at 24 hr) analyzed previously (Figure 3.1B). When we examined HDR in *Brca1*$^{ex11/ex11}$*53bp1*$^{-/-}$ clones #17 and #18, we found that loss of 53BP1 rescued HDR by 4-fold, raising % GFP^+ from 0.13% to ~0.5% (Figure 3.3A). This was still not comparable to the 1.7% in WT J1 cells (Figure 3.1B), but this was likely due to the low levels of baseline HDR in this *Brca1*$^{ex11/ex11}$ #3 cell line used for *53bp1* mutation. In particular, this increase in HDR following 53BP1 loss in *Brca1*$^{ex11/ex11}$ cells was enough to substantially rescue the olaparib sensitivity, as both *Brca1*$^{ex11/ex11}$*53bp1*$^{-/-}$ clones

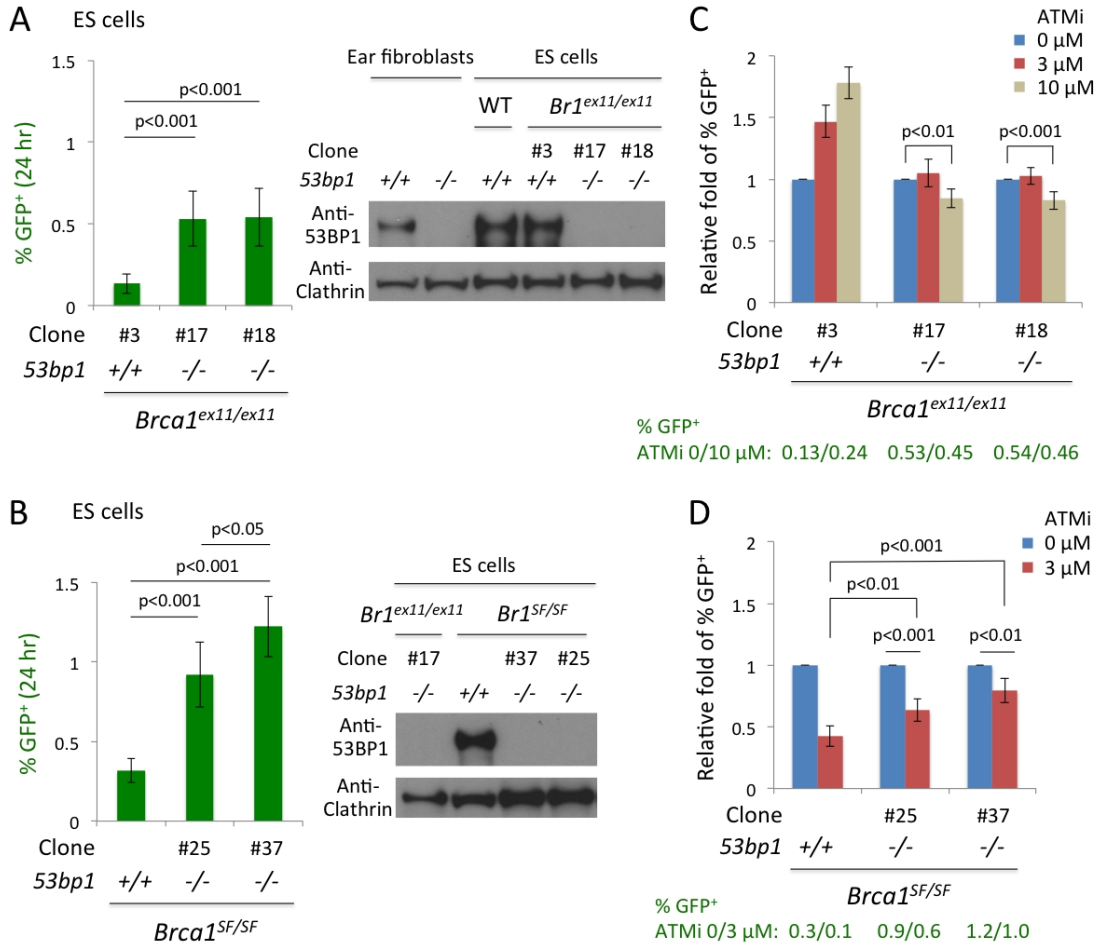

Figure 3.3 Mutation of *53bp1* in *Brca1*^{ex11} cells abolishes the increase in HDR triggered by ATM inhibition.

A. Mutation of *53bp1* rescues the HDR defect in *Brca*$^{ex11/ex11}$ ES cells by 4-fold. Two independent double mutant clones (#17 and #18) are examined. Loss of 53BP1 is confirmed by western blot using *53bp1*$^{-/-}$ primary fibroblasts as a control. *Brca1*$^{ex11/ex11}$ #3: a derivative clone of *Brca1*$^{ex11/ex11}$ DR-GFP ES cells; this clone has lower baseline HDR than the parental cells. (n=5)

B. Mutation of *53bp1* rescues the HDR defect in *Brca1*$^{SF/SF}$ ES cells by 4-fold. Two independent double mutant clones (#25 and #37) are examined. (n=5)

C. Mutation of *53bp1* in *Brca1*$^{ex11/ex11}$ ES cells abolishes the increase in HDR following increasing doses of ATMi treatment (3/10 µM, 24 hr). (n=5)

D. Mutation of *53bp1* in *Brca1*$^{SF/SF}$ ES cells attenuates the extent of HDR reduction following treatment of ATMi (3 µM, 24 hr). (n=5)

showed only a 1.2-fold reduction in colony number even with treatment of 100 nM olaparib, at which dose all *Brca1*$^{ex11/ex11}$ cells were killed (Figure 3.4A, blue bars alone, compare #3 with #17 or #18). These results suggest the exon 11-encoding region of BRCA1 is required for counteracting 53BP1 in response to olaparib-induced damage (26).

For the *Brca1*^{SF} mutant, we found that HDR was rescued by ~3-fold in *Brca1*$^{SF/SF}$*53bp1*$^{-/-}$ clone #25 and ~4-fold in clone #37 compared to *Brca1*$^{SF/SF}$ cells (Figure 3.3B). This significantly increased % GFP^{+} from 0.3% to 1-1.2% (Figure 3.3B), which became only ~1.4-fold lower than the 1.7% in WT cells (Figure 3.1B). The HDR difference between clone #25 and #37 ($p=0.04$) was likely due to clonal variation, which could be followed up in other clones such as #35 (Appendix A.8 F and G). Both *Brca1*$^{SF/SF}$*53bp1*$^{-/-}$ clones showed an almost complete rescue of colony formation in response to 100 nM olaparib, at which dose 70% of the *Brca1*$^{SF/SF}$ colonies were eliminated (Figure 3.4B, blue bars alone, compare #3 with #25 or #37). These results are consistent with the notion that the BRCT domain plays a role in counteracting 53BP1 for HDR, as observed in the mouse primary cell experiments (Chapter 2, (24)).

We next examined whether loss of 53BP1 affects the distinct HDR responses following ATM inhibition in the *Brca1*^{ex11} and *Brca1*^{SF} mutants. Interestingly, we observed that in the *Brca1*^{ex11} mutant, the status of 53BP1 controls whether ATM promotes HDR. In *Brca1*$^{ex11/ex11}$ #3 cells, treatment of ATMi increased HDR by ~1.5-fold compared to DMSO; however, in *Brca1*$^{ex11/ex11}$*53bp1*$^{-/-}$ clones #17 and #18 without 53BP1 expression, the rescued HDR was no longer increased by ATMi compared to DMSO (Figure 3.3C, 3 μM ATMi). Thus, the HDR increase in *Brca1*$^{ex11/ex11}$ cells upon ATM inhibition is dependent on 53BP1.

Conversely, we found in the *Brca1*^{SF} mutant that, while ATM inhibition reduces HDR, the HDR reduction is not more severe in the absence of 53BP1 but rather even somewhat decreased. In *Brca1*$^{SF/SF}$ cells, treatment of ATMi reduced HDR by ~2.5-fold; in *Brca1*$^{SF/SF}$*53bp1*$^{-/-}$ clones #25 and #37, ATMi treatment also reduced HDR, although somewhat less, i.e., by ~1.6- and 1.3-fold, respectively (Figure 3.3D). This is distinct from the reversed trend in the *Brca1*^{ex11} mutant before and after *53bp1* mutation, as described above (Figure 3.3C). The ~1.6-fold reduction in HDR in ATM-treated *Brca1*$^{SF/SF}$*53bp1*$^{-/-}$ clone #25 was similar to that in ATMi-treated WT cells (Figure 3.1B, right panel), whereas the less reduction in clone #37 may be due to the difference in the rescuing effects of 53BP1 loss on the baseline HDR (Figure 3.3B, greater rescue in #37 than #25) or other effects from gene targeting, which can be addressed with more clonal analysis. Nevertheless, the HDR results in the *Brca1*$^{SF/SF}$*53bp1*$^{-/-}$ ES cells were supported by the primary cell data described in Chapter 2 that mutation of *53bp1* in *Brca1*$^{SF/SF}$ ear fibroblasts attenuated the fold of HDR reduction from 5-fold to 1.4-fold upon ATM inhibition. Given that BRCA1 is especially important for HDR in embryonic cells (Chapter 2), the smaller HDR reduction in ATMi-treated *Brca1*$^{SF/SF}$*53bp1*$^{-/-}$ ES cells may also indicate a dependence (either direct or indirect) on ATM to counteract 53BP1 in the *Brca1*^{SF} embryonic contexts, whereas such a dependence on ATM is relieved once 53BP1 is lost.

We also examined the effect of 53BP1 loss in the two *Brca1* mutants to combined treatment with olaparib and ATMi. In the presence of 53BP1, *Brca1*$^{ex11/ex11}$ #3 cells were sensitive to olaparib, but combined treatment with ATMi did not further reduce its colony formation (Figure 3.4A, left panel, compare blue and red bars). Following the loss of 53BP1, *Brca1*$^{ex11/ex11}$*53bp1*$^{-/-}$ clones #17 and #18 became resistant to olaparib; however, upon the combined treatment with olaparib and ATMi, *Brca1*$^{ex11/ex11}$*53bp1*$^{-/-}$ cells now showed a 2-fold reduction in colony formation

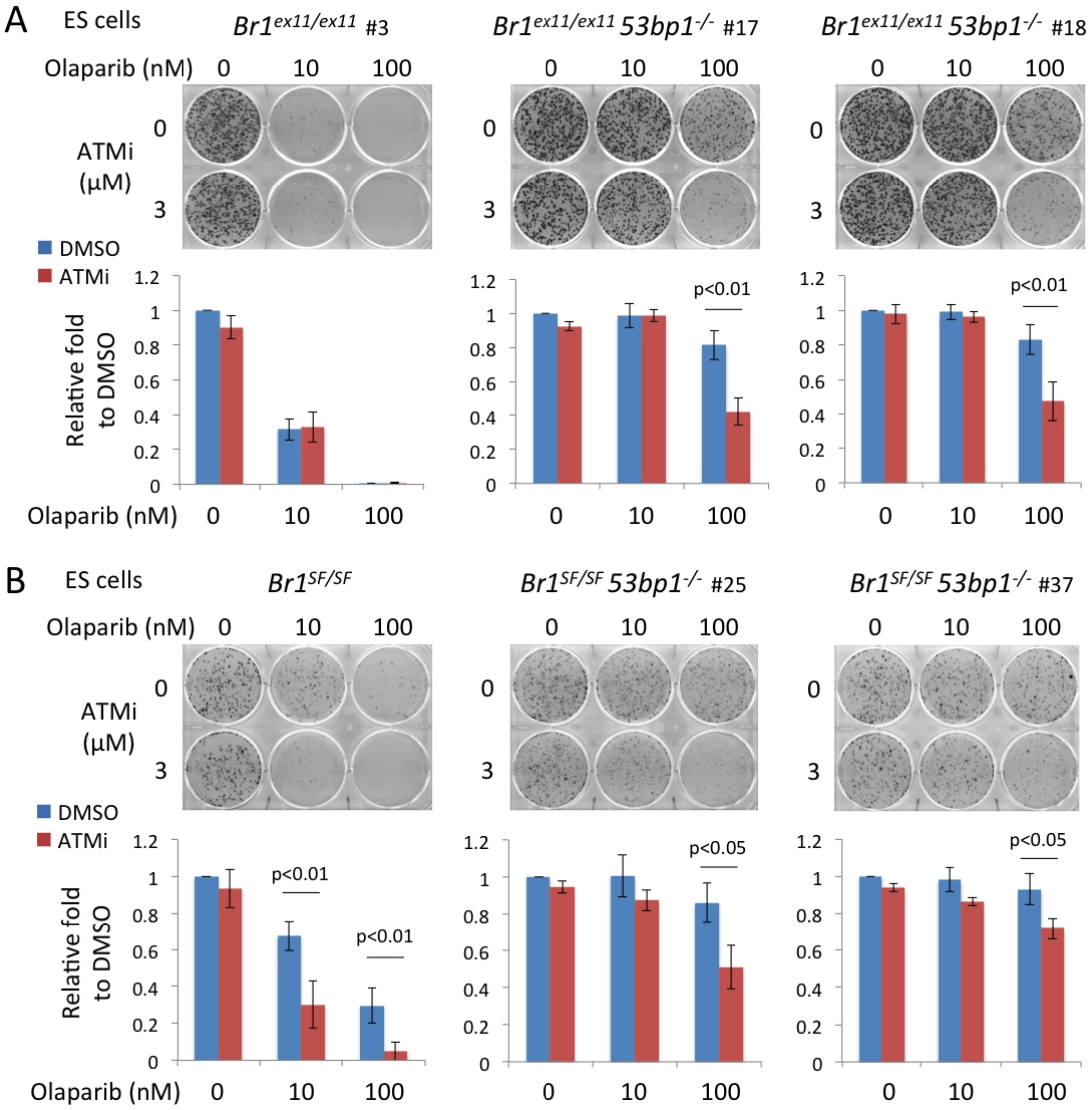

Figure 3.4 Mutation of *53bp1* in *Brca1*^{ex11} cells makes them sensitive to combined treatments with olaparib and ATMi.

A. *Brca1*$^{ex11/ex11}$*53bp1*$^{-/-}$ ES cells are much more resistant to olaparib (48 hr) compared to *Brca1*$^{ex11/ex11}$ cells. Whereas combined treatment with ATMi (continuous) has no effects in *Brca1*$^{ex11/ex11}$ cells, it further reduces colony formation in *Brca1*$^{ex11/ex11}$*53bp1*$^{-/-}$ cells. (n=3)

B. Combination of 48-hr olaparib treatment with continuous ATMi treatment reduces colony formation in both *Brca1*$^{SF/SF}$ and *Brca1*$^{SF/SF}$*53bp1*$^{-/-}$ ES cells, though the fold of decrease is smaller for the latter one. (n=3)

compared to olaparib alone (versus DMSO: 2.5-fold reduction at 100 nM olaparib+ATMi, 1.2-fold reduction at 100 nM olaparib; Figure 3.4A, middle and right panels, compare blue and red bars). This suggests that in cells expressing the BRCA1$^{\Delta 11}$ isoform, ATM contributes to HDR in response to olaparib only when 53BP1 is removed, in agreement with the report that ATM inhibition reduces the formation of RAD51 foci in irradiated *Brca1*$^{\Delta 11/\Delta 11}$*53bp1*$^{-/-}$ B cells (26). The opposing HDR responses to ATM inhibition in the *Brca1*^{ex11} mutant before and after *53bp1* mutation support a modulating role for 53BP1 in this process.

In the presence of 53BP1, *Brca1*$^{SF/SF}$ ES cells showed a further reduction in colony formation upon the combined treatment with olaparib and ATMi (Figure 3.4B, left panel, compare blue and red bars). Following the loss of 53BP1, both *Brca1*$^{SF/SF}$*53bp1*$^{-/-}$ clones gained resistance to olaparib; when combining ATMi with olaparib, the colony formation of *Brca1*$^{SF/SF}$*53bp1*$^{-/-}$ clones #25 and #37 was still reduced by ~1.7- and 1.3-fold, respectively, compared to olaparib treatment alone (Figure 3.4B, middle and right panels, compare blue and red bars at 100 nM olaparib). This suggests that ATM activity supports HDR in the *Brca1*^{SF} mutant in both 53BP1-proficient and -deficient condition, consistent with our analysis in primary cells showing that ATM has independent roles in resection and HDR in the *Brca1*^{SF}-*53bp1* double mutant mice (Chapter 2). To summarize, unlike in *Brca1*^{SF} mutant cells where ATM has a positive role in HDR irrespective of the 53BP1 protein, ATM has ambivalent effects on HDR specifically in *Brca1*^{ex11} mutant cells that are modulated by the status of 53BP1: ATM activity suppresses HDR in the presence of 53BP1 but supports HDR in the absence of 53BP1.

HDR in the *Brca1*^{ex11} mutant is highly suppressed by NHEJ signaling.

To gain more insight into the differential HDR responses, we asked whether ATM-mediated signaling in response to DSBs differs between the two *Brca1* mutants. We

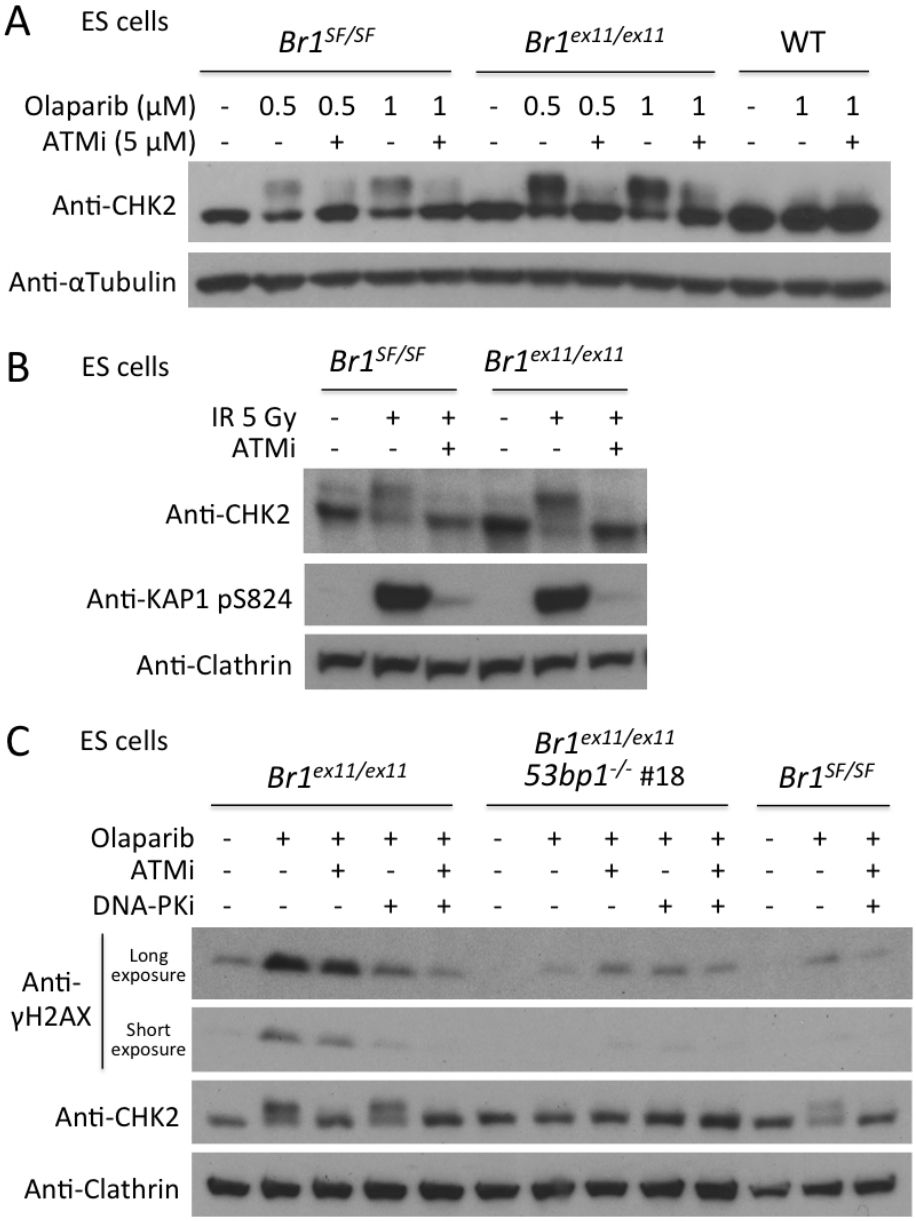

Figure 3.5 *Brca1*^{ex11} cells accumulate high levels of DNA damage upon olaparib treatment due to its HDR defect.

A. *Brca1*$^{ex11/ex11}$ ES cells show higher levels of ATM-dependent phosphorylation of CHK2 (observed by mobility shift) than *Brca1*$^{SF/SF}$ cells following olaparib treatment (20 hr). WT cells do not show a CHK2 shift.

B. Phosphorylation of CHK2 following acute damage by IR is not evidently different between *Brca1*^{SF} and *Brca1*^{ex11} mutant cells. Lysates are collected 1 hr after IR. ATMi: 5 μM.

C. The level of γH2AX is significantly increased in olaparib-treated (0.5 μM, 22 hr) *Brca1*$^{ex11/ex11}$ cells that can be alleviated by combined inhibition of DNA-PKcs (3 μM) and ATM (5 μM) activity.

found that ATM-dependent phosphorylation on its substrate CHK2, as indicated by mobility shifts in western blots, was greater in *Brca1*$^{ex11/ex11}$ than *Brca1*$^{SF/SF}$ ES cells following treatment with 0.5 μM olaparib for 20 hr (Figure 3.5A), suggesting a more profound DNA damage response. WT ES cells are not sensitive to olaparib and thus did not show evidence of CHK2 phosphorylation (Figure 3.5A). The stronger damage response is likely related to the lower HDR in the *Brca1*^{ex11} mutant that results in unresolved olaparib-induced DSBs rather than an intrinsic alteration in ATM activity per se, since the phosphorylation of ATM substrates upon acute DNA breaks by IR was not so different between the two *Brca1* mutants (Figure 3.5B). Consistent with the notion that the HDR defect in *Brca1*^{ex11} mutant leads to more DSB accumulation, loss of 53BP1 in *Brca1*$^{ex11/ex11}$ cells greatly dampened CHK2 phosphorylation and γH2AX formation following olaparib treatment (Figure 3.5C), in accordance with the rescue of HDR (Figure 3.3A). The levels of olaparib-induced γH2AX were also substantially lower in *Brca1*$^{SF/SF}$ than in *Brca1*$^{ex11/ex11}$ cells, suggesting the *Brca1*^{ex11} mutant is a more severe hypomorph (Figure 3.5C).

Given that H2AX can be phosphorylated by redundant kinases ATM and DNA-PKcs, we treated the cells with a DNA-PKcs inhibitor (NU-7441). Although γH2AX is typically promoted by ATM, we found that the elevation of γH2AX in olaparib-treated *Brca1*$^{ex11/ex11}$ cells was greatly suppressed by inhibition of DNA-PKcs but not ATM (Figure 3.5C), indicating particularly high activity of DNA-PKcs at breaks in the *Brca1*^{ex11} mutant. This may be related to the persistent γH2AX formation observed in the developing brain of *Brca1*$^{Δ11/Δ11}$ embryos even after ATM loss (25). Phosphorylation of CHK2 was not affected by DNA-PKcs inhibition (Figure 3.5C). Although ATMi alone had little effect on γH2AX, combined inhibition of ATM and DNA-PKcs further abolished the γH2AX signals to the background level (Figure 3.5C). The reduction in γH2AX by inhibition of ATM and DNA-PKcs could indicate

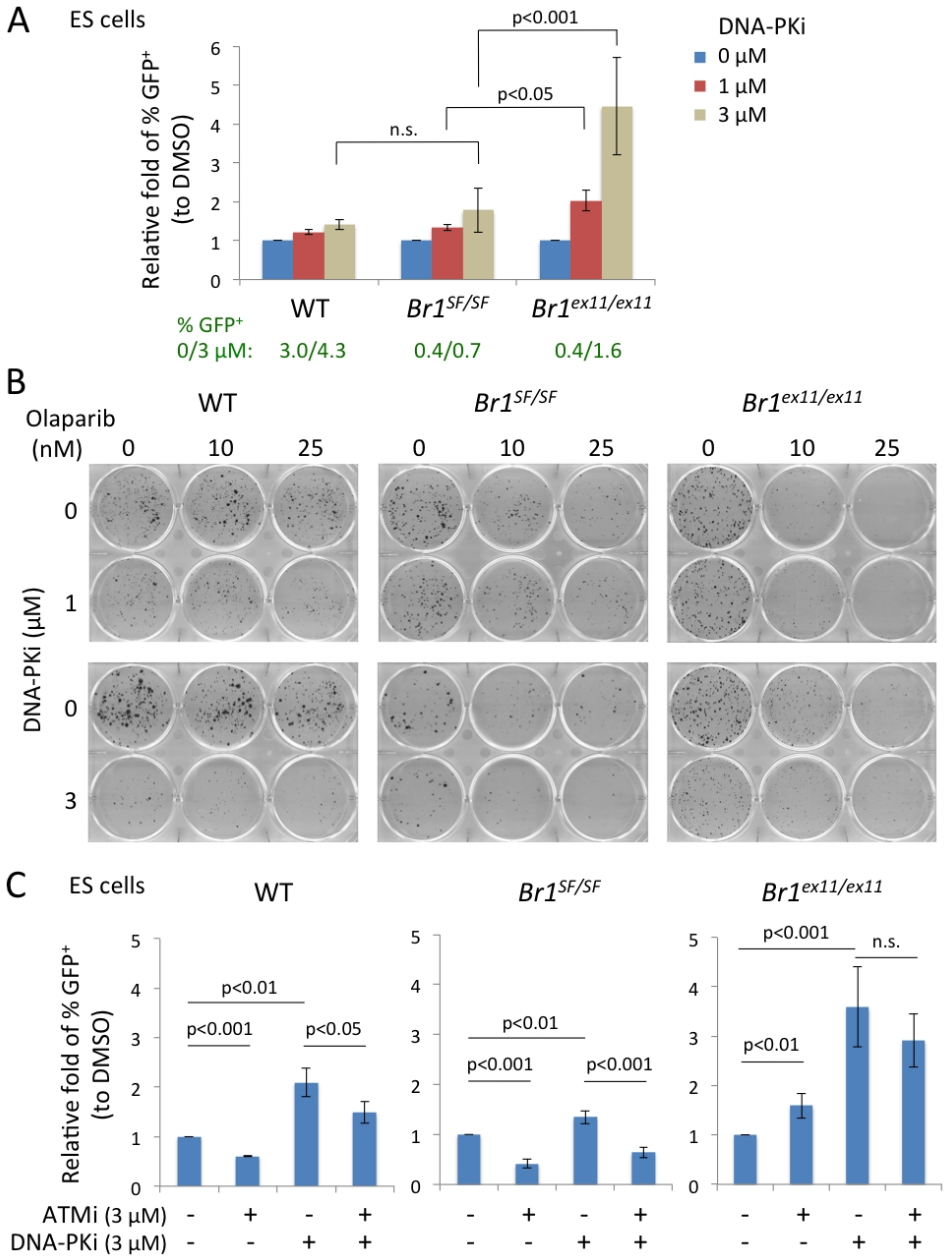

Figure 3.6 HDR in *Brca1*^{ex11} cells is significantly promoted by DNA-PKcs inhibition.

A. Treatment of a DNA-PKcs inhibitor (1/3 µM, 24 hr) increases HDR significantly more in *Brca1*$^{ex11/ex11}$ than *Brca1*$^{SF/SF}$ or WT ES cells. (n≥3)

B. Transient inhibition of DNA-PKcs (48 hr) cannot rescue the sensitivity to olaparib (48 hr) in both *Brca1* mutant ES cells. The two different doses of DNA-PKi are independent experiments. (n=2 for 1 µM DNA-PKi)

C. In WT and *Brca1*$^{SF/SF}$ ES cells, HDR is supported by ATM and inhibited by DNA-PKcs, whereas both ATM and DNA-PKcs contribute to HDR suppression in *Brca1*$^{ex11/ex11}$ cells. DNA-PKi and ATMi: 3 µM, 24 hr. (n≥3)

either the ablation of signaling or the physical repair of breaks, unlike that of 53BP1 loss which likely reflects repair per se; however, the sensitivity to olaparib in *Brca1*^{ex11} mutant cells still cannot be restored by DNA-PKcs inhibition (see below).

Suppression of NHEJ components such as Ku or DNA-PKcs has been shown to increase HDR and promote the survival of HDR-deficient cells following genotoxic damage (32-35). Given the strong DNA damage response and γH2AX accumulation in *Brca1*^{ex11} mutant that are in part dependent on DNA-PKcs, we examined how suppressing NHEJ would affect HDR in the two *Brca1* mutants. Interestingly, inhibition of DNA-PKcs activity led to a more profound increase in HDR in *Brca1*$^{ex11/ex11}$ (~4-fold) than in *Brca1*$^{SF/SF}$ (~1.8-fold) or WT (~1.4-fold) ES cells (Figure 3.6A), suggesting that the repair pathway competition from NHEJ is more prominent in the *Brca1*^{ex11} mutant. Although treatment with the DNA-PKcs inhibitor increased % GFP^{+} in *Brca1*$^{SF/SF}$ and *Brca1*$^{ex11/ex11}$ up to 0.7% and 1.6%, respectively, the levels were still not comparable to the 3% in DMSO-treated WT cells (note that these few experiments with DNA-PKi had higher levels of baseline HDR than those in Figure 3.1B, but since WT and mutants were performed side by side this did not influence the interpretation). The HDR increase in *Brca1*$^{ex11/ex11}$ cells treated with DNA-PKcs inhibitor may also contribute to some degree of the γH2AX reduction in response to olaparib (Figure 3.5C), however it is difficult to separate repair from the signaling aspects.

Despite the increased HDR, we found that DNA-PKcs inhibition in these two *Brca1* mutant ES cell lines did not lessen the sensitivity to low doses of olaparib (Figure 3.6B). This is perhaps analogous to the report that loss of Ku cannot rescue the lethality of *Brca1*$^{\Delta 11}$ mutant mice (32), and we suspect one possibility may be the alternative NHEJ activity in mouse cells that contributes to the toxic end joining events following olaparib-induced damage (36, 37), which will not be suppressed by

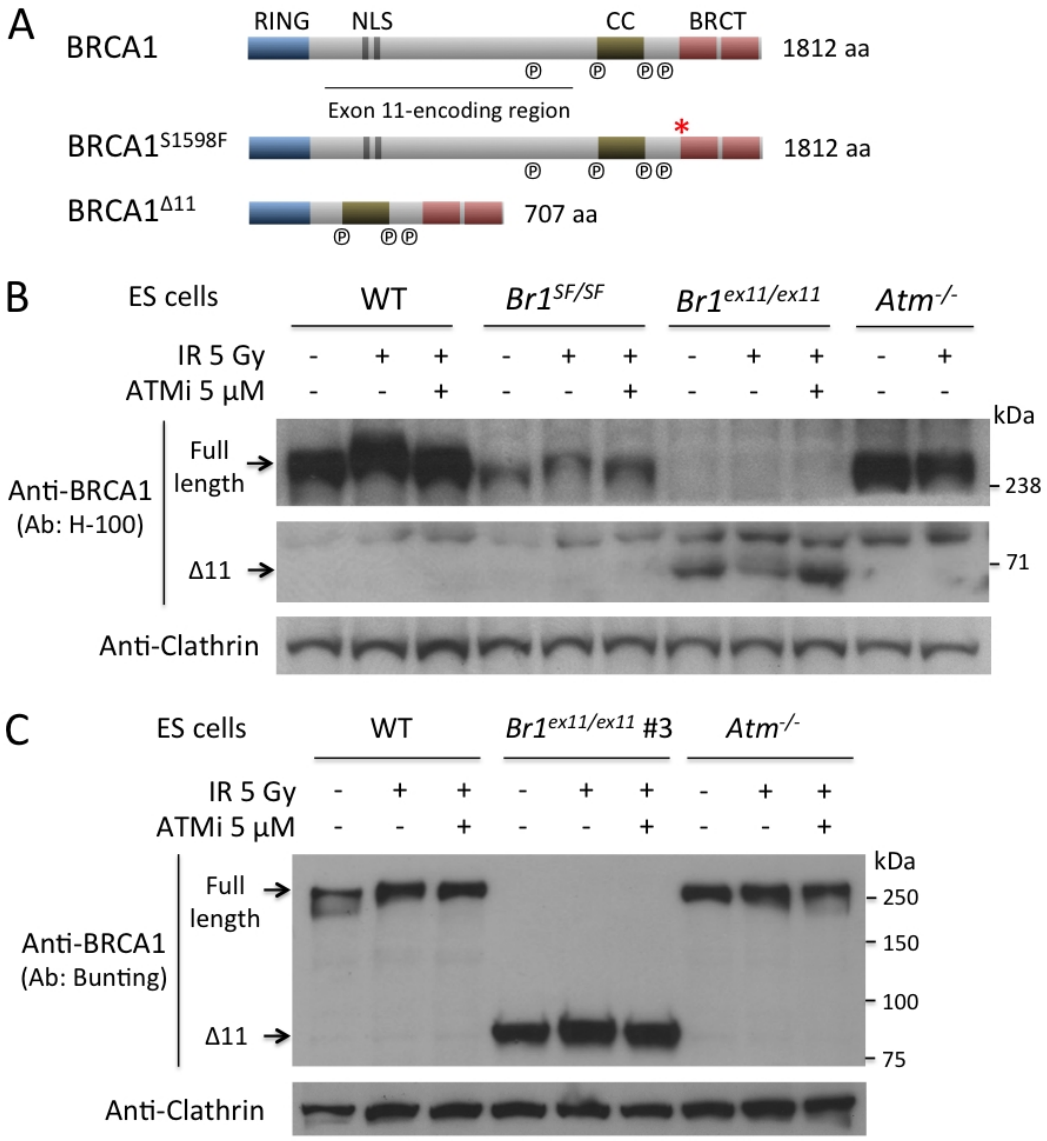

Figure 3.7 BRCA1 protein in WT and *Brca1*^{SF} cells shows an IR-induced mobility shift mediated by ATM.

A. Mouse BRCA1 protein contains at least 4 conserved ATM phosphorylation sites that correspond to human residues S1387, S1466, and S1524 around the coiled-coil domain as well as S1189 in the exon 11-encoding region.

B. The full-length BRCA1 protein in WT and *Brca1*$^{SF/SF}$ ES cells, but not *Atm*$^{-/-}$ cells, shows ATM-dependent mobility shift following IR. The BRCA1 Δ11 isoform does not show apparent mobility shift after IR despite migrating faster than the full-length BRCA1. The samples are separated on a 3-8% Tris-Acetate gradient gel and probed with an anti-BRCA1 polyclonal antibody against the N terminus (SantaCruz H-100).

C. The IR-induced mobility shift of BRCA1 Δ11 protein in *Brca1*$^{ex11/ex11}$ #3 cells is also not very evident on a 10% Tris-Glycine gel. The samples are probed with an anti-BRCA1 monoclonal antibody against the N terminus (provided by Samuel Bunting at Rutgers University).

DNA-PKcs inhibition. We also addressed whether the epistatic relationship of ATM and DNA-PKcs in HDR is different between the two *Brca1* mutants by combining inhibitors targeting either kinase. The results suggest that in $Brca1^{SF/SF}$ and WT ES cells, ATM and DNA-PKcs operate separately: ATM promotes HDR whereas DNA-PKcs suppresses HDR (Figure 3.6C). By contrast, in $Brca1^{ex11/ex11}$ ES cells, both ATM and DNA-PKcs activity lead to the suppression of HDR, with DNA-PKcs being the epistatic factor for this suppression (Figure 3.6C). These observations suggest that in the $Brca1^{ex11}$ mutant, the stronger competition from NHEJ stimulated by active DNA damage signaling likely plays a major role in its more severe HDR defects compared to the $Brca1^{SF}$ mutant.

Discussion

The study in this chapter uncovers an intriguing phenotype that ATM deficiency leads to distinct consequence on HDR depending on different BRCA1 mutations. In the $Brca1^{SF}$ mutant expressing a BRCT-defective peptide (20), ATM activity supports HDR and this regulation is independent of 53BP1, as in the BRCA1-proficient context. This is consistent with the synthetic lethality following ATM loss in $Brca1^{SF/SF}$ mice, which can be rescued by *53bp1* deletion that restores the HDR defect of $Brca1^{SF}$ but not *Atm* mutant (Chapter 2, (24)). By contrast, in the *Brca1* exon 11-skipping mutant, ATM has suppressive effects on HDR specifically in the presence of 53BP1, whereas loss of 53BP1 can restore ATM's supportive roles in HDR. This ambivalent regulation of ATM on HDR resonates with the observation in B cells that ATM can either suppress or promote resection of RAG-induced DSBs depending on the status of H2AX (38), reflecting the dynamic roles of ATM at DSBs.

Previous studies have shown that loss of ATM, CHK2, or p53 rescues the lethality of $Brca1^{\Delta 11/\Delta 11}$ mice via abolishing apoptosis triggered by excessive DNA

damage (17, 25). Intriguingly, ATM loss has stronger rescuing effect than p53 loss on the proliferation defect in the developing brain of mice carrying a *Brca1*^{ex11} allele (together with an exon 5−13 floxed allele) (39), suggesting an involvement of p53-independent functions of ATM in the phenotype of BRCA1$^{\Delta 11}$ mutant. Thus, we speculate that in addition to the relief of apoptosis, the distinct HDR response upon ATM deficiency may also contribute to the viability restoration in *Atm*$^{-/-}$*Brca1*$^{\Delta 11/\Delta 11}$ mice (i.e., ATM loss at least does not exacerbate HDR defect in this context in the presence of 53BP1). Nevertheless, reports show that the *Brca1*$^{\Delta 11/\Delta 11}$ mice rescued by CHK2 loss are still prone to tumorigenesis, unlike those rescued by 53BP1 loss (25, 26, 40). This indicates that the requirement for ATM in checkpoints and apoptosis is still critical for the maintenance of genome integrity on the organismal level (41).

Model 1: The unique structure of BRCA1$^{\Delta 11}$ protein affects interaction with repair proteins.

We hypothesize that the distinct HDR response in the BRCA1 exon 11-skipping mutant could be related to two main possibilities: mutant protein structure or altered DNA damage response.

The first possibility regards the structural difference between BRCA1^{SF} and BRCA1$^{\Delta 11}$ mutant proteins that influences ATM-dependent regulation and/or interaction with repair proteins. Among the mapped ATM phosphorylation sites on human BRCA1, at least four residues are conserved in mice and one of them is in the exon 11-encoding region (42-44) (Figure 3.7A). The significance of ATM phosphorylation on BRCA1-mediated HDR remains to be elucidated. The influence of ATM could also come from its downstream effectors, e.g., phosphorylation on BRCA1 by CHK2 (human S988 in exon 11-encoding region; also conserved in mice) is reported to promote HDR (45, 46). While attempting to address the roles of ATM activity in *Brca1* mutants, our preliminary results found that mouse BRCA1 protein in

WT and *Brca1*$^{SF/SF}$ ES cells, as expected, undergoes an apparent IR-induced mobility shift that could be attenuated by ATM inhibition (Figure 3.7 B and C, full-length position). The BRCA1$^{\Delta 11}$ isoform also appeared to undergo a mobility shift following IR but the change was much less pronounced (Figure 3.7 B and C, Δ11 position) (28). BRCA1$^{\Delta 11}$ isoform still contains some ATM phosphorylation sites (Figure 3.7A) but is reported to lack a putative ATM-interacting region located within the exon 11-encoding region, however this needs to be further studied (43). It is plausible that some alterations of post-translational modification or interaction may contribute to a different interplay with ATM and 53BP1 at breaks. For example, ATM activity could be supporting the hypomorphic functions of BRCA1^{SF} in antagonizing 53BP1, resulting in the dependence on ATM for residual HDR; however, such signaling crosstalk with ATM may be lacking for BRCA1$^{\Delta 11}$, thus leading to more severe defects, as reflected on the inviability of *Brca1*$^{\Delta 11/\Delta 11}$ mice in *53bp1*$^{+/+}$ condition, but no further HDR reduction upon ATM loss (as in olaparib sensitivity assay, Figure 3.4A). Given that BRCA1$^{\Delta 11}$ can localize to chromatin (28), the presence of this structurally distinct mutant may also interfere with repair dynamics or have unidentified biological effects, as observed for another human BRCA1 isoform IRIS (terminate in the intron downstream of exon 11) in stimulating DNA replication (47). For example, perhaps BRCA1$^{\Delta 11}$ can promote ATM and/or DNA-PKcs activity through the interaction of BRCT domain with the BAAT1 protein (48, 49), but it lacks certain feedback regulation to attenuate the signaling. Furthermore, recent studies show that BRCA1 is capable of forming dimers or higher order structures via the BRCA1-A (Abraxas) complex assembly (50, 51), raising the question that if this molecular interaction is preserved for the BRCA1$^{\Delta 11}$ protein that may in turn affect the regulation of the Abraxas/RAP80 complex on chromatin binding and end resection.

Model 2: Excessive DNA damage signaling in BRCA1$^{\Delta 11}$ mutant affects ATM-53BP1 interplay and repair pathway antagonism.

Alternatively, we propose a model that the unique interplay between ATM and 53BP1 in the BRCA1$^{\Delta 11}$ mutant arises from excessive levels of DNA damage signaling that further exacerbates the deficiency in repair pathway antagonism, thus contributing to the different phenotype from the BRCA1^{SF} mutant. Specifically, we found that *Brca1*$^{ex11/ex11}$ cells display highly elevated DNA damage response mediated by ATM and DNA-PKcs following DSB accumulation compared to *Brca1*$^{SF/SF}$ cells. This is in part due to the more severe repair defect of BRCA1$^{\Delta 11}$ mutant protein, which can be rescued by 53BP1 loss (Figure 3.5C), but may also be caused by other unidentified mechanisms (e.g., the aforementioned protein structure model). The elevated DNA damage signaling in the BRCA1$^{\Delta 11}$ mutant presumably acts as a safeguard to stop cell cycle progression, but it could also have a consequence in the regulation of DSB repair pathway choice. For example, given that both ATM and DNA-PKcs phosphorylate 53BP1 and H2AX (52-54), this may promote higher level of 53BP1 function and/or recruitment at breaks that further suppresses the residual HDR. High DNA-PK activity may also promote more NHEJ that can compete with HDR (55) (Figure 3.6A). Therefore, in the presence of 53BP1, HDR in the BRCA1$^{\Delta 11}$ mutant becomes strongly suppressed by this signaling amplification, i.e., in this context, ATM has more involvement in 53BP1-mediated HDR suppression than HDR promotion (Figure 3.8A). This leads to genome instability during embryonic development that in turn triggers ATM/p53-mediated apoptosis and animal lethality. This helps explain our observations that HDR is increased in *Brca1*$^{ex11/ex11}$ cells following ATM inhibition (Figure 3.3C) as well as the rescue of animal lethality by *Atm* mutation (25), since the suppression on HDR by the ATM-53BP1 pathway becomes relieved. Our results also suggest that DNA-PKcs is highly active in *Brca1*$^{ex11/ex11}$ cells and appears to be the

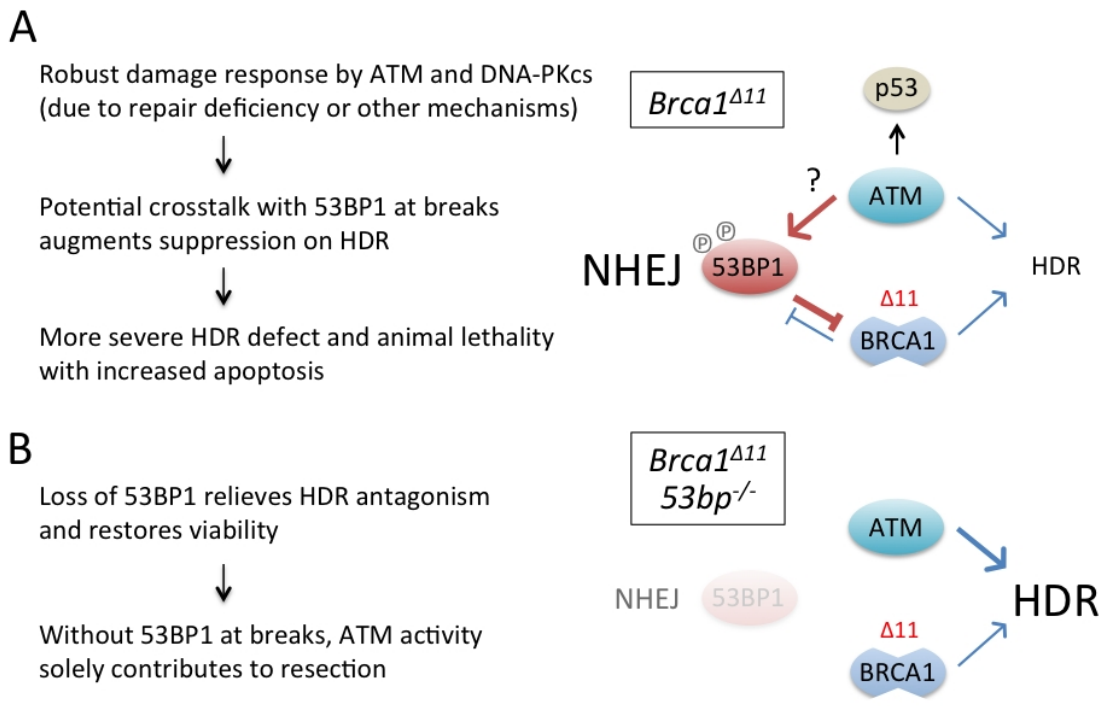

Figure 3.8 Model: ATM-53BP1 interplay contributes to the severe phenotype in *Brca1*$^{\Delta 11}$ mutant mice.
A. We propose a model that the high levels of DNA damage response in the *Brca1*$^{\Delta 11}$ mutant leads to a signaling crosstalk between ATM and 53BP1 at breaks. This ATM-53BP1 interplay exacerbates the imbalance of NHEJ-HDR pathway antagonism and in turn causes animal lethality, apart from ATM's function in triggering apoptosis. See discussion for details.
B. Loss of ATM, 53BP1, or p53 relieves the negative regulation on HDR and viability in *Brca1*$^{\Delta 11}$ mutant mice. In particular, following loss of 53BP1, the signaling amplification due to HDR deficiency is abolished and the repair aspect of ATM activity now only contributes to end resection, thus ATM resumes its positive role in HDR.

predominant kinase at breaks, whose inhibition causes an even higher increase in HDR than ATM inhibition (Figure 3.6C). Overall, this supports the notion that the robust DNA damage signaling in the BRCA1$^{\Delta 11}$ mutant following DSBs leads to a severe imbalance of NHEJ-mediated antagonism against HDR.

On the other hand, whereas loss of 53BP1 rescues HDR defect in *Brca1*$^{ex11/ex11}$ cells, ATM inhibition in *Brca1*$^{ex11/ex11}$*53bp1*$^{-/-}$ cells starts to reduce HDR and augment olaparib sensitivity (Figures 3.3C and 3.4A). This is consistent with the report of Bunting et al. that HDR in *Brca1*$^{\Delta 11/\Delta 11}$*53bp1*$^{-/-}$ B cells is dependent on ATM and that ATM inhibition increases PARPi sensitivity in *Brca1*$^{\Delta 11/\Delta 11}$*53bp1*$^{-/-}$ but not no much in *Brca1*$^{\Delta 11/\Delta 11}$ (p53$^{-/-}$) B cells (see Figure 5 in reference (26)). Loss of 53BP1 in BRCA1$^{\Delta 11}$ mutant restores HDR in the first place that eliminates DSB accumulation and the amplification DNA damage signaling. Furthermore, in the absence of 53BP1 protein at breaks, we think the repair aspect of ATM activity now mainly contributes to end resection factors. Thus, these results probably reflect a shift in the balance of ATM function from 53BP1-mediated NHEJ towards HDR following 53BP1 loss in the BRCA1$^{\Delta 11}$ mutant (Figure 3.8B).

Methods

Mouse ES cell culture and transfection. *Brca1*$^{ex11/ex11}$ (half of exon 11 including splice acceptor replaced by a *Neo*^{R} cassette; also known as *Brca1*$^{\Delta 223\text{-}763}$ (23)) ES cell line was previously integrated with a *Pim1*$^{Hyg/Puro}$ DR-GFP allele by Mary Ellen Moynahan in the lab (21). *Brca1*$^{SF/SF}$ (20) (DR-GFP clone A8) and WT J1 (DR-GFP clone 8) ES cell lines as well as general culture conditions were described in Chapter 2 methods. Typically a total of 3-3.5 × 10^6 cells and 30 μg plasmid DNA were used for each electroporation, which was enough to be split to 3-4 treatment conditions in 6-well plate. The trypsinized cells were resuspended in 600 μl Opti-MEM, mixed with

pCBASce plasmid, and pulsed in a 0.4 cm cuvette at 250 V / 950 μF (sometimes lowered to 230 V / 950 μF when more cell death occurred after pulsing). After pulsing, the cells were mixed with warm growth medium and equally split for different treatments in 6-well plate. For ATM inhibition, the transfection mixture was split to wells containing the ATMi KU-55933 (Calbiochem #118502, 10 mM solution) or equal volume of DMSO, replenished every 24 hr if doing long treatments. For DNA-PKcs inhibition, the DNA-PKi NU-7441 (Tocris #3712) was used.

Mutagenesis of mouse *53bp1*. The method of disrupting mouse *53bp1* gene was previously described (31). Briefly, a DSB was introduced in *53bp1* exon 2 by CRISPR/Cas9 to facilitate the replacement of exon 2 with a promoter-less Hyg^R or Neo^R cassette by HDR. Sequence of *53bp1* gRNA1: 5'-GAC CCT ACT GGA AGT CAA T-3' (19 bp, PAM is not listed). A total 4×10^6 early-passaging cells were electroporated at 250V / 950μF with 10 μg CAGGS-Cas9 plasmid, 10 μg gRNA plasmid, and 20 μg of exon 2 targeting template (circular form). After 48 hr, cells were replated at a density of 5×10^5 cells per 10-cm dish (3-5 dishes total) and selected either in 120 μg/ml Hygromycin B Gold (InvivoGen) or 400 μg/ml G418 (Gibco) for ~1 week until the colonies became visible for picking. After the clones became confluent in 96-well plate, they were trypsinized in 30 μl trypsin, and 10 μl of the cell suspension was transferred to a new 24- or 12-well plate whereas 10 μl was mixed with 30 μl 1X cell lysis buffer (10 mM Tris pH 8, 0.45% NP40, 0.45% Tween 20, and 100 μg/ml fresh Proteinase K). The mixture were incubated at 55°C for 2 hr and then 95°C for 5 min to inactivate the Proteinase K, and the cell lysates can be directly used for PCR genotyping (typically using 1 μl per reaction) or stored at -20°C.

The targeted clones were initially screened using primers amplifying across exon 2 within both homology arms (Universal-F: 5'-CTG AGA AAG TGC TAA GAG CG-3'; Universal-R: 5'-ACC TTT CTG TGG GTG AGA AC-3') and primers

amplifying from the inside of left homology arm to the outside of right homology arm (Universal-F: see above; Check-3R: 5'-CAT CCT GAT ATG CAT AAG ACA CTG-3'). The first primer set (internal PCR) had better amplification efficiency than the latter one (In-Out PCR). Clones showing the *53bp1* exon 2 potentially with targeting cassette integration or with band shifts indicating indels following gRNA cutting were subjected to western blotting directly to examine the status of 53BP1 protein expression. Mutation of *53bp1* was performed in a $Brca1^{ex11/ex11}$ clone #3 previously established by Yu Zhang in the lab that had undergone a first round of CRISPR/Cas9-medated mutagenesis to disrupt a Hyg^{R} marker gene at the $Pim1^{Drgfp}$ allele to allow for the use of Hyg^{R} selection method. Mutation of *53bp1* in $Brca1^{SF/SF}$ cells was performed in the DR-GFP clone A8. Mutation of *53bp1* in WT cells was performed in the J1 DR-GFP clone 8. The targeting experiments and screening processes were performed with the assistance of a volunteering student Megan Mandile in the lab.

Colony formation assay. Mouse ES cells were plated at a density of 1000 cells per well in 6-well plates overnight. For combination with ATMi, cells were pre-treated with 3 μM ATMi or DMSO for 2 hr, and then treated with olaparib in combination with ATMi or equal amount of DMSO for 48 hr. After that, the cells were gently washed with PBS once and then incubated with medium containing only ATMi or DMSO for another 3-4 days until colonies become visible. The colonies were fixed in 100% methanol for 20 min and then stained in 3% Giemsa for 3-4 hr. For combination with the DNA-PK inhibitor NU-7441, cells were treated with olaparib in combination with DNA-PKi or equal amount of DMSO for 48 hr, then washed and changed to blank growth medium for another 3-4 days. Longer incubation (>48 hr) or higher doses of DNA-PKi NU-7441 (>1 μM) has suppressive effects on the general growth of mouse ES cells.

Western blotting. Proliferating cells were scraped from dishes and lysed for 30 min on ice in TEGN buffer with freshly added 1 mM DTT and 1X protease/phosphatase inhibitors. Lysates were centrifuged and the supernatant was collected. See also Chapter 2 methods. Typically an amount of 30 μg protein was loaded for each lane. BRCA1 and 53BP1 were separated on 3-8% Tris-Acetate gels (Invitrogen) and transferred to a PVDF membrane in Tris-Glycine buffer (25 mM Tris, 192 mM glycine) containing 0.01% SDS and 10% methanol at 22 V, 4°C overnight. γH2AX was separated on 4-20% Tris-Glycine eXtended gels (Bio-Rad) and transferred to PVDF membrane in Tris-Glycine buffer containing 20% methanol at 90 V, room temperature (RT) 1 hr. Blocking was performed in 5% non-fat milk in PBST at RT for 1 hr. Primary antibodies were diluted in 2.5% milk or 5% BSA (when mentioned) and incubated at 4°C overnight on a rotator. HRP-conjugated secondary antibodies were diluted 1:10000 in 2.5% milk and incubated at RT for 1 hr on a shaker. Each incubation was followed by three 10-min washes in PBST. Primary antibodies used: Anti-53BP1, 1:4000 (Novus NB100-304); Anti-BRCA1, polyclonal 1:1000 in 5% BSA (Santa Cruz H-100 sc7867, lot # D280, discontinued; epitope human BRCA1 amino acids 1-100) or monoclonal 1:500 in 5% BSA (provided by Samuel Bunting at Rutgers University; epitope mouse BRCA1 amino acids 160-300); Anti-CHK2: 1:1000 (Millipore 05-649); Anti-γH2AX-Ser139: 1:750 in 5% BSA (Millipore 05-636); Anti-KAP1-pSer824: 1:2000 (Bethyl Laboratories A300-767A); Anti-Clathrin heavy chain, 1:10000 (BD Biosciences 610500); Anti-α-Tubulin: 1:10000 (Sigma T9026).

Statistical analysis. Statistical comparisons were calculated using two-tailed Student's t-test. All error bars in figures represent one standard deviation from the mean.

REFERENCES

1. Bouwman P*, et al.* (2013) A high-throughput functional complementation assay for classification of BRCA1 missense variants. *Cancer Discov.* 3(10):1142-1155.
2. Anantha RW*, et al.* (2017) Functional and mutational landscapes of BRCA1 for homology-directed repair and therapy resistance. *Elife* 6.
3. Orban TI & Olah E (2001) Expression profiles of BRCA1 splice variants in asynchronous and in G1/S synchronized tumor cell lines. *Biochem. Biophys. Res. Commun.* 280(1):32-38.
4. Colombo M*, et al.* (2014) Comprehensive annotation of splice junctions supports pervasive alternative splicing at the BRCA1 locus: a report from the ENIGMA consortium. *Hum. Mol. Genet.* 23(14):3666-3680.
5. Tammaro C, Raponi M, Wilson DI, & Baralle D (2012) BRCA1 exon 11 alternative splicing, multiple functions and the association with cancer. *Biochem. Soc. Trans.* 40(4):768-772.
6. Fabbro M, Rodriguez JA, Baer R, & Henderson BR (2002) BARD1 induces BRCA1 intranuclear foci formation by increasing RING-dependent BRCA1 nuclear import and inhibiting BRCA1 nuclear export. *J. Biol. Chem.* 277(24):21315-21324.
7. Westermark UK*, et al.* (2003) BARD1 participates with BRCA1 in homology-directed repair of chromosome breaks. *Mol. Cell. Biol.* 23(21):7926-7936.
8. Paull TT, Cortez D, Bowers B, Elledge SJ, & Gellert M (2001) Direct DNA binding by Brca1. *Proc. Natl. Acad. Sci. U. S. A.* 98(11):6086-6091.
9. Scully R*, et al.* (1997) Association of BRCA1 with Rad51 in mitotic and meiotic cells. *Cell* 88(2):265-275.
10. Zhao W*, et al.* (2017) BRCA1-BARD1 promotes RAD51-mediated homologous DNA pairing. *Nature* 550(7676):360-365.
11. Masuda T, Xu X, Dimitriadis EK, Lahusen T, & Deng CX (2016) "DNA Binding Region" of BRCA1 Affects Genetic Stability through modulating the Intra-S-Phase Checkpoint. *Int J Biol Sci* 12(2):133-143.
12. Wang Y*, et al.* (2016) The BRCA1-Delta11q Alternative Splice Isoform Bypasses Germline Mutations and Promotes Therapeutic Resistance to PARP Inhibition and Cisplatin. *Cancer Res.* 76(9):2778-2790.
13. Xu X*, et al.* (1999) Conditional mutation of Brca1 in mammary epithelial cells results in blunted ductal morphogenesis and tumour formation. *Nat. Genet.* 22(1):37-43.
14. Shen SX*, et al.* (1998) A targeted disruption of the murine Brca1 gene causes gamma-irradiation hypersensitivity and genetic instability. *Oncogene* 17(24):3115-3124.
15. Gowen LC, Johnson BL, Latour AM, Sulik KK, & Koller BH (1996) Brca1 deficiency results in early embryonic lethality characterized by neuroepithelial abnormalities. *Nat. Genet.* 12(2):191-194.

16. Kim SS, *et al.* (2006) Hyperplasia and spontaneous tumor development in the gynecologic system in mice lacking the BRCA1-Delta11 isoform. *Mol Cell Biol* 26(18):6983-6992.
17. Xu X, *et al.* (2001) Genetic interactions between tumor suppressors Brca1 and p53 in apoptosis, cell cycle and tumorigenesis. *Nat. Genet.* 28(3):266-271.
18. Ludwig T, Chapman DL, Papaioannou VE, & Efstratiadis A (1997) Targeted mutations of breast cancer susceptibility gene homologs in mice: lethal phenotypes of Brca1, Brca2, Brca1/Brca2, Brca1/p53, and Brca2/p53 nullizygous embryos. *Genes Dev.* 11(10):1226-1241.
19. Hakem R, de la Pompa JL, Elia A, Potter J, & Mak TW (1997) Partial rescue of Brca1 (5-6) early embryonic lethality by p53 or p21 null mutation. *Nat. Genet.* 16(3):298-302.
20. Shakya R, *et al.* (2011) BRCA1 tumor suppression depends on BRCT phosphoprotein binding, but not its E3 ligase activity. *Science* 334(6055):525-528.
21. Moynahan ME, Cui TY, & Jasin M (2001) Homology-directed dna repair, mitomycin-c resistance, and chromosome stability is restored with correction of a Brca1 mutation. *Cancer Res.* 61(12):4842-4850.
22. Moynahan ME, Chiu JW, Koller BH, & Jasin M (1999) Brca1 controls homology-directed DNA repair. *Mol. Cell* 4(4):511-518.
23. Snouwaert JN, *et al.* (1999) BRCA1 deficient embryonic stem cells display a decreased homologous recombination frequency and an increased frequency of non-homologous recombination that is corrected by expression of a brca1 transgene. *Oncogene* 18(55):7900-7907.
24. Chen CC, *et al.* (2017) ATM loss leads to synthetic lethality in BRCA1 BRCT mutant mice associated with exacerbated defects in homology-directed repair. *Proc. Natl. Acad. Sci. U. S. A.* 114(29):7665-7670.
25. Cao L, *et al.* (2006) ATM-Chk2-p53 activation prevents tumorigenesis at an expense of organ homeostasis upon Brca1 deficiency. *EMBO J.* 25(10):2167-2177.
26. Bunting SF, *et al.* (2010) 53BP1 inhibits homologous recombination in Brca1-deficient cells by blocking resection of DNA breaks. *Cell* 141(2):243-254.
27. Clapperton JA, *et al.* (2004) Structure and mechanism of BRCA1 BRCT domain recognition of phosphorylated BACH1 with implications for cancer. *Nat. Struct. Mol. Biol.* 11(6):512-518.
28. Huber LJ, *et al.* (2001) Impaired DNA damage response in cells expressing an exon 11-deleted murine Brca1 variant that localizes to nuclear foci. *Mol. Cell. Biol.* 21(12):4005-4015.
29. Li M & Yu X (2013) Function of BRCA1 in the DNA damage response is mediated by ADP-ribosylation. *Cancer Cell* 23(5):693-704.
30. Au WW & Henderson BR (2005) The BRCA1 RING and BRCT domains cooperate in targeting BRCA1 to ionizing radiation-induced nuclear foci. *J. Biol. Chem.* 280(8):6993-7001.

31. Zhang Y, Vanoli F, LaRocque JR, Krawczyk PM, & Jasin M (2014) Biallelic targeting of expressed genes in mouse embryonic stem cells using the Cas9 system. *Methods* 69(2):171-178.
32. Bunting SF*, et al.* (2012) BRCA1 functions independently of homologous recombination in DNA interstrand crosslink repair. *Mol. Cell* 46(2):125-135.
33. Chanut P, Britton S, Coates J, Jackson SP, & Calsou P (2016) Coordinated nuclease activities counteract Ku at single-ended DNA double-strand breaks. *Nat Commun* 7:12889.
34. Patel AG, Sarkaria JN, & Kaufmann SH (2011) Nonhomologous end joining drives poly(ADP-ribose) polymerase (PARP) inhibitor lethality in homologous recombination-deficient cells. *Proc. Natl. Acad. Sci. U. S. A.* 108(8):3406-3411.
35. Stark JM, Pierce AJ, Oh J, Pastink A, & Jasin M (2004) Genetic steps of mammalian homologous repair with distinct mutagenic consequences. *Mol. Cell. Biol.* 24(21):9305-9316.
36. Ghezraoui H*, et al.* (2014) Chromosomal translocations in human cells are generated by canonical nonhomologous end-joining. *Mol Cell* 55(6):829-842.
37. Simsek D*, et al.* (2011) DNA ligase III promotes alternative nonhomologous end-joining during chromosomal translocation formation. *PLoS Genet* 7(6):e1002080.
38. Helmink BA*, et al.* (2011) H2AX prevents CtIP-mediated DNA end resection and aberrant repair in G1-phase lymphocytes. *Nature* 469(7329):245-249.
39. Pao GM*, et al.* (2014) Role of BRCA1 in brain development. *Proc. Natl. Acad. Sci. U. S. A.* 111(13):E1240-1248.
40. Cao L*, et al.* (2009) A selective requirement for 53BP1 in the biological response to genomic instability induced by Brca1 deficiency. *Mol. Cell* 35(4):534-541.
41. Callen E*, et al.* (2007) ATM prevents the persistence and propagation of chromosome breaks in lymphocytes. *Cell* 130(1):63-75.
42. Cortez D, Wang Y, Qin J, & Elledge SJ (1999) Requirement of ATM-dependent phosphorylation of brca1 in the DNA damage response to double-strand breaks. *Science* 286(5442):1162-1166.
43. Gatei M*, et al.* (2000) Role for ATM in DNA damage-induced phosphorylation of BRCA1. *Cancer Res.* 60(12):3299-3304.
44. Matsuoka S*, et al.* (2007) ATM and ATR substrate analysis reveals extensive protein networks responsive to DNA damage. *Science* 316(5828):1160-1166.
45. Parameswaran B*, et al.* (2015) Damage-induced BRCA1 phosphorylation by Chk2 contributes to the timing of end resection. *Cell cycle* 14(3):437-448.
46. Zhang J*, et al.* (2004) Chk2 phosphorylation of BRCA1 regulates DNA double-strand break repair. *Mol. Cell. Biol.* 24(2):708-718.
47. ElShamy WM & Livingston DM (2004) Identification of BRCA1-IRIS, a BRCA1 locus product. *Nat Cell Biol* 6(10):954-967.
48. Aglipay JA, Martin SA, Tawara H, Lee SW, & Ouchi T (2006) ATM activation by ionizing radiation requires BRCA1-associated BAAT1. *J. Biol. Chem.* 281(14):9710-9718.

49. So EY & Ouchi T (2011) Functional interaction of BRCA1/ATM-associated BAAT1 with the DNA-PK catalytic subunit. *Exp. Ther. Med.* 2(3):443-447.
50. Kyrieleis OJ*, et al.* (2016) Three-Dimensional Architecture of the Human BRCA1-A Histone Deubiquitinase Core Complex. *Cell Rep* 17(12):3099-3106.
51. Wu Q*, et al.* (2016) Structure of BRCA1-BRCT/Abraxas Complex Reveals Phosphorylation-Dependent BRCT Dimerization at DNA Damage Sites. *Mol. Cell* 61(3):434-448.
52. Callen E*, et al.* (2009) Essential role for DNA-PKcs in DNA double-strand break repair and apoptosis in ATM-deficient lymphocytes. *Mol. Cell* 34(3):285-297.
53. Harding SM & Bristow RG (2012) Discordance between phosphorylation and recruitment of 53BP1 in response to DNA double-strand breaks. *Cell cycle* 11(7):1432-1444.
54. Stiff T*, et al.* (2004) ATM and DNA-PK function redundantly to phosphorylate H2AX after exposure to ionizing radiation. *Cancer Res* 64(7):2390-2396.
55. Pierce AJ, Hu P, Han M, Ellis N, & Jasin M (2001) Ku DNA end-binding protein modulates homologous repair of double-strand breaks in mammalian cells. *Genes Dev.* 15(24):3237-3242.

CHAPTER FOUR

DISCUSSION AND CONCLUSION

The concept of synthetic lethality has been widely recognized in the development of targeted therapies against HDR-deficient tumors. Elucidating the molecular mechanisms of HDR not only helps us understand how cells maintain genome integrity but can also identify more druggable targets for treatment of cancers and related genetic disorders such as Fanconi anemia. In this study, we focus on three key regulators in the early steps of DSB repair: ATM, BRCA1, and 53BP1, and address how their genetic interaction influences DSB repair pathway choice, in particular HDR.

Our work provides evidence that ATM has a context-dependent role in HDR. Loss of ATM in mouse primary cells leads to a moderate reduction in HDR, whereas its deficiency causes a delayed HDR response upon I-SceI-induced DSBs in mouse ES cells, possibly related to certain properties of ES cells (see discussion in Chapter 2). We consider ATM as a minor pathway for end resection and HDR in BRCA1-proficient cells that can operate independently of the BRCA1-53BP1 antagonism. Intriguingly, our genetic analysis shows that the regulation of ATM on HDR can be differentially affected by BRCA1 hypomorphic mutations (Figure 4.1). In the context of a breast cancer-derived $BRCA1^{S1598F}$ mutation in the BRCT domain, ATM becomes essential for supporting the residual HDR and viability, and this positive contribution of ATM to HDR is independent of 53BP1. This is distinct from the phenotype of a $BRCA1^{\Delta 11}$ splicing isoform skipping the exon 11-encoding region, where ATM shows opposing effects on HDR that are modulated by the status of 53BP1, i.e., ATM promotes HDR only in the absence of 53BP1 in mutant cells expressing the $BRCA1^{\Delta 11}$

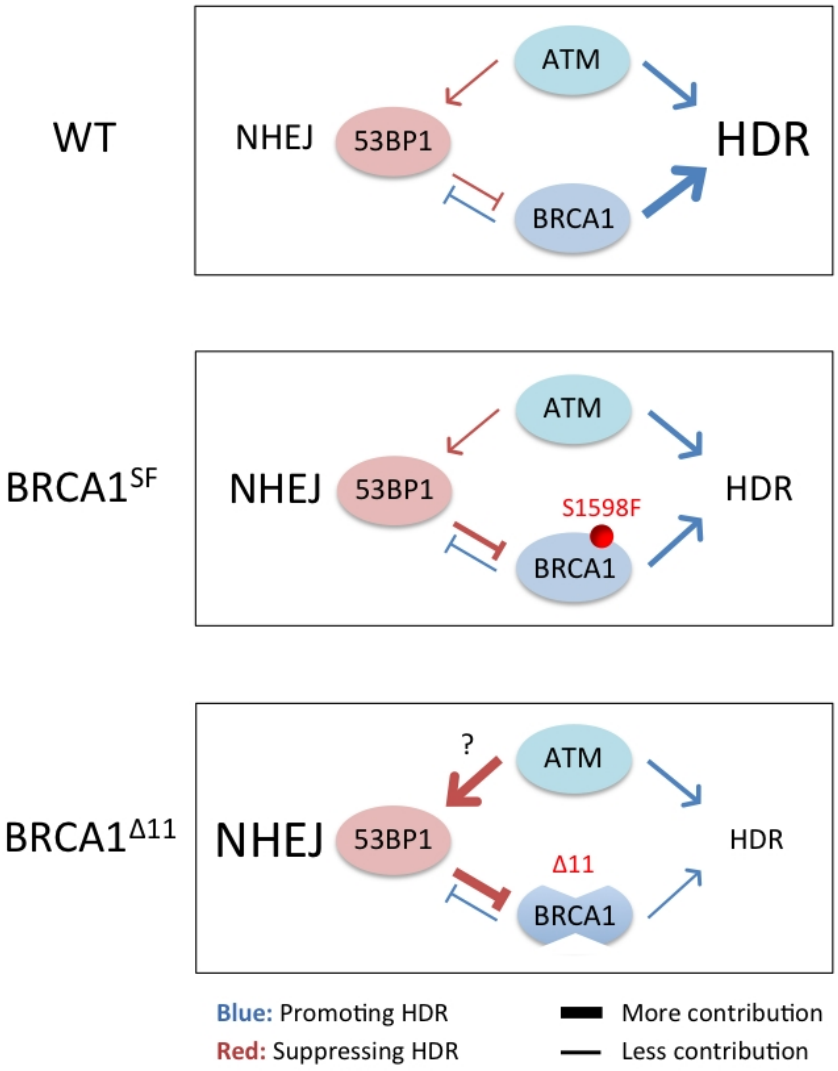

Figure 4.1 Mutations in the BRCT domain and central region of BRCA1 differentially affect how ATM participates in HDR in mice.
In *Brca1*$^{+/+}$ cells (top), BRCA1 has an essential role in HDR via counteracting 53BP1 in S/G2 phases. ATM acts as a minor pathway for HDR but also contributes to 53BP1 function in G1 phase. Both BRCA1^{SF} and BRCA1$^{\Delta 11}$ mutants have compromised HDR and are defective in counteracting 53BP1. In *Brca1*$^{SF/SF}$ cells (middle), ATM becomes crucial for supporting the residual HDR and this process is independent of 53BP1. In *Brca1*$^{ex11/ex11}$ cells (bottom), HDR is suppressed by ATM activity and NHEJ-mediated competition in the presence of 53BP1, whereas loss of 53BP1 allows ATM to resume the supporting role in HDR.

isoform. Our observations demonstrate how mutations on different domains of BRCA1 could drastically change the interplay of HDR and NHEJ pathways, providing clinical implications such as targeting *BRCA1* tumors carrying BRCT mutations specifically with the combination of ATMi and PARPi to achieve better efficacy.

Potential mechanisms for the synthetic lethality of *Atm-Brca1*^{SF} double mutant

Given that HDR is essential for maintaining genome stability during embryonic development and that ATM activity supports the residual end resection (HDR and SSA) in *Brca1*$^{SF/SF}$ cells, we think the most plausible explanation for the synthetic lethality is an exacerbated defect in HDR proficiency that compromises embryogenesis. Strong support for this notion is the rescue of animal lethality by homozygous and even heterozygous mutation of *53bp1*, which correspond to the full and partial HDR restoration in *Brca1*$^{SF/SF}$*53bp1*$^{-/-}$ and *Brca1*$^{SF/SF}$*53bp1*$^{+/-}$ cells, respectively. In addition to HDR, BRCA1 participates in the protection of stalled replication forks and interstrand crosslink (ICL) repair (1-3). Because recent studies suggest that fork protection is not essential for viability (4) and that 53BP1 loss does not rescue the defects in fork protection and ICL repair in BRCA1 mutant cells (2, 5), we think HDR plays an important role in the *Atm-Brca1*^{SF} lethality. We also think the lethality is not likely caused by the lack of ATM-mediated regulation of DNA damage checkpoints and apoptosis, because loss of CHK2 does not lead to synthetic lethality and CHK2 inhibition does not reduce HDR to the significant extent as ATM inhibition in the *Brca1*^{SF} mutant. In fact, heterozygosity of *Atm* (and *Chk2*) partially rescues the sub-viability of *Brca1*$^{SF/SF}$ single mutant, which is contrary to the lethality with homozygous mutation of *Atm* in the *Brca1*$^{SF/SF}$ mutant. These observations suggest that the *Atm-Brca1*^{SF} synthetic lethality is likely related to apoptosis-independent functions of ATM.

We think there are several possibilities regarding why the BRCA1^{SF} BRCT mutation shows synthetic lethality with ATM deficiency. First, the *Brca1*^{SF} mutant may be relying on ATM for regulation of end resection. The BRCT domain of BRCA1 binds to a number of repair proteins including Abraxas, BRIP1, CtIP, ATRIP, and BAAT1 (reviewed in (6)); it also binds DNA-PKcs in a phospho-independent manner (7). The interaction of BRCA1 with CtIP and Abraxas is reported to help modulate the extent of end resection (8-10). A similar role for ATM in fine-tuning resection is also proposed (11-13). As the loss of binding with CtIP alone does not recapitulate the *Brca1*^{SF} phenotype (14, 15), it will be important to determine if loss of interaction with either a specific or combination of factor(s), e.g., Abraxas, contributes to a dependence on ATM to control the length of resected DNA. Given the consensus phosphorylation site (pSer-Pro) in the BRCT-binding motif of these repair proteins (6), it will also be interesting to know if certain responsible kinases are involved in this HDR regulation.

Second, phosphorylation by ATM may be directly affecting the functions of BRCA1^{SF} protein. Mutation of the ATM phosphorylation site on BRCA1 alone or in combination results in phenotypes such as mammary gland abnormalities and radiosensitivity in mice as well as failure to support viability in mouse ES cells (16, 17). However, it is still unclear if ATM-mediated phosphorylation directly regulates the functions of BRCA1 in repair pathway choice, as it does on 53BP1 for recruiting RIF1 and PTIP. For example, it is possible that ATM-mediated phosphorylation is dispensable for BRCA1 WT protein in the antagonism against 53BP1, as the HDR defect of *Atm* mutant is not affected by 53BP1 loss; however, the phosphorylation may have a role in supporting the hypomorphic BRCA1^{SF} protein physically counteract 53BP1, e.g., in 53BP1 spatial reposition (18). This can be addressed by complementing with BRCA1 carrying mutations on ATM phosphorylation sites.

Third, we consider the possibility that other functions of the BRCA1 BRCT domain contribute to the synthetic defect. Studies have shown that the C terminus of BRCA1 contains transactivation activity and can interact with transcription coactivators such as CBP/p300 or with RNA polymerase II holoenzyme (19-23). It will be interesting to determine if ATM has a role in compensating for this regulation in the *Brca1*^{SF} mutant, whose human equivalent S1655F is shown to be defective in the transactivation activity (24). Given that BRCT domain mutations (including human S1655F) impact BRCA1 peptide folding (24), the potential effects of BRCA1^{SF} protein instability on HDR can also be examined, e.g., by comparing the inhibition of the proteasome versus heat shock proteins. In addition, recent studies suggest that BRCA1 suppresses tumor formation in part via regulating anti-oxidant signaling and metabolism (25-27). For example, the BRCT domain of BRCA1 binds and suppresses the acetyl-CoA carboxylase 1, which is linked to lipid anabolism in cancer (28-30). Given the critical function of ATM in cellular redox homeostasis (31), it will be worth knowing whether oxidative stress also plays a part in the synthetic lethality of *Atm-Brca1*^{SF} mice , as reported in the *Atm-H2ax* mice (32).

Potential mechanisms for the distinct HDR response to ATM deficiency in the BRCA1$^{\Delta 11}$ mutant

As discussed extensively in Chapter 3, we propose that the distinct HDR response in the BRCA1 exon 11-skipping mutant upon ATM deficiency may be caused by a more pronounced DNA damage response due to less efficient repair that affects the ATM-53BP1 interplay. Alternatively, it could be caused by the specific structure of this isoform disrupting repair at DSB sites. The exon 11-encoding region of BRCA1 interacts with RAD51, and recent studies suggest that the complex formation of BRCA1 with BARD1, which also has RAD51-binding ability, can stimulate RAD51-mediated strand exchange *in vitro* (33, 34). However, given that both the BRCA1$^{\Delta 11}$

and BRCA1^{SF} proteins retain the BARD1-binding RING domain and that the HDR defect in both mutants is rescued to a similar extent by 53BP1 loss in ES cells, we think the presumed loss of interaction with RAD51 in the BRCA1$^{\Delta 11}$ mutant is not relevant to the different HDR phenotype upon ATM inhibition. The exon 11-encoding region has also been shown to possess DNA binding ability (35), but specific deletion of this region does not appear to have a strong impact on HDR (36). Another study has shown that the BRCA1-Abraxas complex mediates PARylation in the DNA-binding region of BRCA1 to control HDR (37); however, if this is the case, both BRCA1^{SF} (lacking Abraxas binding) and BRCA1$^{\Delta 11}$ (lacking PARylation sites) would be predicted to have similar defective phenotypes. Thus, lacking the DNA-binding function is not likely the main cause for the distinct response to ATMi in BRCA1$^{\Delta 11}$ mutant.

Here we discuss several directions that potentially address the distinct HDR response in the BRCA1$^{\Delta 11}$ mutant, in particular focusing on 53BP1 regulation and BRCT domain-related functions of BRCA1 such as chromatin localization and resection. First, because 53BP1 has opposing effects on how ATM activity affects HDR, we think the priority is to examine if there is any difference in the regulation of ATM-53BP1 pathway. This should preferably be done using an isogenic system to analyze the phenotypes of different BRCA1 mutations under the same cellular context. It will be important to compare the two BRCA1 mutants for the status of 53BP1 chromatin association, levels of ATM-mediated phosphorylation, and RIF1/PTIP recruitment at breaks with and without ATM deficiency. The physical interaction between ATM, BRCA1, and 53BP1 proteins before and after damage can also be examined. Given that Ku-mediated antagonism of HDR is separated from that of 53BP1 (2), we should compare if there is a difference in NHEJ activity per se and the regulation of Ku and DNA-PKcs (e.g., recruitment and autophosphorylation) to

understand why DNA-PK is particularly active at breaks in the BRCA1$^{\Delta 11}$ mutant. Because our model proposes that a high DNA damage response participates in the ATM-53BP1 interplay, it will also be interesting to know if the HDR phenotype is changed in a p53-deficient background.

Second, the localization of BRCA1$^{\Delta 11}$ mutant protein to DSB sites may affect repair dynamics or interplay with other proteins. Unlike the BRCA1^{SF} mutant (38), the BRCA1$^{\Delta 11}$ isoform is expressed at comparable levels as WT BRCA1 and has normal formation of damage foci following DSBs (39, 40). However, this mutant clearly has a more severe impact on HDR and viability than BRCA1^{SF}. As studies on kinase-dead mutants of ATM and DNA-PKcs demonstrate that the recruitment of an inactive protein to breaks results in more severe phenotypes than the absence of protein (41-43), we are interested in knowing if the localization of BRCA1$^{\Delta 11}$ mutant protein to DSB sites somehow alters the functions of other repair proteins including ATM and 53BP1. Given that the BRCT and RING domains help mediate BRCA1 localization, mutations can be introduced in these regions of BRCA1$^{\Delta 11}$ to examine the effects on HDR; alternatively, H2AX can be mutated to disrupt BRCT-dependent recruitment of BRCA1 (44).

Third, the distinct HDR response may arise from residual regulation of end resection mediated by the intact BRCT domain of BRCA1$^{\Delta 11}$ protein. Both the BRCA1^{SF} and BRCA1$^{\Delta 11}$ mutants have reduced HDR and SSA, indicating impaired end resection (14, 45). The main cause of this defect is likely the loss of antagonism against 53BP1, but there may also be difference in the resection regulation between the two BRCA1 mutants, leading to distinct responses to ATM inhibition. For example, because the BRCT domain of BRCA1$^{\Delta 11}$ presumably still binds Abraxas and CtIP, this may reduce the requirement for ATM in supporting resection and also contribute to the limited increase in HDR observed following ATM inhibition, as

opposed to that in BRCA1^{SF} lacking this interaction. This can be addressed by specifically disrupting the BRCT domain in the BRCA1$^{\Delta 11}$ protein to examine the interplay with Abraxas and CtIP upon DSBs. A physical end resection assay can also help elucidate any difference between the two BRCA1 mutants.

Concluding remarks

The functions of ATM, BRCA1, and 53BP1 in the maintenance of genome integrity have been widely studied since their discovery. However, the data presented in this work demonstrate that more needs to be done to elucidate the complex genetic interaction between these critical players in DSB repair. Future work is also needed to extend the significance of this study to a human context such as breast and ovarian cancers. For the therapeutic perspective, our study highlights the importance of identifying the mutation spectrum of DSB repair genes in patients and considering how they potentially impact protein interactions that could alter the response to chemotherapies and development of resistance mechanisms.

REFERENCES

1. Schlacher K, Wu H, & Jasin M (2012) A distinct replication fork protection pathway connects Fanconi anemia tumor suppressors to RAD51-BRCA1/2. *Cancer Cell* 22(1):106-116.
2. Bunting SF*, et al.* (2012) BRCA1 functions independently of homologous recombination in DNA interstrand crosslink repair. *Mol. Cell* 46(2):125-135.
3. Sawyer SL*, et al.* (2015) Biallelic mutations in BRCA1 cause a new Fanconi anemia subtype. *Cancer Discov.* 5(2):135-142.
4. Feng W & Jasin M (2017) BRCA2 suppresses replication stress-induced mitotic and G1 abnormalities through homologous recombination. *Nat Commun* 8(1):525.
5. Ray Chaudhuri A*, et al.* (2016) Replication fork stability confers chemoresistance in BRCA-deficient cells. *Nature* 535(7612):382-387.
6. Wu Q, Jubb H, & Blundell TL (2015) Phosphopeptide interactions with BRCA1 BRCT domains: More than just a motif. *Prog. Biophys. Mol. Biol.* 117(2-3):143-148.
7. Davis AJ*, et al.* (2014) BRCA1 modulates the autophosphorylation status of DNA-PKcs in S phase of the cell cycle. *Nucleic Acids Res.* 42(18):11487-11501.
8. Cruz-Garcia A, Lopez-Saavedra A, & Huertas P (2014) BRCA1 Accelerates CtIP-Mediated DNA-End Resection. *Cell Rep.* 9(2):451-459.
9. Hu Y*, et al.* (2011) RAP80-directed tuning of BRCA1 homologous recombination function at ionizing radiation-induced nuclear foci. *Genes Dev.* 25(7):685-700.
10. Coleman KA & Greenberg RA (2011) The BRCA1-RAP80 complex regulates DNA repair mechanism utilization by restricting end resection. *J. Biol. Chem.* 286(15):13669-13680.
11. Wang H*, et al.* (2013) The interaction of CtIP and Nbs1 connects CDK and ATM to regulate HR-mediated double-strand break repair. *PLoS Genetics* 9(2):e1003277.
12. Kijas AW*, et al.* (2015) ATM-dependent phosphorylation of MRE11 controls extent of resection during homology directed repair by signalling through Exonuclease 1. *Nucleic Acids Res* 43(17):8352-8367.
13. Bolderson E*, et al.* (2010) Phosphorylation of Exo1 modulates homologous recombination repair of DNA double-strand breaks. *Nucleic Acids Res* 38(6):1821-1831.
14. Chen CC*, et al.* (2017) ATM loss leads to synthetic lethality in BRCA1 BRCT mutant mice associated with exacerbated defects in homology-directed repair. *Proc. Natl. Acad. Sci. U. S. A.* 114(29):7665-7670.
15. Reczek CR, Szabolcs M, Stark JM, Ludwig T, & Baer R (2013) The interaction between CtIP and BRCA1 is not essential for resection-mediated DNA repair or tumor suppression. *J. Cell Biol.* 201(5):693-707.

16. Kim SS, *et al.* (2009) Impaired skin and mammary gland development and increased gamma-irradiation-induced tumorigenesis in mice carrying a mutation of S1152-ATM phosphorylation site in Brca1. *Cancer Res* 69(24):9291-9300.
17. Chang S, Biswas K, Martin BK, Stauffer S, & Sharan SK (2009) Expression of human BRCA1 variants in mouse ES cells allows functional analysis of BRCA1 mutations. *J. Clin. Invest.* 119(10):3160-3171.
18. Kakarougkas A, *et al.* (2013) Co-operation of BRCA1 and POH1 relieves the barriers posed by 53BP1 and RAP80 to resection. *Nucleic Acids Res* 41(22):10298-10311.
19. Scully R, *et al.* (1997) BRCA1 is a component of the RNA polymerase II holoenzyme. *Proc Natl Acad Sci U S A* 94(11):5605-5610.
20. Pao GM, Janknecht R, Ruffner H, Hunter T, & Verma IM (2000) CBP/p300 interact with and function as transcriptional coactivators of BRCA1. *Proc Natl Acad Sci U S A* 97(3):1020-1025.
21. Monteiro AN, August A, & Hanafusa H (1996) Evidence for a transcriptional activation function of BRCA1 C-terminal region. *Proc Natl Acad Sci U S A* 93(24):13595-13599.
22. Chapman MS & Verma IM (1996) Transcriptional activation by BRCA1. *Nature* 382(6593):678-679.
23. Hatchi E, *et al.* (2015) BRCA1 recruitment to transcriptional pause sites is required for R-loop-driven DNA damage repair. *Mol Cell* 57(4):636-647.
24. Lee MS, *et al.* (2010) Comprehensive analysis of missense variations in the BRCT domain of BRCA1 by structural and functional assays. *Cancer Res.* 70(12):4880-4890.
25. Gorrini C, *et al.* (2013) BRCA1 interacts with Nrf2 to regulate antioxidant signaling and cell survival. *J Exp Med* 210(8):1529-1544.
26. Gorrini C, *et al.* (2014) Estrogen controls the survival of BRCA1-deficient cells via a PI3K-NRF2-regulated pathway. *Proc Natl Acad Sci U S A* 111(12):4472-4477.
27. Yi YW, Kang HJ, & Bae I (2014) BRCA1 and Oxidative Stress. *Cancers (Basel)* 6(2):771-795.
28. Magnard C, *et al.* (2002) BRCA1 interacts with acetyl-CoA carboxylase through its tandem of BRCT domains. *Oncogene* 21(44):6729-6739.
29. Moreau K, *et al.* (2006) BRCA1 affects lipid synthesis through its interaction with acetyl-CoA carboxylase. *J Biol Chem* 281(6):3172-3181.
30. Brunet J, *et al.* (2008) BRCA1 and acetyl-CoA carboxylase: the metabolic syndrome of breast cancer. *Mol Carcinog* 47(2):157-163.
31. Ditch S & Paull TT (2012) The ATM protein kinase and cellular redox signaling: beyond the DNA damage response. *Trends Biochem Sci* 37(1):15-22.
32. Zha S, Sekiguchi J, Brush JW, Bassing CH, & Alt FW (2008) Complementary functions of ATM and H2AX in development and suppression of genomic instability. *Proc. Natl. Acad. Sci. U. S. A.* 105(27):9302-9306.

33. Zhao W, *et al.* (2017) BRCA1-BARD1 promotes RAD51-mediated homologous DNA pairing. *Nature* 550(7676):360-365.
34. Scully R, *et al.* (1997) Association of BRCA1 with Rad51 in mitotic and meiotic cells. *Cell* 88(2):265-275.
35. Paull TT, *et al.* (2000) A critical role for histone H2AX in recruitment of repair factors to nuclear foci after DNA damage. *Curr Biol* 10(15):886-895.
36. Masuda T, Xu X, Dimitriadis EK, Lahusen T, & Deng CX (2016) "DNA Binding Region" of BRCA1 Affects Genetic Stability through modulating the Intra-S-Phase Checkpoint. *Int J Biol Sci* 12(2):133-143.
37. Hu Y, *et al.* (2014) PARP1-driven poly-ADP-ribosylation regulates BRCA1 function in homologous recombination-mediated DNA repair. *Cancer Discov* 4(12):1430-1447.
38. Shakya R, *et al.* (2011) BRCA1 tumor suppression depends on BRCT phosphoprotein binding, but not its E3 ligase activity. *Science* 334(6055):525-528.
39. Huber LJ, *et al.* (2001) Impaired DNA damage response in cells expressing an exon 11-deleted murine Brca1 variant that localizes to nuclear foci. *Mol Cell Biol* 21(12):4005-4015.
40. Westermark UK, *et al.* (2003) BARD1 participates with BRCA1 in homology-directed repair of chromosome breaks. *Mol Cell Biol* 23(21):7926-7936.
41. Daniel JA, *et al.* (2012) Loss of ATM kinase activity leads to embryonic lethality in mice. *J Cell Biol* 198(3):295-304.
42. Yamamoto K, *et al.* (2012) Kinase-dead ATM protein causes genomic instability and early embryonic lethality in mice. *J Cell Biol* 198(3):305-313.
43. Jiang W, *et al.* (2015) Differential phosphorylation of DNA-PKcs regulates the interplay between end-processing and end-ligation during nonhomologous end-joining. *Mol Cell* 58(1):172-185.
44. Li M & Yu X (2013) Function of BRCA1 in the DNA damage response is mediated by ADP-ribosylation. *Cancer Cell* 23(5):693-704.
45. Stark JM, Pierce AJ, Oh J, Pastink A, & Jasin M (2004) Genetic steps of mammalian homologous repair with distinct mutagenic consequences. *Mol Cell Biol* 24(21):9305-9316.

APPENDIX

Figure A.1 Supporting data of *Atm-Brca1^{SF}-53bp1* mutant mice.
A. Dead *Atm$^{-/-}$Brca1$^{SF/SF}$* mouse can be found at birth and is smaller than the other 6 littermates, which include control and *Atm* or *Brca1^{SF}* single mutants and all are alive at birth (left). This litter is from a F3 backcross cage of *Atm-Brca1^{SF}* mice with 129/SvJ mice. The same double mutant is also compared to a *Brca1$^{SF/SF}$* single mutant dead pup from a different cage (right).
B. Both *Atm$^{-/-}$* and *Brca1$^{SF/SF}$* MEFs are more sensitive to olaparib than control MEFs in MTT assay in the absence of ATMi (n≥5). The similar olaparib sensitivity between these two mutants resembles that of ES cells in colony assays and different from the results that *Brca1$^{SF/SF}$* MEFs have more HDR reduction than *Atm$^{-/-}$* MEFs (Chapter 2), suggesting ATM is particularly required for the repair of olaparib-induced damage. To measure cell growth using Vybrant MTT Kit, MEFs are plated in 96-well plates (4000 cells/well) overnight and treated with olaparib continuously for 5 days, replenished once after 2 days. The cells are pulsed with 1.1 mM MTT for 4 hr, lysed in 0.05% SDS/HCl for 18 hr, and measured absorbance at OD 570 nM.
C. Mutations of *Brca1^{SF}* and/or *53bp1* do not significantly affect the survival of *Atm$^{-/-}$* mice, the majority of which die around age 3-4 months: 68 out of 72 dissected mice carrying *Atm$^{-/-}$* genotype, regardless of the *Brca1^{SF}-53bp1* status, have enlarged thymus indicating thymic lymphoma; 3 other mice without thymic lymphoma have tumors at neck, liver, and inguinal mammary gland, respectively. *53bp1$^{-/-}$* single mutant can live over one year: 3 out of 6 dead *53bp1$^{-/-}$* mice are dissected and do not show signs of thymic lymphoma. Although loss of *53bp1* is reported to accelerate lymphoid malignancy in *Atm$^{-/-}$* mice on the 129/Sv background (Rybanska-Spaeder et al., 2013), we do not see such difference in our colony under mixed backgrounds (blue versus green curve). Mice in this cohort carry the combination of *DR-GFP* and/or *I-SceI/CMV-rtTA* alleles. Median survival days: *Atm$^{-/-}$* 102; *Atm$^{-/-}$ 53bp1$^{+/-}$* 155; *Atm$^{-/-}$ 53bp1$^{-/-}$* 123; *Atm$^{-/-}$ Br1$^{SF/SF}$ 53bp1$^{+/-}$* 103; *Atm$^{-/-}$ Br1$^{SF/SF}$ 53bp1$^{-/-}$* 123; *53bp1$^{-/-}$* 495.
D. Most mutant ear fibroblasts have a similar ~20% reduction in cell proliferation compared to WT (n≥3), except *Atm$^{-/-}$Brca1$^{SF/SF}$53bp1$^{+/-}$* which shows a more severe ~40% reduction (n=2). Primary ear fibroblasts are plated in 12-well plates (4×10^4 cells/well) in duplicates overnight. Cell number is counted on hemocytometer on the next day and again after 2 days. The 48-hr cell number is normalized to the starting number to obtain a 48-hr growth ratio, which is then normalized to the WT in each experiment to account for the variation of each harvest.
E. 53BP1 loss restores the number of IR-induced nuclear RPA foci in *Brca1^{SF}* and *Atm* mutants (blue lines) to the similar level as WT cells. However, unlike in *Brca1^{SF}*, recombination (e.g., RAD51 foci, DR-GFP) cannot be rescued in the *Atm* mutant by 53BP1 loss (Chapter 2). Each genotype consists of at least 3 mice, each with ~30-50 nuclei counted for the number of RPA foci following IR. Data are graphed using Tukey blot with median indicated by the horizontal line in the box.

Figure A.1

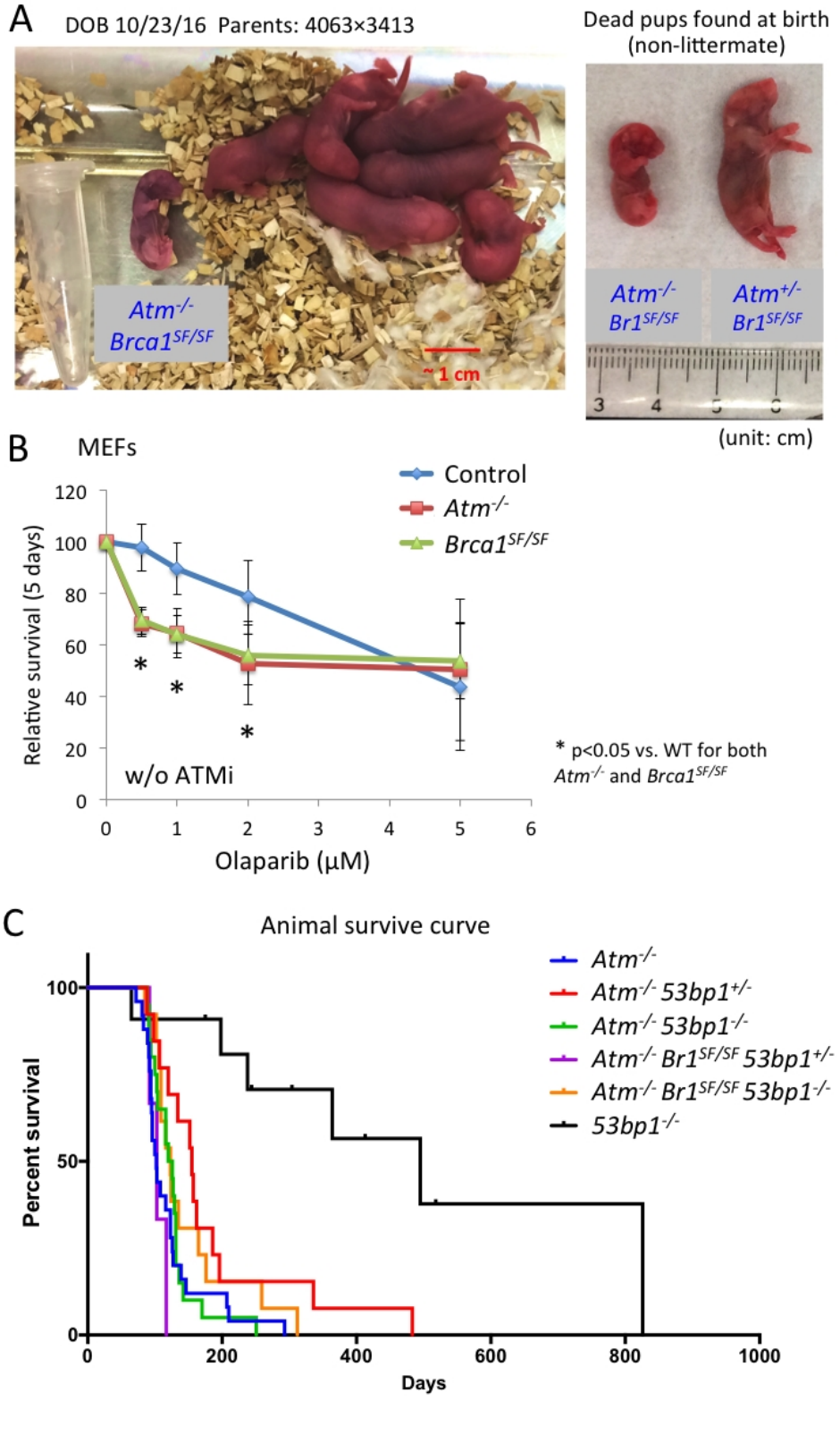
A
DOB 10/23/16 Parents: 4063×3413
Atm-/- Brca1SF/SF
~ 1 cm
Dead pups found at birth (non-littermate)
Atm-/- Br1SF/SF
Atm+/- Br1SF/SF
(unit: cm)
B
MEFs
Control
Atm-/-
Brca1SF/SF
Relative survival (5 days)
w/o ATMi
Olaparib (μM)
* p<0.05 vs. WT for both Atm-/- and Brca1SF/SF
C
Animal survive curve
Atm-/-
Atm-/- 53bp1+/-
Atm-/- 53bp1-/-
Atm-/- Br1SF/SF 53bp1+/-
Atm-/- Br1SF/SF 53bp1-/-
53bp1-/-
Percent survival
Days

Figure A.1 (Continued)

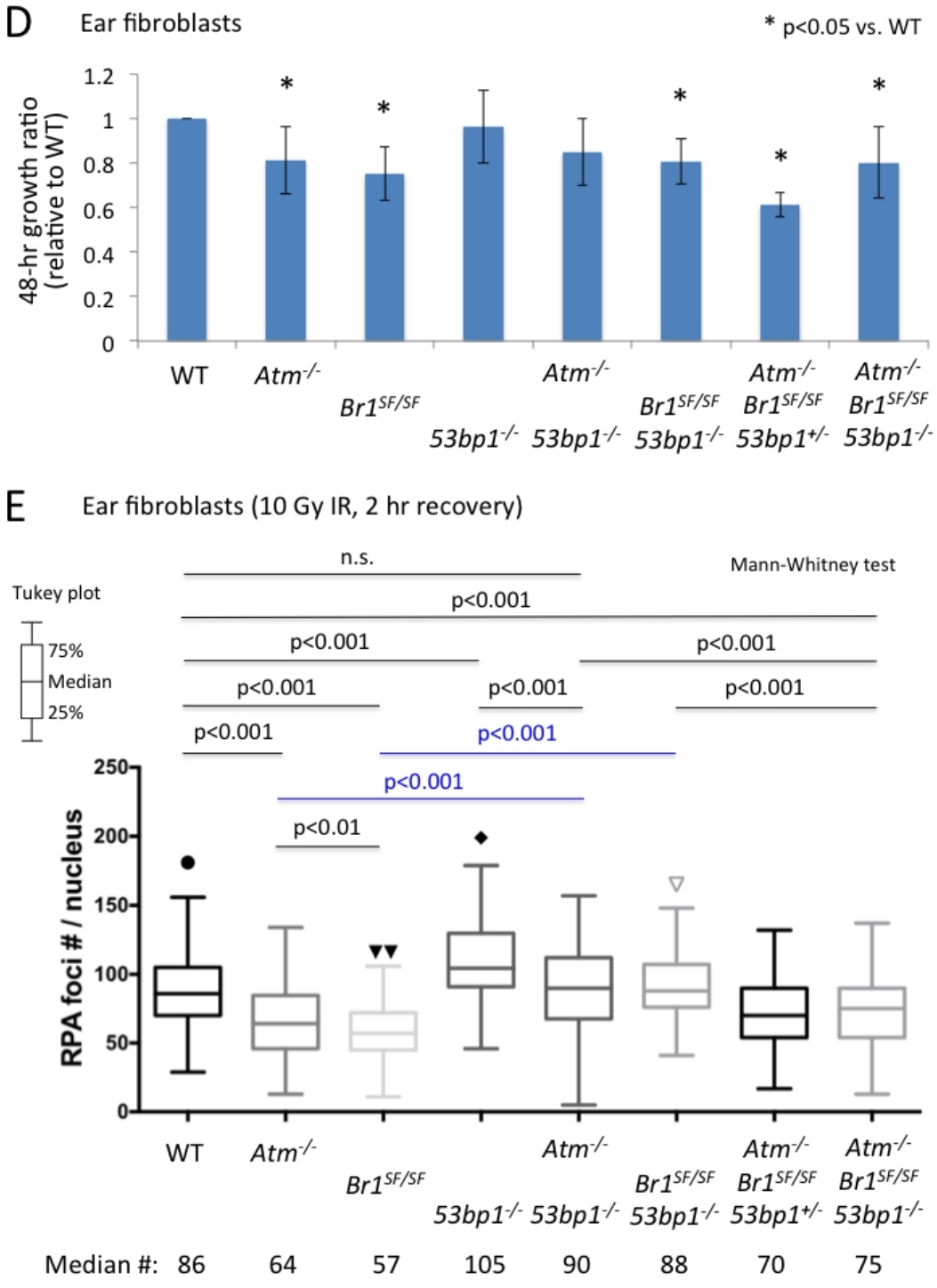

Figure A.2 Genetic interaction of *Atm* and *Brca1^{tr}* mutations.
A. Comparison of mouse WT BRCA1 with S1598F, Δ11, and tr mutant proteins. The *Brca1^{tr}* allele (Ludwig et al., 2001) has sequence insertion in the middle of exon 11 that results in frameshift and stop codon at the downstream sequence. This is predicted to express a BRCA1^{tr} protein truncated after the first 924 amino acids, retaining ~60% of exon 11 region while lacking the C-terminal coiled-coil and BRCT domains. This *Brca1^{tr}* allele mimics a breast cancer founder mutation *2800delAA*.
B. The ratio of *Brca1$^{tr/tr}$* mice is lower than the Mendelian frequency but can be rescued by *Atm* heterozygosity, which is likely related to the functions of ATM in checkpoints. However, viable *Atm$^{-/-}$Brca1$^{tr/tr}$* double mutant mice are not recovered at weaning except for one animal, suggesting complete loss of ATM further compromises *Brca1$^{tr/tr}$* animal viability. The double mutant mouse is smaller than littermates (shown in the photo, no weight measurement) and died after 99 days, but the cause is uncertain due to festered carcass. The contrasting phenotypes of *Atm$^{+/-}$* versus *Atm$^{-/-}$* in *Brca1^{tr}* mice have similarity with that of *Brca1^{SF}* mice, suggesting the *Brca1^{tr}* mutation may have partial synthetic lethality with ATM deficiency.
C. *Atm$^{-/-}$Brca1$^{tr/tr}$* double mutant embryo can be found at mid-embryogenesis (E12.5) and appears smaller than *Brca1$^{tr/+}$* or *Atm$^{-/-}$* littermate embryos but grossly normal with visible heartbeats. Unlike *Brca1^{SF}*, MEFs can be derived from the E12.5 *Atm$^{-/-}$ Brca1$^{tr/tr}$* embryo which show slightly slower growth than *Brca1$^{tr/+}$* or *Atm$^{-/-}$* counterparts. The comparison between embryos and newborn pups suggests the compound defects may be affecting the late embryonic stage.
D. Examining HDR in *Atm-Brca1^{tr}* primary ear fibroblasts carrying the DR-GFP/inducible I-SceI system. The *Brca1$^{tr/tr}$* ear fibroblasts show a moderate ~1.4-fold reduction in HDR (n≥3 except n=2 for WT;). However, HDR is severely reduced by ~10-fold in *Atm$^{-/-}$Brca1$^{tr/tr}$* fibroblasts (n=1, site loss 22%) compared to WT cells. % HDR: % GFP^{+} normalized to % I-SceI site loss. All mice are from the *Atm-Brca1^{tr}* colony. * *Brca1$^{+/+}$* or $^{tr/+}$
E. Treatment with ATMi (3 μM) in *Brca1$^{tr/tr}$* ear fibroblasts inhibits HDR to a greater extent than in control cells (2- versus 1.6-fold reduction), though not as much as the extent of reduction (4-fold) in *Brca1$^{SF/SF}$* cells (n≥3). These results suggest that HDR in the *Brca1^{tr}* mutant may also have some dependence on ATM, but not to the similar level as the *Brca1^{SF}* allele. The fold is relative to the % GFP^{+} of DMSO treatment of each animal. The dataset consists of mice from *Brca1^{SF}* and *Brca1^{tr}* colonies.
F. Cell cycle profiles of *Atm$^{-/-}$Brca1$^{tr/tr}$* tail fibroblasts are similar to WT cells.
G. *Brca1$^{tr/tr}$* primary MEFs show an ~4-fold reduction in HDR. * *Atm$^{+/+}$* or $^{+/-}$ (n≥3)
H. In *Brca1$^{tr/tr}$* primary MEFs, treatment with ATMi does not reduce HDR to a greater extent than in WT MEFs, unlike the phenotype in *Brca1^{SF}* MEFs (Chapter 2). One possibility could be that the HDR defect of *Brca1^{tr}* allele is less severe than the *Brca1^{SF}* allele that mitigates the requirement for ATM in MEFs. This may be related to the observation that *Brca1^{tr}* ear fibroblasts also have smaller HDR reduction than *Brca1^{SF}* upon ATM inhibition (see above). In addition, ATM deficiency has less pronounced effects on HDR in embryonic cells (Chapter 2). * *Atm$^{+/+}$* or $^{+/-}$ (n≥3)

Figure A.2

A

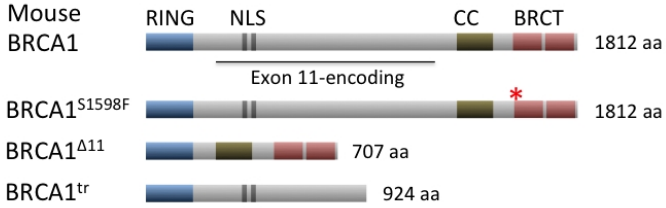

B Viable pups at weaning

Atm$^{+/-}$ *Brca1*$^{tr/+}$ x *Atm*$^{+/-}$ *Brca1*$^{tr/+}$ (Total: 173) * 1 other dead pup found at birth

Atm	+/+			+/-			-/-		
Brca1^{tr}	+/+	tr/+	tr/tr	+/+	tr/+	tr/tr	+/+	tr/+	tr/tr
Observed	16	21	3	24	56	18	15	19	1*
Expected	10.8125	21.625	10.8125	21.625	43.25	21.625	10.8125	21.625	10.8125

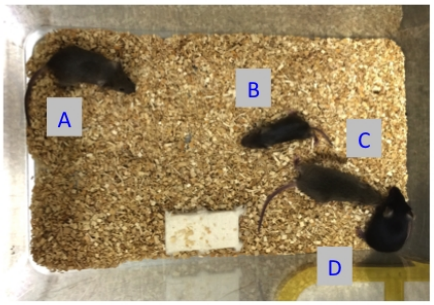

3-week-old
A: *Atm*$^{+/-}$ *Brca1*$^{tr/tr}$
B: *Atm*$^{-/-}$ *Brca1*$^{tr/tr}$
C: *Atm*$^{-/-}$
D: WT

C Embryos at E12.5 - E14.5

Atm$^{+/-}$ *Brca1*$^{tr/+}$ x *Atm*$^{+/-}$ *Brca1*$^{tr/+}$ (Total: 32)

Atm	+/+			+/-			-/-		
Brca1^{tr}	+/+	tr/+	tr/tr	+/+	tr/+	tr/tr	+/+	tr/+	tr/tr
Observed	2	4	2	4	7	5	2	5	1
Expected	2	4	2	4	8	4	2	4	2

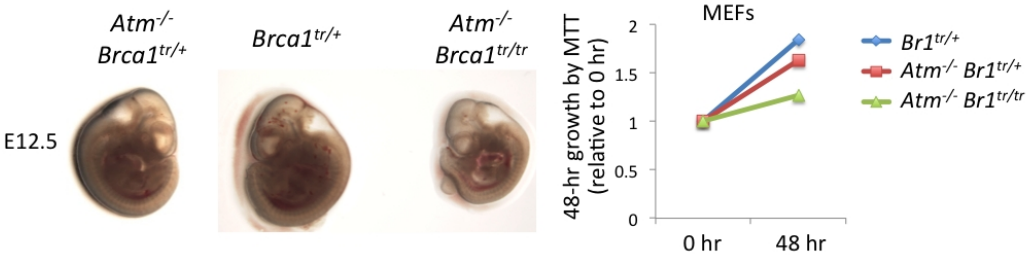

Figure A.2 (Continued)

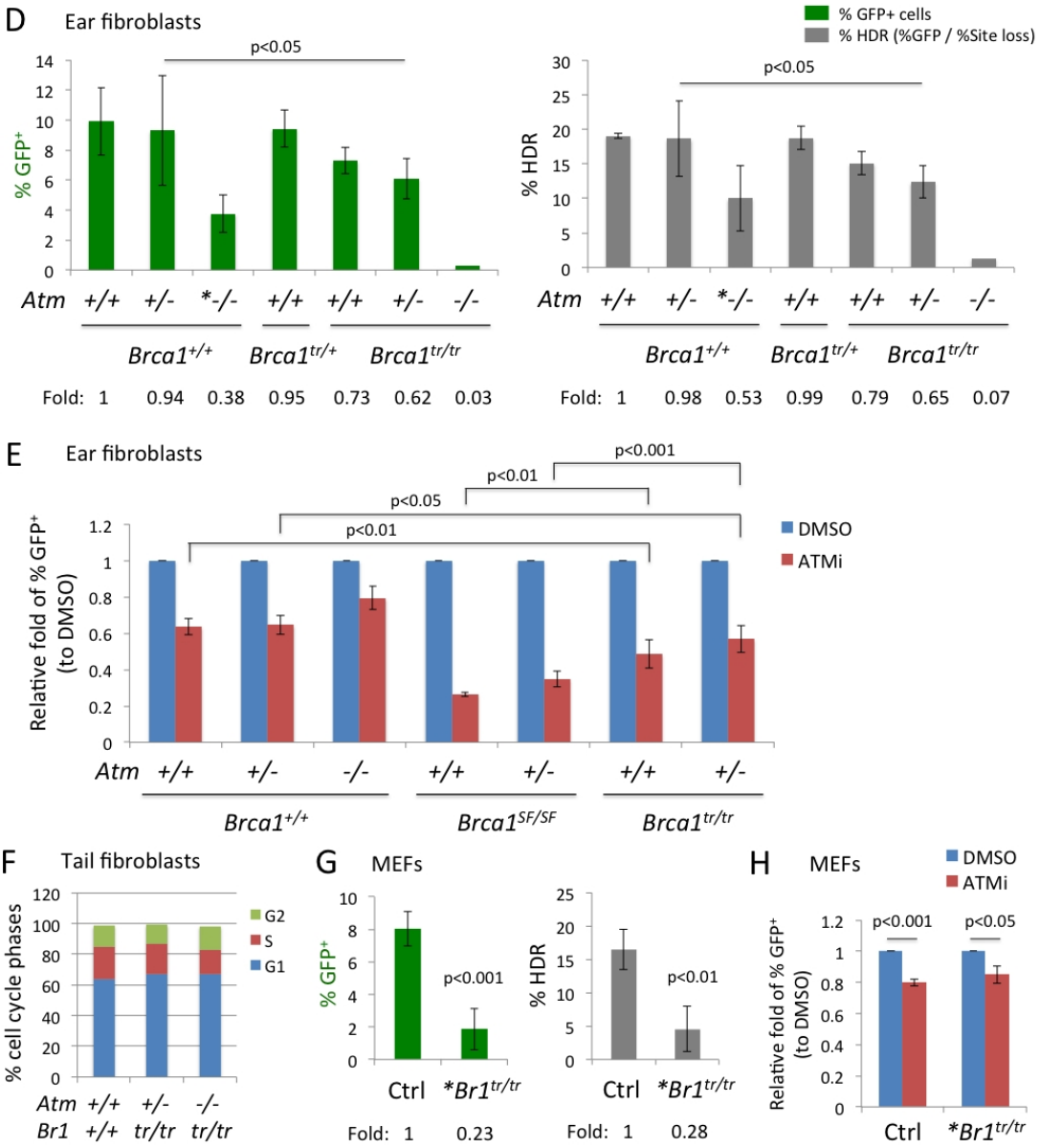

Figure A.3 I-SceI transfection experiments in *Atm* mutant primary cells.
(Part of which is published in Kass et al., PNAS, 2013)
A. The kinase domain of ATM (residues 2722-2972, UniProt, www.uniprot.org) is encoded by exons 56-63 (Ensemble, useast.ensembl.org). The Atm^{b} allele (Xu and Baltimore, 1996) contains a deletion of a portion of the kinase-encoding domain (exon 59 and part of exon 60; deleting residues 2816-2875). The Atm^{w} allele (Barlow et al., 1996) contains a Neo^{R} inserted in a reversed orientation that replaces exon 37. All *Atm* mutant experiments in the thesis are performed with the Atm^{b} allele, except in Chapter 2 Figure 2.5G where the Atm^{w} allele is used.

To analyze the transcripts of the two *Atm* mutant alleles, reverse transcription is performed using RNA prepared from ear fibroblasts from WT, $Atm^{w/w}$, and $Atm^{b/b}$ mice (Kass et al., 2013; *w/w* or *b/b* indicates homozygous mutant). PCR is performed on the prepared cDNA with three different primer sets to amplify exons upstream of the targeted mutations (exons 13-16; serve as a control) and at the site of the targeted mutations. The exons 13-16 product is detected from both $Atm^{w/w}$ and $Atm^{b/b}$ mice but at reduced levels, suggesting unstable mutant transcripts. The normal exons 34-42 product is observed for $Atm^{b/b}$ mice at reduced levels but absent from $Atm^{w/w}$ mice; instead, $Atm^{w/w}$ mice have a lower level of an alternatively spliced product (denoted with asterisk). Sequencing of cloned PCR products indicates that it corresponds to a splicing event from exon 36 to exon 38 that skips the Neo^{R} cassette (18 sequences analyzed by TOPO cloning), resulting in frameshift and truncation of ATM after residue 1838. The normal exons 54-62 product, encoding the kinase domain, is present at low levels in $Atm^{w/w}$ mice but absent from $Atm^{b/b}$ mice.
B. A former lab member, Hildur Helgadottir, performed HDR analysis in the Atm^{w} mutant by transfecting an I-SceI expression plasmid (pCBASce) in $Atm^{w/w}$ fibroblasts carrying the DR-GFP reporter but did not observe a significant HDR reduction (Kass et al., 2013). A similar experiment is performed in the Atm^{b} mutant carrying the DR-GFP reporter. Primary ear fibroblasts harvested from WT or $Atm^{b/b}$ mice are cultured to passage 3 to obtain enough cells for electroporation with the pCBASce plasmid (350 V / 950 μF; 3×10^{6} cells with 30 μg plasmid). GFP-positive cells are analyzed 48 hr after electroporation. The graphs presented here are the means of three experiments included in the Kass 2013 paper (bottom tables, experiments 1-3) and three additional ones; error bars indicate one standard deviation from the mean.

The overall % GFP^{+} is low (0.4-0.6%) following pCBASce transfection in primary fibroblasts. Similar to the Atm^{w} mutant, HDR in $Atm^{b/b}$ ear fibroblasts is not significantly different from WT cells in this assay (upper left, p=0.33). However, a trend of ~1.4-fold reduction in $Atm^{b/b}$ fibroblasts can be noticed (n=6). The transfection efficiency, as examined by an independent electroporation of an NZ-EGFP plasmid, is ~25% for both genotypes (upper right). In comparison, the tetracycline-inducible I-SceI system has much higher efficiency (Kass et al., 2016; Chapter 2): Induction of I-SceI by doxycycline treatment can achieve ~50% DSB efficiency (as determined by site loss assay) and give rise to ~10% GFP-positive cells in WT fibroblasts. Thus, we think the robustness of the inducible I-SceI system allows for a better delineation of the modest HDR reduction in *Atm*-null primary cells compared to the transfection-based method.

C. Treatment with an ATMi KU-55933 reduces HDR in WT ear fibroblasts following pCBASce transfection, whereas HDR in $Atm^{b/b}$ fibroblasts is not affected by ATMi (n=5). The ~1.7-fold reduction in HDR in WT cells treated with 3 μM ATMi is similar to reduction fold in the inducible I-SceI system undergoing the same treatment (Chapter 2). The fold is relative to the % GFP^+ of DMSO treatment.
D.-E. The expression of ATM protein and the DNA damage response in primary ear fibroblasts from $Atm^{w/w}$ and $Atm^{b/b}$ mice are examined by western blotting in **D** and **E**, respectively. *Atm* mutant fibroblasts from both mouse strains do not have detectable ATM protein expression using an antibody against the C terminus of ATM (Abcam 2C1, epitope human residues 2577-3056). Whereas WT fibroblasts display phosphorylation of ATM-targeted substrates (CHK2 and p53) following irradiation that can be abolished by ATMi treatment, both *Atm* mutant fibroblasts do not show visible phosphorylation events.

Figure A.3

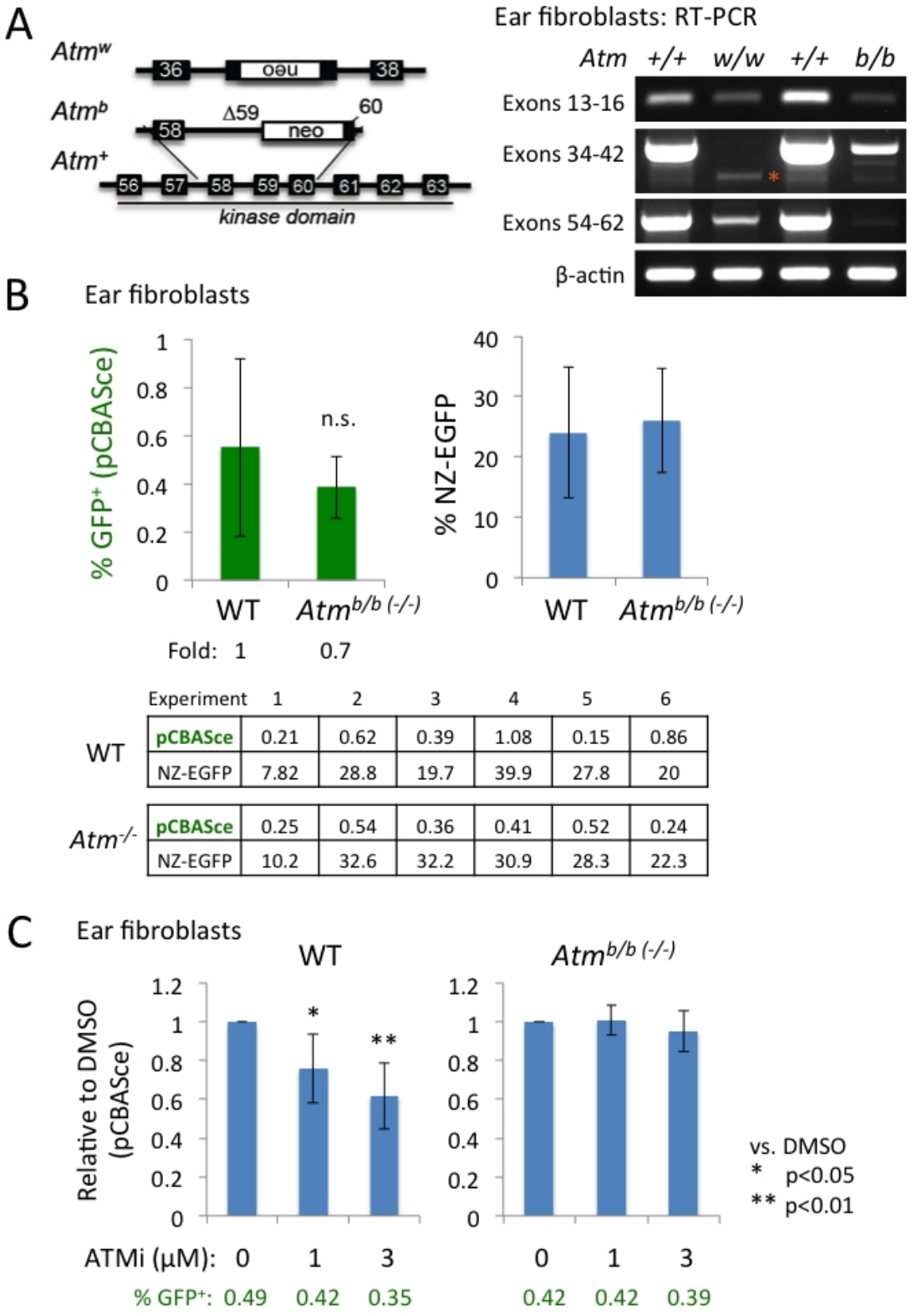
A
Atm^w
36
oəu
38
Atm^b
Δ59
60
58
neo
Atm+
56 57 58 59 60 61 62 63
kinase domain
Ear fibroblasts: RT-PCR
Atm +/+ w/w +/+ b/b
Exons 13-16
Exons 34-42
Exons 54-62
β-actin
B
Ear fibroblasts
% GFP+ (pCBASce)
n.s.
WT
Atm^b/b (-/-)
Fold: 1 0.7
% NZ-EGFP
WT
Atm^b/b (-/-)
Experiment 1 2 3 4 5 6
WT
pCBASce 0.21 0.62 0.39 1.08 0.15 0.86
NZ-EGFP 7.82 28.8 19.7 39.9 27.8 20
Atm-/-
pCBASce 0.25 0.54 0.36 0.41 0.52 0.24
NZ-EGFP 10.2 32.6 32.2 30.9 28.3 22.3
C
Ear fibroblasts
WT
Atm^b/b (-/-)
Relative to DMSO (pCBASce)
vs. DMSO
* p<0.05
** p<0.01
ATMi (μM): 0 1 3 0 1 3
% GFP+: 0.49 0.42 0.35 0.42 0.42 0.39

Figure A.3 (Continued)

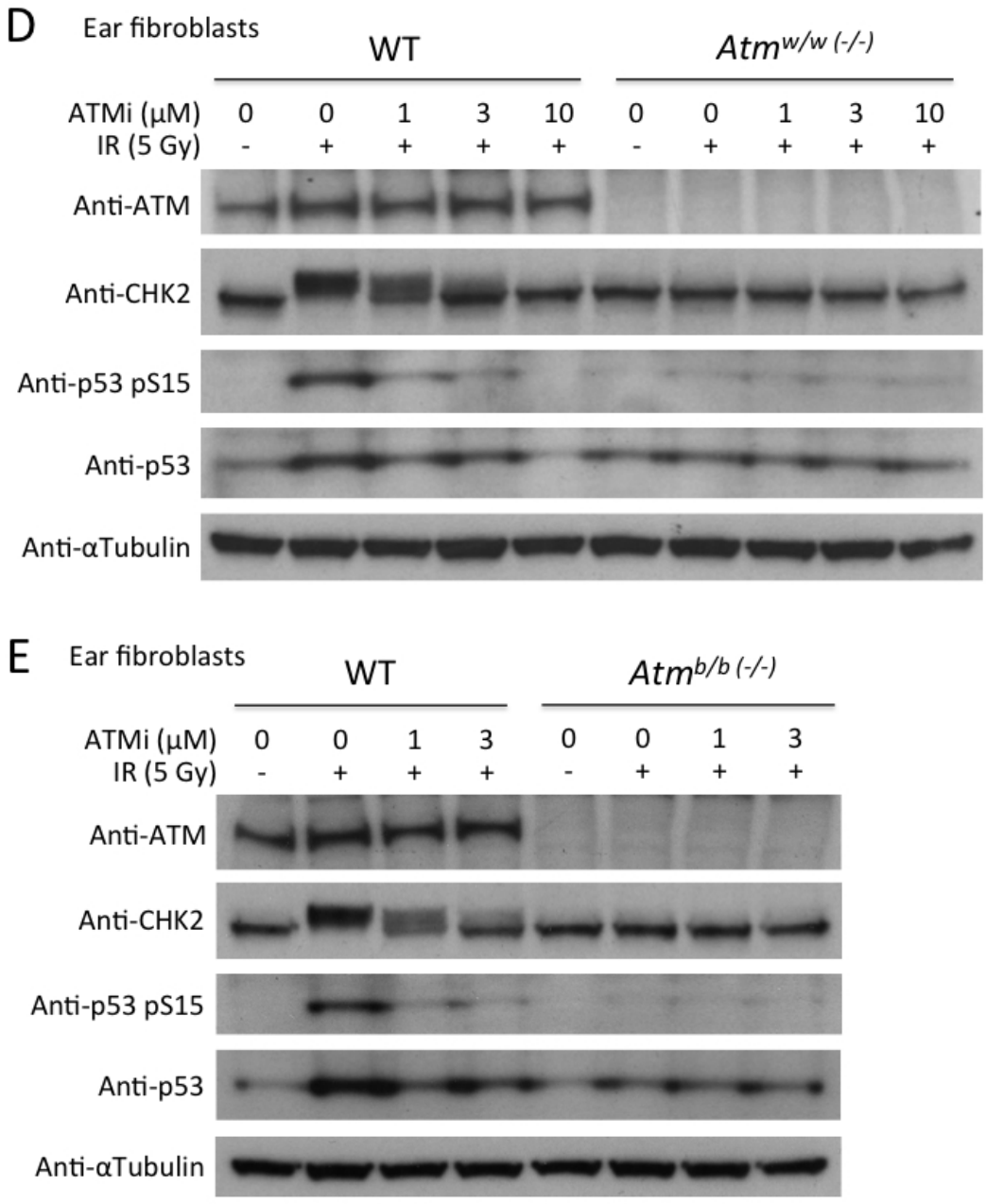

Figure A.4 Effects of HDAC inhibition on HDR in ES cells.
A. Given that ATM has a role in transcriptional silencing in the vicinity of DSBs (Shanbhag et al., 2010) and heterochromatin-associated repair (Goodarzi et al., 2008), we examine how chromatin perturbation influences HDR in ATM-deficient ES cells by treatment with a pan HDAC inhibitor Trichostatin A (TSA) that promotes chromatin relaxation.

In DMSO-treated condition, HDR in *Atm*$^{-/-}$ ES cells is ~1.7-fold lower than WT at 24 hr after transfection of an I-SceI expressing plasmid pCBASce ($p<0.05$), however the difference is not observed at 48 hr, which we refer to in Chapter 2 as a delayed HDR in *Atm*$^{-/-}$ ES cells (top panel). Treatment with TSA (5/10 nM) significantly increases HDR in both cells lines, but the extent of increase is higher in WT than *Atm*$^{-/-}$ cells, such that a difference in 48-hr HDR can now be observed showing that TSA-treated WT cells have ~2-fold higher HDR than *Atm*$^{-/-}$ cells ($p<0.01$). This implies that the status of repressive chromatin may contribute to the diminished difference in HDR between WT and *Atm*$^{-/-}$ ES cells at later time points of repair. (n=3)

The similar increase in % NZ-EGFP in both WT and *Atm*$^{-/-}$ ES cells suggests that the protein expression from transfected plasmids is not differentially altered by inhibition of HDAC (bottom panel).
B. Analysis of site loss assay in ES cells (see Chapter 2 methods). Although % I-SceI site loss is low in pCBASce transfection experiments (compared with empty vector pCAGGS), it is increased by TSA treatment similarly in both WT and *Atm*$^{-/-}$ ES cells, suggesting no difference in overall repair between the two genotypes after HDAC inhibition (n=3). This also suggests that factors other than DSB efficiency contribute to the distinct change in HDR between WT and *Atm*$^{-/-}$ cells. For example, there may be more utilization of HDR versus NHEJ, increased DNA mobility, or less local silencing effects following TSA-induced chromatin relaxation in WT cells, and the activity of ATM is involved in these processes, leading to a difference between WT and *Atm*$^{-/-}$ cells.
C. % HDR (i.e., % GFP^{+} normalized to % I-SceI site loss) of WT and *Atm*$^{-/-}$ ES cells treated with TSA shows similar trend as the analysis of % GFP^{+} shown above.
D. We examine the effects of TSA in other cell types and find that treatment with TSA (10 nM, 48 hr) does not have a significant effect on HDR in primary ear fibroblasts carrying the inducible I-SceI system (n=4); however, a small increase in HDR can be seen in the immortalized WT MEFs (n=2). This suggests that the effects of TSA on HDR in ES cells may be context-dependent, e.g., in embryonic cells.
E. Given that acetylation by Tip60 following chromatin perturbation contributes to ATM activation (Kaidi and Jackson, 2013), we analyze if TSA affects ATM activity but do not observe significant changes in ATM-dependent DNA damage signaling in irradiated WT ES cells pretreated with TSA. However, this could be re-examined with lower dose of IR to better visualize any phosphorylation change on ATM substrates.

F. Given that DNA-PKcs activity contributes to NHEJ and also to break-induced transcriptional silencing (Pankotai et al., 2012), we examine how DNA-PKcs inhibition affects HDR in ES cells. Treatment with a DNA-PKcs inhibitor NU-7441 (3 μM) promotes a ~1.6- and 2-fold increase in HDR in WT cells at 24 and 48 hr, respectively, whereas the increase is ~1.2-fold in *Atm*$^{-/-}$ ES cells. This leads to a difference at 48 hr between the two genotypes such that HDR in WT is ~1.5-fold higher than *Atm*$^{-/-}$ cells. Whether this is related to the loss of NHEJ competition or chromatin silencing needs to be further examined. (n=3)

Summary of HDAC and DNA-PKcs inhibitor experiments:
We propose in the discussion of Chapter 2 that alternative mechanisms, such as ATR and EXO1, compensate for the delayed HDR in *Atm*$^{-/-}$ ES cells (see Appendix Figures A.5 and A.6). However, a different possibility is that some phenotypes change in the context of WT rather than *Atm*$^{-/-}$ cells, creating the difference between the two cell lines.

Here, we hypothesize that the chromatin conformation around the break site may change after DSBs in WT ES cells and become more compact. This somehow alters pathway utilization towards more NHEJ at later time points (similar to the context of heterochromatin) and thus a diminished difference between WT and *Atm*$^{-/-}$ ES cells at 48 hr. Such NHEJ usage can be suppressed by DNA-PKcs inhibition to promote ATM-mediated HDR in WT cells at 48 hr. Treatment of TSA relaxes the chromatin and thus also promotes HDR utilization in WT cells at 48 hr. It is unclear if the process of repressive chromatin formation, if any, is entirely ATM-dependent or partially, since TSA treatment also increases HDR in *Atm*$^{-/-}$ ES cells (albeit not as much as in WT). The molecular mechanisms of TSA-induced effects on chromatin and HDR remain to be elucidated.

Alternatively, a possibility is that TSA simply activates more ATM in WT cells causing higher HDR, however we do not see an increase in ATM signaling by TSA treatment in the preliminary western blot results. Furthermore, this is more difficult to explain the delayed HDR response in *Atm*$^{-/-}$ versus WT cells between 24 and 48 hr, i.e., why ATM is less activated in WT at 48 hr if this is the case.

Figure A.4

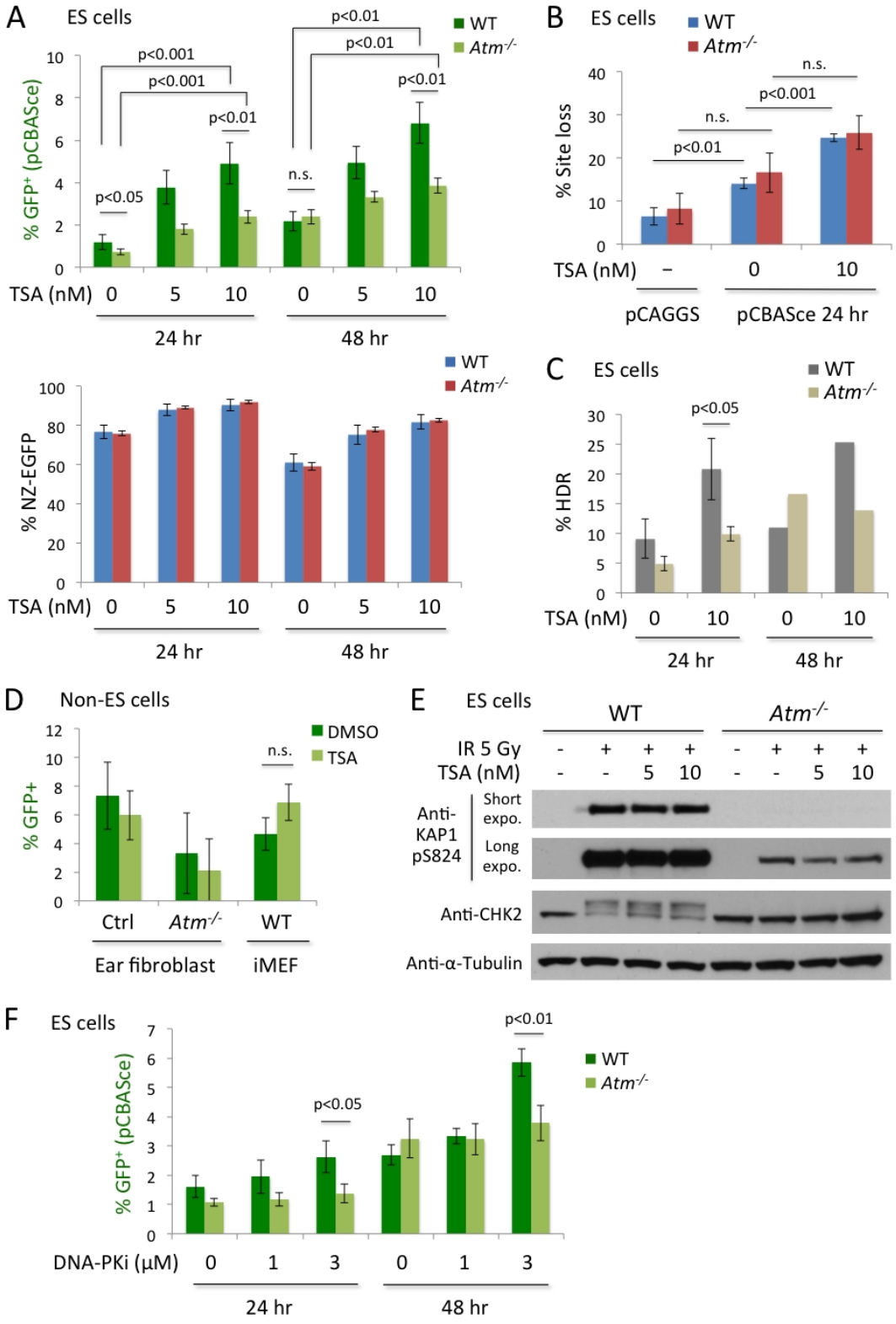
A
ES cells
WT
Atm-/-
% GFP+ (pCBASce)
p<0.001
p<0.001
p<0.01
p<0.05
p<0.01
p<0.01
n.s.
p<0.01
TSA (nM) 0 5 10 0 5 10
24 hr
48 hr
% NZ-EGFP
TSA (nM) 0 5 10 0 5 10
24 hr
48 hr
B
ES cells
WT
Atm-/-
% Site loss
n.s.
p<0.001
n.s.
p<0.01
TSA (nM) – 0 10
pCAGGS
pCBASce 24 hr
C
ES cells
WT
Atm-/-
% HDR
p<0.05
TSA (nM) 0 10 0 10
24 hr
48 hr
D
Non-ES cells
DMSO
TSA
% GFP+
n.s.
Ctrl
Atm-/-
WT
Ear fibroblast
iMEF
E
ES cells
WT
Atm-/-
IR 5 Gy - + + + - + + +
TSA (nM) - - 5 10 - - 5 10
Anti-KAP1 pS824
Short expo.
Long expo.
Anti-CHK2
Anti-α-Tubulin
F
ES cells
% GFP+ (pCBASce)
p<0.05
p<0.01
WT
Atm-/-
DNA-PKi (μM) 0 1 3 0 1 3
24 hr
48 hr

Figure A.5 Effects of ATR kinase inhibition on HDR.
(Part of which is published in Vriend et al., NAR, 2016)
A. Because ATR kinase can promote end resection independently of ATM in the EXO1-proficient condition (Peterson et al., 2013), we examine how inhibition of ATR affects HDR. Treatment with an ATR kinase inhibitor VE-821 (1 μM) suppresses HDR by ~1.4-fold in WT ES cells, suggesting ATR activity plays a role in HDR. ATR inhibition in *Atm*$^{-/-}$ ES cells also causes a similar ~1.4-fold reduction in HDR, suggesting ATR still contributes to HDR even in the absence of ATM. Despite the similar fold of HDR reduction, whether ATR promotes HDR through the same mechanism in WT and *Atm*$^{-/-}$ cells needs to be further examined. (n=3)
B. Treatment with 1 μM ATRi slightly increases the S-phase population of ES cells at 24 hr ($p<0.01$ for WT but not significant for *Atm*$^{-/-}$). At a higher dose of 3 μM, cells start to show S-phase accumulation and cannot be consistently plotted by the FlowJo cell cycle analysis tool; examples of population distribution are shown in the right panel. (n=4)
C. Treatment with hydroxyurea (HU) induces replication stress by depleting nucleotide pools. This leads to ATR activation in WT ES cells and phosphorylation of its substrate CHK1 on S345 (equivalent to human S345), which can be ablated by treatment with an ATR inhibitor. On the other hand, ATR inhibition increases CHK2 phosphorylation (indicated by the mobility shift) in response to HU, which is likely an indication of DSB accumulation due to the blockade of S-phase repair by ATRi treatment.
D. ATR inhibition does not affect CHK2 phosphorylation in response to IR, which is predominantly phosphorylated by ATM.
E.-F. Given that treatment with ATRi or ATMi inhibits HDR in human U2OS cells (Vriend et al., 2016), we confirm that these inhibitors are effectively suppressing the corresponding DNA damage signaling pathways in this cell line. In **E**, ATRi treatment blocks the phosphorylation of ATR substrate CHK1 on S345 in a dose-dependent manner upon HU-induced replication stress. ATR inhibition also leads to increased DSB formation particularly in the HU-treated condition as indicated by the increased autophosphorylation of ATM on S1981. This is similar to the increased CHK2 phosphorylation in mouse ES cells described above. In **F**, ATMi treatment blocks ATM-mediated phosphorylation on its substrate CHK2 and KAP1 in a dose-dependent manner following IR.

Primary antibodies are diluted in 2.5% milk as listed below: Anti-CHK1 pS345, 1:750 (Cell Signaling #2341); Anti-CHK1, 1:750 (Santa Cruz sc-8408); Anti-ATM pS1981, 1:2000 (Rockland 200-301-400); Anti-CHK2 pT68, 1:1000 (Cell Signaling #2661).

Figure A.5

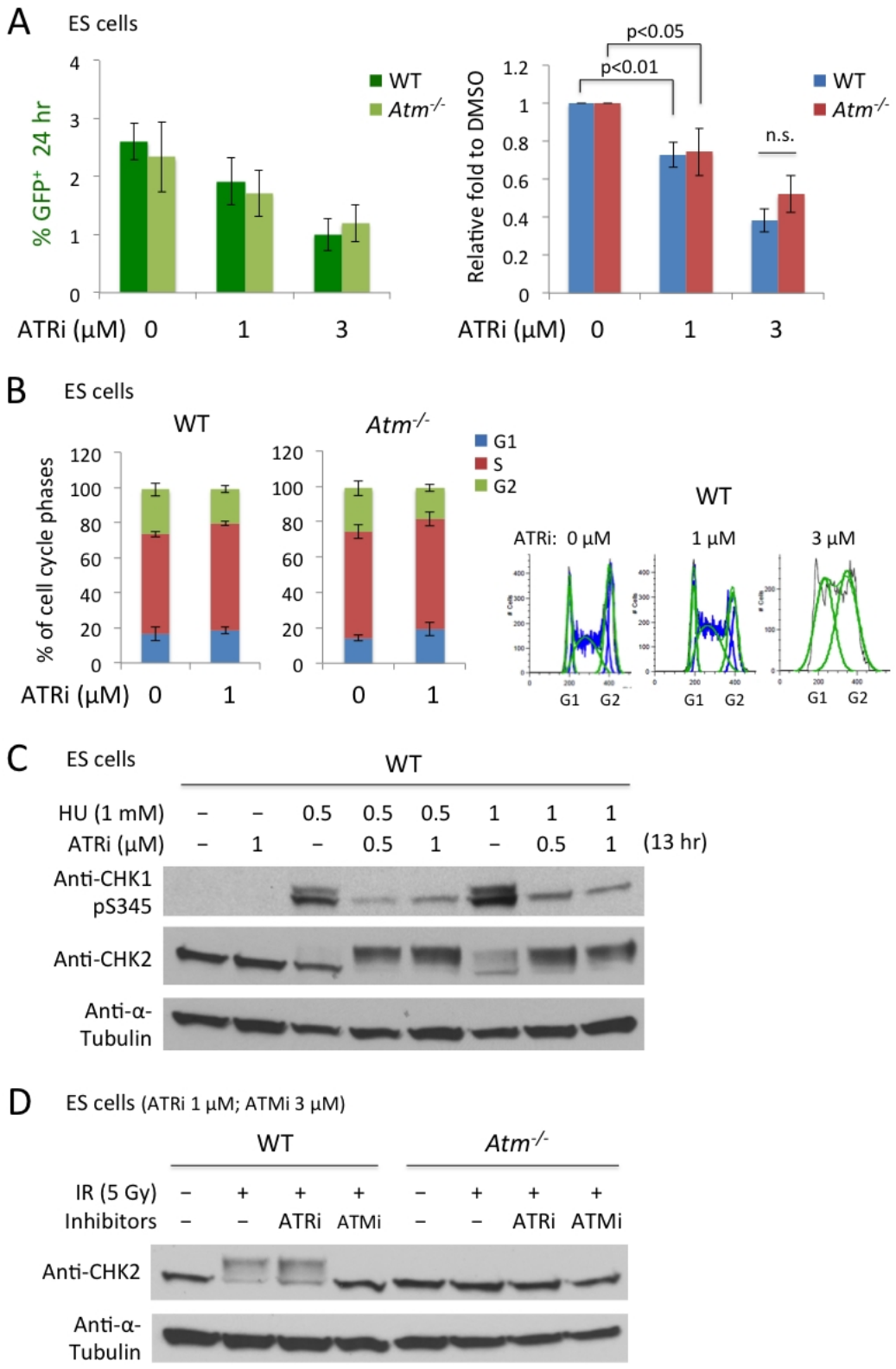
A
ES cells
% GFP+ 24 hr
WT
Atm-/-
ATRi (μM) 0 1 3
Relative fold to DMSO
p<0.05
p<0.01
n.s.
B
ES cells
WT
Atm-/-
% of cell cycle phases
G1
S
G2
ATRi (μM) 0 1 0 1
WT
ATRi: 0 μM
1 μM
3 μM
G1 G2
C
ES cells
WT
HU (1 mM) – – 0.5 0.5 0.5 1 1 1
ATRi (μM) – 1 – 0.5 1 – 0.5 1 (13 hr)
Anti-CHK1 pS345
Anti-CHK2
Anti-α-Tubulin
D
ES cells (ATRi 1 μM; ATMi 3 μM)
WT
Atm-/-
IR (5 Gy) – + + + – + + +
Inhibitors – – ATRi ATMi – – ATRi ATMi
Anti-CHK2
Anti-α-Tubulin

Figure A.5 (Continued)

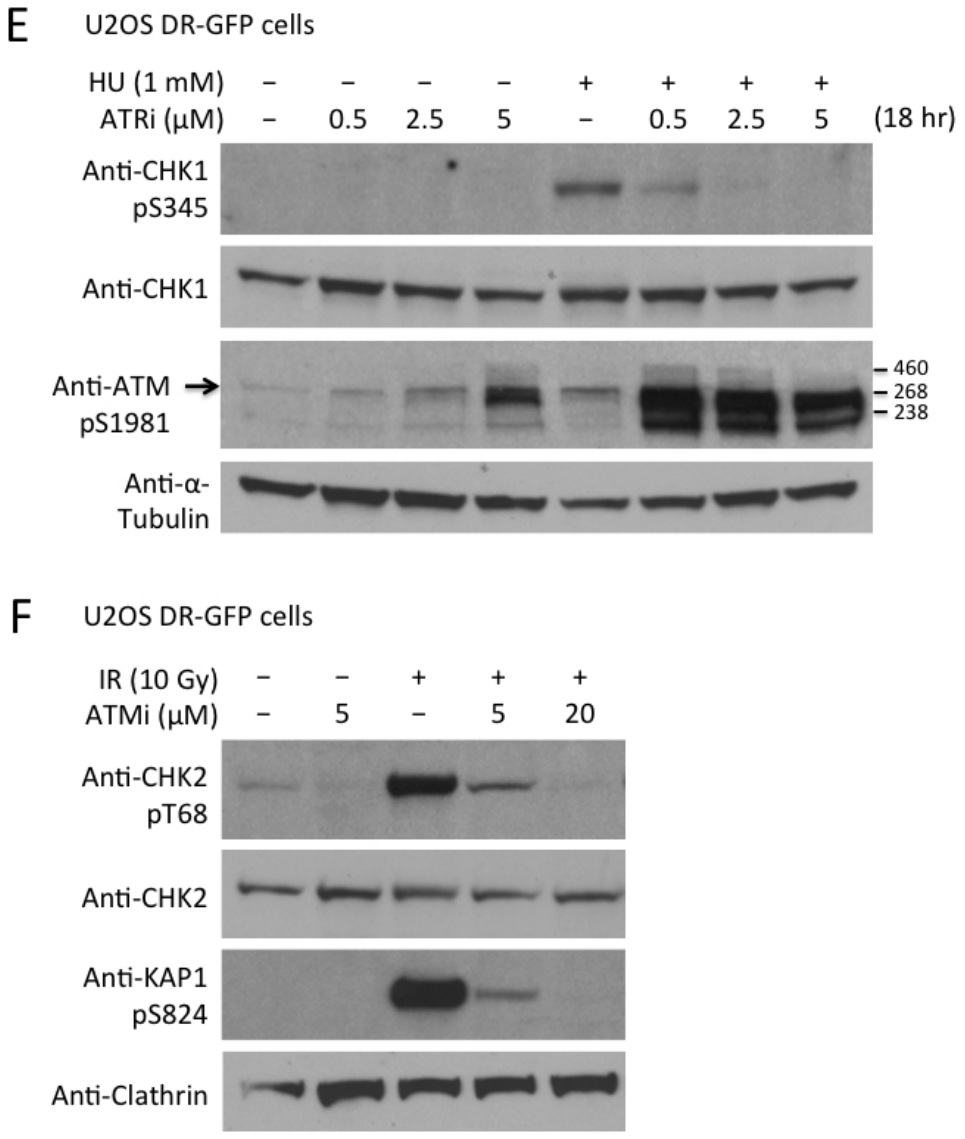

Figure A.6 The role of EXO1 in HDR between diverged sequences.
(Part of which is published in Chen et al., DNA Repair, 2017)
A. EXO1 is a 5' to 3' exonuclease that functions in the mismatch match repair with the MutSα complex (MSH2-MSH6) and also in the extensive step of end resection of DSB repair. We examine how loss of EXO1 affects HDR in *Exo1*$^{-/-}$ mouse ES cells integrated with the DR-GFP reporter (see Figure A.7C for Southern blots of these clones). The average levels of HDR of two *Exo1*$^{-/-}$ DR-GFP clones do not have significant difference compared to that of WT J1 ES cells at 24 and 48 hr after pCBASce transfection (left and middle panels). HDR of individual clones show a similar trend (right). These results suggest that EXO1 loss generally does not impair HDR following I-SceI-induced DSBs, possibly due to the redundancy of resection machinery or the length of resection tract required for revealing homology.
B. ATM inhibition (3 μM) reduces HDR by ~1.5-fold in both WT and *Exo1*$^{-/-}$ DR-GFP ES ells at 24 hr. Interestingly, at 48 hr, HDR in WT cells shows a less pronounced response to ATM inhibition, whereas HDR in *Exo1*$^{-/-}$ cells is still reduced by ~1.4-fold ($n \geq 5$). The smaller extent of HDR reduction at 48 hr is not due to loss of effect of the inhibitor, as the inhibitor-containing medium is replenished every 24 hr; a more frequent change of the inhibitor (every 4-6 hr) in WT cells also yields similar results (not shown). One interpretation is that the smaller effects of ATMi at 48 hr in WT ES cells is analogous to the delayed HDR response observed in *Atm*$^{-/-}$ ES cells (Chapter 2). Given that EXO1 is able to compensate for the resection of clean DSBs upon ATM deficiency (Peterson et al., 2013), it may be acting as an alternative resection pathway to support HDR at later time points. Thus, ATM inhibition in EXO1-deficient cells leads to more persistent HDR suppression compared to EXO1-proficient cells. This hypothesis can be further examined by depleting the redundant resection factors in ATM-deficient cells.
C. To examine how the mismatch repair function of EXO1 influences HDR between diverged sequences, Jeannine LaRocque in the lab modified the DR-GFP reporter to carry 11 silent mutations in the *iGFP* gene (i.e., DR-GFP-11mu; 1.4% increase in divergence; see top diagram) that cause mismatch with the *SceGFP* sequence during homologous pairing (Chen et al., 2017). 3.5×10^6 parental *Exo1*$^{-/-}$ ES cells are electroporated (225 V / 950 μF) with 16 μg of DR-GFP original (denoted by +) or 11mu plasmid together with 16 μg each of pCBASce and/or pCAGGS-mouse EXO1 expression plasmid and analyzed for HDR at 48 hr. In *Exo1*$^{-/-}$ cells complemented with the EXO1 WT protein, HDR between diverged sequences is suppressed by 10-fold compared to that between identical sequences (compare DR-GFP 11mu versus +; % GFP$^+$ in left panel, relative fold in right panel). In *Exo1*$^{-/-}$ cells transfected with an empty vector or a nuclease-inactive D173A mutant (Shao et al., 2014), HDR between diverged sequences is both reduced by only ~1.6-fold. These results suggest that EXO1 inhibits recombination between diverged sequences in a manner dependent on its nuclease activity. The small 1.6-fold reduction in HDR between diverged sequences in the absence of EXO1 also suggests that other mismatch repair factors can still contribute to heteroduplex rejection. (n=3)

The pCAGGS-mouse EXO1 D173A plasmid is provided by Winfried Edelmann at Albert Einstein College of Medicine and the point mutation is confirmed by sequencing (GAC to GCC).

D. Western blots confirm the expression of EXO1 WT and D173A protein in *Exo1*$^{-/-}$ parental cells at the 48-hr time point of flow cytometry. Expression levels from transfected plasmids are typically much lower at 48 hr than 24 hr in ES cells (see below), thus only a faint band of EXO1 protein is detected in the blot (arrow). Expression of the HA-tagged I-SceI is similar among all pCBASce-transfected *Exo1*$^{-/-}$ cells.

Primary antibodies used: Anti-EXO1, 1:1000 in 5% BSA (Bethyl Laboratories A302-640A); Anti-HA, 1:1000 in 2.5% milk (Convance MMS-101P).

E. Western blots of a different EXO1 complementation condition. 5×10^6 *Exo1*$^{-/-}$ DR-GFP cells are electroporated (230 V / 950 μF) with 20 μg of pCBASce and 20 μg of pCAGGS-mouse EXO1 WT or empty vector. Lysates are collected at 24- and 48-hr time points of flow cytometry. The expression of EXO1 protein in complemented *Exo1*$^{-/-}$ cells is comparable to the endogenous level in WT J1 cells at 24 hr but becomes much lower at 48 hr. A similar 24-48 hr difference is observed for the I-SceI expression.

Figure A.6

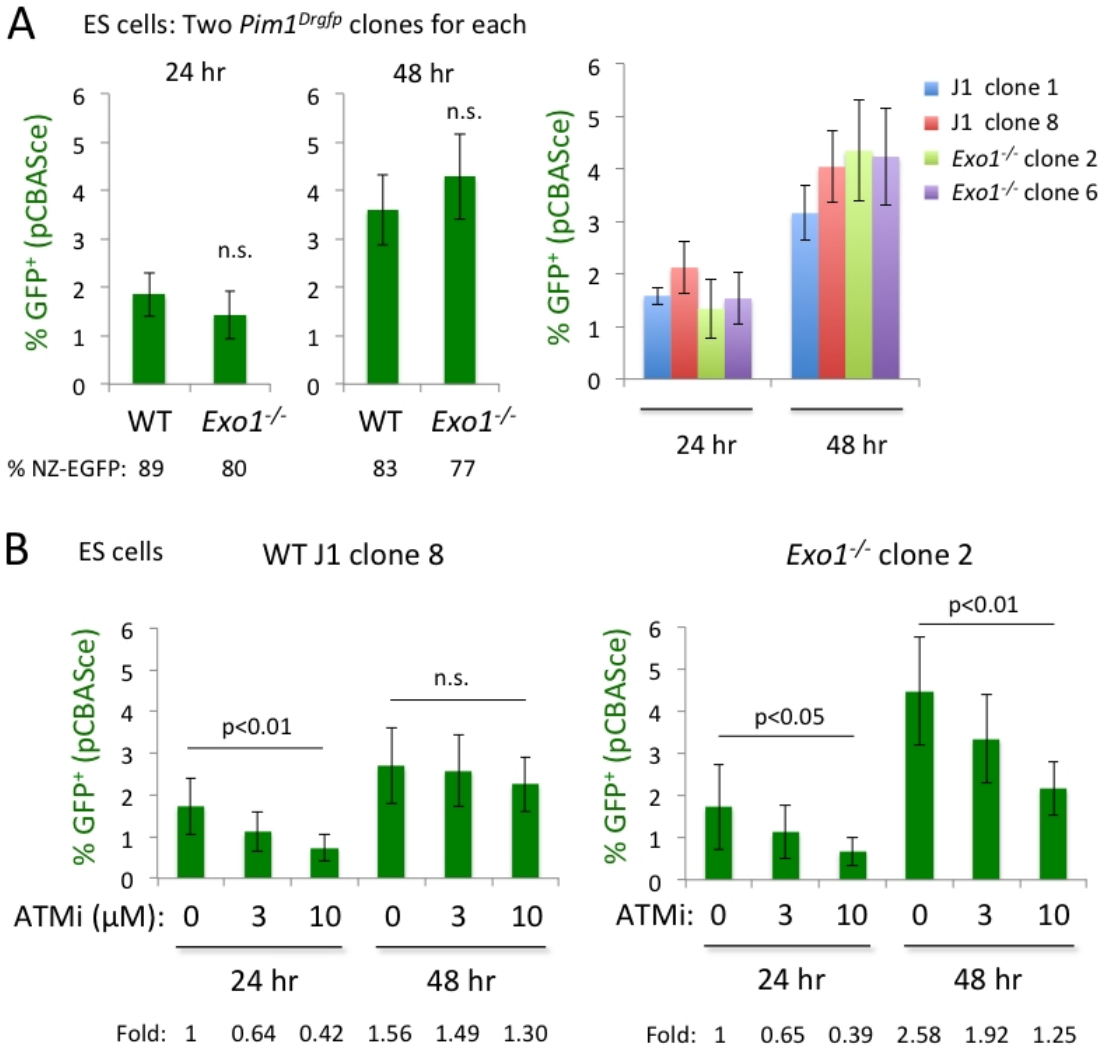
A
ES cells: Two Pim1Drgfp clones for each
24 hr
48 hr
% GFP+ (pCBASce)
n.s.
n.s.
WT
Exo1-/-
WT
Exo1-/-
% NZ-EGFP: 89 80 83 77
J1 clone 1
J1 clone 8
Exo1-/- clone 2
Exo1-/- clone 6
24 hr
48 hr
B
ES cells
WT J1 clone 8
Exo1-/- clone 2
p<0.01
n.s.
p<0.05
p<0.01
ATMi (μM): 0 3 10 0 3 10
ATMi: 0 3 10 0 3 10
24 hr
48 hr
Fold: 1 0.64 0.42 1.56 1.49 1.30
Fold: 1 0.65 0.39 2.58 1.92 1.25

Figure A.6 (Continued)

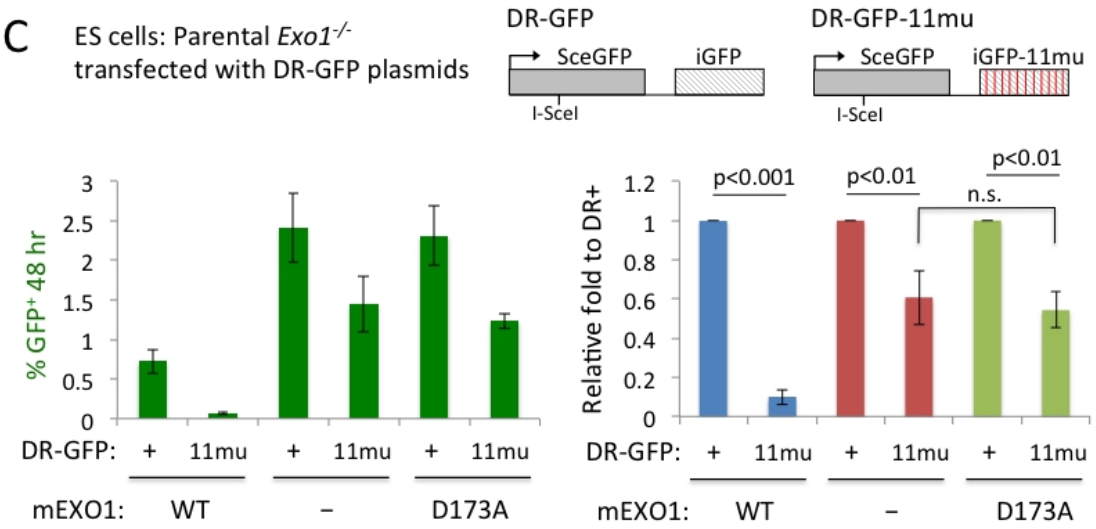

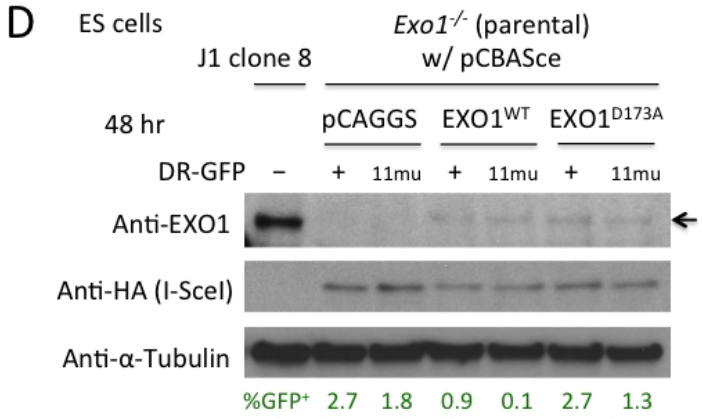

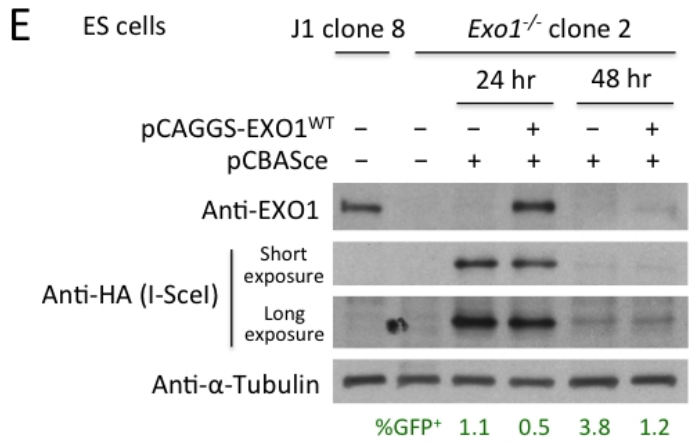

Figure A.7 Southern blots of J1, *Atm*$^{-/-}$, and *Exo1*$^{-/-}$ DR-GFP clones.
A.-C. WT J1**,** *Atm*$^{-/-}$ (Xu et al., 1996), and *Exo1*$^{-/-}$ (Schaetzlein et al., 2013) ES cell lines are integrated with a DR-GFP reporter to the *Pim1* locus using a gene trapping method described previously (Moynahan et al., 2001). 1-2×10^7 ES cells are transfected with 75 μg linealized p59xDR-GFP6 plasmid (XhoI digestion for 7 hr and gel-purified), electroporated at 250 V / 950 μF, and plated to 2-3 10-cm dishes. After 48 hr, the cells are double-selected in 110 μg/ml hygromycin and 1 μg/ml puromycin for ~10 days and the resistant colonies are isolated for genomic DNA purification using Gentra Puregene Tail kit. 5 μg genomic DNA is digested in 20 U HincII (30 μl total volume) for 7 hr, and the reaction is replenished with additional 5 U HincII for overnight digestion. The digested DNA is separated on a 0.8% long gel at 120 V for 6 hr and transferred to a nylon membrane (GeneScreen Plus) in the alkaline buffer overnight. To prepare the *Pim1* probe template, the p22 probe plasmid is first digested in BstXI overnight (10 μg plasmid × 3 reactions) and separated on a 0.8% gel. The 1.7-kb fragment is purified and digested again in HincII overnight (2.2 μg eluted DNA × 3 reactions). After separating on a 0.8% gel, the 1.1-kb fragment is eluted in TE buffer (61 ng/μl × 30 μl total). The probe is synthesized using Prime-It II Random Primer Labeling Kit with 240 ng template and α-^{32}P-dATP and then used for membrane hybridization at 65°C overnight following standard protocols (Pierce and Jasin, 2005). A DR-GFP-targeted allele shows a 2.4-kb band for this probe, whereas the endogenous *Pim1* allele is 3.6 kb.

The results of Southern blotting and EtBr-stained gel images for WT J1, *Atm*$^{-/-}$, and *Exo1*$^{-/-}$ cells are shown in **A**, **B**, and **C**, respectively. Note that in **A**, the genomic DNA of parental J1 control is lost and thus does not show up on the Southern blot (blue asterisk). This has been repeated in the following experiments shown in **B**. A WT ES cell line carrying a *Pim1*^{Drgfp} allele previously established in the lab (Moynahan et al., 2001) is used as a positive control. The J1 clones 1/3/8 and *Atm*$^{-/-}$ clones 1/3/4 are used for HDR analysis in Chapter 2, Figure 2.1. The *Exo1*$^{-/-}$ clones 2 and 6 are analyzed in Appendix Figure A.6.

Figure A.7

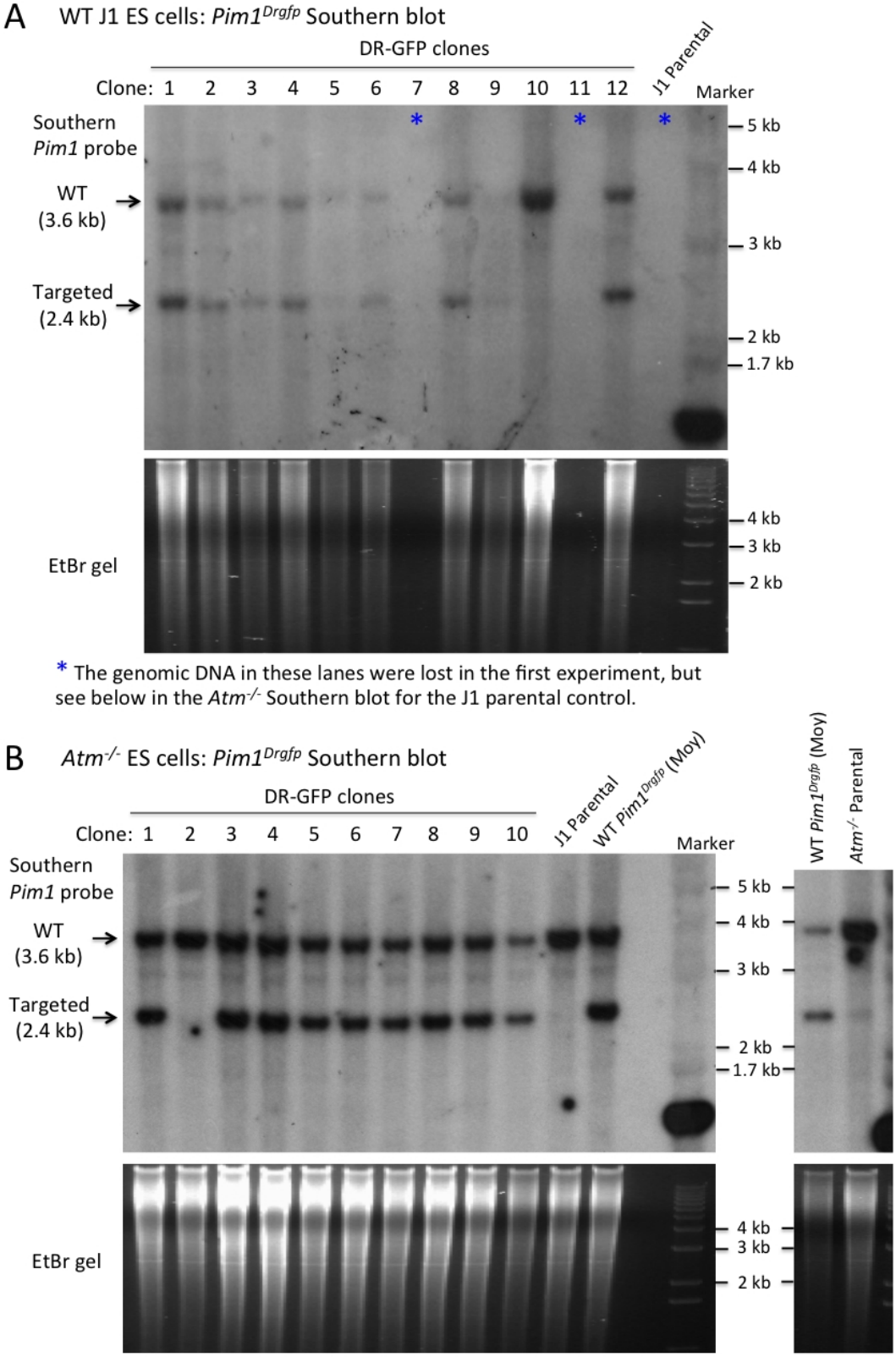
A
WT J1 ES cells: Pim1Drgfp Southern blot
DR-GFP clones
Clone: 1 2 3 4 5 6 7 8 9 10 11 12
J1 Parental
Marker
Southern Pim1 probe
WT (3.6 kb)
Targeted (2.4 kb)
5 kb
4 kb
3 kb
2 kb
1.7 kb
EtBr gel
4 kb
3 kb
2 kb
* The genomic DNA in these lanes were lost in the first experiment, but see below in the Atm-/- Southern blot for the J1 parental control.
B
Atm-/- ES cells: Pim1Drgfp Southern blot
DR-GFP clones
Clone: 1 2 3 4 5 6 7 8 9 10
J1 Parental
WT Pim1Drgfp (Moy)
Marker
WT Pim1Drgfp (Moy)
Atm-/- Parental
Southern Pim1 probe
WT (3.6 kb)
Targeted (2.4 kb)
5 kb
4 kb
3 kb
2 kb
1.7 kb
EtBr gel
4 kb
3 kb
2 kb

Figure A.7 (Continued)

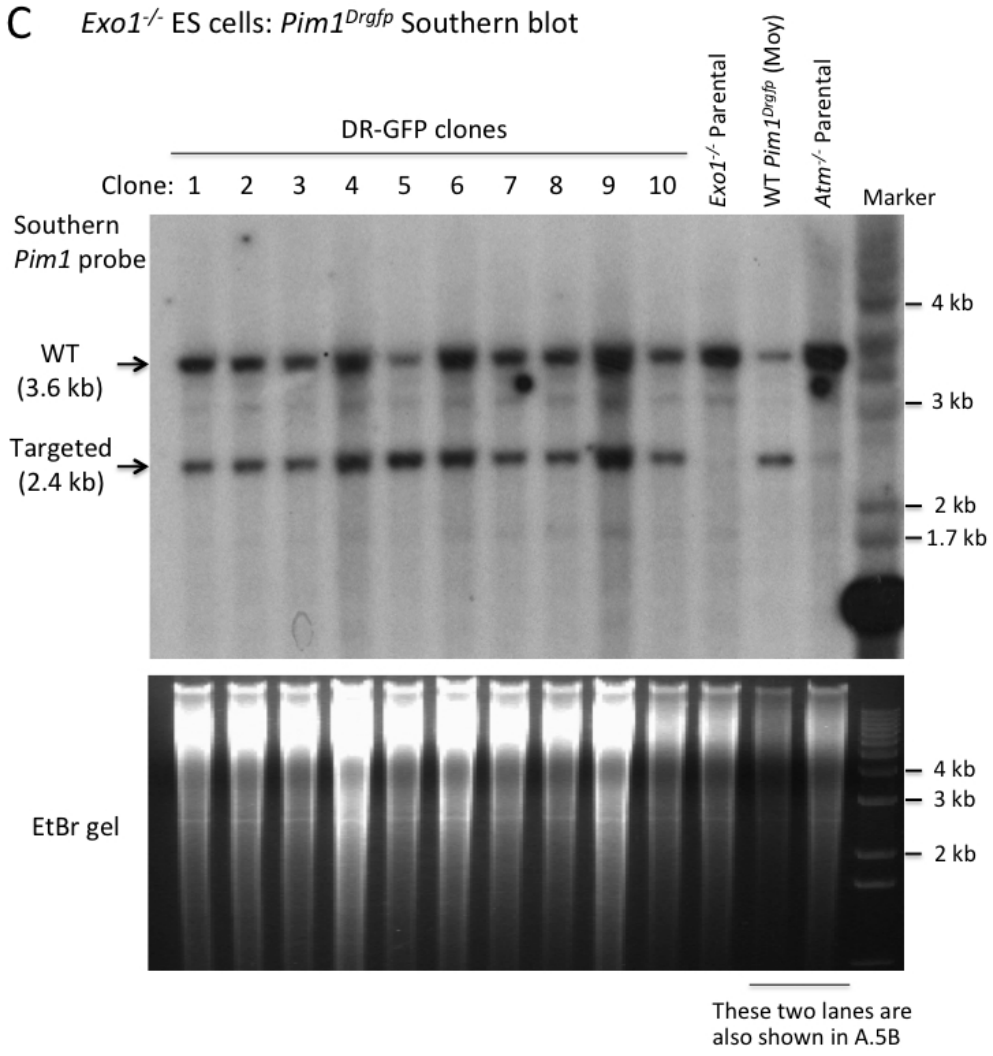

Figure A.8 Construction of *53bp1* mutant ES cell lines.
A.-C. *53bp1* single mutant.
A. To mutate the *53bp1* gene, we follow a previously described method in the lab (Zhang et al., 2014). As shown in the scheme, CRISPR/Cas9 is used to introduce a DSB into exon 2 of *53bp1* to facilitate the replacement of exon 2 with an in-frame resistance cassette (Neo^R is depicted here) via homologous recombination, leading to the disruption of the *53bp1* reading frame. All resistant clones are first screened by PCR amplification across the targeted exon 2 using primers internal to the homology arms (red forward/red reverse), labeled as internal PCR on the scheme. This primer set cannot distinguish targeted versus random integrations, but has robust efficiency to facilitate the screening process. A Neo^R targeting event (or random integration) will produce a ~1.6-kb band in this internal PCR, whereas the WT band is 0.5 kb.

PCR results are analyzed with stringent criteria: Thus, even though many clones show a faint band at the 1.6-kb position that could represent successful targeting of the *Neo* gene (asterisk, below) together with a stronger 0.5-kb WT band (e.g., #64), they are not further pursued. (Note: Amplification efficiency of the much smaller fragment is significantly better.) Only the clones that show potential biallelic modifications, i.e., with the predicted pattern of cassette integration (~1.6 kb) in conjunction with loss of the WT exon 2 band (0.5 kb) or distinguishable shifts to this band, indicating insertions/deletions on the endogenous allele, are further characterized. The second PCR analysis, labeled as In-Out PCR on the scheme, uses primers amplifying from intron 1 (red forward, which anneals to either the 5' homology arm or the endogenous locus) to intron 4 (green reverse, anneals to the endogenous locus only) of *53bp1* to identify correct integration of the template. A correct Neo^R integration will produce a ~2.3-kb band in the In-Out PCR, whereas the WT band is 1.2 kb. The selected clones are then analyzed by western blotting to determine the expression of the 53BP1 protein. The derivative clones that have lost 53BP1 expression are referred to below and in the main texts as $53bp1^{-/-}$.
B. *53bp1* targeting is performed in WT J1 ES cells with a Neo^R template because of a Hyg^R marker at the $Pim1^{Drgfp}$ locus of this cell line. Among the 94 resistant clones analyzed by internal PCR, 11 clones potentially have bi-allelic modifications (all of them show a single band shifted from the 0.5-kb WT position likely due to insertions, e.g., #26 and #55, or deletions, e.g., #36 and #66). Three clones show mono-allelic modification together with a WT band, e.g. #42 (insertion) and #45 (deletion). Two clones do not have an amplified exon 2 band but have a faint band at 1.6 kb, i.e., #31 and #53. Many clones show a faint upper band together with a WT band but this internal PCR cannot tell if it is mono-allelic targeting or random integration, e.g. #27 and #64.

Further analysis using the In-Out PCR suggests that #26 has a potentially targeted allele and another allele with insertions. #66 has a potentially targeted allele and another allele with deletions. #42 has a WT allele and insertions on the other allele. Clones from targeted $Brca1^{ex11}$ cells are used as positive and negative controls here.
C. Nine *53bp1*-targeted J1 clones are examined for 53BP1 expression. #26 shows the absence of 53BP1 band (blue arrow), whose position is determined based on $53bp1^{-/-}$

primary cells in other experiments (see A.6E below). #31 retains the full-length 53BP1 band along with a smaller band slightly above 268 kDa, which can also be seen in the remaining clones. Clone #26 was selected as the *53bp1*$^{-/-}$ single mutant (i.e., *Brca1*$^{+/+}$) for further analysis (Figure 3.2).

D.-E. *Brca1*$^{ex11/ex11}$ *53bp1* double mutant.

D. *53bp1* targeting is performed in a derivative clone (#3) of *Brca1*$^{ex11/ex11}$ ES cells in which the existing *Hyg*^{R} gene was previously disrupted by Cas9. Thus, a *Hyg*^{R} template could be used for this targeting. Among the 161 resistant clones analyzed by internal PCR, 14 clones potentially have bi-allelic modifications (#17, #18, and #62 show a single band between 1-1.7 kb and no 0.5-kb WT band; the remaining show a band shifted from the 0.5-kb position, e.g., #95 and #100). One clone, #22, potentially has mono-allelic targeting together with a WT band. Four clones do not have amplified products, e.g., #31 and #40. Some clones may have cassette integration on a single allele, but it is difficult to conclude due to the faint upper band, e.g., #30.

Further analysis using the In-Out PCR suggests that #17 and #18 have potential cassette integration on one or both alleles (though the upper band is slightly lower than the predicted ~2.3 kb); it is also possible that one allele has modification beyond the red forward primer binding site. Clone #22 has a potentially targeted allele (marked by the green asterisk) and a WT allele.

E. Seven *53bp1*-targeted *Brca1*$^{ex11/ex11}$ clones are examined for 53BP1 expression. All of them, except #22, show the absence of 53BP1 band (blue arrow). #22 has a faint band at the full-length 53BP1 position after longer exposure, suggesting it may be a *53bp1* heterozygous or mixed clone. The *53bp1*$^{-/-}$ control is derived from primary mouse fibroblasts. Clones #17 and #18 were selected as *Brca1*$^{ex11/ex11}$*53bp1*$^{-/-}$ double mutants for further analysis (Figure 3.3).

F.-G. *Brca1*$^{SF/SF}$ *53bp1* double mutant.

F. *53bp1* targeting is performed in *Brca1*$^{SF/SF}$ ES cells using a *Hyg*^{R} template. Among the 64 resistant clones analyzed by internal PCR, 7 clones potentially have bi-allelic modifications (#35, #37, and #41 show a single band ~1.7 kb and no 0.5-kb WT band; the rest of them show a band shifted from the 0.5-kb position, e.g. #39). One clone, #13 (see below), has mono-allelic targeting together with a WT band. Two clones do not have amplified products, e.g. #30.

Further analysis on a few clones using the In-Out PCR suggests that #35, #37, and #41 have potential targeting either on both alleles (maybe #41 due to stronger band intensity) or on one allele in conjunction with loss of primer-binding site on the other allele. #25 may have insertions either on both alleles or on one allele together with loss of primer-binding site on the other allele. #33 has a potentially targeted allele and another allele with insertions. #13 has a WT allele and another allele with insertions.

G. Nine *53bp1*-targeted *Brca1*$^{SF/SF}$ clones are examined for 53BP1 expression and 5 of them showed absence of the 53BP1 protein (blue arrow). The *Brca1*$^{SF/SF}$*53bp1*$^{-/-}$ #25 and #37 have the cleanest background in the blot (i.e., without the faint band at the bottom) and are selected for HDR analysis (Figure 3.3). #13 may be a *53bp1* heterozygous clone. #39 has full-length 53BP1 protein band but may still have in-frame small deletions due to the shift in internal PCR.

Figure A.8

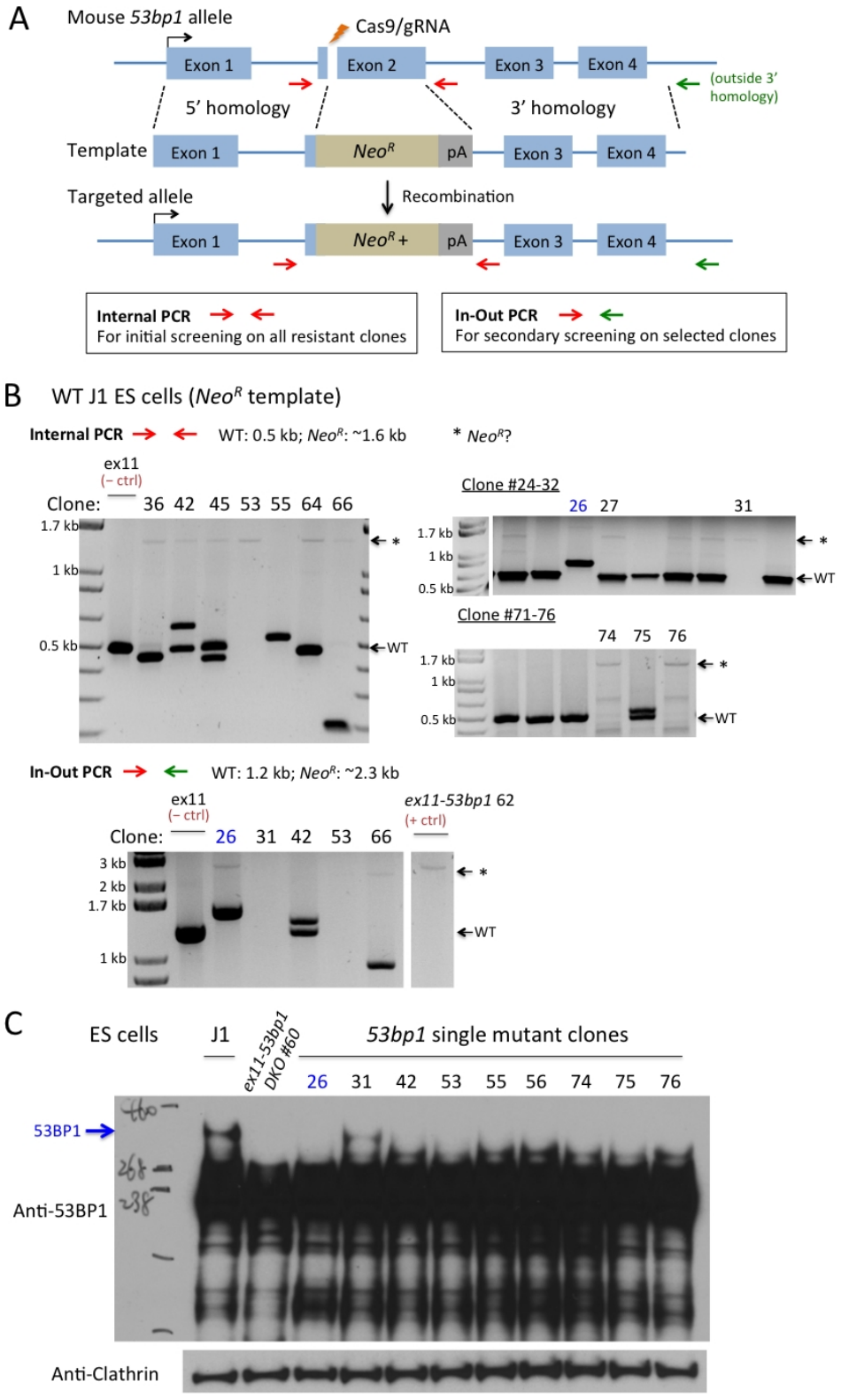
A
Mouse 53bp1 allele
Cas9/gRNA
Exon 1
Exon 2
Exon 3
Exon 4
(outside 3' homology)
5' homology
3' homology
Template
Neo^R
pA
Targeted allele
Recombination
Neo^R +
Internal PCR
For initial screening on all resistant clones
In-Out PCR
For secondary screening on selected clones
B
WT J1 ES cells (Neo^R template)
Internal PCR
WT: 0.5 kb; Neo^R: ~1.6 kb
* Neo^R?
ex11
(– ctrl)
Clone: 36 42 45 53 55 64 66
1.7 kb
1 kb
0.5 kb
WT
Clone #24-32
26 27 31
Clone #71-76
74 75 76
In-Out PCR
WT: 1.2 kb; Neo^R: ~2.3 kb
ex11-53bp1 62
(+ ctrl)
Clone: 26 31 42 53 66
3 kb
2 kb
1.7 kb
1 kb
C
ES cells
J1
ex11-53bp1 DKO #60
53bp1 single mutant clones
26 31 42 53 55 56 74 75 76
53BP1
Anti-53BP1
Anti-Clathrin

Figure A.8 (Continued)

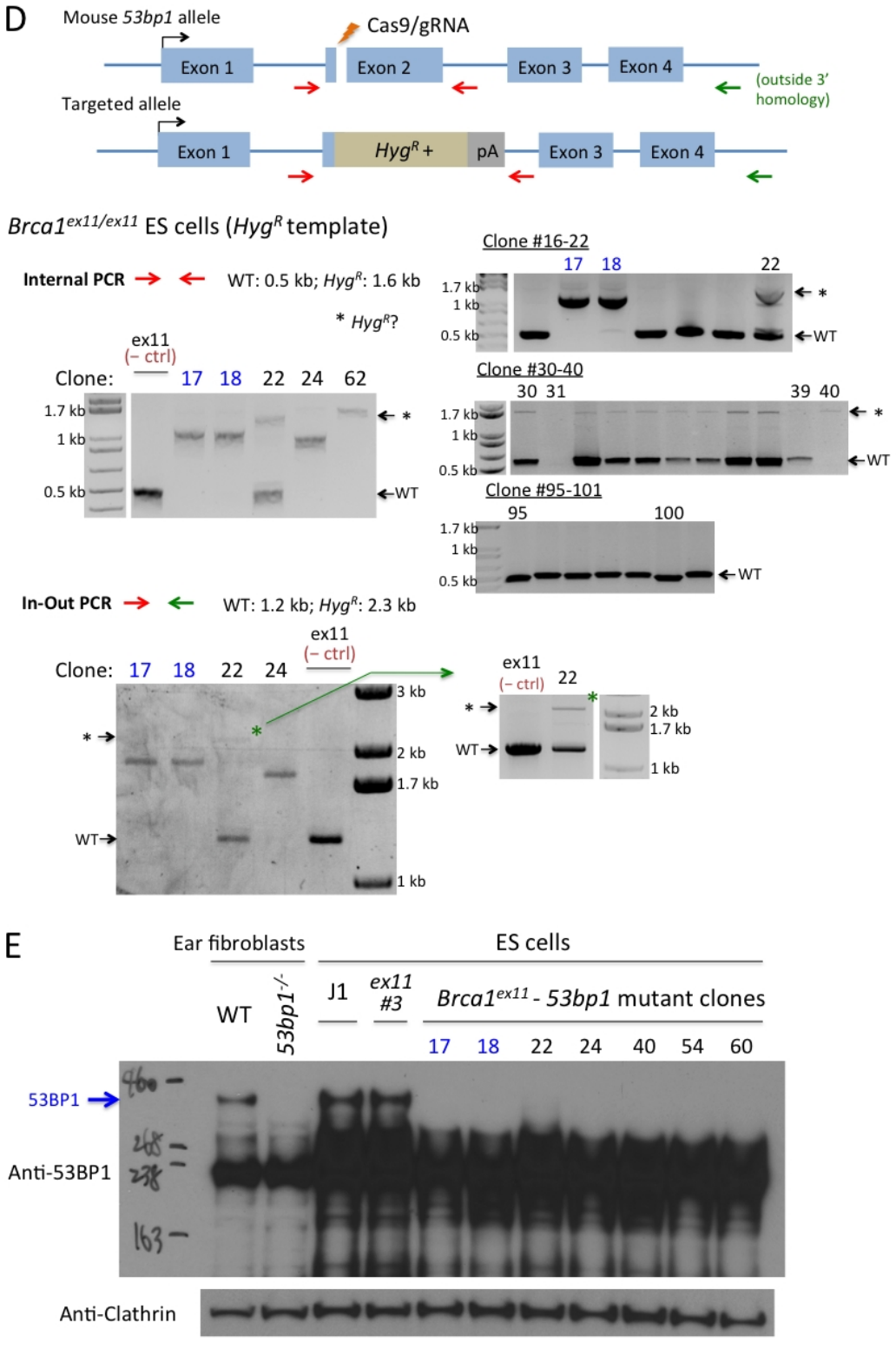

Figure A.8 (Continued)

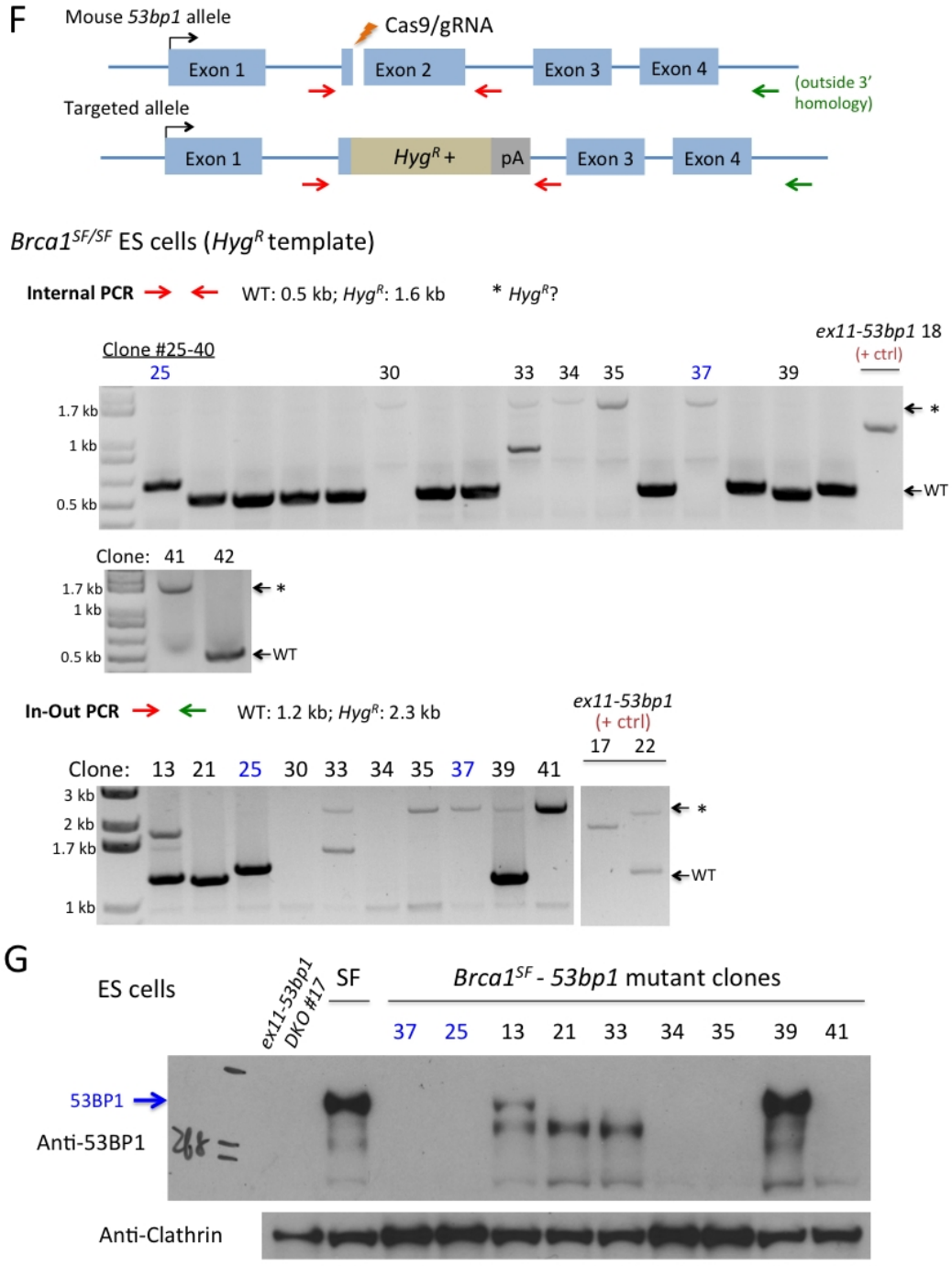

Figure A.9 Supporting data of *Brca1*^{SF} and *Brca1*^{ex11} mutant ES cells.
A. BRCA1^{SF} protein is expressed at a lower level than WT BRCA1 in ES cells, likely due to the folding defect of BRCT domain mutation, however it can be transiently stabilized by treatment with a proteasome inhibitor MG-132 for 6 hr. Anti-BRCA1: dilution 1:500 in 5% BSA overnight (o/n), monoclonal against mouse BRCA1 amino acids 160-300 (provided by Samuel Bunting at Rutgers University).
B. Phosphorylation of CtIP by ATM, as indicated by the mobility shift, following 20 Gy IR shows similar patterns between WT, *Brca1*$^{SF/SF}$, and *Brca1*$^{ex11/ex11}$ ES cells and is not observed in *Atm*$^{-/-}$ cells. Anti-CtIP: dilution 1:250 in 5% BSA o/n (provided by Richard Baer at Columbia University)
C. The 53BP1 protein in *Brca1*$^{ex11/ex11}$ ES cells shows a more prominent mobility shift than in *Brca1*$^{SF/SF}$ cells following olaparib treatment for 20 hr. ATM inhibition can attenuate but not completely abolish the shift of 53BP1. This suggests that ATM may be inducing higher levels of 53BP1 phosphorylation in the *Brca1*^{ex11} mutant, but more molecular characterization is needed. Anti-53BP1: dilution 1:4000 in 2.5% milk (Novus NB100-304); 7.5% Tris-Gly gel transferred at 22 V o/n.
D.-G. Analyzing chromatin association of 53BP1
D. Inhibition of ATM appears to increase the levels of chromatin-bound 53BP1 particularly in olaparib-treated *Brca1*$^{SF/SF}$ cells, suggesting ATM may have a role in counteracting the localization of 53BP1 to DNA upon damage in the *Brca1*^{SF} mutant. See below for quantification. It is interesting to note that CtIP binding to chromatin also increases in the olaparib-treated *Brca1*^{SF} mutant and shows a slightly shifted pattern not suppressed by ATMi, but it is unclear if this means that the cells attempt to perform resection/HDR or if CtIP is blocked at the DSB sites from dissociation; in total cell lysates, the IR-induced shift of CtIP is similar between the two *Brca1* mutants (see Figure A.9B above).

The ES cells are treated with olaparib (0.5 μM) with or without ATMi (5 μM) for 20 hours. Cells are trypsinized and 2×10^6 cells were fractionated using Thermo Fisher Subcellular Protein Fractionation Kit to isolate chromatin-bound proteins for western blot. The blots are quantified using ImageJ. The band intensity of 53BP1 is normalized to that of internal control HDAC2 first and then compared between the two *Brca1* mutants on the same blot for each experiment. Three out of five experiments are shown here.
E. In the condition with olaparib treatment, combination with ATMi in *Brca1*$^{SF/SF}$ ES cells leads to a significant increase in chromatin-bound 53BP1 compared to olaparib alone. Such change is not evident in the *Brca1*$^{ex11/ex11}$ or WT cells. The fold is relative to the sample treated with olaparib alone in each genotype. (n=5 except n=1 for WT)
F. In the undamaged condition, *Brca1*$^{ex11/ex11}$ cells show slightly higher levels of chromatin-bound 53BP1 than *Brca1*$^{SF/SF}$ cells, perhaps related to its more severe HDR defect at baseline level. The fold is relative to the *Brca1*$^{SF/SF}$ sample treated with only DMSO. (n=5)
G. The BRCA$^{\Delta11}$ protein can be found localized to the chromatin (more obvious with olaparib treatment), whereas the BRCA^{SF} protein is not very observable in part due to the instability of BRCT mutant peptide. Two experiments are shown here. Anti-BRCA1: 1:1000 in 5% BSA o/n (Santa Cruz H-100).

Figure A.9

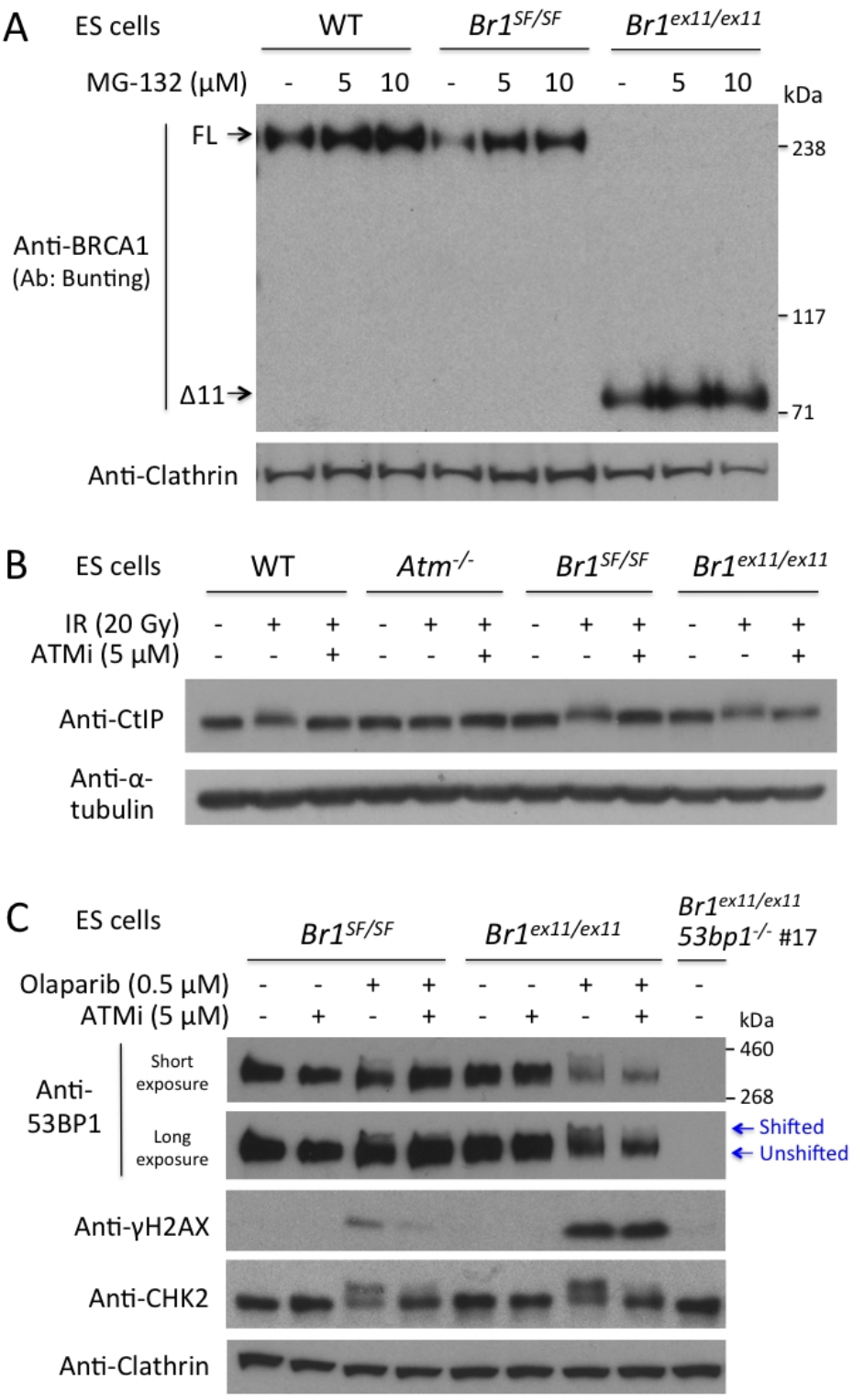
A
ES cells
WT
Br1SF/SF
Br1ex11/ex11
MG-132 (μM)
- 5 10 - 5 10 - 5 10
kDa
FL
Δ11
238
117
71
Anti-BRCA1
(Ab: Bunting)
Anti-Clathrin
B
ES cells
WT
Atm-/-
Br1SF/SF
Br1ex11/ex11
IR (20 Gy)
ATMi (5 μM)
Anti-CtIP
Anti-α-tubulin
C
ES cells
Br1SF/SF
Br1ex11/ex11
Br1ex11/ex11 53bp1-/- #17
Olaparib (0.5 μM)
ATMi (5 μM)
kDa
460
268
Anti-53BP1
Short exposure
Long exposure
Shifted
Unshifted
Anti-γH2AX
Anti-CHK2
Anti-Clathrin

Figure A.9 (Continued)

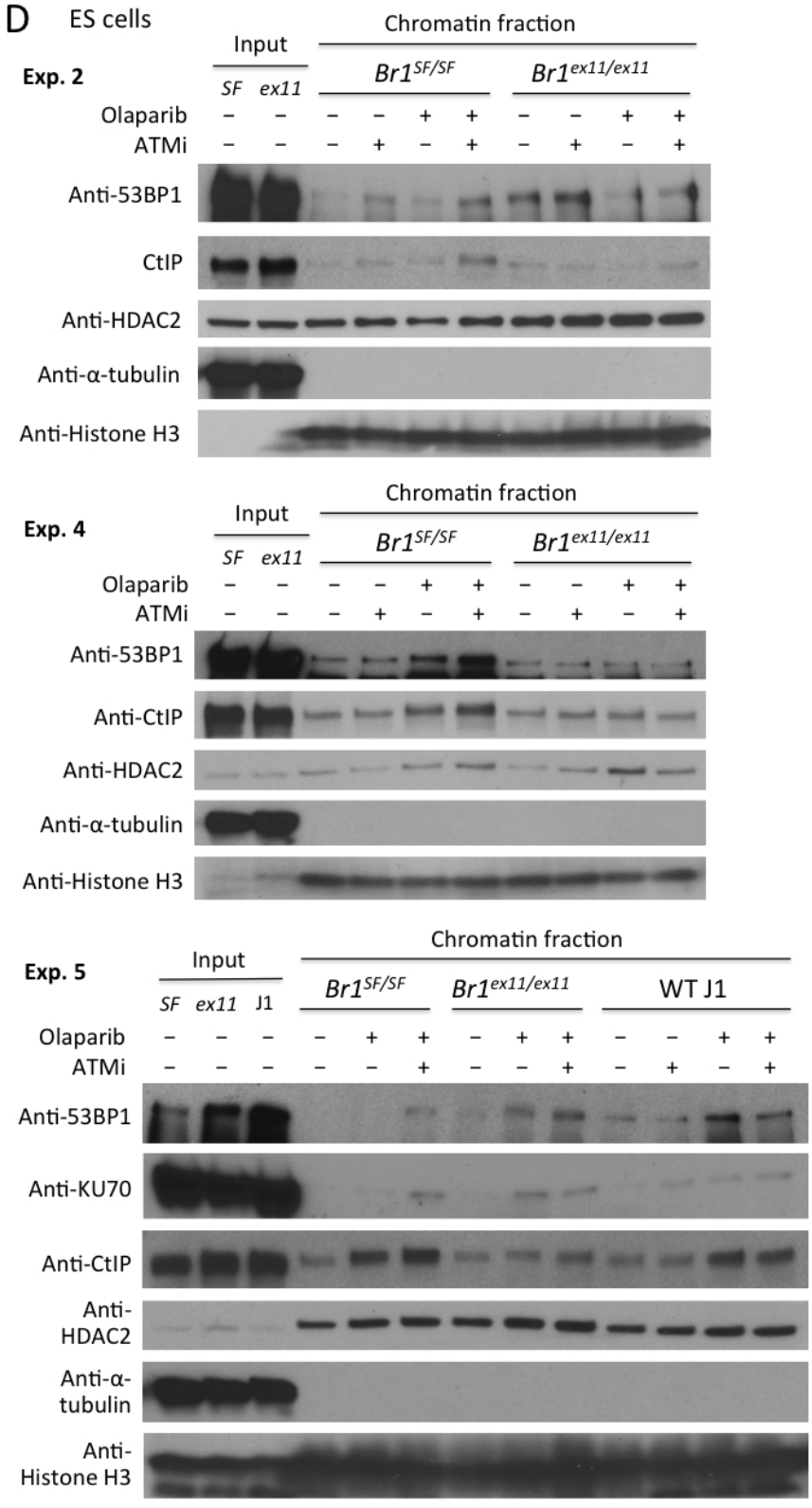

Figure A.9 (Continued)